Theoretical Study of σ-Bond Activation Reactions by Transition Metal Complexes(Dissertation_全文)

AUTHOR(S):

Ochi, Noriaki

Theoretical Study of σ-Bond Activation Reactions by Transition Metal Complexes

Noriaki Ochi

2009

Preface

Nowadays, theoretical and computational methods are used in wide areas of chemistry from fundamental to applied chemistries. Not only theoretical chemists but also experimental chemists investigate various chemical issues with theoretical and computational method. One of the strong points of theoretical and computational study is the ability to present such important information as molecular geometry, bonding nature, electronic structure, relative energy, and so on. These theoretical informations are indispensable for well understanding and prediction of various compounds and chemical reactions.

Various structures, electronic structures, bonding natures, and reaction behavior are found in transition metal complexes as well known. Also, transition metal complexes play important roles as catalyst in organic chemistry, organic synthesis, and catalytic chemistry. To understand correctly their catalyses, we need correct knowledge of the intermediate and transition state. However, it is not easy to experimentally obtain such knowledge, because the intermediate is very reactive and its concentration is very low in general. On the other hand, theoretical and computational method is very useful and powerful to present theoretical knowledge of intermediate and transition state. Actually, many theoretical studies of the reactions have been reported and catalytic reaction mechanisms have been clarified so far. Despite of those many theoretical studies, there remain important issues to be investigated theoretically. One of them is σ-bond activation reactions of alkanes and aromatic hydrocarbons by transition metal complexes.

In this thesis, I wish to report theoretical studies of the σ-bond activation reaction by transition metal complexes with electronic structure theory. Chapter 1 reports the theoretical investigation of heterolytic σ-bond activation of methane with titanium-imido complex. In this chapter, we disclosed that the titanium-imido complex is considerably reactive for C-H

σ-bond activation of alkane and that the important orbital interaction of heterolytic σ-bond activation. Considering these results, we investigated various σ-bond activations by the titanium-imido complex. In chapter 2, we report our computational results of the O-H, Si-H, and C-Si σ-bond activation reactions. In chapter 3, we theoretically investigated regioselective {2 + 2} cycloaddition reaction of C≡C triple bond across the titanium-imido bond. This reaction is interesting because this is the symmetry forbidden by the Woodward-Hoffmann rule but easily occurs. We disclosed the reason based on the orbital interaction diagram. Chapter 4 reports the electronic structure of new palladium(II) complex of P,S-containing hybrid calixphyrin and its unexpectedly high reactivity for oxidative addition of phenyl bromide (PhBr). In chapter 5, the interconversion reaction between H_2 and H_2O with ruthenium-germanium dinuclear complex is reported. This reaction, which is model of hydrogenase, occurs via heterolytic H-H σ-bond activation.

These studies were carried out at Department of Molecular Engineering, Graduate School of Engineering, Kyoto University. I would like to express my deepest appreciation to Professor Shigeyoshi Sakaki for his careful discussion and valuable suggestions. His versatile knowledge of theoretical chemistry, organometallic chemistry, and inorganic chemistry supported my all studies. My studies did not achieve without his collaboration. I should express a lot of thanks to Associate Professor Hirofumi Sato and Assistant Professor Yoshihide Nakao for their fruitful suggestions and technical advices. I should express my appreciation to Associate Professor Yoshihiro Matano and Assistant Professor Tsuyoshi Matsumoto for their valuable suggestions. They warm-heartedly collaborated in study of chapters 4 and 5, respectively.

I also would like to express my appreciation to Professors Kosuke Shobatake, Atsushi Satsuma, Associate Professor Kyoichi Sawabe, and Assistant Professor Kenichi Shimizu in Nagoya University. They kindly provided me with academic comments in various fields. I wish to express my acknowledgments also to all members of Sakaki laboratory. Especially, I

appreciate doctoral students for informal seminar, which gave me great opportunities to learn a lot in many fields. I also wish to present my grate thanks to Mr. Hideo Ando for his advices in various cases.

I thank Japan Society for Promotion of Science (JSPS) for financial support (Grant-in-Aid for JSPS Fellows).

Finally, I sincerely appreciate to Masaaki Ochi and Atsuko Ochi. They have been understanding and supporting my academic works.

Noriaki Ochi

November, 2009

Contents

General Introduction

1. Importance of Theoretical Study of Transition Metal Complex

Transition metal complexes have attracted a lot of interests for their enormous applications in inorganic chemistry, catalytic chemistry, organometallic chemistry, and organic synthesis. Especially, the catalysis of the transition metal complex is of considerable importance in recent fundamental and applied chemistry. For example, transition metal complexes are employed as catalyst in many industrial reactions such as polymerization, hydrogenation of alkene and alkyne, and hydroformylation.[1] Also, transition metal complexes are often applied as catalyst to fine synthetic reactions such as asymmetric synthesis and cross-coupling reaction.[2-4]

There are many strong points in the transition metal complexes for catalyst: (1) Yield and selectivity of the catalytic reaction are considerably high in many cases. (2) Transition metal complexes are indispensable as catalysts for many synthetic reactions which are useful for fine syntheses of medicine and various chemicals. And, (3) fine tuning of reactivity and selectivity can be achieved by selecting proper transition metal center and designing appropriate ligand. However, it is still difficult to design excellent ligand and to select proper metal center because the catalytic reaction is very complicated and catalyses of transition metal complexes are not clear in many cases.

Theoretical and computational study of catalytic reaction by transition metal complex provides us with correct understanding of reaction mechanism and catalysis. Such understanding is indispensable to make further development of catalytic chemistry by transition metal complexes and to design new excellent catalyst. Actually, many theoretical and computational studies have been carried out so far and various important reports have been presented on reaction mechanism and catalytic functions of transition metal complexes.

2. Theoretical and Computational Chemistry of Catalytic Reaction by Transition Metal Complex

Catalytic reactions by transition metal complexes very often consist of many common elementary steps, such as σ-bond activation, insertion of alkene and alkyne into M-H and M-R bonds, reductive elimination, nucleophilic attack to coordinating ligand, and so on. In this regard, the correct knowledge of each elementary step is necessary for the well understanding of catalytic reactions by transition metal complexes.

Various elementary steps involved in catalytic reactions were theoretically investigated first with extended Hückel MO and semi-empirical MO methods. In these studies, fundamental understanding of the reactions were presented based on orbital interaction diagram rather than computational results of energy and geometry arguments.[5, 6] In 1980's to 1990's, ab initio MO method was applied to such theoretical and computational studies of catalytic reactions, and now density functional theory (DFT) method[7] is very often applied to theoretical and computational studies of catalytic reactions based on computational results of geometry and energy. In those studies, theoreticians succeeded in reporting geometry and energy changes of various important elementary steps involved by catalytic reactions and presenting quantitatively, at least semi-quantitatively, correct understanding of those reactions. For example, Sakaki and coworkers investigated oxidative addition of silane and methane to platinum(0) complex and reported transition state and activation barrier with ab initio MO method.[9]

Recently, not only elementary step but also whole catalytic cycle is theoretically investigated with electronic structure theory, because big developments have been achieved in electronic structure theory and computer performance. Actually, many theoretical studies of whole catalytic cycle have been reported so far. From those results, we can obtain rate-determining step and know the most favorable reaction course. One good example is theoretical study of hydrosilylation of alkene;[10] the reaction mechanism is different between

Pt and Rh complexes, and also different between the late transition metal and early transition metal complexes. As shown in Scheme 1, this catalytic reaction occurs through Chalk-Harrod mechanism in the case of Pt catalyst, but through modified Chalk-Harrod mechanism in the case of Rh catalyst. The reason of the difference was clearly elucidated by theoretical studies. In the case of Cp_2Zr catalyst, much more complicated reaction mechanism was theoretically presented and the reason was disclosed based on the characteristic features of transition metal center;[11] see Scheme 2.

The other important example is theoretical studies of palladium-catalyzed Suzuki-Miyaura cross-coupling reaction.[12] In this study, the whole catalytic cycles with neutral $Pd(PMe_3)_2$, anionic $[Pd(PMe_3)_2OAc]^-$, and $[Pd(PMe_3)OAc]^-$ model complexs were theoretically investigated. Although the energy changes of anionic complex are most favorable in these model systems, the difference is small. From these results, it was suggested that several catalytic pathways involving neutral and anionic palladium complexes contribute to the catalytic mechanism. These results are consistent with experimental foundings.

As described above, theoretical and computational studies are very important and indispensable in catalytic chemistry by transition metal complexes.

Scheme 1 (From Ref. 10)

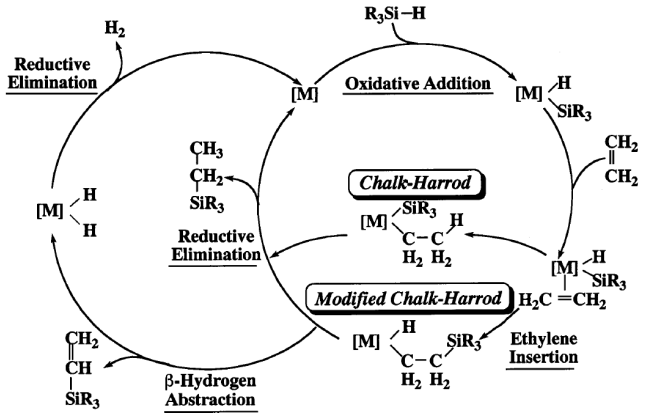

Scheme 2 (From Ref. 11)

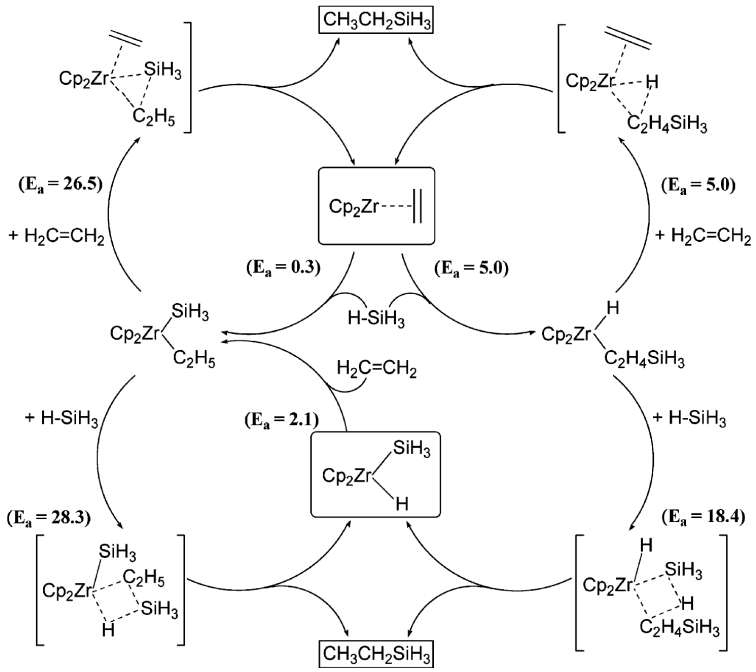

3. Theoretical Studies of σ-Bond Activation with Transition Metal Complex

The σ-bond activation reaction is one of the most important research targets in organometallic chemistry and catalytic chemistry, because σ-bond activation is a key step of various catalytic reactions and metallo-enzyme reactions. The σ-bond activation reactions are classified into two categories (eqs 1 and 2).

$$M + A{-}B \longrightarrow M\begin{matrix}A\\B\end{matrix} \qquad (1)$$

$$ML + A{-}B \longrightarrow M{-}A + L{-}B \qquad (2)$$

As well known, the σ-bond activation in eq. 1 is called oxidative addition and its characteristic features have been explored from both experimental and theoretical points of

view.[13-26] Theoretical and computational studies considerably contributed to the understanding of reaction features and electronic process of the oxidative addition reaction.

On the other hand, theoretical studies of heterolytic σ-bond activations (eq. 2) have been limited except for a few pioneering theoretical works, as follows: In Shilov reaction, methane is converted into methanol with Pt(II) complex. The key reaction step is C-H σ-bond activation of methane, in which two different mechanisms have been suggested (eqs 3 and 4).

$$Pt(II) + H_3C{-}H \longrightarrow H_3C{-}Pt(IV){-}H \qquad (3)$$

$$Pt(II) + H_3C{-}H \longrightarrow H_3C{-}Pt(II)^{-} \quad H^{+} \qquad (4)$$

Siegbahn and Crabtree theoretically investigated the σ-bond activation of methane with model complex $PtCl_2$ with several water molecules, using B3LYP and PCI-80 methods.[27] In their theoretical study, the C-H σ-bond activation occurs through intermediate η^1-methane complex and transition state, to afford product complex $Pt(HCl)Cl(H_2O)_2$. They indicated that the activation occurs via σ-bond metathesis with moderate activation barrier of 27.0 kcal/mol. It is noted that the activated H atom has positive atomic charge of +0.23 and +0.26 in transition state and η^1-methane complex, respectively. The atomic charges of the other H atoms of methane are in the range +0.19 to +0.22. In other words, the activated H atom becomes slightly proton-like. Thus, the C-H bond of methane is moderately polarized in transition state, which is different from that of oxidative addition. Another example was reported by Sakaki and cowerkers; In Fujiwara-Moritani reaction,[28] the C-H σ-bond activation of benzene is performed by Pd(II)-acetate complex. This elementary step was theoretically investigated with DFT, MP2-MP4(SDQ), and CCSD(T) method.[29] As shown in Figure 1, the C-H σ-bond activation occurs through precursor complex (**PC1**) and transition state (**TS1a**), to afford the intermediate (**I1**). In **TS1a**, the Pd-O distance lengthens and C-H

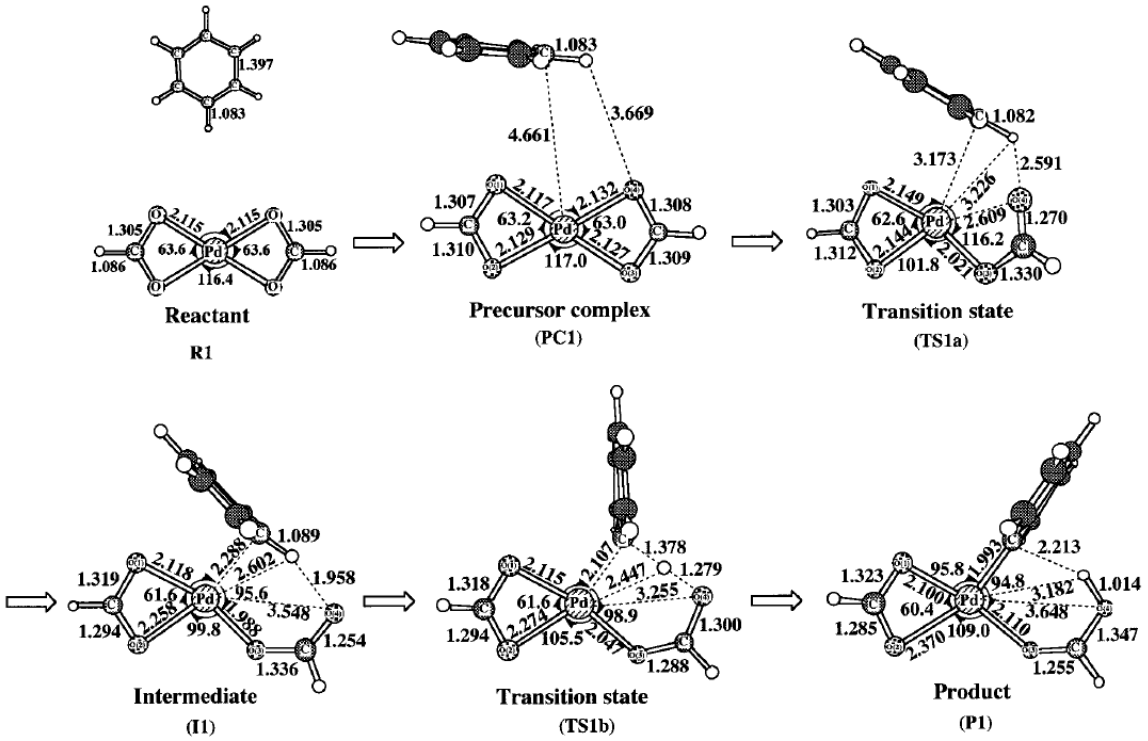

Figure 1. Geometry changes in the C-H bond activation of benzene by $Pd(\eta^2\text{-}O_2CH)_2$. Bond lengths are in angstroms and bond angles are in degrees. (From Ref. 29)

distance of benzene does not change. Starting from **I1**, product complex (**P1**) was formed through transition state (**TS1b**). In **TS1b**, the C-H distance considerably lengthens, indicating that the C-H σ-bond is broken. This characteristic feature of the reaction is found in population changes of the phenyl group and the H atom. As shown in Figure 2, the population of the phenyl group increases but that of the H atom decreases in the reaction, indicating that the phenyl group and H atom become negatively and positively charged, respectively. In other words, this reaction occurs in heterolytic manner. This is the first theoretical report which clearly shows the heterolytic σ-bond activation reaction.

However, there remain a lot of important issues to be theoretically elucidated; one of those issues is orbital interaction in heterolytic σ-bond activation. In the oxidative addition

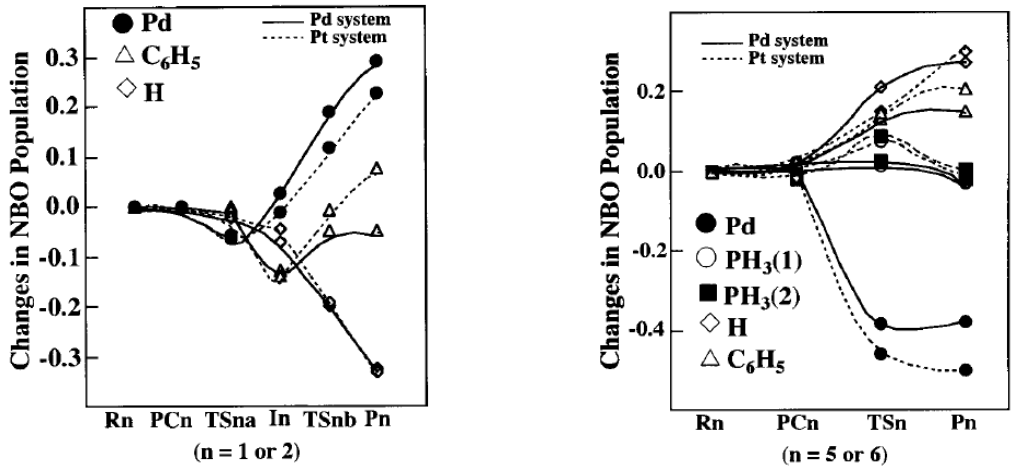

(A) C-H activation of benzene by $M(\eta^2\text{-}O_2CH)_2$

(B) C-H activation of benzene by $M(PH_3)_2$

Figure 2. Population changes in the C-H bond activations of benzene by $M(\eta^2\text{-}O_2CH)_2$ and $M(PH_3)_2$ (M = Pd or Pt). A positive value represents an increase in population (vice versa). Solid lines represent population change for M = Pd, and dotted lines represent population changes for M = Pt. (From Ref. 29)

reaction, the important orbital interaction has been discussed very previously.[30] On the other hand, it is not clear what orbital interaction plays important roles in the heterolytic σ-bond activation. The other is what type of σ-bond can be activated by this reaction. Also, it is important to clarify characteristic features of heterolytic σ-bond activation reaction in comparison with the σ-bond activation by the oxidative addition. I believe that further theoretical study is necessary for both of oxidative addition and heterolytic σ-bond activation reactions.

4. Aims of This Thesis

In this thesis, I wish to report the theoretical investigations of σ-bond activation by transition metal complex and provide new and fundamental understanding for σ-bond

activation reaction.

In chapter 1, I theoretically investigated C-H σ-bond activation of methane by titanium-imido complex [$(Me_3SiO)_2Ti(NSiMe_3)$] (eq. 5). In this reaction, the CH_3 and H groups of methane are bound with Ti and N, respectively; see eq. 5

(5)

Theoretical calculations clearly show that this C-H σ-bond activation occurs in a heterolytic manner, in which the electron population of CH_3 increases but that of H decreases. In other words, the CH_3 and H groups become negatively and positively charged, respectively, in the reaction. The purposes in this chapter are to present well understanding of the heterolytic σ-bond activation and clarify the differences between the oxidative addition and the heterolytic σ-bond activation. Also, I investigated the possibility of the N-H σ-bond activation of ammonia with titanium-imido complex and titanium-alkylidyne complex to present theoretical prediction what type transition metal complex can be applied to the N-H σ-bond activation which is one of difficult reactions.

Considering the conclusions in chapter 1, I theoretically investigated the possibility of O-H σ-bond activation of methanol, Si-H σ-bond activation of silane, and Si-C σ-bond activation of methylsilane with the titanium-imido complex (eq. 6) in chapter 2.

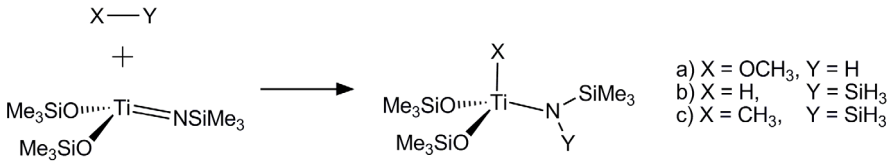

(6)

The purposes here are to clarify the characteristic features of these σ-bond activation reactions, to present correct understandings of these reaction, and finally to theoretically predict that the

titanium-imido complex is useful for O-H, Si-H, and Si-C σ-bond activation reactions.

In chapter 3, {2 + 2} cycloaddition of alkynes across the Ti=N bond of titanium-imido complex (eq. 7) was theoretically investigated.

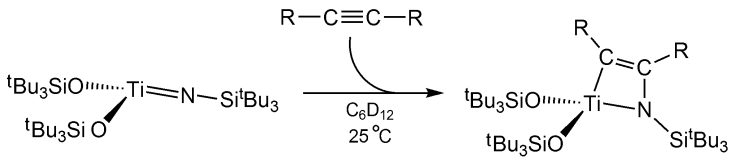

(7)

Though this cycloaddition is symmetry forbidden in a formal sense by the Woodward-Hoffmann rule, this cycloaddition easily occurs with moderate activation barrier and considerably large exothermicity. Considering the symmetry forbidden character of this reaction, I carefully investigated this reaction with CASSCF and MRMP2 methods as well as CCSD(T) method. The purposes in this chapter are to present detail knowledge of the {2 + 2} cycloaddition, to clarify the reason why this cycloaddition easily occurs, and to provide the well understanding in terms of orbital interactions. The computational results clearly indicate that the high reactivity of the titanium-imido complex for both of the heterolytic σ-bond activation and the {2 + 2} cycloaddition arises from the polarized Ti=N bond.

In chapter 4, I investigated electronic structure of new palladium complex of P,S-containing hybrid calixphyrin and its flexible behavior in the oxidative addition of phenyl bromide (PhBr). As shown in Scheme 3, this palladium complex takes two kinds of valence tautomer: Pd(II) form and Pd(0) form.

Scheme 3

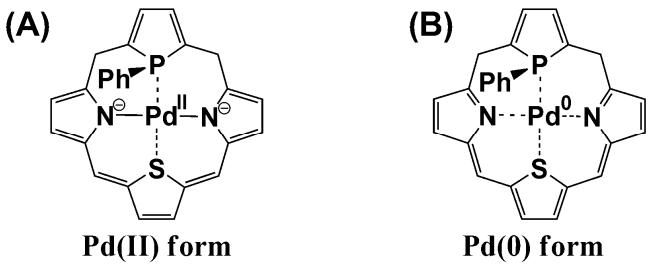

Pd(II) form **Pd(0) form**

This chapter reports that Pd(II) form is favorable but interestingly oxidative addition to this Pd(II) form occurs easily, though the oxidative addition to Pd(II) complex is difficult in general. The purpose of this chapter is to investigate the electronic structure of palladium complex of P,S-containing hybrid calixphyrin and clarify the reason why the oxidative addition easily occur to this Pd(II) complex.

In chapter 5, I investigated the interconversion reaction between H_2 and H_2O with hydroxo/sulfido-bridged ruthenium-germanium dinuclear complex (eq. 8), which is synthesized as model of hydrogenase enzyme. The purpose of this chapter is to clarify the mechanism and characteristic features of interconversion reaction and what roles Ru and Ge centers play in this reaction.

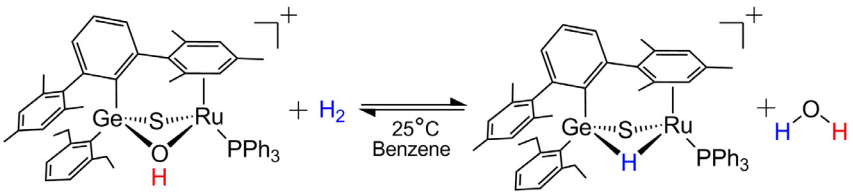

(8)

Through these studies, I wish to present well understanding of σ-bond activation reaction, especially heterolytic σ-bond activation, propose theoretical prediction of N-H, O-H, Si-H, and Si-C σ-bond activation, and clarify interesting reactivities of P,S-containing calixphyrin palladium complex in the oxidative addition reaction and that of the Ru-Ge dinuclear complex in the interconversion between H_2 and H_2O.

References

(1) Kameoka, H.; Inoue, S. *Industrial Organic Chemistry*; Shokabo: Tokyo, 2004

(2) (a) Noyori, R.; Takaya, H. *Acc. Chem. Res.* **1990**, *23*, 345. (b) Knowles, W. S.; Noyori, R. *Acc. Chem. Res.* **2007**, *40*, 1238.

(3) Miyaura, N.; Suzuki, A. *Chem. Rev.* **1995**, *95*, 2457.

(4) Hegedus, L. S. *Transition Metals in the Synthesis of Complex Organic Molecules 2nd Ed.*; University Science Books: California, 1999.

(5) Thorn, D. L.; Hoffmann, R. *J. Am. Chem. Soc.* **1978**, *100*, 2079.

(6) Sakaki, S.; Nishikawa, M.; Ohyoshi, A. *J. Am. Chem. Soc.* **1980**, *102*, 4062.

(7) Koch, W.; Holthausen, M. C. *A Chemist's Guide to Density Functional Theory* Vch Verlagsgesellschaft Mbh, 2000.

(8) (a) Tatsumi, K.; Hoffmann, R.; Yamamoto, A.; Stille, J. K. *Bull. Chem. Soc. Jpn.* **1981**, *54*, 1857. (b) Elian, M.; Hoffmann, R. *Inorg. Chem.* **1975**, *14*, 1058.

(9) Sakaki, S; Ieki, M. *J. Am. Chem. Soc.* **1993**, *115*, 2373.

(10) (a) Sakaki, S.; Mizoe, N.; Sugimoto, M.; Musashi, Y. *Coord. Chem. Rev.* **1999**, *190*, 933. (b) Sakaki, S.; Sumimoto, M.; Fukuhara, M.; Sugimoto,M.; Fujimoto, H.; Matsuzaki, S. *Organometallics* **2002**, *21*, 3788.

(11) Sakaki, S.; Takayama, T.; Sumimoto, M.; Sugimoto, M. *J. Am. Chem. Soc.* **2004**, *126*, 3332.

(12) (a) Goossen, L. J.; Koley, D.; Hermann, H. L., Thiel, W. *J. Am. Chem. Soc.* **2005**, *125*, 11102. (b) Goossen, L. J.; Koley, D.; Hermann, H. L., Thiel, W. *Organometallics* **2006**, *25*, 54. (c) Braga, A. A. C.; Ujaque, G.; Maseras, F. *Organometallics* **2006**, *25*, 3647.

(13) Arndtsen, B. A.; Bergman, R. G.; Mobley, T. A.; Peterson, T. H. *Acc. Chem. Res.* **1995**, *28*, 154.

(14) Crabtree, R. H. *Chem. Rev.* **1995**, *95*, 987.

(15) Shilov, A. E.; Shul'pin, G. B. *Chem. Rev.* **1997**, *97*, 2879.

(16) Crabtree, R. H. *J. Chem. Soc., Dalton Trans.* **2001**, 2437.

(17) Labingerand, J. A.; Bercaw, J. E. *Nature* **2002**, *417*, 507.

(18) Tamura, H.; Yamazaki, T.; Sato, H.; Sakaki, S. *J. Am. Chem. Soc.* **2003**, *125*, 16114.

(19) (a) Musaev, D. G.; Froese, R. D. J.; Morokuma, K. *Organometallics*, **1998**, *17*, 1850. (b) Tomita, T.; Takahama, T.; Sugimoto, M.; Sakaki, S. *Organometallics*, **2002**, *21*. 4138.

(20) (a) Kitaura, K.; Obara, S.; Morokuma, K. *J. Am. Chem. Soc.* **1981**, *103*, 2891. (b) Obara, S.; Kitaura, K.; Morokuma, K. *J. Am. Chem. Soc.* **1984**, *106*, 7482.

(21) (a) Low, J. J.; Goddard, W. A. *J. Am. Chem. Soc.* **1986**, *108*, 6115. (b) Low, J. J.; Goddard, W. J. *Organometallics* **1986**, *5*, 609.

(22) (a) Sakaki, S.; Ieki, M. *J. Am. Chem. Soc.* **1993**, *115*, 2373. (b) Sakaki, S.; Ogawa, M.; Musashi, Y.; Arai, T. *Inorg. Chem.* **1994**, *33*, 1660. (c) Sakaki, S.; Ogawa, M.; Kinoshita, M. *J. Phys. Chem.* **1995**, *99*, 9933.

(23) Su, M. -D.; Chu, S. -Y. *J. Am. Chem. Soc.* **1997**, *119*, 5373.

(24) Espinosa-Garcia, J.; Corchado, J. C.; Truhlar, D. G. *J. Am. Chem. Soc.* **1997**, *119*, 9891.

(25) Hill, G. S.; Puddephatt, R. J. *Organometallics* **1998**, *17*, 1478.

(26) (a) Heiberg, H.; Swang, O.; Ryan, O. B.; Gropen, O. *J. Phys. Chem. A* **1999**, *103*, 10004. (b) Heiberg, H.; Johansson, L.; Gropen, O.; Ryan, O. B.; Swang, O.; Tilset, M. *J. Am. Chem. Soc.* **2000**, *122*, 10831.

(27) Siegbahn, P. E. M.; Crabtree, R. H. *J. Am. Chem. Soc.* **1996**, *118*, 4442.

(28) (a) Moritani, I.; Fujiwara, Y. *Tetrahedron Lett.* **1967,** *1119*. (b) Fujiwara, Y.; Takagi, Y.; Taniguchi, Y. *Synlett* **1996**, *591*.

(29) Biswas, B.; Sugimoto, M.; Sakaki, S. *Organometallics* **2000**, *19*, 3895.

(30) Tatsumi, K.; Hoffmann, R.; Yamamoto, A.; Stille, J. K. *Bull. Chem. Soc. Jpn.* **1981**, *54*,

1857.

(31) Barros, N.; Eisenstein, O.; Maron, L. *J. Chem. Soc., Dalton Trans.* **2006**, 3052.

Chapter 1

Theoretical Study of C-H and N-H σ-Bond Activation Reactions by Titanium(IV)-Imido Complex. Good Understanding Based on Orbital Interaction and Theoretical Proposal for N-H σ-Bond Activation of Ammonia

1.1. Introduction

C-H σ-bond activation of alkane by transition-metal complex is one of the challenging reactions in organometallic chemistry, inorganic chemistry, and catalytic chemistry, because functional group can be introduced into alkane via C-H σ-bond activation.[1] In the recent review articles,[1] we found three categories of σ-bond activation, as follows; (1) C-H σ-bond activation via oxidative addition reaction by late transition-metal complexes, (2) C-H σ-bond activation via σ-bond metathesis by lanthanide and actinide complexes, and (3) C-H σ-bond activation via addition of the C-H σ-bond across M=N and M=C multiple bonds by early to middle transition-metal complexes.

The oxidative addition of C-H σ-bond to late transition-metal complexes such as platinum(0) and platinum(II) complexes has been theoretically investigated by many groups.[2-15] From those theoretical studies, we have now detailed knowledge about the oxidative addition reaction. The C-H σ-bond addition across the M=N bond in the early transition-metal complexes has been theoretically investigated by Cundari and his collaborators in the last decade.[16] They also investigated interesting bonding nature of the transition-metal imido complexes, transition-metal alkylidene complexes, and their methane adducts.[17] Recently, the C-H σ-bond activation of benzene by the Ti-alkylidyne complex was also experimentally succeeded and theoretically investigated with the DFT method.[18]

However, many issues to be investigated still remain; for instance, comparison of the C-H σ-bond activation between early and late transition-metal complexes has not been made yet, to our knowledge, despite that such comparison is of considerable interest. Also, it is not clear what orbital interaction plays important role in the C-H σ-bond activation by the M=N bond.

N-H σ-bond activation of ammonia by transition-metal complexes is another challenging research target. Though one successful result has been reported recently,[19] the N-H σ-bond activation of ammonia is still difficult. Ammonia can form stable complexes with late transition-metal elements, while early transition-metal complexes of ammonia are less known than the late transition-metal complexes. Because the formation of too stable reactant complex of ammonia is one of the important reasons for difficulty of the N-H σ-bond activation of ammonia,[19] it is of considerable interest to investigate whether or not early transition-metal complexes can be utilized for the N-H σ-bond activation of ammonia.

In this theoretical work, we investigated the C-H σ-bond activation of methane and the N-H σ-bond activation of ammonia with Ti-imido complex by DFT, MP2 to MP4(SDQ), and CCSD(T) methods. Our purposes here are to show the differences in the C-H σ-bond activation between early and late transition metal complexes, to clarify what orbital interaction plays important role in the C-H σ-bond activation by this complex, and to present theoretical prediction whether or not the Ti-imido complex can be applied to the N-H σ-bond activation of ammonia. The N-H σ-bond activation by Ti-alkylidyne complex was also theoretically investigated, because the C-H σ-bond activation of benzene was achived by Ti-alkylidyne complex.[18]

1.2. Computational Details

Geometries were optimized with the DFT method, where the B3LYP functional was used for exchange-correlation term.[20-22] We ascertained that each equilibrium geometry

exhibited no imaginary frequency and each transition state exhibited one imaginary frequency. We carried out IRC calculation, to check that transition state connected reactant and product. Energy and population changes were evaluated with the DFT(B3LYP), MP2 to MP4(SDQ), and CCSD(T) methods, using the DFT-optimized geometries. In MP2 to MP4(SDQ) and CCSD(T) calculations, core orbitals were excluded from active space. Two kinds of basis set systems were used. The smaller system (BS1) was used for geometry optimization. In this BS1, core electrons of Ti (up to 2p) and Pt (up to 4f) were replaced with effective core potentials (ECPs),[23] and their valence electrons were represented with (541/541/311) and (541/541/111) basis sets,[23, 24] respectively. For Si and P, core electrons (up to 2p) were replaced with ECPs,[25] and their valence electrons were represented with (21/21/1) basis sets,[25] where a d-polarization function was added.[26] For H, C, N, and O, 6-31G* basis sets[27] were employed, where a p-polarization function was added for the active H atom that reacts with Ti complexs to form either C-H or N-H bond, and a diffuse function was added to the N atom. The better basis set system (BS2) was used for evaluation of energy changes. In this BS2, (5311/5311/311/1) and (5311/5311/111/1) basis sets[23, 24, 29] were employed for Ti and Pt, respectively, where the same ECPs as those of BS1 were employed for core electrons. For H, C, N, O, Si, and P, the 6-311G* basis sets were employed,[30, 31] while a p-polarization function was added to the active H atom and a diffuse function was added for the N atom. And the C atom which binds with the Ti atom of Ti-alkylidyne complex was supplemented with a diffuse function. Zero-point energy was evaluated with the DFT/BS1 method, under assumption of harmonic oscillator.

The Gaussian 03 program package[32] was used for all calculations. Population analysis was carried out with the method of Weinhold et al.[33] Molecular orbitals were drawn with the MOLEKEL program package.[34]

1.3. Results and Discussion

1.3.1. Geometry and Energy Changes by the C-H σ-Bond Activation of Methane by Ti-Imido Complex, $[(Me_3SiO)_2Ti(=NSiMe_3)]$ 1

The C-H σ-bond activation of methane by a Ti-imido complex, $[(Me_3SiO)_2Ti(=NSiMe_3)]$ **1** takes place through precursor complex (**PC1a**) and transition state (**TS1a**), to afford product complex (**PRD1a**), as shown in Figures 1.

In $[(Me_3SiO)_2Ti(=NSiMe_3)]$ **1**, the Ti-N-Si moiety is almost linear (175 degrees), which agrees well with the experimental value (175 degrees) of the similar complex.[35] This linear geometry of the $Ti=NSiMe_3$ group indicates that the $NSiMe_3$ moiety is considered to be anion, as reported.[17a, d] The Ti-N bond (1.697 Å) is moderately shorter and the N-Si bond (1.746 Å) is moderately longer than those of the similar complex,[36] though the differences are not large. We optimized the model complex with several functionals and variety of basis sets but found moderately longer Ti-N and moderately shorter N-Si distances in all the optimized geometries (see Appendix Figure A1 and Tables A1 and A2). In **PC1a**, methane approaches the Ti center, where the Ti-C^{α} and Ti-H distances are 2.621 Å and 2.209 Å, respectively, where C^{α} represents the C atom of methane, hereafter. The C^{α}-H bond slightly lengthens to 1.108 Å, which is similar to that of the agostic interaction system. Because no d-orbital is occupied in the Ti(IV) center in a formal sense, the charge-transfer (CT) from the C-H bonding orbital to the empty d-orbital of Ti is considered to be origin of the bonding interaction. This is essentially the same as the agostic interaction.[37-39] In **TS1a**, the Ti-C^{α} distance shortens to 2.269 Å which is similar to that of **PRD1a**. The C^{α}-H distance considerably lengthens to 1.442 Å, whereas the N-H distance (1.385 Å) is still long. The H atom that is moving from the C^{α} atom to the N atom is at middle position between C^{α} and N atoms. The similar geometry changes were reported in the theoretical study of the heterolytic C-H σ-bond activation of methane by $Pd(\eta^2\text{-}O_2CH)_2$ and $Pt(\eta^2\text{-}O_2CH)_2$.[7e] The product **PRD1a** takes pseudo-tetrahedral structure, as expected from the d^0 electron configuration.

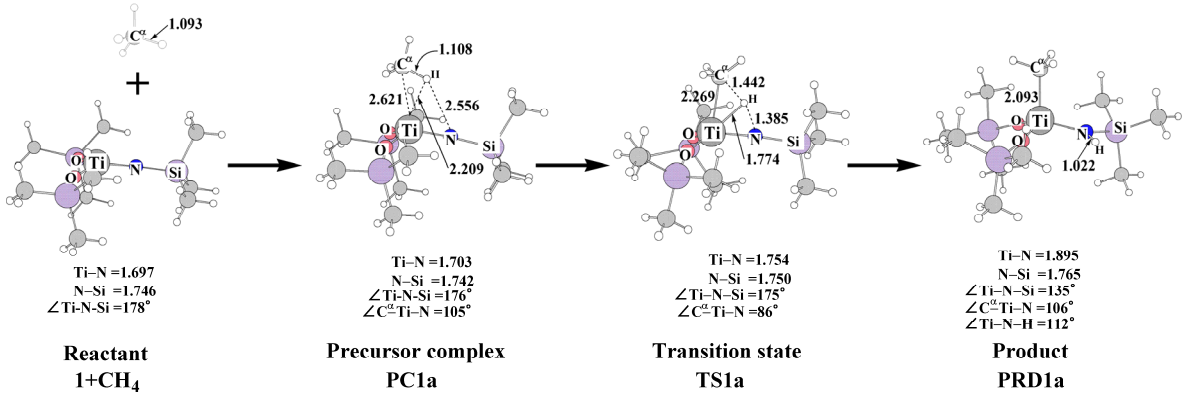

Figure 1. Geometry changes in the C-H σ-bond activation of methane by $(Me_3SiO)_2Ti(=NSiMe_3)$ **1**. Bond lengths are in angstrom and bond angles are in degree.

Binding energy (*BE*), activation barrier (E_a), and reaction energy (ΔE) are defined as the energy differences between **PC1a** and the sum of reactants, between **PC1a** and **TS1a**, and between **PRD1a** and the sum of reactants, respectively. Negative ΔE value means that the C-H σ-bond activation is exothermic and vice versa. First, we calculated *BE*, E_a, and ΔE values in the reaction of a model Ti-imido complex, $[(H_3SiO)_2Ti(=NSiH_3)]$ **1m**, in which the methyl groups are replaced by the H atoms, because **1** is too large to perform CCSD(T) calculations; geometry changes of this model reaction are given in Appendix Figure A2. In the reaction of **1m**, the *BE* value little fluctuates upon going to CCSD(T) from MP2, as shown in Table 1, while the DFT-calculated *BE* value is somewhat smaller than the others.[40] These results indicate that the *BE* values calculated by the DFT and MP4(SDQ) methods are reliable. The E_a and ΔE values somewhat fluctuate around MP2 and MP3 levels but much less upon going to CCSD(T) from MP3. The DFT- and MP4(SDQ)-calculated *BE*, E_a, and ΔE values are little different between **1** and **1m**, suggesting that the model system is useful to investigate this type of C-H σ-bond activation. It is noted that the DFT-calculated E_a and ΔE values are similar to those of the CCSD(T)-calculated values, while the MP4(SDQ)-calculated E_a value is considerably larger and the MP4(SDQ)-calculated exothermicity is considerably smaller than the CCSD(T)-calculated values.

Table 1. Binding energy (*BE*), activation barrier (E_a), and reaction energy (ΔE) of the C-H σ-bond activation of methane by $(Me_3SiO)_2Ti(=NSiMe_3)$ **1** and $(H_3SiO)_2Ti(=NSiH_3)$ **1m**

	$(Me_3SiO)_2Ti(=NSiMe_3) + CH_4$			$(H_3SiO)_2Ti(=NSiH_3) + CH_4$		
	BE^a	$E_a{}^b$	ΔE^c	BE^a	$E_a{}^b$	ΔE^c
MP2	-9.8	17.6	-16.5	-9.6	18.7	-14.9
MP3	-7.1	12.7	-36.5	-7.0	12.9	-35.4
MP4(DQ)	-7.8	18.0	-25.3	-7.8	18.7	-24.2
MP4(SDQ)	-9.4	21.5	-16.5	-9.4	22.8	-14.6
CCSD(T)	-	-	-	-9.0	17.0	-22.7
DFT(B3LYP)	-4.5	14.6	-22.7	-5.5	15.5	-22.6

In kcal/mol unit. [a] $BE = E_t$(precursor complex) – E_t(sum of reactants). [b] $E_a = E_t$(transition state) – E_t(precursor complex). [c] $\Delta E = E_t$(product) – E_t(sum of reactants).

Though the DFT method underestimates the *BE* value, we employed the DFT method to discuss the E_a and ΔE values of the reaction of **1**, because our main purpose is to investigate how much easily the C-H σ-bond activation takes place; note that **1** + CH_4 is too large to perform CCSD(T) calculation.

1.3.2. Important Orbital Interactions in the C-H σ-Bond Activation by Ti-Imido Complex.

It is of considerable importance to clarify the characteristic features of the C-H σ-bond activation of methane by the Ti-imido complex. We compared the C-H σ-bond activation reaction with the oxidative addition of methane to $Pt(PH_3)_2$ **2**, because the latter reaction is one of typical C-H σ-bond activations through the oxidative addition. We optimized the precursor complex, the transition state, and the product of this oxidative addition, using the DFT/BS1 method. The explanation of geometry and energy changes are omitted here

because this reaction was theoretically investigated previously[4,7a,d] and no essential difference from the previous works was observed; see Appendix Figure A3 for the geometry changes.

Electron population changes are compared between the C-H σ-bond activation reactions by **1** and **2**, as shown in Figure 2. In the oxidative addition of methane to **2**, the electron populations of H and CH_3 groups increase but the Pt atomic population considerably decreases, as the reaction proceeds (Figure 2(B)). These population changes are consistent with our understanding that this is the oxidative addition. Population changes in the C-H σ-bond activation by **1** are significantly different from those in the reaction by **2**, as follows: (1) The electron population of CH_3 increases very much, as shown in Figures 2(A). (2) The H atomic population considerably decreases upon going from **PC1a** to **PRD1a** in the reaction of **1**. (3) The Ti atomic population considerably increases upon going to **TS1a** from **PC1a** but then considerably decreases upon going to **PRD1a** in the reaction of **1**. And, (4) the electron population of $NSiMe_3$ moiety moderately decreases upon going to **TS1a** from reactant but considerably increases upon going to **PRD1a** from **TS1a**. Most important differences in population changes between the Ti complex and the Pt(0) complex are found in the electron populations of Ti, H, and CH_3 groups. The increase in the Ti atomic population at **PC1a** is attributed to the CT from methane to the Ti center; remember that the C^{α}-H bond of methane interacts with the Ti center in **1** like agostic interaction, which involves the CT from the C-H bonding orbital to the Ti center.[37-39] In **TS1a**, the CH_3 electron population considerably increases but the H atomic population considerably decreases, while both electron populations of H and CH_3 groups increase in **TS2**. These differences indicate that the C-H σ-bond activation by the Ti complex can be understood in terms of heterolytic C-H σ-bond activation unlike the oxidative addition by **2**. Also, it is noted that the Ti atomic population increases in **TS1a** but the Pt atomic population decreases in **TS2**. These results suggest that the CT from methane to the Ti center participates in **TS1a** but the CT from the Pt center to methane participates in **TS2**, which will be discussed below in more detail.

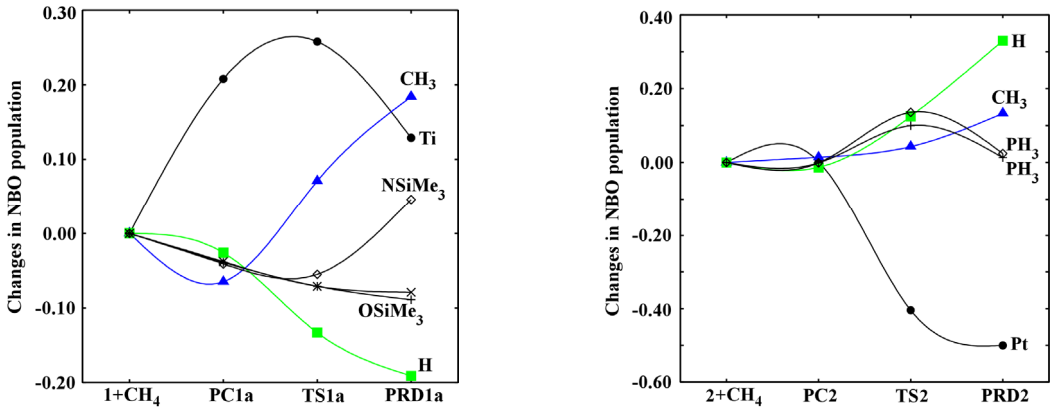

(A) $(Me_3SiO)_2Ti(=NSiMe_3)$ **1** (B) $Pt(PH_3)_2$ **2**

Figure 2. Population changes in C-H σ-bond activations of methane by (A) $(Me_3SiO)_2Ti(=NSiMe_3)$ **1** and (B) $Pt(PH_3)_2$ **2**. The positive value represents the increase in electron population, and vice versa. The B3LYP/BS2 method was employed.

Though important orbital interaction was well understood in the oxidative addition reaction,[2,7f,41] the orbital interaction has not been discussed yet in the heterolytic C-H σ-bond activation. Thus, it is worth investigating what type of orbital interaction is important in the heterolytic C-H σ-bond activation. As shown in Figure 3, the 83-th MO in **PC1a** becomes stable in energy upon going from **PC1a** to **PRD1a**. This MO mainly consists of the sp^3 orbital of the CH_3 group and the d_π-p_π orbital of the Ti-N moiety, as shown in Figure 4(A). To inspect the orbital picture, we analyzed this MO by representing with linear combination of molecular orbitals of fragments;

$$\psi_i(\mathrm{AB}) = \sum_m C_{im}^A \varphi_m(\mathrm{A}) + \sum_n C_{in}^B \varphi_n(\mathrm{B}) \qquad (1)$$

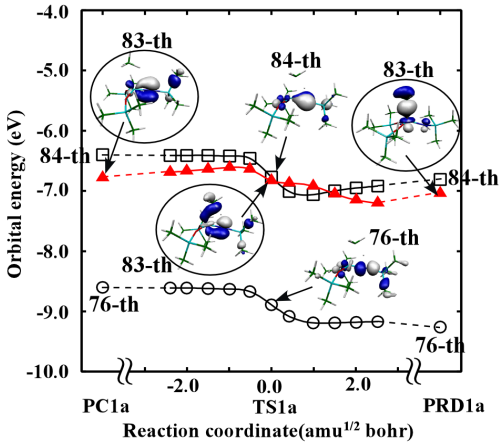

Figure 3. Orbital energy changes in C-H σ-bond activations of methane by $(Me_3SiO)_2Ti(=NSiMe_3)$ **1**.

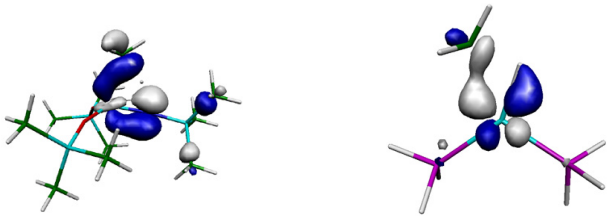

83-th MO of **TS1a** 32-th MO of **TS2**

(A) Important MOs of **TS1a** and **TS2**

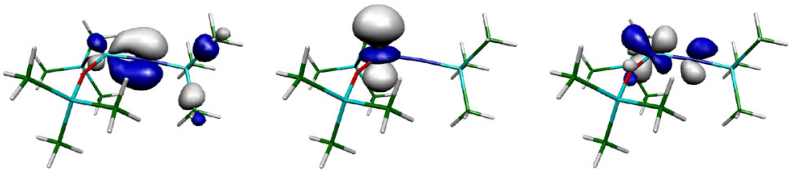

78-th MO 80-th MO 82-th MO

(B) Important MOs of $(Me_3SiO)_2Ti(=NSiMe_3)$ **1**

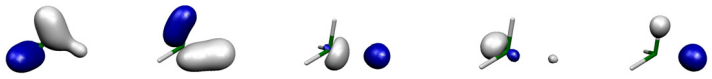

3-th MO 5-th MO 6-th MO 7-th MO 10-th MO

(C) Important MOs of CH_4

Figure 4. Important MOs in **TS1a** and **TS2**, and fragment MOs of $(Me_3SiO)_2Ti(=NSiMe_3)$ **1** and methane. The B3LYP/BS2 method was employed.

Table 2. The weight of fragment MOs calculated with the B3LYP/BS2 method

	$(Me_3SiO)_2Ti(=NSiMe_3)$		$Pt(PH_3)_2$ [a]	
	82-th MO	3.1%	28-th MO	0.0%
unocc	80-th MO	7.3%		
occ	78th-MO	56.8%	27-th MO	78.4%
			23-th MO	1.0%
			22-th MO	0.0%
	CH_4		CH_4	
	10-th MO	1.2%	10-th MO	0.8%
	7-th MO	2.0%	7-th MO	2.5%
unocc	6-th MO	10.4%	6-th MO	11.4%
occ	5-th MO	10.3%	5-th MO	0.6%
	3-th MO	5.3%	3-th MO	4.2%

[a] The analysis was made at the same C-H distance of methane as that of **TS1a**

where ψ_i(AB) represents the i-th MO of the system AB, φ_m(A) is the m-th MO of the fragment A, and C^A_{im} is expansion coefficient of φ_m(A). Here, we separate the reaction system into methane and the Ti-imido complex. The weights of fragment orbitals are summarized in Table 2;[42] see Figure 4 for the important MOs of the reaction system and fragments. In the reaction by **1**, the 83-th MO of the reaction system largely consists of the d_π-p_π bonding orbital of the Ti-imido moiety and somewhat consists of HOMO and LUMO of methane. Also, the d_{z2} orbital of Ti, which is unoccupied orbital in a formal sense, moderately participates in the 83-th MO. These orbital mixings are schematically shown in Scheme 1; the d_π-p_π bonding orbital suffers from anti-bonding overlap with the C-H σ-bonding orbital (HOMO) of methane, because the HOMO of methane is at lower energy than the d_π-p_π bonding orbital. The C-H σ*-anti-bonding orbital (LUMO) of methane mixes with the d_π-p_π bonding orbital in a bonding way, because the LUMO is at higher energy than the $d_\pi-p_\pi$ bonding orbital. These orbital mixings decrease the contribution of the H 1s orbital to the MO of the reaction system and increase that of the CH_3 sp^3 orbital. As a result, the CH_3

Scheme 1

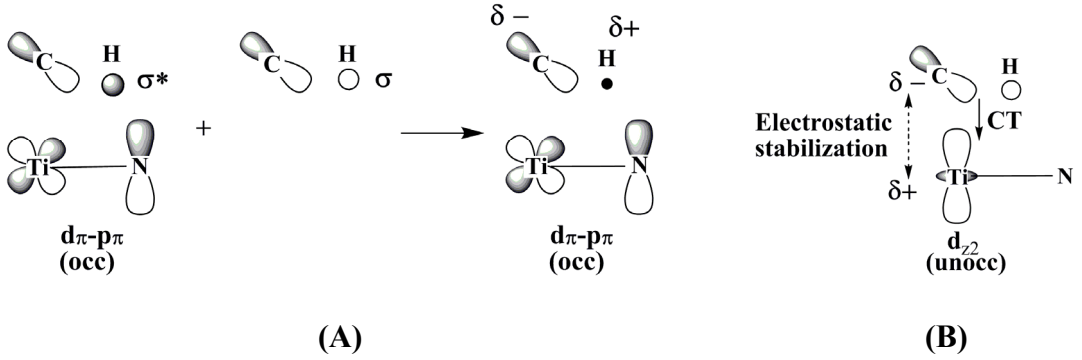

electron population increases and the H atomic population decreases; in other words, the H atom becomes proton-like and the CH_3 group becomes anionic. The empty d_{z2} orbital overlaps with the CH_3 sp^3 orbital in a bonding way to form the CT interaction with the negatively charged CH_3 group, which increases the Ti atomic population. Thus, the orbital mixings shown in Scheme 1 clearly explain population changes by the heterolytic C-H σ-bond activation, and Ti-CH_3 and C-H bond formations. In the reaction by **2**, the 32-th MO of the reaction system is important. This mainly consists of the Pt d_π orbital and the LUMO of methane which is C-H σ*-anti-bonding orbital, as shown in Table 2; see Figure 4 and Figure A4 for these orbital pictures. It is noted that the HOMO of methane, which is C-H σ-bonding orbital, little participates in this 32-th MO. This means that only CT from $Pt(PH_3)_2$ to methane is important in the reaction by **2**, which is consistent with the population changes of this reaction (see Figure 2(B)); remember that the Pt atomic population decreases and both H and CH_3 electron populations increase in the reaction.

Because the occupied d_π-p_π bonding orbital and the unoccupied d_{z2} orbital play important roles in these orbital mixings around transition state, the higher the occupied d_π-p_π bonding orbital energy is and the lower unoccupied d_{z2} orbital energy is, the easier heterolytic C-H σ-bond activation becomes.

Upon going to **PRD1a** from **TS1a**, the Ti atomic population considerably decreases but

the electron populations of $NSiMe_3$ considerably increase in the reaction by **1**. Those population charges are different from those observed upon going to **TS1a** from **PC1a**, indicating that the origin of those population changes are different from the above discussed orbital interaction. One of the plausible reasons of these population changes is that the proton-like H atom binds with $NSiMe_3$ to suppress the electron donation from these ligands to the Ti center. As a result, the Ti atomic population considerably decreases and the electron population of the $NSiMe_3$ moiety considerably increases.

1.3.3. Effects of the OR Ligand on the C-H σ-Bond Activation:

Here, we wish to mention ligand effects of the C-H σ-bond activation, because the O atom effect on the O-H σ-bond activation was discussed recently. To clarify how much the OR ligand of **1** facilitates the C-H σ-bond activation, we compared the reactivity of $(HO)_2Ti(=NSiH_3)$ $\mathbf{1_{OH}}$ with that of $(HS)_2Ti(=NSiH_3)$ $\mathbf{1_{SH}}$, where $\mathbf{1_{OH}}$ is a good model of **1** because the C-H σ-bond activation reaction by $\mathbf{1_{OH}}$ occurs with similar *BE*, E_a, and Δ*E* values to those of the reaction by **1**; see Appendix Tables A3 and A4 and Figure A5 for energy, population, and geometry changes by the reactions of $\mathbf{1_{OH}}$ and $\mathbf{1_{SH}}$. Interestingly, the C-H σ-bond activation by $\mathbf{1_{SH}}$ takes place with a considerably larger E_a value (19.6 kcal/mol) and considerably smaller exothermicity (Δ*E* = -12.4 kcal/mol) than those of the reaction by $\mathbf{1_{OH}}$ (E_a) 15.5 kcal/mol and Δ*E* = -21.9 kcal/mol), where the DFT/BS2//DFT/BS1 method was employed. The d_π-p_π and d_{z2} orbitals of $\mathbf{1_{SH}}$ are at lower energy (-8.13 and -3.33 eV, respectively) than those of **1OH** (-7.35 and -2.94 eV, respectively), where Kohn-Sham orbital energies are given. It is noted also that the Ti center is much more positively charged and the N atom is more negatively charged in $\mathbf{1_{OH}}$ than in $\mathbf{1_{SH}}$; the Ti and N atomic charges are +1.779 e and -1.227 e, respectively, in $\mathbf{1_{OH}}$ and +1.194 e and -1.062 e, respectively, in $\mathbf{1_{SH}}$, where the DFT/BS2-calculated charges are given. These results suggest that $\mathbf{1_{OH}}$ forms the stronger CT from the d_π-p_π orbital to the C-H σ*-antibonding orbital and the stronger electrostatic

stabilizations between the negatively charged CH_3 group and the positively charged Ti atom and between the positively charged H and negatively charged N atoms than does $\mathbf{1_{SH}}$. Because of these factors, $\mathbf{1_{OH}}$ is more reactive than $\mathbf{1_{SH}}$; in other words, the OR group facilitates the heterolytic C-H σ-bond activation than the similar SR group.

1.3.4. Why does the H atom bind not with the Ti center but with the N atom?

In the C-H σ-bond activation reaction by **1**, the methyl group is bound with the Ti center and the H atom is bound with the N atom.[36] It is of considerable interest to clarify the reason why the methyl group is bound not with the N atom but with the Ti center, and why the H atom is bound not with the Ti center but with the N atom.

We investigated the C-H σ-bond activation of methane leading to the formation of $(Me_3SiO)Ti(H)\{N(CH_3)\}(SiMe_3)$ **PRD1a**, which involves the Ti-H and N-CH_3 bonds. This is called the reverse regioselective reaction. In the precursor complex **PC1b**, methane approaches the Ti center in the different orientation from that in **PC1a**, as shown in Figures 5. In the transition states **TS1b**, the C^{α}-H distance of methane lengthens by 0.639 Å. This distance is longer than that of **TS1a**. The Ti-H distance in **TS1b** is almost the same as that of the product, **PRD1b**. These features indicate that **TS1b** is characterized to be more product-like than **TS1a.** **PRD1b** takes pseudo-tetrahedral geometry similar to that of **PRD1a**.

As shown in Table 3, the *BE* value of **PC1b** is almost the same as that of **PC1a**. However, the E_a value for **TS1b** is much larger than that for **TS1a**. Consistent with the larger E_a value, the ΔE value of the reverse regioselective reaction is less negative than that of the normal one. These results indicate that the reverse regioselective reaction is thermodynamically and kinetically less favorable than the normal one. To understand the

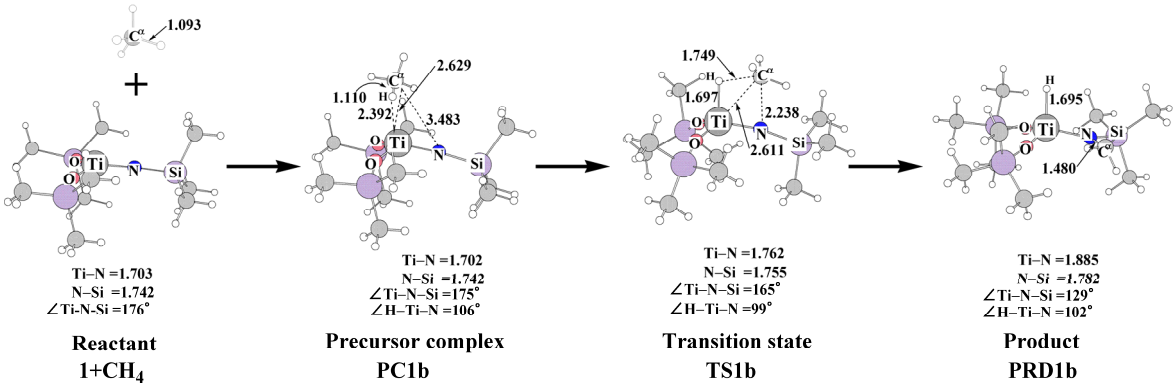

Figure 5. Geometry changes in the C-H σ-bond activation of methane by $(Me_3SiO)_2Ti(=NSiMe_3)$ **1** leading to formations of Ti-H and N-CH_3 bonds. Bond lengths are in angstrom and bond angles are in degree.

Table 3. Binding energy (*BE*), activation barrier (E_a), and reaction energy (ΔE) of the C-H σ-bond activation of methane by $(Me_3SiO)_2Ti(=NSiMe_3)$ **1** leading to formations of $(Me_3SiO)_2Ti(H)\{N(CH_3)(SiMe_3)\}$.

	$(Me_3SiO)_2Ti(=NSiMe_3) + CH_4$		
	BE^a	$E_a{}^b$	ΔE^c
MP2	-9.8	70.7	3.1
MP3	-7.2	61.8	-15.5
MP4(DQ)	-7.9	69.3	-5.9
MP4(SDQ)	-9.5	75.5	1.4
DFT(B3LYP)	-4.2	60.4	-1.2

In kcal/mol unit. [a] $BE = E_t$ (precursor complex) – E_t (sum of reactants). [b] $E_a = E_t$ (transition state) – E_t (precursor complex). [c] $\Delta E = E_t$ (product) – E_t (sum of reactants).

reasons why the normal regioselective reaction more favorably occurs than the reverse one, we evaluated here the Ti-H, Ti-CH_3, N-CH_3, and N-H bond energies, considering following assumed reactions; the Ti-H and Ti-CH_3 bond energies of the Ti-imido complex were calculated with eqs 2 to 5. The other bond energies were defined as energy changes by eqs 6 and 7.

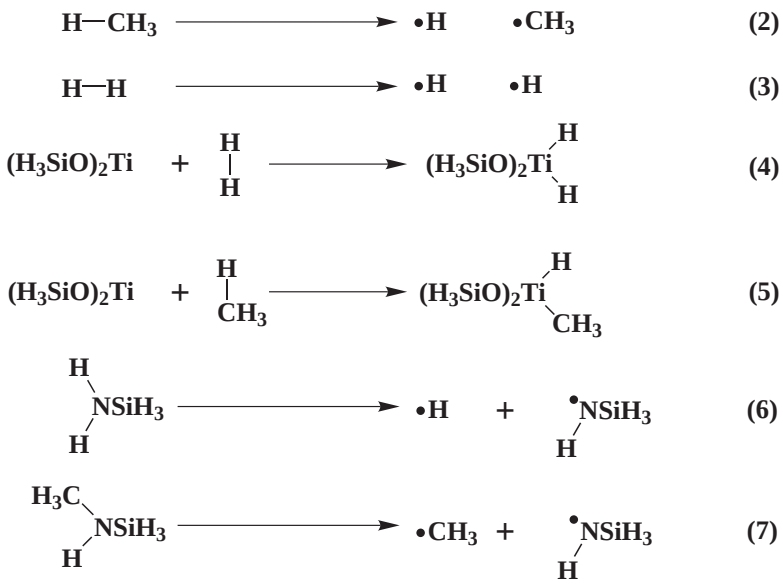

These bond energies are summarized in Table 4. The N-H bond energy little depends on the computational methods. The N-CH_3 bond energy moderately fluctuates upon going to MP3 level from MP2 level but converges upon going to CCSD(T) level from MP3 level. Moreover, the MP4(SDQ)-, CCSD(T)-, and DFT-calculated N-CH_3 bond energies are similar to each other, suggesting that these methods present reliable N-CH_3 bond energy. Though the Ti-H and Ti-CH_3 bond energies moderately fluctuate around MP2 level, they converge upon going to MP4(SDQ) and CCSD(T) levels from MP3 level. Also, the CCSD(T)-calculated Ti-H and Ti-CH_3 bond energies are similar to the MP4(SDQ)-calculated values, indicating that these values are reliable. Though the DFT-calculated Ti-H, Ti-CH_3, and Ti-NH_2 bond energies are moderately smaller than the CCSD(T)- and MP4(SDQ)-calculated values, the relative values of these bond energies are similarly

Scheme 2

(A) Normal regioselective reaction (B) Reverse regioselective reaction

Table 4. Ti-H, Ti-CH_3, Ti-NH_3, N-H, and N-CH_3 bond energies[a]

	B3LYP	MP2	MP3	MP4(DQ)	MP4(SDQ)	CCSD(T)
Ti-H	73.4	79.9	74.8	76.0	81.1	80.4
Ti-CH_3	77.2	92.4	81.8	81.0	86.3	87.6
Ti-NH_2	100.6	119.1	102.0	102.7	110.4	111.0
N-H	114.8	116.0	112.9	113.0	113.0	113.2
N-CH_3	89.0	98.2	90.5	89.9	90.3	91.6

[a] The BS2 was used. In kcal/mol unit.

calculated by the DFT, MP4(SDQ), and CCSD(T) methods. Thus, the conclusion does not depend on the computational method.

Apparently, the N-H bond is considerably stronger than the N-CH_3 bond, while the Ti-CH_3 bond is moderately stronger than the Ti-H bond. As a result, the normal regioselective reaction is more favorable than the reverse regioselective one from the thermodynamic point of view.

The higher E_a value of the reverse regioselective reaction is easily interpreted in terms of the smaller overlap of the C-H σ*-anti-bonding orbital with the d_π-p_π orbital of the Ti-imido moiety than in the normal regioselective reaction. Methane approaches the Ti-N

moiety with the H atom in the lead, as shown in Figure 1, because the H atom is less bulky than the CH_3 group. This approach leads to formation of larger overlap between the H 1s orbital and the Ti-N d_π-p_π orbital in the normal regioselective reaction than in the reverse one, as shown in Scheme 2A, because the p orbital of imido group more contributes to the d_π-p_π orbital than the d_π orbital of Ti (Figure 4). In the reverse regioselective reaction, on the other hand, the H 1s orbital must interact with the d_π orbital of Ti. The methyl sp^3 orbital interacts with the imido p orbital, but it is much more distant from the imido group in the reverse regioselective reaction than the H atom is in the normal one (see Figures 5). As a result, the overlap is much small in the reverse regioselective reaction, as shown in Scheme 2B. Because of the smaller overlap, the reverse regioselective reaction needs the larger E_a value, and therefore, the reverse regioselective reaction is less favorable kinetically than the normal one.

1.3.5. The N-H σ-Bond Activation of Ammonia.

It is of considerable interest to investigate whether or not the N-H σ-bond activation of ammonia can be achieved by Ti-imido complex, because this σ-bond activation is believed to be very difficult and only one successful result was recently reported with (PCP)(η^2-propene)Ir.[19] We investigated here the N-H σ-bond activation of ammonia by **1**. The Ti-N^α distance is 2.199 Å in **PC1c**, as shown in Figures 6, where N^α represents the N atom of ammonia and N represents that of the imido ligand, hereafter. The short Ti-N^α distance indicates that the typical coordinate bond is formed between Ti and NH_3, in contrast with the weak interaction between the Ti moiety and methane. Starting from **PC1c** the N-H σ-bond activation takes place through transition state **TS1c,** to afford a product **PRD1c**. In **TS1c**, the N^α-H distance lengthens to 1.349 Å, which is considerably longer than that of free ammonia. The N-H distance between ammonia and imido groups in **TS1c** is still long (1.338 Å). The Ti-N^α distance of **TS1c** is moderately longer than that of **PRD1c** but

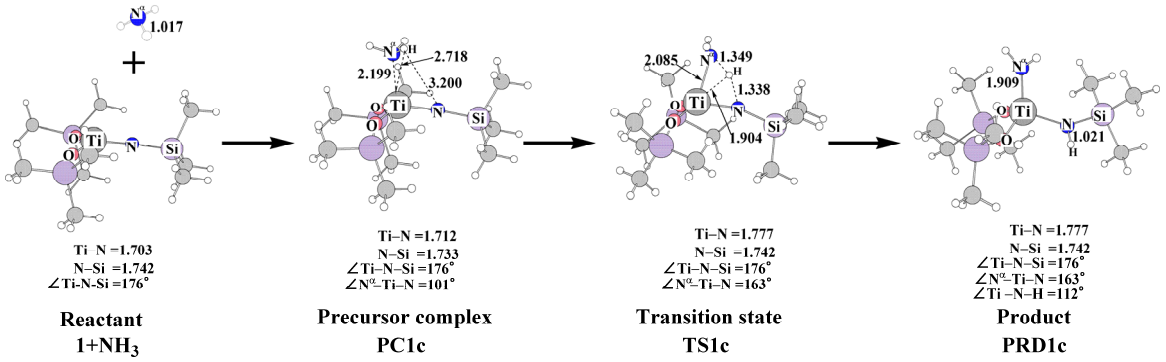

Figure 6. Geometry changes in the N-H σ-bond activation of ammonia by $(Me_3SiO)_2Ti(=NSiMe_3)$ **1**. Bond lengths are in angstrom and bond angles are in degree.

Table 5. Binding energy (*BE*), activation barrier (E_a), and reaction energy (ΔE) of the N-H σ-bond activation of ammonia by $(Me_3SiO)_2Ti(=NSiMe_3)$ **1** and $(PNP)Ti(\equiv CSiMe_3)$ **2**.

	$(Me_3SiO)_2Ti(=NSiMe_3) + NH_3$			$(PNP)Ti(\equiv CSiMe_3) + NH_3$		
	BE^a	$E_a{}^b$	ΔE^c	BE^a	$E_a{}^b$	ΔE^c
MP2	-36.0	25.0	-39.1	-30.4	13.2	-52.3
MP3	-37.1	18.9	-56.6	-29.6	5.7	-74.0
MP4(DQ)	-35.8	24.7	-46.4	-29.6	13.6	-57.6
MP4(SDQ)	-35.7	27.9	-39.4	-30.8	15.3	-56.1
DFT(B3LYP)	-31.4	19.0	-45.0	-24.8	7.5	-60.2

In kcal/mol unit. ^{a} $BE = E_t$ (precursor complex) – E_t (sum of reactants).
^{b} $E_a = E_t$ (transition state) – E_t (precursor complex). ^{c} $\Delta E = E_t$ (product) – E_t (sum of reactants).

moderately shorter than that of **PC1c**. In **PRD1c**, the NH_2 moiety is planar, indicating that the NH_2 moiety is considered to be imido anion.

As shown in Table 5, the *BE* value is considerably larger than those of the C-H σ-bond activation of methane, against our expectation. This is because ammonia coordinates with the Ti center by the CT from the lone pair of ammonia to the empty d-orbital of Ti. Actually,

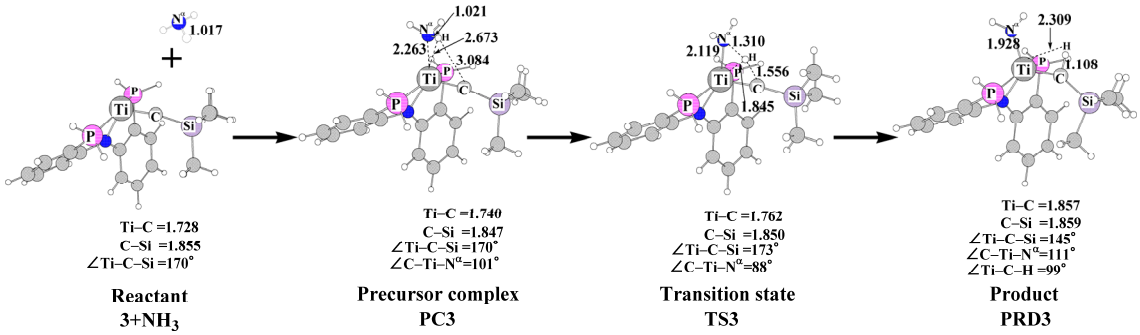

Figure 7. Geometry changes in the N-H σ-bond activation of ammonia by (PNP)Ti(≡CSiMe$_3$) **3**. Bond lengths are in angstrom and bond angles are in degree.

the electron population of ammonia decreases very much in **PC1c**, as shown in Figure 8. The E_a value somewhat fluctuates around MP2 and MP3 levels but much less upon going to MP4(SDQ) level from MP3 level. The DFT method presents considerably smaller E_a value. However, it is noted that all the computational methods present moderately larger E_a value and much larger exothermicity than those of the C-H σ-bond activation. This result suggests that the N-H σ-bond activation can be achieved by the Ti-imido complex, in which the activation barrier is moderately larger than the C-H σ-bond activation.

To search another complex which can perform easily the N-H σ-bond activation, we investigated the N-H σ-bond activation by Ti-alkylidyne complex (PNP)Ti(≡CSiMe$_3$) **3**, because the C-H σ-bond activation of benzene by **3** was recently reported in the experimental field.[18] This N-H σ-bond activation takes place through precursor complex **PC3** and transition state **TS3**, to afford product complex **PRD3**, as shown in Figure 7. Because the geometry changes are similar to those of the N-H σ-bond activation by **1**, we wish to omit detailed explanation but mention several important points. In **TS3**, the N$^{\alpha}$-H distance (1.310 Å) is shorter and the C-H distance (1.556 Å) is longer than the corresponding N$^{\alpha}$-H and N-H distances of **TS1c**, indicating that **TS3** is more reactant-like than **TS1c**. In **PRD3**, the Ti-H distance is 2.309 Å and the Ti-C-H angle is 99 degrees. These geometrical features indicate

that the α-agostic interaction is formed in **PRD3**, which is in contrast to the absence of the agostic interaction in **PRD1c**. This interesting difference is easily interpreted in term of the energy levels of N-H and C-H σ-bonding orbitals. The C-H σ-bonding orbital is at -10.7 eV but the N-H σ-bonding orbital is at -17.1 eV, where Kohn-Sham orbital energies are given. Because the agostic interaction is formed by the CT from the C-H σ-bonding orbital to the empty d-orbital, the C-H σ-bond is more favorable for the agostic interaction than the N-H σ-bond.

Consistent with the more reactant-like TS, the E_a value of this reaction is much smaller than that of the N-H σ-bond activation by **1**. It is noted that the E_a value is much smaller than that of the C-H σ-bond activation by **1**, which actually occurs experimentally. Thus, we wish to propose that the N-H σ-bond activation of ammonia can be easily achieved by the Ti-imido and Ti-alkylidyne complex and that the latter complex is much more reactive than the former one.

In this N-H σ-bond activation, the N^{α}-H bond should be broken, and the Ti-$N^{\alpha}H_2$ bond and either N-H or C-H bond are formed. The considerably large exothermicity of the N-H σ-bond activation arises from the formation of the very strong Ti-$N^{\alpha}H_2$ bond as shown in Table 4. Because of this very strong Ti-$N^{\alpha}H_2$ bond, the product is more stable than the reactant complex.

Population changes show somewhat different features from those of the C-H σ-bond activation, as shown in Figure 8. As mentioned above, the electron population of ammonia considerably deceases in the precursor complexes **PC1c** and **PC3**, indicating that the strong CT interaction is formed between the Ti center and ammonia. In the transition state, the electron population of the NH_2 moiety considerably increases. The H atomic population further decreases in the reaction by **1** but slightly increases in the reaction by **3**, while its atomic charge is still positive; the H atomic population is 0.449 e and 0.389 e in the reactions by **1** and **3**, respectively. These features indicate that the NH_2 moiety is becoming anion-like

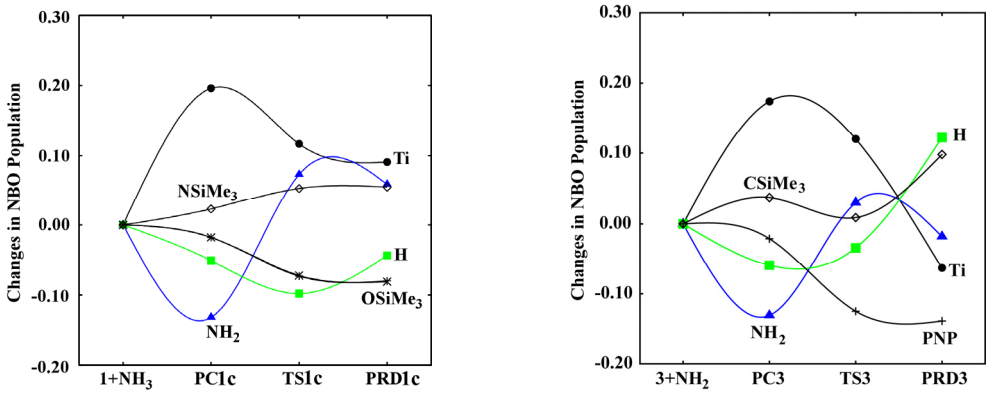

(A) $(Me_3SiO)_2Ti(=NSiMe_3)$ **1** (B) $(PNP)Ti(\equiv CSiMe_3)$ **3**

Figure 8. Population changes in N-H σ-bond activation of ammonia by (A) $(Me_3SiO)_2Ti(=NSiMe_3)$ **1** and (B) $(PNP)Ti(\equiv CSiMe_3)$ **3**. The positive values represent the increase in electron population, and vice versa. The B3LYP/BS2 method was employed.

and the H atom is becoming proton-like in the transition state; in other words, the N-H σ-bond activation occurs in heterolytic manner like the C-H σ-bond activation. Upon going to **PRD1c** and **PRD3** from **TS1c** and **TS3**, respectively, the Ti atomic population decreases. The reason is the same as that discussed in the C-H σ-bond activation of methane by **1**. The H atomic population is recovered in the reaction by **1**, because the H atom is again bound with the N atom. On the other hand, it considerably increases in the reaction by **3**, because it is bound with the C atom which is less electronegative than the N atom.

1.4. Conclusions

The C-H σ-bond activation of methane and the N-H σ-bond activation of ammonia by $(Me_3SiO)_2Ti(=NSiMe_3)$ **1** was theoretically investigated with the DFT, MP2 to MP4(SDQ), and CCSD(T) methods. The C-H σ-bond activation of methane proceeds through the precursor complex and the transition state, to afford the product $(Me_3SiO)_2Ti(Me)(NHSiMe_3)$. The activation barrier (E_a) is 14.6 (21.5) kcal/mol and the reaction energy (ΔE) is -22.7

(-16.5) kcal/mol, where the DFT- and MP4(SDQ)-calculated values are given without and in parentheses, respectively.

The analysis of the electron redistribution of this reaction shows interesting features, as follows: (1) The electron population of the CH_3 group considerably increases in the reaction, while the population of the H atom that reacts with the Ti-imido moiety considerably decreases in the transition state. These population changes indicate that the C-H σ-bond activation can be understood in terms of heterolytic C-H σ-bond activation unlike the oxidative addition. (2) The Ti atomic population considerably increases upon going to the transition state from the precursor complex, which indicates the CT from methane to the Ti center becomes stronger in the transition state. These characteristic features arise from orbital interactions among the d_π-p_π bonding and d_{z2} non-bonding orbitals of the Ti-imido moiety and the C-H σ-bonding and σ*-anti-bonding orbitals of methane. The CT interaction is formed between the d_π-p_π bonding orbital and the C-H σ*-anti-bonding orbital, into which the C-H σ-bonding orbital mixes in an anti-bonding way with the d_π-p_π bonding orbital. This orbital mixing decreases the H atomic population and increases the CH_3 electron population; in other words, the C-H bond to be broken is polarized by this orbital mixing. The negatively charged CH_3 group interacts with the empty d_{z2} orbital of the Ti center, to yield stabilization energy by the CT interaction. These population changes and orbital interactions are completely different from those of the oxidative addition of methane to $Pt(PH_3)_2$.

The reverse regioselective C-H σ-bond activation leading to $(Me_3SiO)_2Ti(H)\{N(Me)SiMe_3\}$ takes place with larger E_a value and smaller exothermicity than the normal one. These results are interpreted in terms of bond energy and orbital overlap in the transition state. The Ti-CH_3 and N-H bonds are stronger than the Ti-H and N-CH_3 bonds, respectively, indicating that the normal regioselective C-H σ-bond activation is thermodynamically more favorable than the reverse one. Also, the H 1s orbital better

overlaps with the d_π-p_π bonding orbital of the Ti-imido moiety in the normal regioselective reaction than in the reverse one, indicating that the E_a value of the normal regioselective reaction is smaller than that of the reverse one.

The N-H σ-bond activations of ammonia by **1** and (PNP)Ti(≡CSiMe$_3$) **3** (PNP = N-[2-(PH$_3$)$_2$-phenyl]) take place with moderate activation barrier and considerably large exothermicity. Several important results are summarized, as follows: (1) The *BE* value is considerably large, -31.4 (-35.7) and -24.8 (-30.8) kcal/mol for **1** and **3**, respectively. (2) Consistent with the large *BE* value, the electron population of the ammonia considerably decreases in precursors, **PC1c** and **PC3**, which indicates that the strong CT interaction is formed between the Ti center and NH$_3$. (3) The E_a and ΔE values are 19.0 (27.9) and -45.0 (-39.4) kcal/mol, respectively, in the reaction by **1** and 7.5 (15.3) and -60.2 (-56.1) kcal/mol, respectively, in the reaction by **3**. And, (4) the N-H σ-bond activation of ammonia occurs in a heterolytic manner like the C-H σ-bond activation of methane. From these computational results, we wish to propose that the N-H σ-bond activation can be achieved by Ti-imido and Ti-alkylidyne complexes.

In summary, we presented here clear picture of orbital interaction in the heterolytic C-H σ-bond activation and theoretical proposals that Ti-imido and Ti-alkylidyne complexes can be applied to many heterolytic σ-bond activation including N-H σ-bond activation.

1.5. Appendix

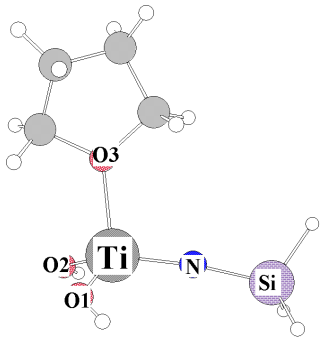

Figure A1. Model complex $(HO)_2(THF)Ti(=NSiH_3)$ **1THF** (THF = tetrahydrofuran)

Table A1. Comparing experimental structure ($^{t}Bu_3O)_2Ti(=NSi^{t}Bu_3)$ (THF) with optimized structure of **1THF** with several basis sets

Basis set	BS1	BS2	BS3	BS4	BS5	BS6	Exp[c]
Ti	ECP[a]+(541/541/311)	ECP[b]+(7511/6621/411)	ECP[a]+(541/541/311)	ECP[a]+(541/541/311)	cc-pVTZ	m6-31G*	
Si	6-31G(d)	6-31G(d)	D95(d)	cc-pVDZ	cc-pVTZ	6-31G(d)	
C	6-31G(d)	6-31G(d)	D95(d)	cc-pVDZ	cc-pVTZ	6-31G(d)	
N	6-31+G(d)	6-31G(d)	D95(d)	aug-cc-pVDZ	aug-cc-pVTZ	6-31G(d)	
O	6-31G(d)	6-31G(d)	D95(d)	cc-pVDZ	cc-pVTZ	6-31G(d)	
H	6-31G(d)	6-31G(d)	D95(d)	cc-pVDZ	cc-pVTZ	6-31G(d)	
Structure							
Ti-N[Å]	1.712	1.712	1.712	1.712	1.715	1.714	1.772(3)
N-Si	1.717	1.718	1.728	1.739	1.713	1.713	1.685(3)
Ti-O1	1.844	1.853	1.845	1.842	1.851	1.841	1.821(2)
Ti-O2	1.843	1.851	1.843	1.842	1.850	1.839	1.827(3)
Ti-O3	2.081	2.096	2.078	2.081	2.087	2.086	2.037(2)
Ti -N -Si[°]	174.6	172.4	173.1	172.6	173.6	171.4	174.9(2)
N-Ti-O1	114.4	113.9	114.5	114.7	114.9	114.6	114.38(12)
N-Ti -O2	114.7	114.4	114.5	114.8	115.0	114.6	118.52(13)
O1-Ti-O2	113.4	114.4	113.3	113.2	113.5	112.5	115.14(11)
O3-Ti-N	104.0	103.9	104.4	104.0	103.7	104.0	101.40(11)
O3 -Ti-O1	104.6	104.2	104.2	104.3	103.8	104.3	103.17(10)
O3-Ti -O2	104.1	104.4	104.4	104.1	104.1	105.3	100.51(10)

[a] by Hay-Wadt [b] by Christiansen [c] Bennett, J. L.; Wolczanski, P. T. *J. Am. Chem. Soc.* **1997**, *119*, 10696.

Table A2. Comparing experimental structure ($^{t}Bu_3O)_2Ti(=NSi^{t}Bu_3)(THF)$ with optimized structure of **1THF** with several functional

Functional	B3LYP	B3PW91	B3P86	Exp[b]
Basis set	BS1	BS1	BS1	
Ti	ECP[a]+(541/541/311)	ECP[a]+(541/541/311)	ECP[a]+(541/541/311)	
Si	6-31G(d)	6-31G(d)	6-31G(d)	
C	6-31G(d)	6-31G(d)	6-31G(d)	
N	6-31+G(d)	6-31+G(d)	6-31+G(d)	
O	6-31G(d)	6-31G(d)	6-31G(d)	
H	6-31G(d)	6-31G(d)	6-31G(d)	
Structure				
Ti-N[Å]	1.712	1.705	1.704	1.772(3)
N-Si	1.717	1.714	1.711	1.685(3)
Ti-O1	1.844	1.838	1.835	1.821(2)
Ti-O2	1.843	1.837	1.834	1.827(3)
Ti-O3	2.081	2.075	2.063	2.037(2)
Ti-N-Si[°]	174.6	174.5	174.9	174.9(2)
N-Ti-O1	114.4	114.0	114.1	114.38(12)
N-Ti-O2	114.7	114.3	114.4	118.52(13)
O1-Ti-O2	113.4	114.0	114.0	115.14(11)
O3-Ti-N	104.0	103.6	103.1	101.40(11)
O3-Ti-O1	104.6	105.0	105.0	103.17(10)
O3-Ti-O2	104.1	104.5	104.4	100.51(10)

[a] by Hay-Wadt [b] Bennett, J. L.; Wolczanski, P. T. *J. Am. Chem. Soc.* **1997**, *119*, 10696.

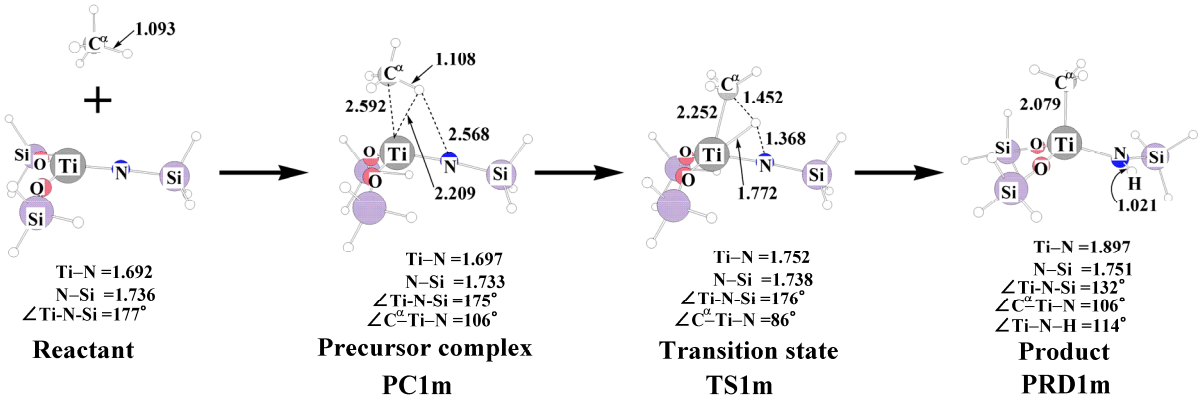

Figure A2. Geometry changes in the C-H σ-bond activation of methane by model Ti-imido complex $(H_3SiO)_2Ti(=NSiH_3)$ **1m**. Bond lengths are in angstrom and bond angles are in degree.

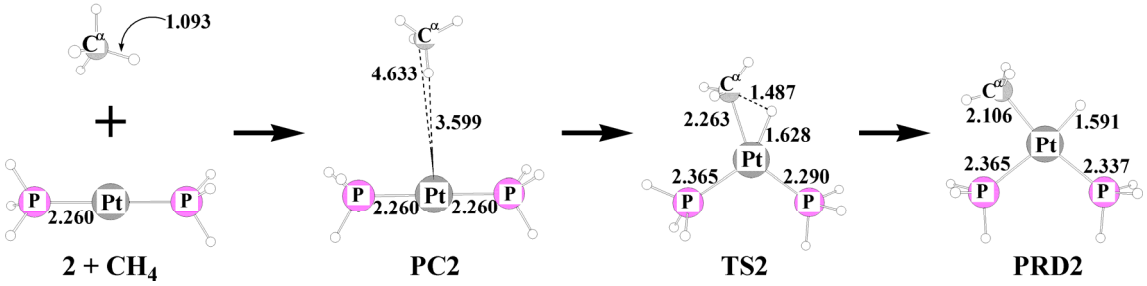

Figure A3. Geometry changes in the C-H σ-bond activation of methane by $Pt(PH_3)_2$ complex. Bond lengths are in angstrom and bond angles are in degree.

22-th MO 23-th MO 27-th MO 28-th MO

Fragment orbitals of $Pt(PH_3)_2$

Figure A4. These MOs are fragment MOs of $Pt(PH_3)_2$ **2**.

Table A3. Binding energy $(BE)^a$, activation barrier $(E_a)^a$, and reaction energy $(\Delta E)^a$ of the C-H σ-bond activation of methane by $(L)_2Ti(=NSiH_3)$ (L = OH or SH).

	L = OH			L = SH		
	BE	E_a	ΔE	*BE*	E_a	ΔE
DFT(B3LYP)	-5.7	15.5	-22.8	-6.0	19.4	-12.8
	$(-5.1)^b$	$(15.5)^b$	$(-21.9)^b$	$(-5.9)^b$	$(19.6)^b$	$(-12.4)^b$

In kcal/mol unit. [a] $BE = E_t$(precursor complex) – E_t(sum of reactants).

$E_a = E_t$(transition state) – E_t(precursor complex). $\Delta E = E_t$(product) – E_t(sum of reactants).

[b] A diffuse function was added to the O atom, also.

Table A4. NBO charge of the C-H σ-bond activation of methane by $(L)_2Ti(=NSiH_3)$ (L = OH or SH).

	L = OH			
	Reactant	**PC**	**TS**	**PRD**
Ti	1.779	1.566	1.531	1.651
N	-1.227	-1.198	-1.244	-1.337
OH	-0.506	-0.478	-0.446	-0.423
OH	-0.523	-0.460	-0.428	-0.432
	L = SH			
	Reactant	**PC**	**TS**	**PRD**
Ti	1.194	0.937	0.916	1.073
N	-1.062	-1.054	-1.136	-1.286
SH	-0.326	-0.251	-0.220	-0.217
SH	-0.315	-0.267	-0.231	-0.214

Table A5. Binding energy (*BE*), activation barrier (E_a), and reaction energy (ΔE) of the N-H σ-bond activation of ammonia by (PNP)Ti(≡$CSiMe_3$) **3**.

	BS2			BS2 without diffuse function on alkylidyne C atom[a]		
	BE	E_a	ΔE	*BE*	E_a	ΔE
MP2	-30.7	13.3	-52.5	-30.4	13.2	-52.3
MP3	-29.8	5.8	-74.1	-29.6	5.7	-74.0
MP4(DQ)	-29.8	13.7	-57.8	-29.6	13.6	-57.6
MP4(SDQ)	-31.2	15.4	-56.3	-30.8	15.3	-56.1
DFT(B3LYP)	-24.8	7.5	-60.2	-24.8	7.5	-60.2

In kcal/mol unit. [a] This C atom binds to the Ti atom.

Table A6. The destabilization energies (kcal/mol) of the heterolytic C-H σ-bond cleavage of methane [a]

	H^- + CH_3^+	H^+ + CH_3^-
MP2	338.9	444.9
MP3	336.7	446.5
MP4(DQ)	335.5	446.7
MP4(SDQ)	335.7	446.4
CCSD(T)	336.4	446.0
DFT(B3LYP)	364.3	442.3

In kcal/mol unit. [a] Geometries were optimized with the DFT/BS1 method and energy changes were evaluated with the BS2 system.

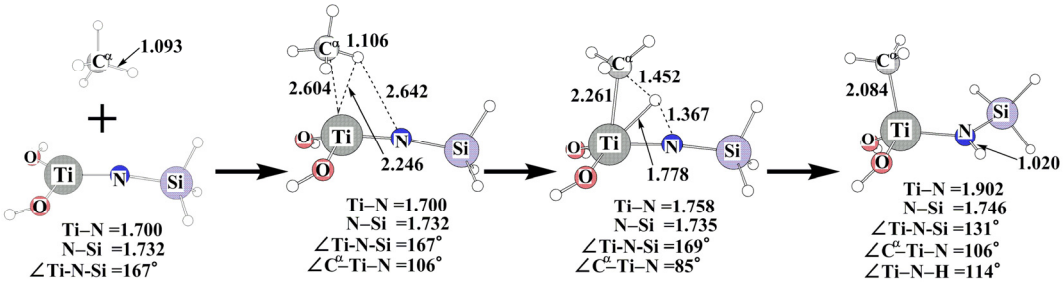

(A) L = OH

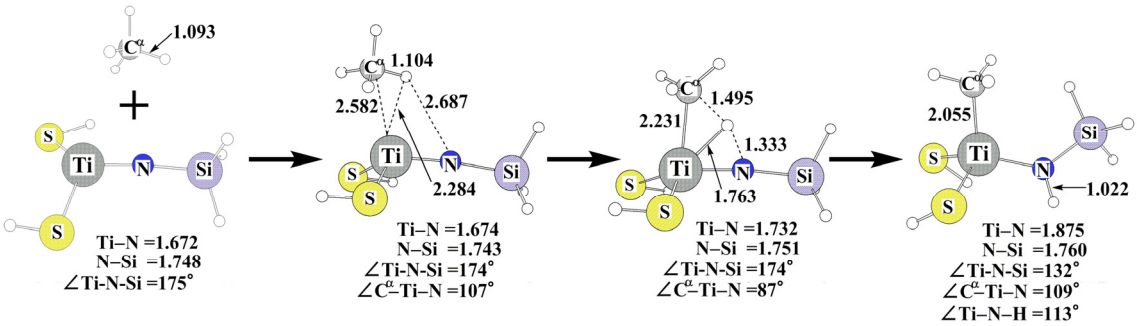

(B) L = SH

Figure A5. Geometry changes in the C-H σ-bond activation of methane by $(L)_2Ti(=NSiMe_3)$ (L = OH, SH). Bond lengths are in angstrom and bond angles are in degree.

Reference

(1) Recent reviews; (a) Arndtsen, B. A.; Bergman, R. G.; Mobley, T. A.; Peterson, T. H. *Acc. Chem. Res.* **1995**, *28*, 154. (b) Shilov, A. E.; Shul'pin, G. B. *Chem.Rev.* **1997**, *97*, 2879. (c) Jones, W. D. *Top. Organomet. Chem.* **1999**, *3*, 9. (d) Sen, A. *Top. Organomet. Chem.* **1999**, *3*, 81. (e) Crabtree, R. H. *J. Chem. Soc., Dalton*, **2001**, 2437. (f) Labingerand, J. A.; Bercaw, J. E. *Nature* **2002**, *417*, 507.

(2) Saillard, J. -Y.; Hoffmann. R. *J. Am. Chem. Soc.* **1984**, *106*, 2006.

(3) (a) Obara, S.; Kitaura, K.; Morokuma, K. *J. Am. Chem. Soc.* **1984**, *106*, 7482. (b) Koga, N.; Morokuma, K. *J. Phys. Chem.* **1990**, *94*, 5454. (c) Koga, N.; Morokuma, K. *J. Am. Chem. Soc.* **1993**, *115*, 6883. (d) Matsubara, T.; Koga, N.; Musaev, D. G.; Morokuma, K. *J. Am. Chem. Soc.* **1998**, *120*, 12692.

(4) (a) Low, J. J.; Goddard III, W. A. *J. Am. Chem. Soc.* **1986**, *108*, 6115. (b) Low, J. J.; Goddard III, W. A. *Organometallics* **1986**, *5*, 609.

(5) (a) Blomberg, M. R. A.; Siegbahn, P. E. M.; Nagashima, U.; Wennerberg, J. *J. Am. Chem. Soc.* **1991**, *113*, 424. (b) Svensson, M.; Blomberg, M. R. A.; Siegbahn, P. E. M. *J. Am. Chem. Soc.* **1991**, *113*, 7076. (c) Blomberg, M. R. A.; Siegbahn, P. E. M.; Svensson, M. *J. Am. Chem. Soc.* **1992**, *114*, 6095. (d) Siegbahn, P. E. M.; Blomberg, M. R. A.; Svensson, M. *J. Am. Chem. Soc.* **1993**, *115*, 4191. (e) Blomberg, M. R. A.; Siegbahn, P. E. M.; Svensson, M. *J. Phys. Chem.* **1994**, *98*, 2062. (f) Siegbahn, P. E. M.; Blomberg, M. R. A. *Organometallics* **1994**, *13*, 354. (g) Siegbahn, P. E. M. *Organometallics* **1994**, *13*, 2833. (h) Siegbahn, P. E. M.; Svensson, M. *J. Am. Chem. Soc.* **1994**, *116*, 10124. (i) Siegbahn, P. E. M. *J. Am. Chem. Soc.* **1996**, *118*, 1487. (j) Siegbahn, P. E. M.; Crabtree, R. H. *J. Am. Chem. Soc.* **1996**, *118*, 4442.

(6) (a) Song, J.; Hall, M. B. *Organometallics* **1993**, *12*, 3118. (b) Jimenez-Catano, R.; Hall, M. B. *Organometallics* **1996**, *15*, 1889. (c) Niu, S. -Q.; Hall, M. B. *J. Am. Chem. Soc.* **1998**, *120*, 6169.

(7) (a) Sakaki, S.; Ieki, M. *J. Am. Chem. Soc.* **1993**, *115*, 2373. (b) Sakaki, S.; Biswas, B.; Sugimoto, M. *J. Chem. Soc., Dalton Trans.* **1997**, 803. (c) Sakaki, S.; Biswas, B.; Sugimoto, M. *Organometallics* **1998**, *17*, 1278. (d) Sakaki, S.; Mizoe, M.; Musashi, Y.; Biswas, B.; Sugimoto, M. *J. Phys. Chem. A.* **1998**, *102*, 8027. (e) Biswas, B.; Sugimoto, M.; Sakaki, S. *Organometallics* **2000**, *19*, 3895. (f) Sakaki, S. *Topics Organomet. Chem.* **2005**, *12*, 31.

(8) Hinderling, C.; Feichtinger, D.; Plattner, D. A.; Chen, P. *J. Am. Chem. Soc.* **1997**, *119*, 10793.

(9) Su, M. -D.; Chu, S. -Y. *J. Am. Chem. Soc.* **1997**, *119*, 5373.

(10) Espinosa-Garcia, J.; Corchado, J. C.; Truhlar, D. G. *J. Am. Chem. Soc.* **1997**, *119*, 9891.

(11) Hill, G. S.; Puddephatt, R. J. *Organometallics* **1998**, *17*, 1478.

(12) (a) Heiberg, H.; Swang, O.; Ryan, O. B.; Gropen, O. *J. Phys. Chem. A.* **1999**, *103*, 10004. (b) Heiberg, H.; Johansson, L.; Gropen, O.; Ryan, O. B.; Swang, O.; Tilset, M. *J. Am. Chem. Soc.* **2000**, *122*, 10831.

(13) Ustynyuk, Y. A.; Ustynyuk, L. Y.; Laikov, D. N.; Lunin, V. V. *J. Organomet. Chem.* **2000**, *597*, 182.

(14) Bartlett, K. L.; Goldberg, K. I.; Borden, W. T. *Organometallics* **2001**, *20*, 2669.

(15) (a) Kua, J.; Xu, X.; Periana, R. A.; Goddard III, W. A. *Organometallics* **2002**, *21*, 511. (b) Xu, X.; Kua, J.; Periana, R. A.; Goddard III, W. A. *Organometallics* **2003**, *22*, 2057.

(16) (a) Cundari, T. R. *J. Am. Chem. Soc.* **1992**, *114*, 10557. (b) Cundari, T. R. *Organometallics* **1993**, *12*, 1998. (c) Cundari, T. R., *Organometallics* **1993**, *12*, 4971. (d) Cundari, T. R. *J. Am. Chem. Soc.* **1994**, *116*, 340. (e) Benson, M. T.; Cundari, T. R.; Moody, E. W. *J. Organomet. Chem.* **1995**, *504*, 1. (f) Cundari, T. R.; Matsunaga, N.; Moody, E. W. *J. Phys. Chem.* **1996**, *100*, 6475. (g) Cundari, T. R.; Klinchkman, T. R.; Wolczanski, P. T. *J. Am. Chem. Soc.* **2002**, *124*, 1481.

(17) (a) Cundari, T. R. *Chem. Rev.* **2000**, *100*, 807. (b) Cundari, T. R.; Gordon, M. S. *J. Am. Chem. Soc.* **1991**, *113*, 5231. (c) Cundari, T. R.; Gordon, M. S. *J. Am. Chem. Soc.* **1992**, *114*, 539. (d) Cundari, T. R. *J. Am. Chem. Soc.* **1992**, *114*, 7879. (e) Cundari, T. R. *J. Am. Chem. Soc.* **1992**, *114*, 10557. (f) Cundari, T. R. *Organometallics*, **1993**, *12*, 1998.

(18) Bailey, B. C.; Fan, H.; Baum, E. W.; Huffman, J. C.; Baik, M.-H.; Mindiola, D. J. *J. Am. Chem. Soc.* **2005**, *127*, 16016.

(19) (a) Zhao, J.; Goldman, A. S.; Hartwig, J. F. *Science* **2005**, *307*, 1080. (b) Kanzelberger, M.; Zhang, X.; Emge, T. J.; Goldman, A. S.; Zhao, J; Incarvito, C.; Hartwig, J. F. *J. Am. Chem. Soc.* **2003**, *125*, 13644.

(20) Becke, A. D. *Phys. Rev.* **1988**, *A38*, 3098.

(21) Becke, A. D. *J. Chem. Phys.* **1983**, *98*, 5648.

(22) Lee, C.; Yang, W.; Parr, R. G. *Phys. Rev.* **1988**, *B37*, 785.

(23) Hay, P. J.; Wadt, W. R. *J. Chem. Phys.* **1985**, *82*, 299.

(24) Couty, M.; Hall, M. B. *J. Comput. Chem.* **1996**, *17*, 1359.

(25) Wadt, W. R.; Hay, P. J. *J. Chem. Phys.* **1985**, *82*, 284.

(26) Höllowarth, A.; Böhme, M.; Dapprich, S.; Ehlers, A. W.; Gobbi, A.; Jonas, V.; Köhler, K. F.; Stegmann, R.; Veldkamp, A.; Frenking, G. *Chem. Phys. Lett.* **1993**, *208*, 237.

(27) (a) Hariharan, P. C.; Pople, J. A. *Theor. Chim. Acta* **1973**, *28*, 213. (b) Hariharan, P. C.; Pople, J. A. *Mol. Phys.* **1974**, *27*, 209.

(28) Krishnan, R.; Binkley, J. S.; Seeger, R.; Pople, J. A. *J. Chem. Phys.* **1980**, *72*, 650.

(29) Ehlers, A. W.; Böhme, M.; Dapprich, S.; Gobbi, A.; Höllwarth, A.; Jonas, V.; Köhler, K. F.; Stegmann, R.; Veldkamp, A.; Frenking, G. *Chem. Phys. Lett.* **1993**, *208*, 111.

(30) McLean, A. D.; Chandler, G. S. *J. Chem. Phys.* **1980**, *72*, 5639.

(31) Blaudeau, J. -P.; McGrath, M. P.; Curtiss, L. A.; Radom, L. *J. Chem. Phys.* **1997**, *107*, 5016.

(32) Pople, J. A. , et al. *Gaussina 03* (Revision C.02), Gaussian, Inc., Wallingford CT 2004.

(33) Reed, A. E.; Curtiss, L. A.; Weinhold, F. *Chem. Rev.* **1988**, *88*, 899.

(34) Flükiger, P. and; Lüthi, H. P.; Portann, S.; Weber, J. MOLEKEL, v.4.3; Scientific Computing: Manno, Switzerland, 2002-2002. Portman, S.; Lüthi, H. P. *CHIMIA* **2000**, *54*, 766

(35) (a) Haymore, B. L.; Maatta, E. A.; Wentworth, R. D. *J. Am. Chem. Soc.* **1979**, *101*, 2063. (b) Parkin, G.; van Asselt, A.; Leahy, D. J.; Whinnery, L.; Hua, N. G.; Quan, R. W.; Henling, L. M.; Schaefer, W. P.; Santarsiero, B. D.; Bercaw, J. E. *Inorg. Chem.* **1992**, *31*, 82.

(36) Bennett, J. L.; Wolczanski, P. T. *J. Am. Chem. Soc.* **1997**, *119*, 10696.

(37) Koga, N; Obara, S: Morokuma, K. *J. Am. Chem. Soc.* **1984**, *106*, 4625.

(38) Goddard, R. J.; Hoffmann, R.; Jemmis, E. D. *J. Am. Chem. Soc.* **1980**, *102*, 7667.

(39) Obara, S.; Koga, N.; Morokuma, K. *J. Organomet. Chem.* **1984**, *270*, C33.

(40) (a) The interaction energy between π-conjugated systems and $Pt(PH_3)_2$ is also underestimated by the DFT method, similarly.[40b] (b) Kameno, Y.; Ikeda, A.; Nakao, Y.; Sato, H.; Sakaki, S. J. Phys. Chem. **2005**, 109, 8055.

(41) (a) McKinney, R. J.; Thorn, D. L.; Hoffmann, R.; Stockis, A. *J. Am. Chem. Soc.* **1981**, *103*, 2595. (b) Tatsumi, K.; Hoffmann, R.; Yamamoto, A.; Stille, J. K. *Bull. Chem. Soc. Jpn.* **1981**, *54*, 1857.

(42) The weight was evaluated with Mulliken approximation.

Chapter 2

Theoretical Prediction of O-H, Si-H, and Si-C σ-Bond Activation Reactions by Titanium(IV)-Imido Complex

2.1. Introduction

The σ-bond activation of saturated molecule by transition-metal complex is one of the important reactions in organometallic chemistry, inorganic chemistry, and catalytic chemistry, because active species is produced by this reaction in many cases.[1] There are several categories of σ-bond activation: (i) The first is the σ-bond activation via oxidative addition reaction by late transition-metal complexes. This reaction has been theoretically investigated well by many groups.[2-15] (ii) The second is the σ-bond activation via metathesis by lanthanide and actinide complexes, which was theoretically investigated by Eisenstein and her coworkers.[16] (iii) The third is the σ-bond activation by metal-ligand single bond such as the platinum(II)-chloride, Palladium(II)-acetate, and iridium(III)-acetate bonds,[17-19] which were theoretically investigated by Siegbahn et al.,[20] Sakaki et al.,[21] Ziegler et al.,[22] Goddard et al.,[23] and Schwarz et al.[24] And, (iv) the last is the σ-bond activation via addition of C-H σ-bond across M=N multiple bond by early to middle transition-metal complexes.[25] This σ-bond activation was theoretically investigated by Cundari and his collaborators in the last decade.[26] Recently, the C-H σ-bond activation of benzene by the titanium(IV)-alkylidyne complex was experimentally succeeded and theoretically investigated with the DFT method by Mindiola group.[27] We also theoretically investigated the C-H σ-bond activation of methane by the titanium(IV)-imido complex recently, and clearly showed that not only the charge-transfer (CT) from the Ti=N moiety to the σ*-anti-bonding orbital but also the reverse CT from the C-H σ-bonding orbital to the Ti empty d-orbital plays important role in this σ-bond activation.[28]

In our previous work,[28] we presented theoretical prediction that N-H σ-bond activation of ammonia can be achieved by the titatnium(IV)-imido and titanium(IV)-alkylidyne complexes. Though one successful N-H σ-bond activation of ammonia has been reported recently,[29] it is still difficult. Considering that the titanium(IV)-imido complex is useful for the C-H and N-H σ-bond activations, one can expect that this complex can be also applied to other σ-bond activations of O-H, Si-H, and Si-C bonds. Because the O-H bond is strong like the N-H bond, its activation is interesting. Also, the Si-H σ-bond activation is important because it is involved in many catalytic reactions producing organosilicon compounds. The Si-C σ-bond activation is challenging, because it is difficult as well known.

In this theoretical work, we investigated the O-H σ-bond activation of methanol, the Si-H σ-bond activation of silane, and the Si-C σ-bond activation of methylsilane with titanium(IV)-imido complex, $(Me_3SiO)_2Ti(NSiMe_3)$, by DFT and MP2 to MP4(SDQ) methods. This complex was used for many experimental works by Wolczanski group.[25] Our purposes here are to show the differences of the O-H, Si-H, and Si-C σ-bond activations from the C-H σ-bond activation, to present theoretical prediction if the titanium(IV)-imido complex can be utilized for these σ-bond activations, and to clarify what factor is important in these σ-bond activations.

2.2. Computational Details

Geometries were optimized by the DFT method with the B3LYP functional.[30-32] We ascertained that each equilibrium geometry has no imaginary frequency and each transition state has only one imaginary frequency. Two kinds of basis set systems were used. The smaller system (BS1) was used for geometry optimization. In this BS1, core electrons of Ti (up to 2p) were replaced with effective core potentials (ECPs),[33] and their valence electrons were represented with (311111/2111/411/1) basis set.[33] For H, C, N, O, and Si, 6-31G* basis

sets[34] were employed, where a p-polarization function[35] was added to the active H atom that reacts with the Ti complex to form either Ti-H or N-H bond. The better basis set system (BS2) was used for evaluation of energy changes. In this BS2, (311111/2111/411/11) basis set was employed for Ti,[33, 36] where the same ECPs as those of BS1 were employed for core electrons. For H, C, N, O, and Si, the 6-311G* basis sets were employed,[37-39] where a p-polarization function was added to the active H atom and a diffuse function was added to the imido N atom. Zero-point energy was evaluated with the DFT/BS1 method under assumption of harmonic oscillator. The energy changes are presented here after correction of zero-point energy.

The Gaussian 03 program package[40] was used for all calculations. Population analysis was carried out with the method of Weinhold et al.[41] Molecular orbitals were drawn with the MOLEKEL program package.[42]

2.3. Results and Discussion

2.3.1. Geometry and Energy Changes in the O-H σ-Bond Activation of Methanol by Titanium(IV)-Imido Complex, [$(Me_3SiO)_2Ti(NSiMe_3)$] R

The O-H σ-bond activation of methanol by $(Me_3SiO)_2Ti(NSiMe_3)$ **R** occurs through precursor complex (**PC1**) and transition state (**TS1**) to afford product complex (**PRD1**), as shown in Figure 1. The optimized geometry of **R** agrees well with the experimental one[43, 44] except for the moderate discrepancies in the Ti-N and N-Si bond distances, as reported previously.[26, 28] We stop to discuss the moderate discrepancies here because we presented the discussion in our recent work.[28] In **PC1**, the O atom of methanol approaches the Ti center, where the Ti-O distance is 2.109 Å, but the H atom is considerably distant from the N atom. The O-H bond little lengthens in **PC1**, which is different from the moderately elongated C-H bond in the precursor complex of the C-H σ-bond activation of

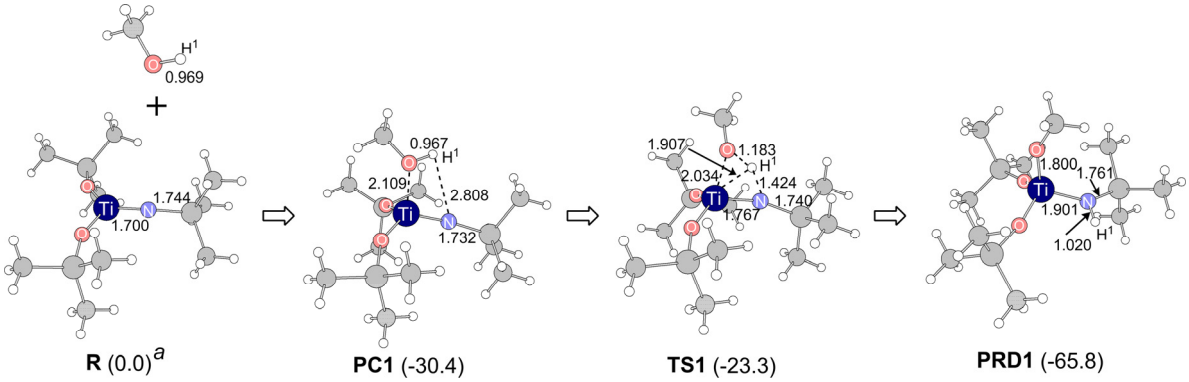

Figure 1. Geometry changes in O-H σ-bond activation of methanol by $(Me_3SiO)_2Ti(NSiMe_3)$ **R**. Bond lengths are in angstroms, and bond angles are degree. [a] In parenthesis is relative energy calculated by DFT(B3LYP)/BS2 method.

methane. This difference will be discussed below in more detail. In **TS1**, the Ti-O distance becomes shorter to 2.034 Å, which is moderately longer than that of **PRD1**. The O-H distance is moderately elongated to 1.183 Å, and the N-H distance (1.424 Å) is still considerably long. The moderate elongation of the O-H distance in **TS1** is in contrast to the considerable elongation of the C-H bond in the transition state of the C-H σ-bond activation of methane.[28] The product **PRD1** takes pseudo-tetrahedral structure, as expected from the d^0 electron configuration of Ti(IV).

Binding energy (*BE*), activation barrier (E_a), and reaction energy (ΔE) are defined as the energy differences between **PC1** and the sum of reactants, between **PC1** and **TS1**, and between **PRD1** and the sum of reactants, respectively. Negative ΔE value means that the σ-bond activation is exothermic, and vice versa. The *BE* value is -30.4 (-36.6) kcal/mol, as shown in Table 1, where DFT- and MP4(SDQ)-calculated values are presented without and in parenthesis hereafter. This large *BE* value indicates that methanol strongly coordinates with the Ti center to afford **PC1** unlike the methane complex.[28] This difference is interpreted, as follows: Because methanol has the lone pair orbital on the O atom, the charge-transfer (CT)

Table 1. Binding Energy (*BE*), Activation Barrier (E_a), and Reaction Energy (ΔE) of the Si-H σ-bond activation of silane, O-H σ-bond activation of methanol, and C-Si σ-bond activation of methylsilane by $(Me_3SiO)_2Ti(NSiMe_3)$ **R**.[a]

	CH_3O-H			$H-SiH_3$						CH_3-SiH_3			$H-CH_3$[e]		
				path A			path B								
	BE [b]	E_a [c]	ΔE[d]	BE [b]	E_a [c]	ΔE[d]	BE [b]	E_a [c]	ΔE[d]	BE [b]	E_a [c]	ΔE[d]	BE [b]	E_a [c]	ΔE[d]
DFT(B3LYP)	-30.4	7.1	-65.8	-6.0	9.7	-27.7	-6.8	2.6	-32.5	-8.1	19.1	-33.9	-4.5	14.6	-22.7
MP2	-36.6	12.4	-59.7	-13.7	11.0	-24.3	-14.9	4.0	-32.7	-17.2	16.5	-38.0	-9.8	17.6	-16.5
MP3	-36.3	9.0	-74.2	-11.2	10.6	-42.2	-13.0	0.5	-50.6	-14.7	13.1	-54.9	-7.1	12.7	-36.5
MP4(DQ)	-35.5	13.4	-65.4	-12.3	13.4	-32.4	-13.5	3.4	-40.9	-15.7	17.6	-44.4	-7.8	18.0	-25.3
MP4(SDQ)	-36.6	14.6	-61.4	-13.9	15.0	-26.4	-15.2	4.3	-34.1	-17.5	18.6	-37.7	-9.4	21.5	-16.5

[a] In kcal/mol unit. [b] BE = E(precursor complex) − E(sum of reactants). [c] E_a = E(transition state) − E(precursor complex). [d] ΔE = E(product) − E(sum of reactants). [e] Ref. 28

occurs from the lone pair orbital to the Ti empty d-orbital. Also, the O atom forms considerably strong electrostatic interaction with the positively charged Ti(IV) center, because the O atom is much negatively charged. In the precursor complex of methane, the CT occurs from the C-H bonding orbital to the Ti empty d-orbital like agostic interaction,[28] but the CT is weak because the C-H bonding orbital energy is much lower than the O lone pair of CH_3OH. Because the CT occurs from the O lone pair to the Ti empty d orbital in **PC1**, the O-H σ-bonding orbital little participates in the CT, which induces little elongation of the O-H bond; remember that the C-H bond is moderately elongated in the precursor complex of the C-H σ-bond activation, because the CT occurs from the C-H bonding orbital to the Ti empty d-orbital.[28] It is also noted that the DFT-calculated *BE* value is similar to the MP4(SDQ)-calculated one here, though the MP4(SDQ)-calculated *BE* value is much larger than the DFT-calculated one in the C-H σ-bond activation of methane (see Table 1). This difference would arise from the fact that van der Waals interaction, as well as the CT, also participates in the weak interaction between the C-H bond and the metal center.

In the O-H σ-bond activation, the E_a value is 7.1 (14.6) kcal/mol, which is much smaller than that of the C-H σ-bond activation of methane, as shown in Table 1. The ΔE value is much more negative than in the C-H σ-bond activation of methane. These results suggest that the titanium(IV)-imido complex can be utilized for the O-H σ-bond activation of alcohol.

2.3.2. Geometry and Energy Changes in the Si-H σ-Bond Activation of Silane SiH_4 by Titanium(IV)-Imido Complex, $[(Me_3SiO)_2Ti(NSiMe_3)]$ R :

In the reaction, we need to consider two possibilities; in one reaction course (course A), the H atom and the SiH_3 group are bound with the N atom and the Ti center, respectively, in the product like the C-H σ-bond activation, while in the other course (course B) the H atom and the SiH_3 group are bound with the Ti center and the N atom, respectively, in the product

unlike the C-H σ-bond activation. The former reaction occurs through precursor complex **PC2a** and transition state **TS2a** to afford product $(Me_3SiO)_2Ti(SiH_3)[NH(SiMe_3)]$ **PRD2a**, as shown in Figure 2. In **PC2a**, the Ti-H distance is 2.029 Å, which is shorter than that of the precursor complex in the C-H σ-bond activation of methane. Also, the Si-H distance is moderately elongated to 1.511 Å. These results indicate that the agostic interaction of the Si-H σ-bond with the Ti center more contributes to the stabilization of **PC2a** than does the C-H σ-bond. This is because the Si-H σ-bonding orbital exists at higher energy than the C-H σ-bonding orbital. In **TS2a**, the Si-H bond is moderately elongated to 1.762 Å, and the Ti-Si distance becomes shorter to 2.777 Å, which is slightly longer than that of **PRD2a**. But, the N-H distance is still long. These geometrical features indicate that **TS2a** is more reactant-like than the transition state of the C-H σ-bond activation. **PRD2a** is four-coordinate pseudo-tetrahedral titanium(IV)-alkyl amino complex, as expected.

In the course B, the precursor complex **PC2b** is formed. As shown in Figure 3, its Si-H distance is moderately elongated to 1.522 Å like that of **PC2a**. The Ti-H distance is 1.975 Å and the Si-N distance is very long. In the transition state **TS2b**, the Si-H distance is moderately elongated to 1.623 Å, and the Ti-H and N-Si distances become shorter to 1.835 Å and 2.253 Å, respectively. The Ti-H distance is somewhat and the N-Si distance is considerably longer than those of the product $(Me_3SiO)_2Ti(H)[N(SiH_3)(SiMe_3)]$ **PRD2b**, indicating that **TS2b** is reactant-like, too. **PRD2b** is a four-coordinate titanium(IV) hydride disilylamino complex, geometry of which is pseudo-tetrahedral.

In the reaction course A, the *BE* value is -6.0 (-13.9) kcal/mol, which is somewhat larger than that of the precursor complex of the C-H σ-bond activation. This is because the CT from the Si-H σ-bonding orbital to the Ti empty d-orbital is stronger than that from the C-H σ-bonding orbital to the Ti empty d-orbital; remember that the Si-H σ-bonding orbital exists at higher energy than the C-H σ-bonding orbital. The E_a value is 9.7 (15.0) kcal/mol and the ΔE value is -27.7 (-26.4) kcal/mol. This E_a value is much smaller than that of the

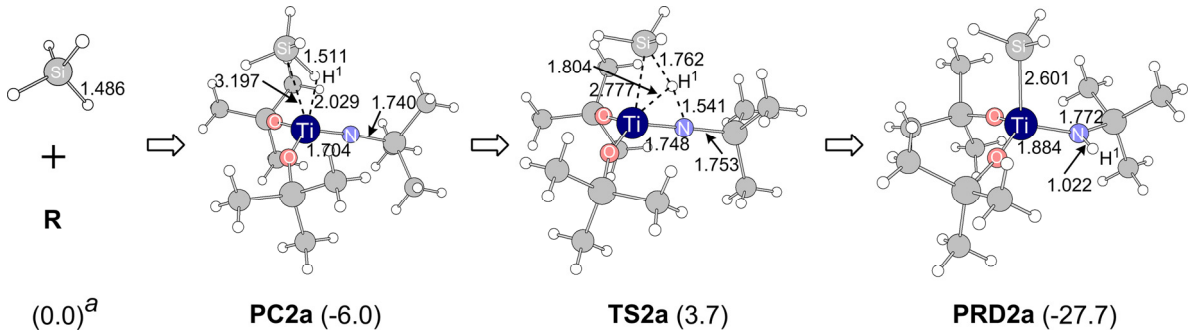

Figure 2. Geometry changes in Si-H σ-bond activation of silane by $(Me_3SiO)_2Ti(NSiMe_3)$ **R** (reaction course A). In this reaction course, Ti-SiH_3 and N-H bonds were formed. Bond lengths are in angstroms, and bond angles are degree. [a] In parenthesis is relative energy calculated by DFT(B3LYP)/BS2 method.

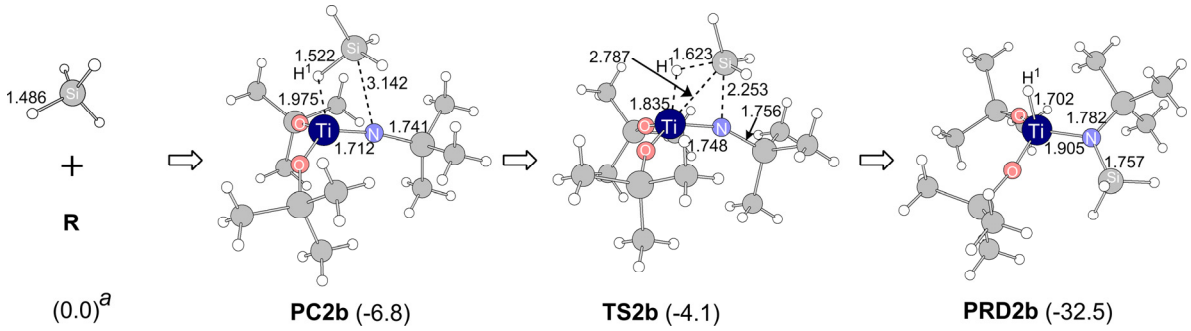

Figure 3. Geometry changes in Si-H σ-bond activation of silane by $(Me_3SiO)_2Ti(NSiMe_3)$ **R** (reaction course B). In this reaction course, Ti-H and N-SiH_3 bonds were formed. Bond lengths are in angstroms, and bond angles are degree. [a] In parenthesis is relative energy calculated by DFT(B3LYP)/BS2 method.

C-H σ-bond activation, but moderately larger than that of the O-H σ-bond activation. In the reaction course B, the *BE* value is similar to that of the course A. However, the E_a value (2.7 (4.3) kcal/mol) is much smaller and the ΔE value (-32.5 (-34.1) kcal/mol) is much more negative than those of the course A. These results clearly show that the course B is easier than the course A and the titanium(IV)-hydride disilylamino complex

$(Me_3SiO)_2Ti(H)[N(SiH_3)(SiMe_3)]$ **PRD2b** is a product of the Si-H σ-bond activation. It is noted that the E_a value is much smaller than those of the C-H and O-H σ-bond activations, and that the ΔE value is much more negative than that of the C-H σ-bond activation but much less negative than that of the O-H σ-bond activation. The reasons will be discussed below in detail.

2.3.3. Geometry and Energy Changes in the Si-C σ-Bond Activation of Methylsilane SiH_3-CH_3 by Titanium(IV)-Imido Complex, $[(Me_3SiO)_2Ti$-$(NSiMe_3)]$ R:

The precursor complex **PC3** is formed by the CT interaction of the Si-H σ-bond with the Ti empty d orbital like **PC2b**, as shown in Figure 4. In the transition sate **TS3**, the Ti-C distance is 2.259 Å and the N-Si distance is 2.117 Å, which are not very much longer than those of the product **PRD3**. Also, the Si-C distance is moderately elongated to 2.150 Å. These geometrical features suggest that **TS3** is understood to be more product-like than **TS1** and **TS2b** but more reactant-like than the transition state of the C-H σ-bond activation. The product **PRD3** is a titanium(IV) methyl disilylamino complex $(Me_3SiO)_2Ti(CH_3)[N$-$(SiH_3)(SiMe_3)]$, geometry of which is pseudo-tetrahedral, as expected.

The *BE* value is similar to that of **PC2b**. The E_a value is 19.1 (18.6) kcal/mol and the ΔE value is -33.9 (-37.7) kcal/mol. The E_a value is similar to and the ΔE value is much larger than those of the C-H σ-bond activation reaction. Considering that the C-H σ-bond activation by the titanium(IV)-imido complex was reported experimentally,[25] these E_a and ΔE values suggest that the Si-C σ-bond activation can be achieved by the titanium(IV)-imido complex.

2.3.4. Comparisons of the Population Changes among O-H, Si-H, and Si-C σ-Bond Activations:

In the O-H σ-bond activation, the H atomic population little decreases and the electron population of the OCH_3 group little increases in the reaction, as shown in Figure 5. On the other hand, the Ti atomic population increases in **PC1** because of the CT from the O lone pair to the Ti empty d-orbital, while it moderately decreases upon going from **PC1** to **PRD1**. These population changes are quite different from those of the C-H σ-bond activation, in which the H atomic population considerably decreases and the electron population of the CH_3 moiety considerably increases. The moderate population changes by the O-H σ-bond activation are easily interpreted in terms of the highly polarized O-H bond of CH_3OH; actually, the positive charge of the H atom and the negative charge of the OCH_3 group are considerably large in CH_3OH. In the product, the H atom is bound with the N atom, electronegativity of which is not different very much from that of the O atom. The OCH_3 group is anionic in the product because it is bound with the Ti center. Because the OCH_3 group is sufficiently anionic in CH_3OH, as discussed above, the electron redistribution does not considerably occur in the O-H σ-bond activation.

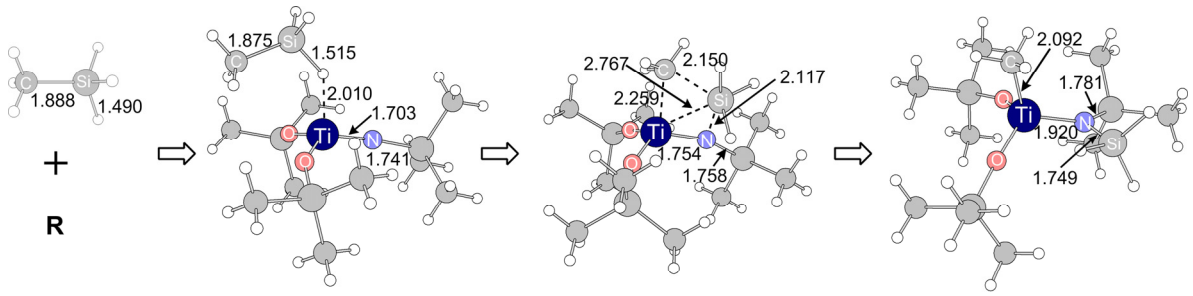

(0.0)[a] **PC3** (-8.1) **TS3** (11.0) **PRD3** (-33.9)

Figure 4. Geometry changes in Si-C σ-bond activation of methylsilane by $(Me_3SiO)_2Ti(NSiMe_3)$ **R**. Bond lengths are in angstroms, and bond angles are degree. [a] In parenthesis is relative energy calculated by DFT(B3LYP)/BS2 method.

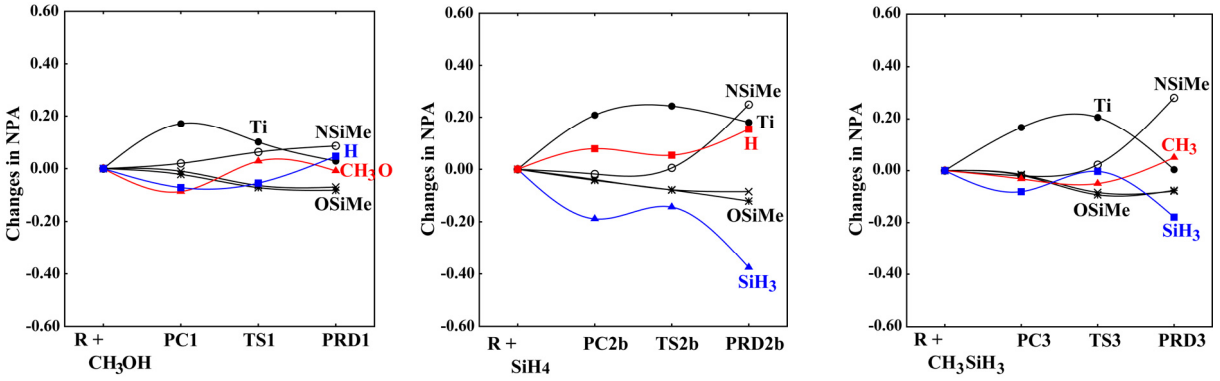

(A) The O-H σ-bond activation of CH_3OH

(B) The Si-H σ-bond activation of SiH_4 (course B)

(C) The Si-C σ-bond activation of CH_3SiH_3

Figure 5. Population changes in (A) O-H σ-bond activation of methane, (B) Si-H σ-bond activations of silane (course B), and (C) Si-C σ-bond activation of methylsilane by $(Me_3SiO)_2Ti(NSiMe_3)$ **R**. The positive value represents the increase in electron population, and vice versa. The DFT(B3LYP)/BS2 method was employed.

In the Si-H σ-bond activation via the course B, the total electron population of H-SiH_3 moderately decreases by 0.113 e and the electron population of the Ti-imido complex moderately increases by 0.113 e upon going to **PC2b** from **R**. Also, the Ti atomic population increases. These population changes arise from the fact that the net CT occurs from the Si-H bond to the Ti empty d-orbital in **PC2b**, as discussed above. Interestingly, the H atomic population increases and the electron population of SiH_3 decreases upon going to **PC2b** from **R**, as shown in Figure 5(B). The increase in the H atomic population and the decrease in the SiH_3 electron population are interpreted in terms of the polarization, as follows; because the H atom and the SiH_3 moiety approach the positively charged Ti center and the negatively charged N atom, respectively, in **PC2b**, the polarization occurs so as to increase the H atomic population and decrease the electron population of the SiH_3 moiety. Little population change occurs upon going from **PC2b** to **TS2b**, because **TS2b** is reactant-like; remember that the Si-H distance is elongated by only 0.1 Å upon going to **TS2b**

from **PC2b**. However, the populations considerably change upon going to **PRD2b** from **TS2b**, in which the H atomic population considerably increases and the electron population of SiH_3 considerably decreases. These population changes indicate that the Si-H σ-bond cleavage occurs via heterolytic σ-bond activation. It is noted that the increase in the H atomic population and the decrease in the SiH_3 electron population contrast with those of the C-H σ-bond activation of methane in which the H atomic population considerably decreases but the CH_3 electron population considerably increases. The reason is easily interpreted in terms of the polarized Si-H bond; because of the much small electronegativity of the Si element, the H atom is negatively charged and the Si atom is positively charged in SiH_4. As a result, the H atomic population does not need to increase but rather decreases and the SiH_3 electron population does not need to decrease but rather increases.

In the Si-C σ-bond activation, the populations moderately change, too, as shown in Figure 5(C). The reason is the same as those of the O-H and Si-H σ-bond activations, as follows: Because the SiH_3 group is bound with the N atom and the CH_3 group is bound with the Ti center in **PRD3**, the SiH_3 group is positively charged and the CH_3 group is negatively charged in **PRD3**. In CH_3-SiH_3, the CH_3 group is negatively charged and the SiH_3 group is positively charged, due to the electronegativity difference between C and Si atoms. As a result, the large population changes do not necessarily occur in the reaction, too.

2.3.5. Comparisons of the Reactivity among O-H, Si-H, Si-C, and C-H σ-Bond Activations:

First, we wish to discuss the reason why the course B is easier than the course A in the Si-H σ-bond activation. In the course A, the Ti-SiH_3 and N-H bonds are formed, while the Ti-H and N-SiH_3 bonds are formed in the course B. We evaluated these bond energies, considering assumed reactions shown in Scheme 1. Though the DFT-computed bond energies are moderately smaller than the CCSD(T)-computed values, as shown in Table 2, the

trends are the same in both computational values. Apparently, the N-H bond energy is moderately larger than the N-SiH_3 bond energy by 11.3 kcal/mol at the DFT level and by 6.1 kcal/mol at the CCSD(T) level. However, the Ti-H bond is much stronger than the Ti-SiH_3 bond by 19.5 kcal/mol and 13.3 kcal/mol at the DFT and CCSD(T) levels, respectively. As a result, the course B is easier than the course A.

Scheme 1

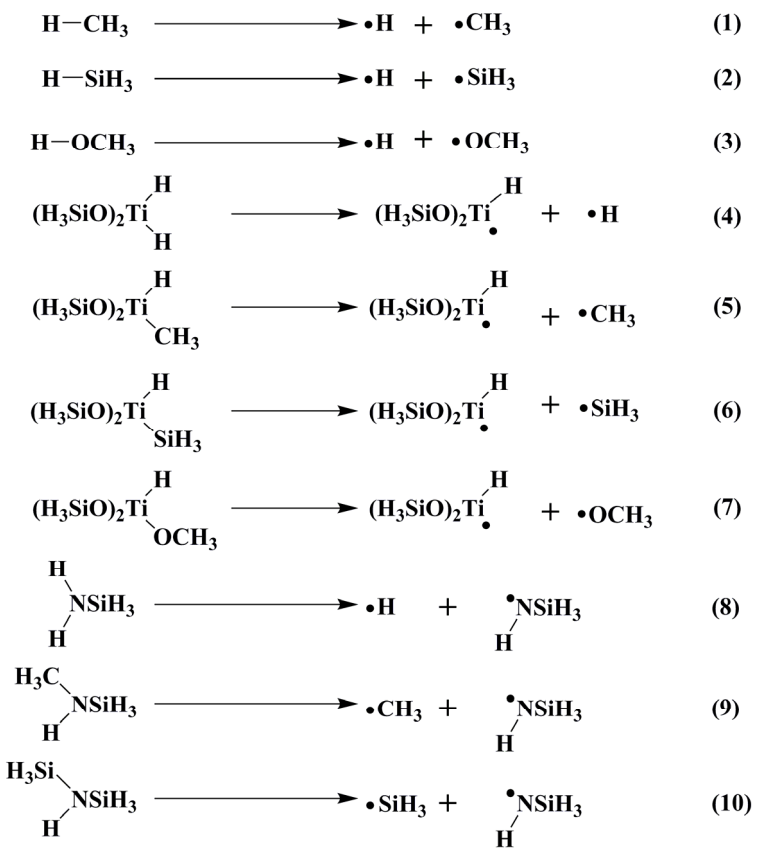

Table 2. Bond energies calculated with DFT(B3LYP), MP2-MP4(SDQ), and CCSD(T)/BS2 methods.

	DFT(B3LYP)	MP2	MP3	MP4(DQ)	MP4(SDQ)	CCSD(T)
Ti-H	65.4	69.9	62.0	64.4	70.1	67.5
Ti-SiH_3	45.9	59.4	47.4	49.0	55.9	54.2
Ti-OCH_3	108.7	130.5	105.6	109.5	119.5	116.8
Ti-CH_3	68.4	83.0	69.0	69.3	75.2	74.5
N-H	115.9	116.9	114.0	114.2	114.2	114.5
N-SiH_3	104.6	114.4	107.9	107.5	107.8	108.4
N-CH_3	100.3	108.4	101.0	100.4	100.8	102.1
C-H	118.4	114.5	115.0	114.9	115.1	115.5
Si-H	94.8	90.6	92.9	93.2	93.3	93.4
O-H	107.2	111.0	106.5	107.1	107.0	107.3
Si-C	96.1	99.0	96.7	95.6	95.9	96.5

[a] In kcal/mol unit.

The O-H σ-bond activation is more exothermic than the Si-H σ-bond activation. In the O-H σ-bond activation, the Ti-OCH_3 and N-H bonds are formed. Though the O-H bond is much stronger than the Si-H bond, its difference (12.4 kcal/mol) is much smaller than the difference between the sum of Ti-OCH_3 and N-H bond energies and that of the Ti-H and N-SiH_3 bond energies, because the Ti-OCH_3 bond is much stronger than the Ti-H bond. This is the reason why the H-OCH_3 σ-bond activation is more exothermic than the Si-H σ-bond activation. However, the O-H σ-bond activation needs larger E_a value than the Si-H σ-bond activation unexpectedly from the above-described exothermicity. One of the important factors to determine the E_a value is the strength of the σ-bond to be broken. The O-H bond is considerably stronger than the Si-H bond. In the transition state, the O-H bond should be cleaved, while the Ti-OCH_3 bond is not completely formed yet. Actually, the elongation of the O-H bond to 1.183 Å gives rise to larger destabilization energy than that of the Si-H bond to 1.623 Å, as shown in Table 3; remember the O-H distance is 1.183 Å and the Si-H distance is 1.623 Å in the transition state. The difference in the destabilization energy between CH_3OH and SiH_4 is similar to the difference in E_a value. Thus, it is concluded that the O-H σ-bond activation needs larger E_a value than the Si-H σ-bond activation because the strong O-H bond should be broken.

Then, we will compare the O-H σ-bond activation with the C-H σ-bond activation. In the C-H σ-bond activation, the Ti-CH_3 and N-H bonds are formed. Though the C-H bond is moderately stronger than the O-H bond, the Ti-CH_3 bond is much weaker than the Ti-OCH_3 bond. Thus, the O-H σ-bond activation much easier occurs than the C-H σ-bond activation.

The difference between the Si-H and C-H σ-bond activations is easily interpreted in terms of bond energy, too, as follows: In the Si-H σ-bond activation, the Ti-H and N-SiH_3 bonds are formed. Though the N-SiH_3 bond is somewhat weaker than the N-H bond and the Ti-H bond is as strong as the Ti-CH_3 bond, the Si-H bond is much weaker than the C-H

Table 3. Distortion energies of CH_3OH and SiH_4 in **TS1** and **TS2b**, respectively[a]

	CH_3OH	SiH_4
DFT(B3LYP)	21.3	16.6
MP2	23.2	18.8
MP3	24.2	18.5
MP4(DQ)	23.6	18.4
MP4(SDQ)	23.3	18.3
CCSD(T)	22.6	17.9

[a] In kcal/mol unit.

bond. As a result, the Si-H σ-bond activation occurs easier than the C-H σ-bond activation. It is worth investigating the reason why the C-H σ-bond activation occurs via the course A which leads to the formation of the Ti-CH_3 and N-H bonds (28), but the Si-H σ-bond activation occurs via the course B leading to the formation of the Ti-H and N-SiH_3 bonds. One of the reasons is that the N-SiH_3 bond is stronger than the N-CH_3 bond. Another reason is that the Ti-SiH_3 bond is much weaker than the Ti-CH_3 bond. This is because the electropositive Si element tends to form a strong bond with the electronegative N atom but a weak bond with the electropositive Ti atom. Also, the electronegative C element trends to form a strong bond with the electropositive Ti center. Because of the formation of this strong N-SiH_3 bond and the weak Ti-SiH_3 bond, the Si-H σ-bond activation occurs via the course B. On the other hand, because the Ti-CH_3 and N-H bonds are stronger than the Ti-H and N-CH_3 bonds, respectively, the C-H σ-bond activation occurs via the course A.

In the Si-C σ-bond activation, the MP4(SDQ)-calculated E_a value is similar to and the DFT-calculated value is moderately larger than those of the C-H σ-bond activation, while the former reaction is more exothermic than the latter one. In the Si-C σ-bond activation, not the bond energy but another factor plays important role to determine the E_a value. This is the same as the difference between the C-H and C-C σ-bond activations.[8a] In general, the

Scheme 2

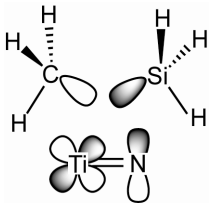

(A) Si-C σ-bond activation

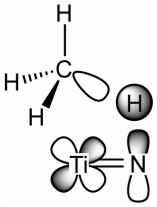

(B) C-H σ-bond activation

C-C σ-bond activation of ethane is much more difficult than the C-H σ-bond activation, though the exothermicity is similar between them. The difference between the C-H and C-C σ-bond activations was interpreted in terms of the distortion of valence orbital.[4, 5a, 45] The difference here is interpreted in the same way, as follows: In the Si-C σ-bond activation, the CH_3 and SiH_3 groups must change their directions toward the Ti center and the N atom, respectively, to form Ti-CH_3 and N-SiH_3 bonds, as shown in Scheme 2, because the valence orbitals of CH_3 and SiH_3 are sp^3-like. Such direction changes give rise to considerably large distortion energy. On the other hand, the C-H σ-bond activation, only the CH_3 group must change its direction toward the Ti center but the H atom can interact with both CH_3 and imido groups because of the spherical 1s orbital. As a result, the Si-C σ-bond activation needs larger E_a value than the C-H σ-bond activation.

2.3.6. Reasons Why Bond Energy Increases in the Order Ti-SiH_3 < Ti-H < Ti-CH_3 < Ti-OCH_3:

Because these bond energies are important factor to determine the reactivity of the σ-bond activation, it is worthy investigating the reason why bond energy increases in the above order. The covalent bond energy ΔE_{cov} is approximately represented by eq. 11,[46] as follows:

$$\Delta E_{cov} = \sqrt{(\varepsilon_A - \varepsilon_B)^2 + 4\beta_{AB}{}^2} \quad (11)$$

$$\Delta E_{cov} \approx |\varepsilon_A - \varepsilon_B| + \frac{2\beta_{AB}^2}{|\varepsilon_A - \varepsilon_B|} \quad (12)$$

If the $|\varepsilon_A - \varepsilon_B|$ value is much larger than the $|\beta_{AB}|$ value, eq. 11 can be further simplified to eq. 12. In the above eqs., ε_A and ε_B are valence orbital energies of A and B, respectively, and β_{AB} is resonance integral between valence orbitals of A and B. As shown in Table 4, the valence orbital energy of $\cdot TiH(OSiH_3)_2$ is calculated to be -5.56 eV, where we employ Kohn-Sham orbital energy. This is much higher than those of $\cdot CH_3$, $\cdot SiH_3$, and $\cdot OCH_3$. Because the valence orbital energy becomes lower in the order $\cdot SiH_3 > \cdot CH_3 > \cdot OCH_3$, as expected from their electronegativities, the $|\varepsilon_A - \varepsilon_B|$ value increases in the order $\cdot SiH_3 < \cdot CH_3 < \cdot OCH_3$. Thus, the Ti-$SiH_3$ bond is the weakest and the Ti-OCH_3 is the strongest in these three bonds (47). In other words, the electronegative group forms strong bond with the Ti center. Also, the Ti-H bond is much stronger than the Ti-SiH_3 bond, because the H 1s orbital is at lower energy (-8.75 eV) than the $\cdot SiH_3$ valence orbital and the $|\varepsilon_A - \varepsilon_B|$ value for the H 1s orbital is considerably larger than that for the $\cdot SiH_3$ valence orbital. Though the H 1s orbital energy is lower than the $\cdot CH_3$ valence orbital, the Ti-H bond is moderately weaker than the Ti-CH_3 bond. This is probably because the $|\beta_{AB}|$ value is larger for the Ti-CH_3 pair than that for the Ti-H pair. It is likely that the CH_3 sp^3 orbital more expands toward the Ti center than the H 1s orbital to provide the larger $|\beta_{AB}|$ value for the Ti-CH_3 pair. Though Hatree-Fock orbital energies are much different from Kohn-Sham orbital energies, the trend is the same between them (see Table 4).

The same explanation can be presented on the N-X bond energy except for the N-H bond energy. The valence orbital energy of $\cdot NH(SiH_3)$ is calculated at -9.18 eV, which is lower than the valence orbital of $\cdot H$, $\cdot CH_3$, and $\cdot SiH_3$. Because the difference in orbital energy between $\cdot CH_3$ and $\cdot NH(SiH_3)$ is the smallest, the N-CH_3 bond is the weakest in these three bonds, as seen in Table 2. Because the energy difference between valence orbital of

Table 4. Orbital energies of ·$TiH(OSiH_3)_2$, ·CH_3, ·SiH_3, ·OCH_3, ·$NH(SiH_3)$, and ·H calculated with DFT(B3LYP)/BS2 and HF/BS2.[a]

	·$TiH(OSiH_3)_2$	·CH_3	·SiH_3	·OCH_3	·$NH(SiH_3)$	·H
SOMO (Kohn-Sham)	-5.56	-7.23	-6.24	-9.33	-9.18	-8.75
SOMO (Hartree-Fock)	-10.68	-11.63	-9.29	-14.38	-12.93	-13.60

[a] In eV unit.

·$NH(SiH_3)$ and ·SiH_3 is the largest, the N-SiH_3 bond is strongest. Though the valence orbitals of ·SiH_3 and ·CH_3 are higher than that of the H atom, the N-H bond is stronger than the N-SiH_3 and N-CH_3 bonds. It is likely that this result arises from the larger $|\beta_{AB}|$ value for the N-H pair because the N-H distance is much shorter than the N-C and N-Si distances due to the small size of H atom.

From these results, we wish to present theoretical prediction that the X-H σ-bond activation by the titanium(IV)-imido complex becomes easier as the X group becomes electronegative, when the X and H are bound with the Ti and N atoms, respectively, in the product. However, the X-H σ-bond activation becomes easier as the X group becomes electropositive, when the X and H are bound with the N and Ti atoms, respectively, in the product.

2.4. Conclusions

The O-H σ-bond activation of methanol, the Si-H σ-bond activation of silane, and the Si-C σ-bond activation of methysilane by $(Me_3SiO)_2Ti(NSiMe_3)$ **R** were theoretically investigated with the DFT and MP2 to MP4(SDQ) methods. The σ-bond activations of methanol and silane (course B) occur much easier than the C-H σ-bond activation to afford the products $(Me_3SiO)_2Ti(OCH_3)[NH(SiMe_3)]$ and $(Me_3SiO)_2Ti(H)[N(SiH_3)(SiMe_3)]$, respectively. Their activation barriers (E_a) are 7.1 (14.6) kcal/mol and 2.7 (4.3) kcal/mol,

respectively, and their exothermicities are 65.8 (61.4) kcal/mol and 32.5 (34.1) kcal/mol. The very large exothermicity and moderate E_a value of the O-H σ-bond activation arise from the formation of the very strong Ti-OCH_3 bond. The very small E_a value and the considerably large exothermicity of the Si-H σ-bond activation arise from the weak Si-H bond.

The Si-C σ-bond activation, which is in general considered to be difficult, occurs with moderate activation barrier and considerably large exothermicity. These results arise from the formations of considerably strong Ti-CH_3 and N-SiH_3 bonds.

In the Si-H σ-bond activation, the other reaction course (course A) leading to the formation of $(Me_3SiO)_2Ti(SiH_3)[NH(SiMe_3)]$ was also investigated. However, the activation barrier is larger and the exothermicity is smaller than those of the course B leading to $(Me_3SiO)_2Ti(H)[N(SiH_3)(SiMe_3)]$. This result is understood in terms of the bond energy; the Ti-SiH_3 bond is considerably weaker than the Ti-H bond, while the N-SiH_3 bond is moderately stronger than the N-H bond. These results of the weak Ti-SiH_3 bond and the strong N-SiH_3 bond arise from the fact that the Si element is considerably electropositive.

From these results, we wish to theoretically propose that the titanium(IV)-imido complex can be utilized for the O-H, Si-H, and Si-C σ-bond activation reactions. In the X-H σ-bond activation (X = CH_3 and OCH_3 etc), the reaction becomes easier as the electronegativity of X increases, when the X and H are bound with the Ti center and the N atom, respectively, in the product. However, the X-H σ-bond activation becomes easier as the X becomes electropositive, when the X and H are bound with the N atom and the Ti center, respectively, in the product. Considering these results, one can construct the reaction system leading to the formation of the Ti-X species through the σ-bond activation of H-X.

References

(1) Recent reviews; (a) Arndtsen, B. A.; Bergman, R. G.; Mobley, T. A.; Peterson, T. H. *Acc. Chem. Res.* **1995**, *28*, 154. (b) Shilov, A. E.; Shul'pin, G. B. *Chem. Rev.* **1997**, *97*, 2879. (c) Jones, W. D. *Top. Organomet. Chem.* **1999**, *3*, 9. (d) Sen, A. *Top. Organomet. Chem.* **1999**, *3*, 81. (e) Crabtree, R. H. *J. Chem. Soc., Dalton.* **2001**, 2437. (f) Labingerand, J. A.; Bercaw, J. E. *Nature* **2002**, *417*, 507. (g) Sakaki, S.; Ochi, N.; Ohnishi, Y. -y. In *Computational Modeling for Homogeneous and Enzymatic Catalysis: A Knowledge-base for Designing Efficient Catalysts* Edited by Morokuma, K. and Musaev, D. G.: Wiley-VCH: Weinheim. 2008. p. 265.

(2) Saillard, J. -Y.; Hoffmann, R. *J. Am. Chem. Soc.* **1984**, *106*, 2006.

(3) (a) Obara, S.; Kitaura, K.; Morokuma, K. *J. Am. Chem. Soc.* **1984**, *106*, 7482. (b) Koga, N.; Morokuma, K. *J. Phys. Chem.* **1990**, *94*, 5454. (c) Koga, N.; Morokuma, K. *J. Am. Chem. Soc.* **1993**, *115*, 6883. (d) Matsubara, T.; Koga, N.; Musaev, D. G.; Morokuma, K. *J. Am. Chem. Soc.* **1998**, *120*, 12692.

(4) (a) Low, J. J.; Goddard III, W. A. *J. Am. Chem. Soc.* **1986**, *108*, 6115. (b) Low, J. J.; Goddard III, W. A. *Organometallics* **1986**, *5*, 609.

(5) (a) Blomberg, M. R. A.; Siegbahn, P. E. M.; Nagashima, U.; Wennerberg, J. *J. Am. Chem. Soc.* **1991**, *113*, 424. (b) Svensson, M.; Blomberg, M. R. A.; Siegbahn, P. E. M. *J. Am. Chem. Soc.* **1991**, *113*, 7076. (c) Blomberg, M. R. A.; Siegbahn, P. E. M.; Svensson, M. *J. Am. Chem. Soc.* **1992**, *114*, 6095. (d) Siegbahn, P. E. M.; Blomberg, M. R. A.; Svensson, M. *J. Am. Chem. Soc.* **1993**, *115*, 4191. (e) Blomberg, M. R. A.; Siegbahn, P. E. M.; Svensson, M. *J. Phys. Chem.* **1994**, *98*, 2062. (f) Siegbahn, P. E. M.; Blomberg, M. R. A. *Organometallics* **1994**, *13*, 354. (g) Siegbahn, P. E. M. *Organometallics* **1994**, *13*, 2833. (h) Siegbahn, P. E. M.; Svensson, M. *J. Am. Chem. Soc.* **1994**, *116*, 10124. (i) Siegbahn, P. E. M. *J. Am. Chem. Soc.* **1996**, *118*, 1487. (j) Siegbahn, P. E. M.; Crabtree, R. H. *J. Am. Chem. Soc.* **1996**, *118*, 4442.

(6) (a) Ziegler, T.; Tschimke, V.; Fan, L.; Becke, A. D. *J. Am. Chem. Soc.* **1989**, *111*, 9177. (b) Bickelhaupt, F. M.; Ziegler, T. *Organometallics* **1995**, *14*, 2288.

(7) (a) Song, J.; Hall, M. B. *Organometallics* **1993**, *12*, 3118. (b) Jimenez-Catano, R.; Hall, M. B. *Organometallics* **1996**, *15*, 1889. (c) Niu, S. -Q.; Hall, M. B. *J. Am. Chem. Soc.* **1998**, *120*, 6169.

(8) (a) Sakaki, S.; Ieki, M. *J. Am. Chem. Soc.* **1993**, *115*, 2373. (b) Sakaki, S.; Biswas, B.; Sugimoto, M. *J. Chem. Soc., Dalton Trans.* **1997**, 803. (c) Sakaki, S.; Biswas, B.; Sugimoto, M. *Organometallics* **1998**, *17*, 1278. (d) Sakaki, S.; Mizoe, M.; Musashi, Y.; Biswas, B.; Sugimoto, M. *J. Phys. Chem. A.* **1998**, *102*, 8027. (e) Biswas, B.; Sugimoto, M.; Sakaki, S. *Organometallics* **2000**, *19*, 3895. (f) Sakaki, S. *Top. Organomet. Chem.* **2005**, *12*, 31.

(9) Hinderling, C.; Feichtinger, D.; Plattner, D. A.; Chen, P. *J. Am. Chem. Soc.* **1997**, *119*, 10793.

(10) Su, M. -D.; Chu, S. -Y. *J. Am. Chem. Soc.* **1997**, *119*, 5373.

(11) Espinosa-Garcia, J.; Corchado, J. C.; Truhlar, D. G. *J. Am. Chem. Soc.* **1997**, *119*, 9891.

(12) Hill, G. S.; Puddephatt, R. J. *Organometallics* **1998**, *17*, 1478.

(13) (a) Heiberg, H.; Swang, O.; Ryan, O. B.; Gropen, O. *J. Phys. Chem. A.* **1999**, *103*, 10004. (b) Heiberg, H.; Johansson, L.; Gropen, O.; Ryan, O. B.; Swang, O.; Tilset, M. *J. Am. Chem. Soc.* **2000**, *122*, 10831.

(14) Ustynyuk, Y. A.; Ustynyuk, L. Y.; Laikov, D. N.; Lunin, V. V. *J. Organomet. Chem.* **2000**, *597*, 182.

(15) Bartlett, K. L.; Goldberg, K. I.; Borden, W. T. *Organometallics* **2001**, *20*, 2669.

(16) (a) Maron, L.; Eisenstein, O. *J. Am. Chem. Soc.* **2001**, *123*, 1036. (b) Maron, L.; Perrin, L.; Eisenstein, O. *J. Chem. Soc., Dalton Trans.* **2002**, 534. (c) Perrin, L.; Maron, L.; Eisenstein, O. *Inorg. Chem.* **2002**, *41*, 4355. (d) Barros, N.; Eisenstein, O.; Maron, L. *J. Chem. Soc., Dalton Trans.* **2006**, 3052.

(17) (a) Moritani, I.; Fujiwara, Y. *Tetrahedron Lett.* **1967**, 1119. (b) Fujiwara, Y.; Takaki, K.; Taniguchi, Y. *Synlett* **1996**, 591, and reference therein.

(18) (a) Periana, R. A.; Taube, D. J.; Evitt, E. R.; Loffler, D. G.; Wentrcek, P. R.; Voss, G.; Masuda, T. *Science* **1993**, *259*, 340. (b) Periana, R. A.; Taube, D. J.; Gamble, S.; Taube, H.; Satoh, T.; Fujii, H. *Science* **1998**, *280*, 560.

(19) Matsumoto, T.; Taube, D. J.; Periana, R. A.; Taube, H.; Yoshida, H. *J. Am. Chem. Soc.* **2000**, *122*, 7414.

(20) Siegbahn, P. E. M.; Crabtree, R. H. *J. Am. Chem. Soc.* **1996**, *118*, 4442.

(21) Biswas, B.; Sugimoto, M.; Sakaki, S. *Organometallics* **2000**, *19*, 3895.

(22) (a) Ziegler, T.; Li, J. *Organometallics* **1995**, *14*, 214. (b) Gilbert, T. M.; Hristov, I.; Ziegler, T. *Organometallics* **2001**, *20*, 1183.

(23) (a) Kua, J.; Xu, X.; Periana, R. A.; Goddard III, W. A. *Organometallics* **2002**, *21*, 511. (b) Xu, X.; Kua, J.; Periana, R. A.; Goddard III, W. A. *Organometallics* **2003**, *22*, 2057.

(24) (a) Böhme, D. K.; Schwarz, H. *Angew. Chem., Int. Ed.* **2005**, *44*, 2336. (b) Schlangen, M.; Schwarz, H. *Angew. Chem., Int. Ed.* **2007** *46*, 5614. (c) Paul, A.; Musgrave, C. B. *Organometallics* **2007**, *26*, 793.

(25) (a) Bennett, J. L.; Wolczanski, P. T. *J. Am. Chem. Soc.* **1994**, *116*, 2179. (b) Bailey, B. C.; Fan, H.; Baum, E.W.; Huffman, J. C.; Baik, M. -H.; Mindiola, D. J. *J. Am. Chem. Soc.* **2005**, *127*, 16016.

(26) (a) Cundari, T. R. J. Am. Chem. Soc. **114**, 10557 (1992); (b) Cundari. T. R. *Organometallics* **1993**, *12*, 1998. (c) Cundari, T. R. *Organometallics* **1993**, *12*, 4971. (d) Cundari, T. R. *J. Am. Chem. Soc.* **1994**, *116*, 340. (e) Benson, M. T.; Cundari, T. R.; Moody, E. W. *J. Organomet. Chem.* **1995**, *504*, 1. (f) Cundari, T. R.; Matsunaga, N.; Moody, E. W. *J. Phys. Chem.* **1996**, *100*, 6475. (g) Cundari, T. R.; Klinchkman, T. R.; Wolczanski, P. T. *J. Am. Chem. Soc.* **2002**, *124*, 1481.

(27) Bailey, B. C.; Fan, H.; Baum, E. W.; Huffman, J. C.; Baik, M. -H.; Mindiola, D. J. *J. Am. Chem. Soc.* **2005**, *127*, 16016.

(28) Ochi, N.; Nakao, Y.; Sato, H.; Sakaki, S. *J. Am. Chem. Soc.* **2007**, *129*, 8615.

(29) (a) Zhao, J.; Goldman, A. S.; Hartwig, J. F. *Science* **2005**, *307*, 1080. (b) Kanzelberger, M.; Zhang, X.; Emge, T. J.; Goldman, A. S.; Zhao, J.; Incarvito, C.; Hartwig, J. F. *J. Am. Chem. Soc.* **2003**, *125*, 13644.

(30) Becke, A. D. *Phys. Rev.* **1988**, *A38*, 3098.

(31) Becke, A. D. *J. Chem. Phys.* **1983**, *98*, 5648.

(32) Lee, C.; Yang, W.; Parr, R. G. *Phys. Rev.* **1988**, *B37*, 785.

(33) Couty, M.; Hall, M. B. *J. Comput. Chem.* **1996**, *17*, 1359.

(34) (a) Hariharan, P. C.; Pople, J. A. *Theor. Chim. Acta* **1973**, *28*, 213. (b) Hariharan, P. C.; Pople, J. A. *Mol. Phys.* **1974**, *27*, 209.

(35) Hehre, W. J.; Ditchfield, R.; Pople, J. A. *J. Chem. Phys.* **1972**, *56*, 2257.

(36) Martin, J. M. L.; Sundermann, A. *J. Chem. Phys.* **2001**, *114*, 3408.

(37) Krishnan, R.; Binkley, J. S.; Seeger, R.; Pople, J. A. *J. Chem. Phys.* **1980**, *72*, 650.

(38) McLean, A. D.; Chandler, G. S. *J. Chem. Phys.* **1980**, *72*, 5639.

(39) Blaudeau, J. -P.; McGrath, M. P.; Curtiss, L. A.; Radom, L. *J. Chem. Phys.* **1997**, *107*, 5016.

(40) Pople, J. A. et al. Gaussina 03 (Revision C.02), Gaussian, Inc., Wallingford CT 2004.

(41) Reed, A. E.; Curtiss, L. A.; Weinhold, F. *Chem. Rev.* **1988**, *88*, 899.

(42) Flükiger, P.; Lüthi, H. P.; Portann, S.; Weber, J. MOLEKEL, v.4.3; Scientific Computing: Manno, Switzerland, 2002-2002. Portman, S.; Lüthi, H. P. *CHIMIA* **54**, 766 (2000).

(43) (a) Haymore, B. L.; Maatta, E. A.; Wentworth, R. D. *J. Am. Chem. Soc.* **1979**, *101*, 2063. (b) Parkin, G.; van Asselt, A.; Leahy, D. J.; Whinnery, L.; Hua, N. G.; Quan, R. W.; Henling, L. M.; Schaefer, W. P.; Santarsiero, B. D.; Bercaw, J. E. *Inorg. Chem.*

1992, *31*, 82.

(44) Bennett, J. L.; Wolczanski, P. T. *J. Am. Chem. Soc.* **1997**, *119*, 10696.

(45) Blomberg, M. R. A.; Brandemark, U.; Siegbahn, P. E. M. *J. Am. Chem. Soc.* **1983**, *105*, 5557 .

(46) Sakaki, S.; Kai, S.; Sugimoto, M. *Organometallics* **1999**, *18*, 4825.

(47) Overlap integral also decreases in the order Ti-O ≈ Ti-C >> Ti-Si.

Chapter 3

{2 + 2} Cycloaddition of Alkyne with Titanium-Imido Complex. Theoretical Study of Determining Factor of Reactivity and Regioselectivity

3.1. Introduction

The {2 + 2} cycloaddition reaction is key elementary process in catalytic C-C coupling reaction mediated by transition metal complexes.[1] Typical examples are ring closing metathesis[2] and cross metathesis,[3, 4] which occur via {2 + 2} cycloaddition of alkene and alkyne across metal-alkylidene (M=C) bond. Because of industrial utilities, a lot of experimental works have been reported over decades.[2-12] On the other hand, the similar alkyne metathesis across metal-imido (M=N) bond has not been investigated well except for a few of pioneering works;[13-15] for instance, Bergman et al,[13] Mountford et al,[14] and Wolczanski et al[15] reported the {2 + 2} cycloaddition of alkyne across the M=N bond. Because this cycloaddition reaction leads to formation of C-N bond, this reaction is expected to be utilized for hydroamination which is important in organic synthesis.

The {2 + 2} cycloaddition of alkene across the M=C bond is also of considerable interest from the point of view of theoretical chemistry, because this reaction easily occurs in spite of the symmetry forbidden character by the Woodward-Hoffmann rule in a formal sense. In this regard, several groups theoretically investigated this reaction. Eisenstein and Hoffmann very previously investigated this reaction with extended Hückel MO method.[16] Upton et al. investigated the {2 + 2} cycloaddition with the Hartree-Fock method and reported that this reaction easily took place with small activation barrier.[17] Cundari and Gordon investigated this reaction with the Hartree-Fock method,[18] too. Ziegler and coworkers carried out the DFT study of this reaction.[19] Other groups reported

the DFT studies of this {2 + 2} cycloaddition.[20-24] On the other hand, the {2 + 2} cycloaddition across the M=N bond has not been theoretically investigated well. Only a few of pioneering works with the DFT method[25, 26] have been reported on the cycloadditions of allene and pyridine across the Ti=N bond, in which energy and geometry changes were mainly presented but neither orbital interaction nor regioselectivity was discussed.

In this work, we investigated the {2 + 2} cycloaddition of alkyne across the Ti=N bond with DFT, MP2 to MP4(SDTQ), CCSD(T), CASSCF, and MRMP2 methods. This reaction (Scheme 1) was experimentally reported to easily occur, though this is symmetry-forbidden {2 + 2} cycloaddition reaction in a formal sense.[15] Our purposes here are to present clear understanding of the electronic process of this reaction including orbital interaction, to elucidate the reason why this symmetry forbidden reaction easily occurs, and to clarify the determining factors for reactivity and regioselectivity.

3.2. Computational Details and Models

Geometries were optimized with the DFT method, where the B3LYP functional was used for exchange-correlation term.[27-29] We ascertained that each equilibrium geometry exhibited no imaginary frequency and that each transition state exhibited one imaginary frequency and the geometry changes induced by the imaginary frequency are consistent with the reaction. Two kinds of basis set system were used. The smaller system (BS1) was used for geometry optimization. Also, zero-point energy was evaluated with the DFT(B3LYP)/BS1 method under assumption of harmonic oscillator. In this BS1, core electrons of Ti (up to 2p) were replaced with effective core potentials (ECPs)[30] and its valence electrons were represented with (311111/22111/411/1) basis set.[30] For H, C, O, and N, 6-31G* basis sets were employed.[31] The better basis set system (BS2) was used for evaluation of energy changes. In this BS2, all electron basis set [21s15p10d6f]/(6s5p4d2f)[32] was employed for Ti. For the other atoms, the cc-pVDZ basis

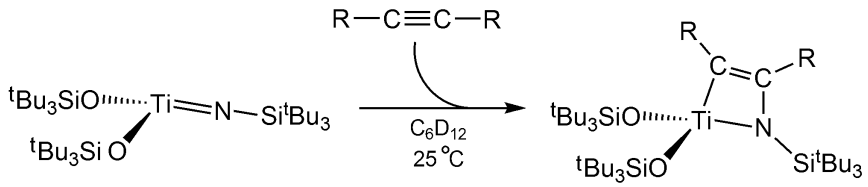

Scheme 1. The {2 + 2} cycloaddition of alkyne across the Ti=N multiple bond of $(H_3SiO)_2Ti(=NSiH_3)$ **1**.[15]

sets[33] were employed. The potential energy curves were evaluated with DFT, MP2-MP4(SDTQ), and CCSD(T) methods. The energy change with correction of zero-point energy is presented in this work. We carried out stability check of the DFT wave function in all stationary structures but found no instability in all the geometries.

In a thermal {2 + 2} cycloaddition, two reference-states are necessary at least to represent wavefunction around transition state, as shown in Scheme A1. This suggests that the multi-reference method should be applied to the thermal {2 + 2} cycloaddition. Thus, we employed CASSCF and MRMP2 methods besides the DFT, MP2 to MP4(SDTQ), and CCSD(T) methods.

Our previous DFT study reported that the optimized Ti-N distance (1.708 Å) of the model complex $[(H_3SiO)_2Ti(=NSiH_3)(THF)]$ **1(THF)** (THF = tetrahydrofuran) was somewhat shorter but the N-Si distance (1.719 Å) was moderately longer than their experimental distances of $[(^tBu_3SiO)_2Ti(=NSi^tBu_3)(THF)]$ **R(THF)** (1.783(3) Å and 1.684(3) Å, respectively).[34] We carried out geometry optimization of **1(THF)** with various computational methods, various basis sets, and several models to examine (1) effects of alkyl groups which were substituted for H atoms in **1(THF)**, (2) dependence of the optimized Ti-N distance on computational method, and (3) basis set effects on the Ti-N distance. The results are summarized, as follows; (1) the optimized geometry of **1(THF)** is little different from that of **R(THF)** except for the moderately shorter Ti-N and moderately longer N-Si distances, and (2) the DFT(B3LYP)/BS1-optimized Ti-N and Si-N

distances of **1(THF)** are little different from MRMP2- and CCSD(T)-optimized ones: see Appendix page 87-89 and Tables A1, A2, A3, A4, Scheme A2, Figures A1, A2, and A3. Based on these results, it is likely concluded that **1(THF)** is a good model of **R(THF)** and the DFT(B3LYP)/BS1 method presents reliable geometry of this reaction system.

In this theoretical work, a model system, $(H_3SiO)_2Ti(=NSiH_3)$ **1,** 2-butyne, and 1-methoxy-1-propyne were employed as a titanium-imido complex and alkyne, respectively.

The Gaussian 03 program package[35] was used for DFT calculations. The GAMESS program package[36] was used for CASSCF and MRMP2 calculations.[37] Population analysis was carried out with the method of Weinhold et al.[38] Molecular orbitals were drawn with the MOLEKEL program package.[39]

3.3. Results and Discussion

3.3.1. Geometry and Energy Changes in {2 + 2} Cycloaddition of 2-Butyne Across Titanium-imido Bond of $[(H_3SiO)_2Ti(=NSiH_3)]$ 1.

As shown in Figure 1, 2-butyne approaches the Ti center of $[(H_3SiO)_2Ti(=NSiH_3)]$ **1** to afford precursor complex (**PC1**). In **PC1**, the Ti-C^{α} and Ti-C^{β} distances are 2.393 Å and 2.527 Å, respectively, the C^{α}-C^{β} distance moderately lengthens to 1.223 Å, and the Me-C^{α}-C^{β} angle moderately bends to 172 degree; see Figure 1 for C^{α} and C^{β}. These geometrical features indicate that this species is understood to be an alkyne complex. Because Ti(IV) is d^0 system, the coordinate bond of 2-butyne is formed by the charge transfer from the π orbital of 2-butyne to the unoccupied d orbital of Ti; actually, the electron population of 2-butyne dereases by 0.141 e upon this coordination. In transition state **TS1**, the Ti-C^{α} and C^{β}-N distances shorten to 2.138 Å and 2.230 Å, respectively, the C^{α}-C^{β} and Ti-N distances moderately lengthen to 1.259 Å, and 1.745 Å, respectively, and the Me$C^{\alpha}C^{\beta}$ and $C^{\alpha}C^{\beta}$Me angles decrease to 148 and 154 degrees, respectively. The

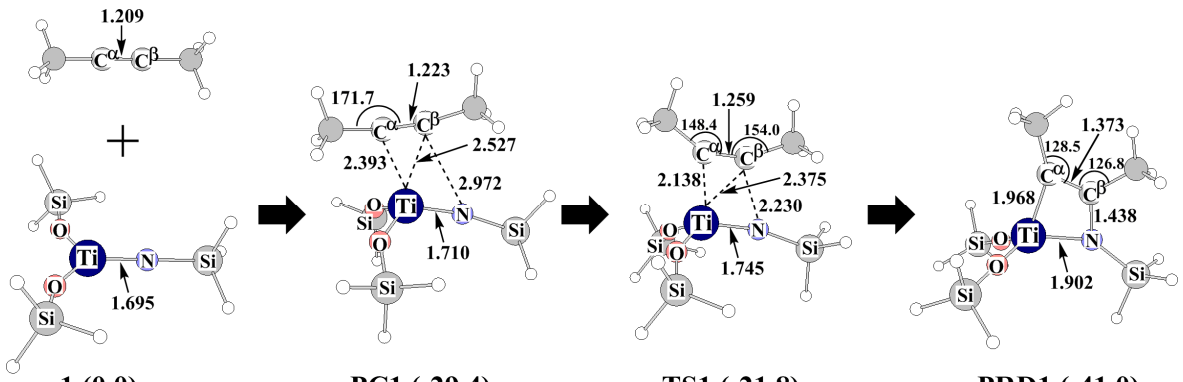

Figure 1. Geometry changes in the {2 + 2} cycloaddition of 2-butyne across the Ti=N bond of $(H_3SiO)_2Ti(=NSiH_3)$ **1**. Bond lengths are in angstroms. Energy (in kcal/mol) was evaluated with the CCSD(T)/BS2 method.

moderate elongations of the C^{α}-C^{β} and Ti-N bonds in **TS1** indicate that this transition state is reactant-like and its bonding nature can be discussed in terms of the interaction between the titanium-imido complex and alkyne; see below. Product **PRD1** contains a distorted four-membered ring in which the Ti-N and C^{α}-C^{β} bonds considerably lengthen to 1.902 Å and 1.373 Å, respectively, and the Ti-C^{α} and C^{β}-N distances become 1.968 Å and 1.438 Å, respectively.

Binding energy (*BE*), activation barrier (E_a), and reaction energy (ΔE) are defined as the energy differences between **PC1** and the sum of reactants, between **PC1** and **TS1**, and between **PRD1** and the sum of reactants, respectively. A negative ΔE value means that the reaction is exothermic and vice versa. The *BE* value little fluctuates when going to CCSD(T) from MP2, as shown in Table 1, while the DFT-calculated *BE* value is somewhat smaller than the others. These results indicate that the reliable *BE* value is calculated by the MP2 to MP4(SDTQ) and CCSD(T) methods but the DFT(B3LYP) method underestimates the *BE* value. The DFT method similarly underestimates the binding energy of transition metal complexes with π-conjugated system.[40] Also, it is noted that the E_a and ΔE values considerably fluctuate when going to CCSD(T) from MP2 and that

Table 1. Binding energy (*BE*), activation barrier (E_a), and reaction energy (ΔE) of the {2+2} cycloaddition of 2-butyne and 1-methoxy-1-propyne across the Ti=N bond of $(H_3SiO)_2Ti(=NSiH_3)$ **1**[a].

	2-butyne			1-methoxy-1-propyne (path A)			1-methoxy-1-propyne (path B)		
	BE^b	E_a^c	ΔE^d	BE^b	E_a^c	ΔE^d	BE^b	E_a^c	ΔE^d
DFT(B3LYP)	-22.4	5.8	-38.7	-25.7	2.5	-51.9	-24.0	6.3	-48.6
MP2	-30.3	9.9	-36.7	-32.4	4.7	-50.1	-31.7	10.5	-46.3
MP3	-26.3	6.8	-48.0	-28.3	2.3	-61.6	-27.1	8.7	-55.3
MP4(SDQ)	-28.5	13.2	-33.9	-30.5	7.1	-47.2	-29.9	12.5	-44.9
MP4(SDTQ)	-33.2	15.5	-27.1	-35.5	8.7	-39.9	-35.5	13.8	-41.3
CCSD(T)	-29.4	7.6	-41.0	-32.3	3.2	-54.3	-31.1	7.9	-50.9

[a] In kcal/mol unit. [b] $BE = E$(precursor complex) − E(sum of reactants). [c] $E_a = E$(transition state) − E(precursor complex).

[d] $\Delta E = E$(product) − E(sum of reactants). [e] Energy was calculated with BS2.

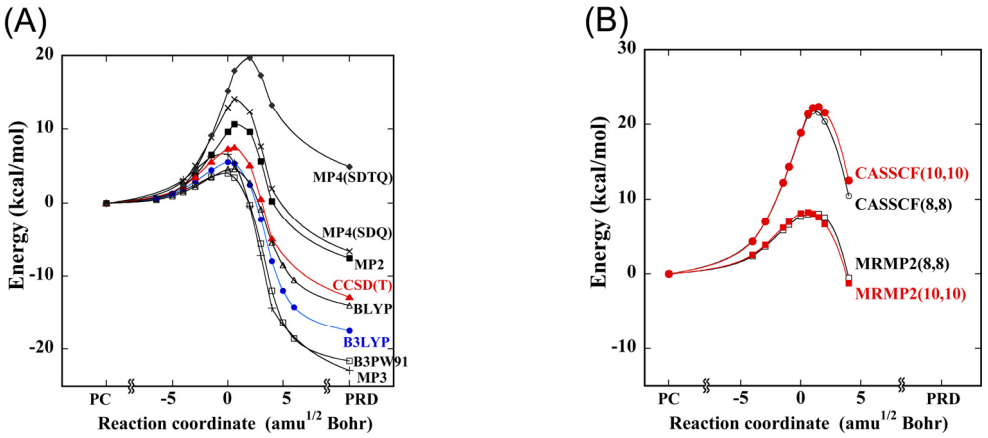

Figure 2. Potential energy curves of the {2 + 2} cycloaddition of 2-butyne across the Ti=N bond of $(H_3SiO)_2Ti(=NSiH_3)$ **1** calculated with (A) DFT(B3LYP), MP2-MP4, and CCSD(T) and (B) CASSCF and MRMP2 methods. The BS2 was employed.

MP4(SDTQ)-calculated E_a and ΔE values are much larger than the CCSD(T)-calculated values, as shown in Table 1 and Figure 2(A). These results indicate that the Møller-Plesset perturbation theory can not be applied to this reaction system; see also Appendix Table A5. The unsuccessful computational results of Møller-Plesset perturbation theory was also reported for the oxidative addition of dihydrogen molecule to nickel(0) complex which is the first-row transition metal complex like the titanium-imido complex.[41] The CCSD(T)-calculated E_a value is moderately larger and the CCSD(T)-calculated ΔE value is moderately more negative than the DFT-calculated values. These results suggest that the DFT method is not bad to investigate this type of {2 + 2} cycloaddition except for the underestimation of *BE*. Because the unsuccessful results of the Møller-Plesset perturbation theory suggest the considerable contribution of static (non-dynamic) correlation, we evaluated the E_a with CASSCF and MRMP2 methods; note that the ΔE could not be evaluated here with these methods because the active space completely changes when going to **PRD1** from **TS1**. We carried out CASSCF(8, 8) calculation with the active space including 8 electrons in such 8 molecular orbitals (MOs) as the bonding

MO (17a") between the Ti d_π and N p_π orbitals perpendicular to the Ti-C^α-C^β-N plane, its anti-bonding counterpart (20a"), the π (18a") and π* (19a") MOs of the $C^\alpha \equiv C^\beta$ triple bond perpendicular to the Ti-C^α-C^β-N plane, the π (34a') and π* (37a') MOs of the $C^\alpha \equiv C^\beta$ triple bond in the Ti-C^α-C^β-N plane, the bonding MO (35a') between the Ti d_π and N p_π orbitals into which the π* MO of the $C^\alpha \equiv C^\beta$ triple bond mixes in a bonding way with the p_π of the N, the anti-bonding MO (36a') between the Ti d_π and N p_π into which the π* of the $C^\alpha \equiv C^\beta$ triple bond mixes in a bonding way with the p_π of the N: see Figure 3. The CASSCF(10, 10) calculation with the active space including 10 electrons in 10 MOs was also carried out to check the reliability of the above active space, where the Ti d_σ-N p_σ bonding MO (33a') and its anti-bonding counterpart (38a') were added to the active space of the CASSCF(8, 8); see Figure 3. As shown in Figure 2(B), the CASSCF(8, 8) and CASSCF(10, 10) calculations present almost the same energy change, indicating that the active space of 8 electrons in 8 MOs is reasonable choice. It is noted that the MRMP2(8, 8) and MRMP2(10, 10) calculations considerably decrease the E_a to 7.9 and 8.3 kcal/mol, respectively. This result indicates the importance of dynamical correlation. These values are similar to the CCSD(T)-calculated E_a value (7.6 kcal/mol).

Based on these results, it should be concluded that the static (non-dynamical) correlation is not very large in this cycloaddition reaction and that the CCSD(T) method presents reliable E_a and ΔE values. The DFT method is also useful for discussing the E_a and ΔE, while it somewhat underestimates the *BE*.

3.3.2. The Reasons Why the {2 + 2} Cycloaddition of Alkyne Across the Titanium-imido Bond Easily Occurs

It is considerably important to understand the reason why single-reference CCSD(T) and DFT methods can be applied to the {2 + 2} cycloaddition of alkyne across the Ti=N bond in spite of its symmetry forbidden character. As shown in Figure 4, the Ti atomic

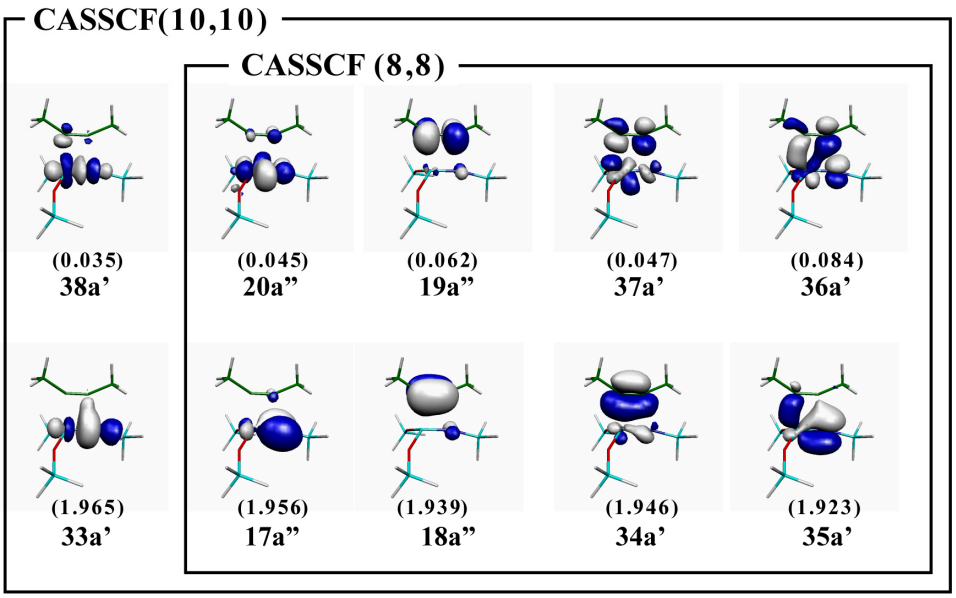

Figure 3. Important natrural orbitals of **TS1**. In parentheses are occupation numbers.

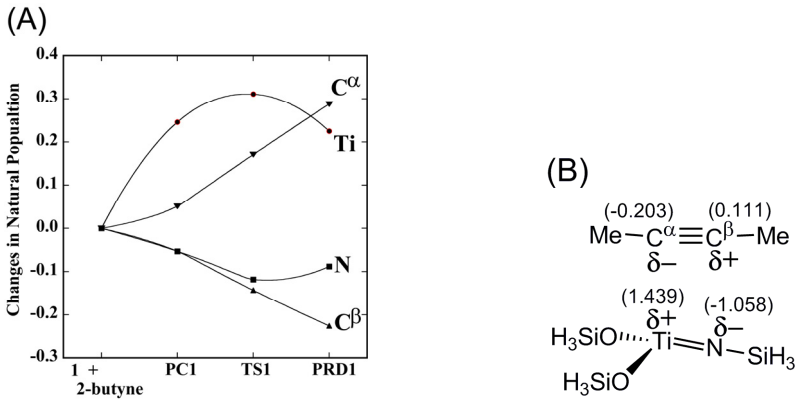

Figure 4. (A) Population changes in the {2 + 2} cycloaddition of 2-butyne across the Ti=N bond of $(H_3SiO)_2Ti(=NSiH_3)$ **1** and (B) population changes in the transition state relative to those of reactants. The positive value represents the increase in electron population, and vice versa. The DFT(B3LYP)/BS2 was employed.

population considerably increases when going to **TS1** from **1** and slightly decreases when going to **PRD1** from **TS1**. On the other hand, the N atomic population considerably decreases when going to **TS1** from **1** and slightly increases when going to **PRD1** from **TS1**. The C^{α} atomic population considerably increases but the C^{β} atomic population considerably decreases when going to **PRD1** from **1**. These results clearly indicate that the $C^{\alpha}\equiv C^{\beta}$ triple bond becomes polar when going to **TS1** from the reactant, which deeply relates to the orbital interaction, as will be discussed below.

We wish to inspect orbital interactions based on Kohn-Sham orbitals because the DFT method is useful for discussion of E_a and ΔE. As shown in Figure 5(A), the HOMO ψ_{HOMO}(TiAc) is the d_{π}-p_{π} bonding MO of the Ti-N moiety perpendicular to the Ti-N-C^{α}-C^{β} plane, where Ti and Ac represent the titanium-imido complex and alkyne, respectively. Thus, the ψ_{HOMO}(TiAc) does not directly participate in this reaction. The HOMO-1 ψ_{HOMO-1}(TiAc) involves the Ti-C^{α} bonding interaction and the HOMO-7 ψ_{HOMO-7}(TiAc) involves the C^{β}-N bonding interaction, as shown in Figures 5(B) and 5(C). It is likely that these two MOs play important roles in this cycloaddition. To inspect the orbital pictures of ψ_{HOMO-1}(TiAc) and ψ_{HOMO-7}(TiAc), we analyzed these MOs by representing them with a linear combination of MOs of fragments,[34, 42]

$$\psi_i(\mathrm{AB}) = \sum_m C_{im}^A \varphi_m(\mathrm{A}) + \sum_n C_{in}^B \varphi_n(\mathrm{B}) \qquad (1)$$

where ψ_i(AB) represents the i-th MO of the system AB, φ_m(A) is the m-th MO of the fragment A, and $C_{im}{}^A$ is the expansion coefficient of φ_m(A). Here, we separate the reaction system into the titanium-imido complex and 2-butyne. This separation is reasonable, because the transition state is reactant-like, as discussed above. The weights of important MOs of fragments are summarized in Table 2. Apparently, the ψ_{HOMO-1}(TiAc) mainly consists of the occupied d_{π}-p_{π} bonding MO $\phi_{d\pi\text{-}p\pi}$ (the 47-th MO) of the titanium-imido complex, somewhat of the π and π^* MOs of alkyne, and the unoccupied MO ϕ_{dz2} (the 49-th

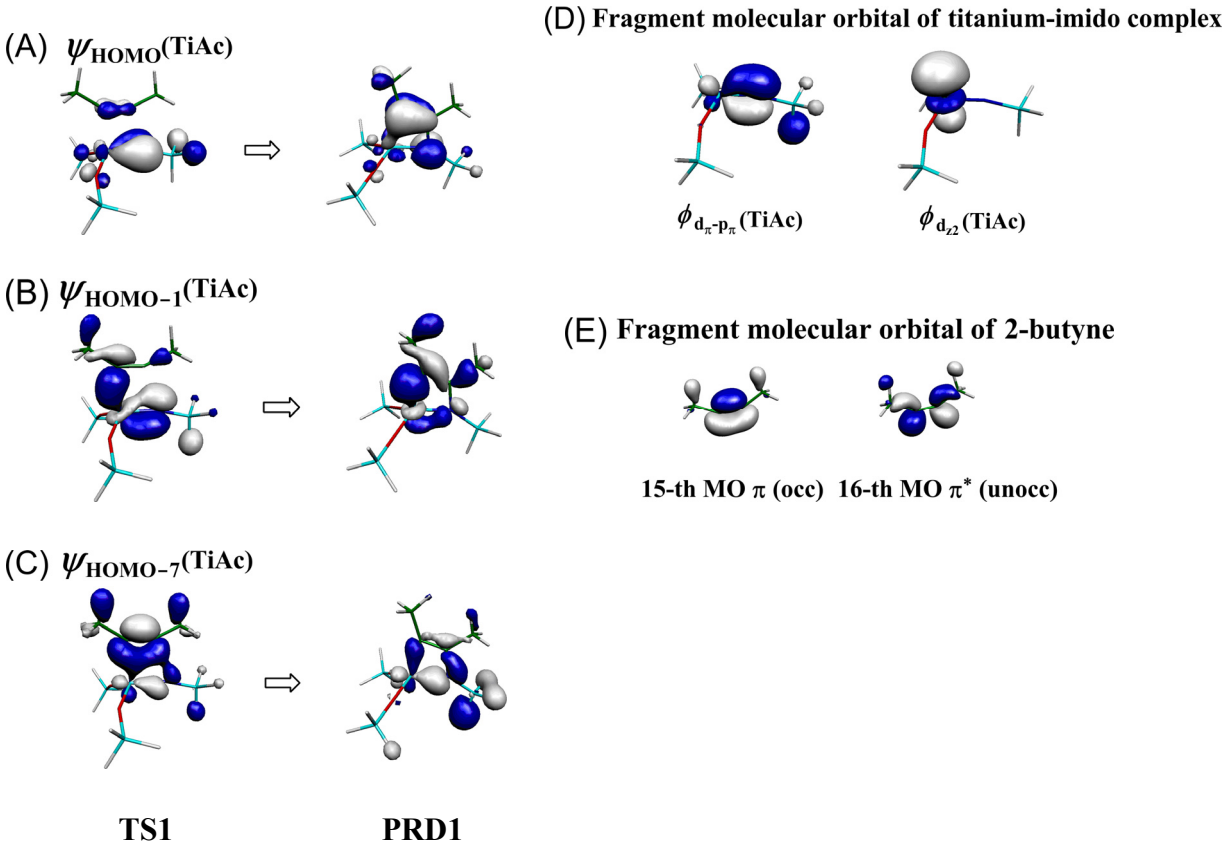

Figure 5. Important Kohn-Sham orbitals in **TS1** and **PRD1**. (A) HOMO, ψ_{HOMO}(TiAc), (B) HOMO−1, ψ_{HOMO-1}(TiAc), (C) HOMO−7, ψ_{HOMO-7}(TiAc), (D) Molecular orbitals of the titanium-imido complex, and (E) Molecular orbitals of 2-butyne.

Table 2. Contributions of fragment MOs to the ψ_{HOMO-1}(TiAc) and ψ_{HOMO-7}(TiAc)[a] of the transition state in the {2+2} cycloadditions of 2-butyne and 1-methoxy-1-propyne across the Ti=N bond of $(H_3SiO)_2Ti(=NSiH_3)$ **1**.

	2-butyne (MeC≡CMe)			1-methoxy-1-propyne (MeC≡COMe)		
		ψ_{HOMO-1}(TiAc)[b]	ψ_{HOMO-7}(TiAc)[b]		ψ_{HOMO-1}(TiAc) (path A)	ψ_{HOMO-1}(TiAc) (path B)
$(H_3SiO)_2Ti(=NSiH_3)$ **1**						
unocc.	49-th MO (d_{z2})	7.5%	6.2%	49-th MO (d_{z2})	2.3%	5.3%
occ.	47-th MO ($d_\pi - p_\pi$)	66.2%	13.3%	47-th MO ($d_\pi - p_\pi$)	82.5%	76.5%
Alkyne						
unocc.	16-th MO (π*)	13.8%	0.0%	20-th MO (π*)	10.5%	10.0%
occ.	15-th MO (π)	8.7%	57.8%	19-th MO (π)	0.1%	4.9%

[a] See Figure 5 for these MOs. [b]Geometries of fragment are fixed to these in the transition state. DFT(B3LYP)/BS2 method was employed.

MO) mainly consisting of Ti d_{z2} orbital. The $\phi_{d\pi\text{-}p\pi}$ involves the d_π-p_π bonding interaction between the occupied p_π orbital of the $NSiH_3$ group and the empty d_π orbital of Ti, as shown in Figure 5(B). The characteristic features of $\psi_{HOMO\text{-}1}$(TiAc) are summarized, as follows: Because the p_π orbital of the N much more contributes to the $\phi_{d\pi\text{-}p\pi}$ than does the d_π orbital of the Ti, the π^* MO of 2-butyne overlaps with the $\phi_{d\pi\text{-}p\pi}$ in a bonding way with the p_π orbital of the N, as shown in Scheme 2(A). As a result, the charge transfer (CT) from the Ti-N moiety to 2-butyne occurs in the $\psi_{HOMO\text{-}1}$(TiAc). Into this interaction, the π MO of 2-butyne mixes in an anti-bonding way with the p_π orbital of the N because the π MO exists at lower energy than the $\psi_{HOMO\text{-}1}$(TiAc). This anti-bonding mixing considerably increases the contribution of the C^α p_π orbital to the $\psi_{HOMO\text{-}1}$(TiAc) but considerably decreases that of the C^β p_π orbital, as shown in Scheme 2(A), leading to the polarized C^α-C^β bond. The unoccupied ϕ_{dz2} forms the CT interaction with the enlarged p_π orbital of the C^α, leading to the formation of the Ti-C^α bonding interaction, as shown in Scheme 2(B). These bonding interactions are certainly found in $\psi_{HOMO\text{-}1}$(TiAc), as shown in Figure 5(B). These polarization and CT interactions are consistent with the population changes discussed above; see Figure 4(A). Also, it is noted that this orbital interaction is essentially the same as that observed in the C-H activation of methane by the titanium-imido complex.[34]

The $\psi_{HOMO\text{-}7}$(TiAc) mainly consists of the π MO of 2-butyne, somewaht of the $\phi_{d\pi\text{-}p\pi}$ and moderately of the ϕ_{dz2} of the titanium-imido moiety, as shown in Table 2. The interactions involved in the $\psi_{HOMO\text{-}7}$(TiAc) are understood, as follows: The π MO of 2-butyne overlaps with the $\phi_{d\pi\text{-}p\pi}$ in a bonding way, into which the ϕ_{dz2} mixes in a bonding way because the ϕ_{dz2} exists at higher energy than the π MO. These orbital mixings lead to the formations of the Ti-C^α and N-C^β bonding interactions in the $\psi_{HOMO\text{-}7}$(TiAc), as schematically shown in Scheme 2(C) and Figure 5(C).

In the usual {2 + 2} cycloaddition of two ethylene molecules, the π-π bonding overlap between two π MOs is formed at the next HOMO $\psi_{HOMO\text{-}1}(\pi + \pi)$ and the π-π

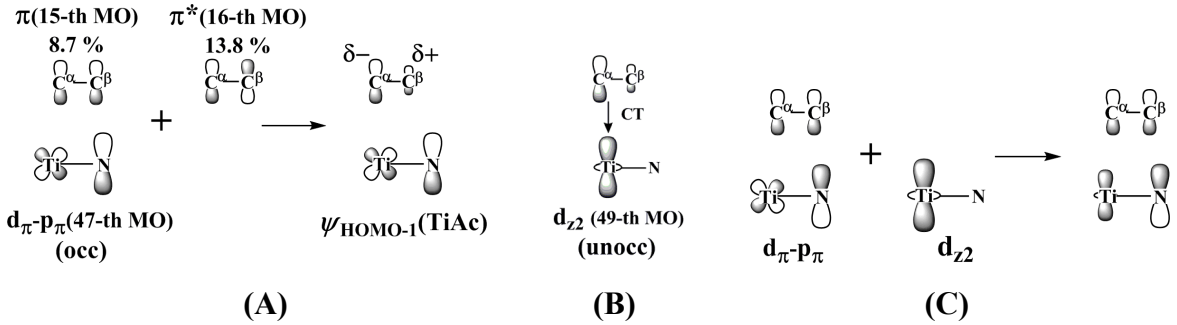

Scheme 2. Schematic pictures of orbital interaction in the ψ_{HOMO-1}(TiAc).

anti-bonding overlap between two π MOs is formed at the HOMO $\psi_{HOMO}(\pi - \pi)$, as schematically shown in Scheme A3, where π + π and π − π represent bonding and antibonding overlaps of π MOs of two ethylene molecules. This π-π bonding overlap corresponds to the ψ_{HOMO-7}(TiA*c*), here. However, the ψ_{HOMO-1}(TiAc) is completely different from the $\psi_{HOMO}(\pi - \pi)$ of the usual {2 + 2} cycloaddition of two ethylene molecules. Because the $\psi_{HOMO}(\pi - \pi)$ gives rise to the symmetry forbidden character of the usual {2 + 2} cycloaddition (see Scheme A3), the different feature of ψ_{HOMO-1}(TiAc) from that of $\psi_{HOMO}(\pi - \pi)$ is responsible for the decrease of the symmetry forbidden character, which leads to the moderate activation barrier of this cycloaddition. The most important feature in the ψ_{HOMO-1}(TiAc) is that the π* MO of alkyne overlaps with the $\phi_{d\pi\text{-}p\pi}$ of the Ti-N bond in a bonding way with the p_π orbital of the N, into which the π MO of alkyne mixes in an antibonding way with the p_π of the N. These orbital mixings induce significantly large polarization of the C-C triple bond and considerably reduce the symmetry forbidden character in the ψ_{HOMO-1}(TiAc).

In conclusion, the highly polarized d_π-p_π bonding MO in the titanium-imido complex induces the unsymmetrical mixings of the π and π* MOs of alkyne into the $\phi_{d\pi\text{-}p\pi}$ of the titanium-imido moiety, which considerably decreases the symmetrical forbidden character of this cycloaddition reaction. As a result, this cycloaddition easily occurs with moderate

activation barrier.

3.3.3. Reactivity and Rgioselectivity of the {2 + 2} Cycloaddition of Unsymmetrically Substituted Alkyne:

It is expected that the orbital mixing in the ψ_{HOMO-1}(TiAc) much more easily occurs when the π and π* MOs of alkyne are polarized. To inspect the effects of polarized π and π* MOs of alkyne, we investigated the {2 + 2} cycloaddition of 1-methoxy-1-propyne ($MeC^{\alpha}\equiv C^{\beta}OMe$) across the Ti=N bond of **1**. In this cycloaddition, two reaction courses must be investigated. In path A, the C^{α} and the C^{β} approach the Ti and the N, respectively; see Scheme 3 for C^{α} and C^{β}. In path B, the C^{α} and the C^{β} approach the N and the Ti, respectively. We investigated both reaction courses. Like the cycloaddition of 2-butyne, the cycloaddition of 1-methoxy-1-propyne occurs through precursor complex (**PC2a** and **PC2b**) and transition state (**TS2a** and **TS2b**) to afford product complex (**PRD2a** and **PRD2b**); see Figure A4. Because the geometry changes are similar to those of the reaction of 2-butyne, detailed discussion is omitted here.

The activation barrier of the path A is 3.2 kcal/mol, which is considerably smaller than that (7.6 kcal/mol) of the reaction of 2-butyne, where the CCSD(T)-calculated values are presented. That of the path B is 7.9 kcal/mol, which is slightly larger than that of the reaction with 2-butyne. In the DFT calculation, the activation barrier of the path B is somewhat larger than that of the reaction of 2-butyne. These results clearly indicate that the introduction of methoxy group accelerates the {2 + 2} cycloaddition across the Ti=N bond. It is noted that the difference in activation barrier between paths A and B is significantly large. This difference leads to the very large regioselectivity; the ratio of **PRD2a** to **PRD2b** is estimated to be about 100 at 298 K under assumption that the activation entropy change is similar between these two paths, indicating that only **PRD2a** is formed as a product.

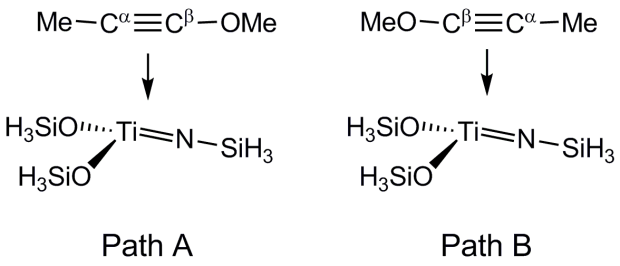

Scheme 3. Two reaction courses of the cycloaddition of 1-methoxy-1-propyne

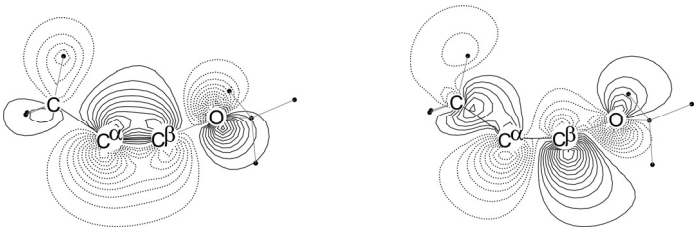

19-th MO (π) 20-th MO (π*)

Figure 6. π and π* orbital of 1-methoxy-1-propyne taking distorted geometry in the transition state. The DFT(B3LYP)/BS2 method was employed.

It is worth investigating the origin of this regioselectivity. As shown in Figure 6, the p_π orbital of the C^α more contributes to the π MO of this alkyne than that of the C^β, while the p_π orbital of the C^β more contributes to the π* MO than that of the C^α. Because of this polarized π* MO, the $\phi_{d\pi\text{-}p\pi}$ of the titanium-imido complex overlaps larger with the π* MO in the path A than in the path B; remember that the C^β approaches the N in the path A. Also, the CT from the π MO to the unoccupied ϕ_{dz2} occurs stronger in the path A than in the path B, because the p_π orbital of the C^α is larger in the π MO than that of the C^β. All these features are completely opposite to those of the path B. As a result, the {2 + 2} cycloaddition of 1-methoxy-1-propyne occurs with smaller activation barrier in the path A than in the path B.

There results clearly indicate the polarized d_π-p_π bonding MO of the Ti=N bond and the polarized π and π* MOs of alkyne are key factors for the reactivity and regioselectivity of the {2 + 2} cycloaddition. Also, it is expected that the activation barrier decreases as these d_π-p_π, π, and π* MOs become polar.

3.4. Conclusions

We theoretically investigated the {2 + 2} cycloaddition of 2-butyne across the Ti=N bond of $[(H_3SiO)_2Ti(=NSiH_3)]$ **1**. The Møller-Plesset perturbation theory can not be applied to this reaction but the CCSD(T) and MRMP2 present reliable results. The DFT method presents also similar results to those of CCSD(T) except for the considerable underestimation of *BE*.

Though this reaction is symmetry forbidden by the Woodward-Hoffmann rule in a formal sense, this cycloaddition easily occurs with moderate activation barrier (7.6 kcal/mol) and considerably large exothermicity (41.0 kcal/mol), where the CCSD(T)-calculated values are presented. To clarify the reason, we inspected the ψ_{HOMO-1}(TiAc) in the transition state, because this MO plays important roles in the cycloaddition reaction. The ψ_{HOMO-1}(TiAc) mainly consists of the d_π-p_π bonding MO $\phi_{d\pi\text{-}p\pi}$ of the Ti=N bond and somewhat of the π and π* MOs of alkyne: Because the p_π orbital of the N largely and the d_π orbital of the Ti moderately participate in the $\phi_{d\pi\text{-}p\pi}$, the π* MO of alkyne interacts with the $\phi_{d\pi\text{-}p\pi}$ so as to form large bonding overlap with the p_π orbital of the N, into which the π MO of 2-butyne mixes in an anti-bonding way with the p_π orbital of the N. As a result, the ψ_{HOMO-1}(TiAc) becomes considerably different from the HOMO of {2 + 2} cycloaddition of two ethylene molecules and the symmetry forbidden character becomes considerably weak in the ψ_{HOMO-1}(TiAc); in other words, this cycloaddition occurs easily because the d_π-p_π bonding MO is very polarized.

Also, we investigated the {2 + 2} cycloaddition of 1-methoxy-1-propyne

(MeC$^{\alpha}$≡C$^{\beta}$OMe), where two reaction courses were examined; in path A, the C$^{\alpha}$ and the C$^{\beta}$ approach the Ti and the N, respectively, and in path B, the C$^{\alpha}$ and the C$^{\beta}$ approach the N and the Ti, respectively. The activation barrier of the path A is considerably smaller but that of the path B is slightly larger than that of 2-butyne. The p_{π} orbital of the C$^{\alpha}$ more contributes to the π MO of 1-methoxy-1-propyne than that of the C$^{\beta}$, while the p_{π} orbital of the C$^{\beta}$ more contributes to the π* MO than that of the C$^{\alpha}$. The polarized π* MO of this alkyne leads to the formation of larger overlap between the π* MO of this alkyne and the $\phi_{d\pi\text{-}p\pi}$ of the titanium-imido complex in the path A than in the path B. The polarized π MO of alkyne is also more favorable for the CT from the π to the unoccupied ϕ_{dz2} of the Ti in the path A than in the path B. As a result, the path A is more favorable than the path B in the {2 + 2} cycloaddition of 1-methoxy-1-propyne, indicating that the regioselective cycloaddition can be performed by introducing π-electron donating group on one C atom. It is theoretically predicted that the C atom bearing the π-electron donating group is bound with the N atom and the other C atom is bound with the Ti atom. The regioselectivity is expected to be very large.

3.5. Appendix

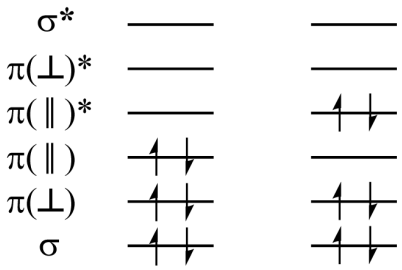

Scheme A1. Schematic representation of important electron-configurations. See Figure A2 for these orbitals.

3.5.1. The Computational Method Applied to the Present System

In the geometry optimization of **1(THF)**, we investigated (1) effects of alkyl groups which were substituted for H atoms in **1(THF)**, (2) dependence of the optimized Ti-N distance on computational method, and (3) basis set effects.

First, we employed methyl (Me) and *tert*-butyl (^{t}Bu) groups as alkyl group (R) of $[(R_3SiO)_2Ti(=NSiR_3)(THF)]$ (see Scheme A2). As shown in Table A1, the Ti-N distance little changes upon going from **1(THF)** (R=H) to **2(THF)** (R=Me) but moderately lengthens to 1.730 Å upon going to the real complex **R(THF)** (R=^{t}Bu). The N-Si distance somewhat lengthens to 1.761 Å from 1.719 Å upon going to **R(THF)** from **1(THF)**; Apparently, the discrepancy in the N-Si distance becomes larger in **R(THF)** than in **1(THF)**. These results indicate that substituent effect is not responsible for the discrepancy. Also, the Ti-N and N-Si distances of **1(THF)** little depend on the basis sets, as shown in Table A2, where we employed triple-zeta quality basis sets for Ti and double- and triple-zeta quality basis sets for the other atoms.

The geometry of **1(THF)** was optimized with pure functional BLYP and hybrid functional B3PW91, where the BS1 was employed. Although the BLYP-optimized Ti-N distance (1.730 Å) is slightly closer to the experimental value than the B3LYP-optimized one, as shown in Table A3, and the BLYP-optimized N-Si distance (1.732 Å) is considerably longer than the experimental value; in other words, the discrepancy in the N-Si distance increases. To examine the possibility that the neglect of dispersion interaction between ligands gives rise to the longer N-Si distance which further leads to shorter Ti-N distance, we employed MP2 method in geometry optimization. However, the MP2-optimized N-Si distance becomes longer and the MP2-optimized Ti-N distance (1.711 Å) is similar to that of B3LYP.

We were also afraid of the possibility that the longer N-Si bond leaded to the shorter Ti-N bond. To optimize the Ti-N distance with the correct N-Si distance, the N-Si distance

was taken to be the same as experimental value (1.685 Å) and the potential energy curves (PECs) were evaluated against the Ti-N distance with various computational methods, as shown in Figure A1, where the BS2 was employed and the geometry of the other moiety was optimized with the DFT(B3LYP)/BS1 method. Although the PECs of hybrid functionals B3PW91 and PBE1PBE are similar to that of B3LYP, the PEC by BLYP is somewhat different. The optimized Ti-N distance is 1.715 Å, 1.691 Å, and 1.699 Å, and 1.740 Å at B3LYP, B3PW91, PBE1PBE and BLYP levels, respectively, as shown in Table A4.[1] All of them are somewhat shorter than the experimental value. Though the Ti-N distance by the BLYP optimization is better than the others, the N-Si distance by the BLYP optimization is much longer than the experimental value (Table A4), indicating that BLYP can not be applied to this complex. As shown in Figure A1(B), the PECs considerably fluctuate upon going to MP4(SDTQ) from MP2; The optimized Ti-N distance is 1.723 Å, 1.682 Å, 1.752 Å, 1.845 Å, and 1.729 Å at MP2, MP3, MP4(SDQ), MP4(SDTQ), and CCSD(T) levels, respectively. Although the optimized Ti-N distance approaches the experimental value upon going to MP4(SDQ) from MP2, the discrepancy in the Ti-N distance considerably increases upon going from MP4(SDQ) to MP4(SDTQ). Also, the MP4(SDTQ)-calculated value is considerably different from the CCSD(T)-calculated value. These results indicate that the Møller-Plesset perturbation method cannot be applied to this compound; in other words, electron correlation effect is very large in this compound.

In CASSCF(6, 6) calculation, six electrons in such six orbitals as σ, $\pi(\parallel)$, $\pi(\perp)$, σ^*, $\pi(\parallel)^*$, and $\pi(\perp)^*$ were involved in active space; see Figure A2 for these orbitals. The BS2 was employed in CASSCF and MRMP2 calculations. As shown in Figure A1(C), the Ti-N distance is optimized to be 1.698 Å and 1.726 Å, respectively, by CASSCF and MRMP2 methods. These bond distances are somewhat shorter than the experimental value. As shown in Scheme A1, the configuration 1 is the Hartree-Fock configuration and the second leading term, configuration 2, involves two-electron excitation from $\pi(\parallel)$ to $\pi(\parallel)^*$.

Though the weight of configuration 1 moderately decreases and that of configuration 2 moderately increases with lengthening of the Ti-N distance, as shown in Figure A3, the weight of the configuration 1 is always larger than 90 %, and that of the configuration 2 is always smaller than 3 %. Consistent with these results, the occupation number of the π(∥) orbital moderately decreases but that of the π(∥)* orbital moderately increases, as the Ti-N distance becomes longer; see Figure A3. It is also noted that the CCSD(T)-optimized Ti-N distance (1.729 Å) is almost the same as the MRMP2-optmized distance (1.726 Å).

Because all of CCSD(T), MRMP2, and DFT(B3LYP) methods present somewhat shorter Ti-N distance than the experimental one, it is likely that the significant discrepancy between optimized and experimental Ti-N distances arises from another factor such as crystal packing. In fact, the PECs calculated by CCSD(T), MRMP2, and DFT(B3LYP) are considerably shallow, indicating that the Ti-N distance easily changes with moderate influence from surrounding atmosphere; for instance, the energy difference between the optimized and experimental Ti-N distance is very small, 1.0 , 1.0, 1.8 kcal/mol, by CCSD(T), MRMP2, and DFT(B3LYP) calculations, respectively.

These results indicate that the Møller-Plesset perturbation theory can not be applied to this complex, the static correlation effect is not very large, and the CCSD(T) method as well as MRMP2 and DFT(B3LYP) methods present reliable results.

Table A1. Important optimized geometrical parameters of several model complexes.[a]

	1(THF)	**2(THF)**	**R(THF)**[b]	Experiment[c]
R	H	Me	^{t}Bu	^{t}Bu
Ti-N [Å]	1.708	1.714	1.730	1.783(3)
N-Si	1.719	1.730	1.761	1.685(3)
Ti-O^{1}	1.845	1.843	1.867	1.821(2)
Ti-O^{2}	1.845	1.843	1.867	1.827(3)
Ti-O^{3}	2.067	2.078	2.098	2.037(2)
Ti-N-Si [degree]	171.3	170.9	178.7	174.9(2)
Ti-O^{1}-Si	149.8	152.5	174.4	175.6(2)
Ti-O^{2}-Si	149.5	151.0	175.1	172.6(2)

[a] The DFT(B3LYP)/BS1 was employed. [b] The ONIOM method was employed. [c] Ref. 3.

Table A2. Basis set effect on important optimized geometrical parameters of model complex $[(H_3SiO)_2Ti(=NSiH_3)(THF)]$ **1(THF)**.

	BS1	BS2	BS3	BS4	Experiment[d]
Ti	ECP[a]+(311111/22111/411/1)	[6s5p4d2f][b]	[6s5p4d2f][b]	ECP[c]+(5311/5311/311/1)	
C, Si	6-31G*	cc-pVDZ	cc-pVTZ	6-311G*	
N, O	6-31G*	cc-pVDZ	cc-pVTZ	6-311G*	
H	6-31G	cc-pVDZ	cc-pVTZ	6-311G	
Ti-N [Å]	1.708	1.711	1.709	1.708	1.783(3)
N-Si	1.719	1.728	1.718	1.719	1.685(3)
$Ti-O^1$	1.845	1.853	1.854	1.845	1.821(2)
$Ti-O^2$	1.845	1.850	1.852	1.845	1.827(3)
$Ti-O^3$	2.067	2.085	2.080	2.067	2.037(2)
Ti-N-Si [degree]	171.3	172.8	172.3	171.3	174.9(2)
$Ti-O^1-Si$	149.8	149.5	154.3	149.8	175.6(2)
$Ti-O^2-Si$	149.5	149.5	154.7	149.5	172.6(2)

[a] Ref. 3. [b] Ref. 4. [c] Ref. 5. [d] Ref. 3.

Table A3. Comparison between DFT- and MP2-optimized geometrical parameters[a] of **1(THF)**.

	BLYP	B3PW91	MP2	Expt.[c]
Ti-N [Å]	1.730	1.701	1.711	1.783(3)
N-Si	1.732	1.717	1.747	1.685(3)
Ti-O^{1} [b]	1.860	1.840	1.866	1.821(2)
Ti-O^{2} [b]	1.860	1.839	1.853	1.827(3)
Ti-O^{3} [b]	2.084	2.061	2.059	2.037(2)
Ti-N-Si [degree]	171.3	171.2	174.0	174.9(2)
Ti-O^{1}-Si	148.0	146.5	135.2	175.6(2)
Ti-O^{2}-Si	148.4	147.2	145.9	172.6(2)

[a] BS1 was used. [b] see Scheme 2 for O^{1}, O^{2}, and O^{3}. [c] Ref. 3.

Table A4. Comparison of the Ti-N distance optimized by various computational methods.[a]

	Ti-N bond distance (Å)
B3LYP	1.715
B3PW91	1.691
PBE1PBE	1.699
BLYP	1.740
HF	1.681
MP2	1.723
MP3	1.682
MP4(SDQ)	1.752
MP4(SDTQ)	1.845
CCSD(T)	1.729
CASSCF(6,6)	1.698
MRMP2(6,6)	1.726
Expt.[b]	1.783(3)

[a] Only the Ti-N distance was optimized, where the N-Si distance was taken to be the same as the experimental value (1.685 Å)[3] and the geometry of the other moiety was optimized with the DFT(B3LYP)/BS1 method. [b] Ref. 3.

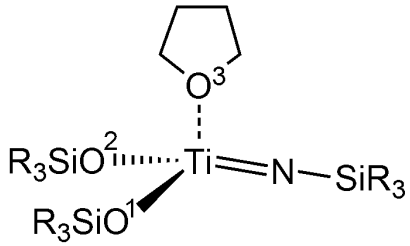

Scheme A2. Titanium complex $[(R_3SiO)_2Ti(=NSiR_3)(THF)]$ (THF = tetrahydrofuran) (**1(THF)** for R = H, **2(THF)** for R = Me, and **R(THF)** for R = ^{t}Bu)

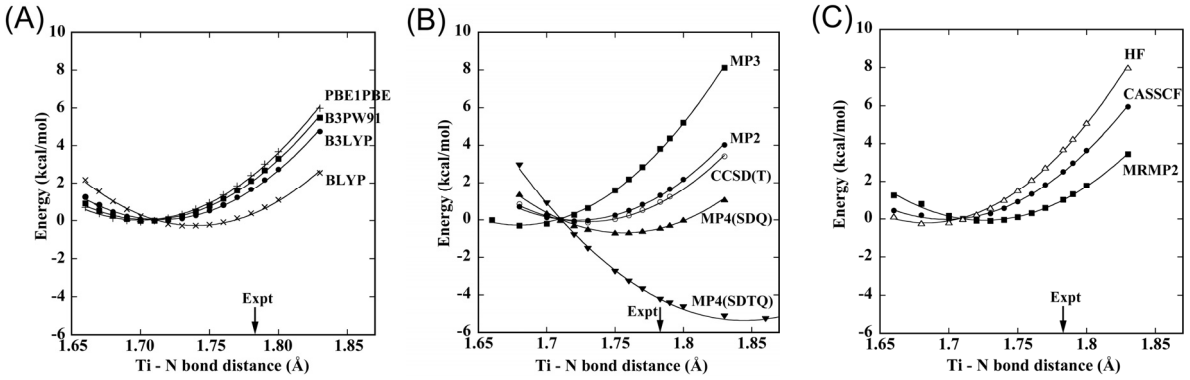

Figure A1. Potential energy curves against the Ti-N bond distance in the Ti imido complex **1(THF)** calculated with (A) DFT method with various functional, (B) MP2-MP4 and CCSD(T) methods, and (C) CASSCF and MRMP2 methods.[a] Arrow means the experimental Ti-N bond distance. [a]Only the Ti-N distance was optimized, where the N-Si distance was taken to be the same as the experimental value (1.685 Å)[3] and the geometry of the other moiety was optimized with the DFT(B3LYP)/BS1 method. [b] Ref. 3.

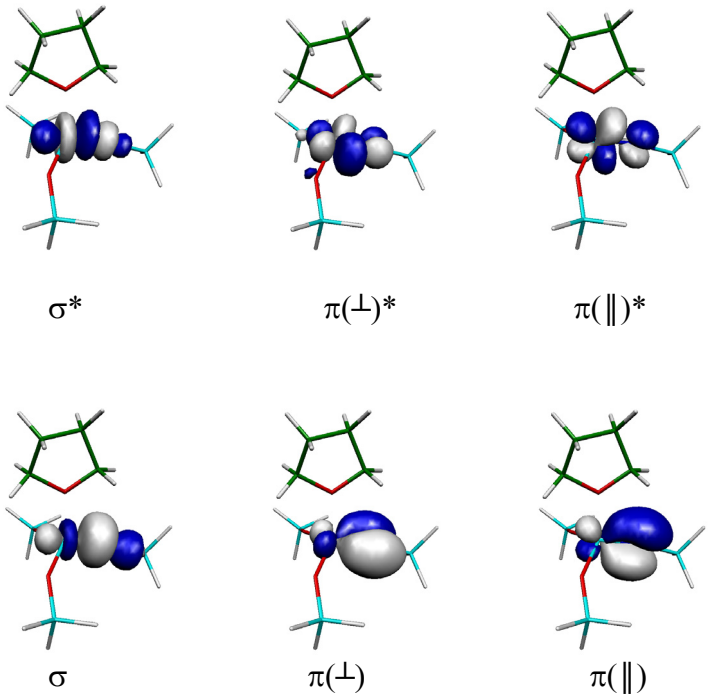

Figure A2. Natural orbitals in CASSCF(6, 6) calculation.

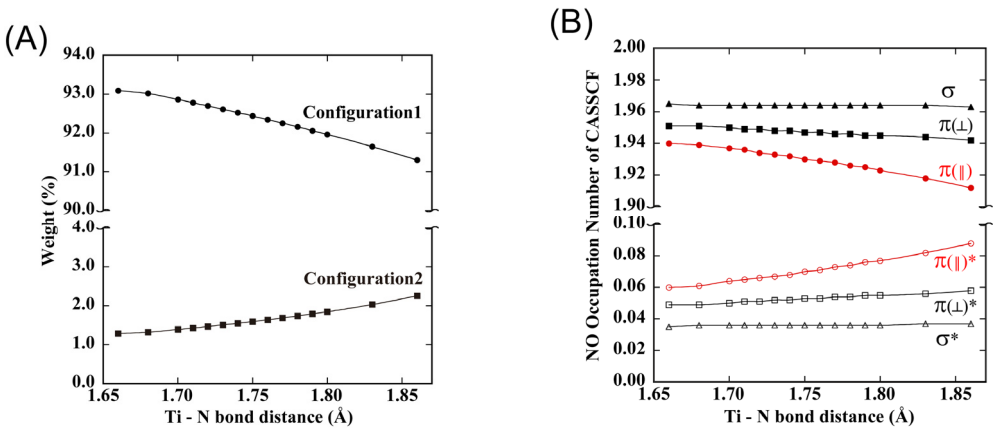

Figure A3. (A) Weights of several important configurations of CASSCF(6, 6) calculation and (B) natural orbital occupation number.

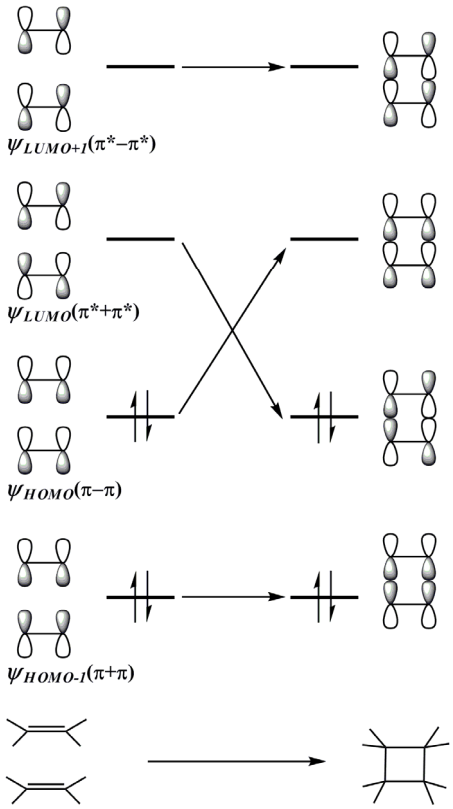

Scheme A3. Orbital interactions in the {2 + 2} cycloaddition of two ethylene molecules. The signs of + and – represent bonding and anti-bonding pairs of orbitals, respectively.

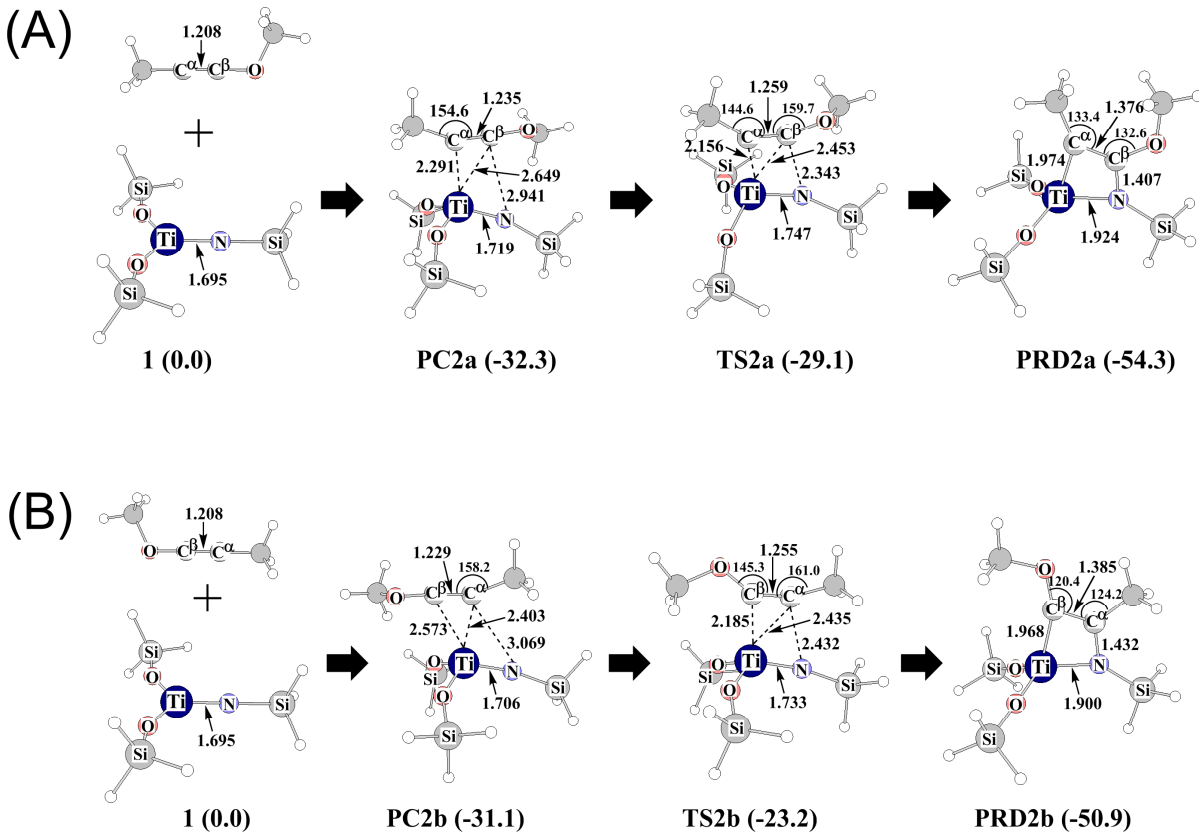

Figure A4. Geometry changes in the {2 + 2} cycloaddition of 1-methoxy-1-propyne across the Ti=N bond of $(H_3SiO)_2Ti(=NSiH_3)$ **1** through (A) path A and (B) path B. Bond lengths are in angstroms. Energy (in kcal/mol) was evaluated with the CCSD(T)/BS2 method.

Table A5. The correlation energies (in Hartree) at the 2'nd to 4-th orders of the MP method

	2nd order correction	3rd order correction	4th order correction
1	-1.0167755	0.0062743	-0.1547410
PC1	-1.5776286	-0.0205675	-0.0870091
TS1	-1.5815247	-0.0254486	-0.0767809
PRD1	-1.5570557	-0.0449779	-0.0611021
PC2a	-1.7574462	-0.0189657	-0.2042901
TS2a	-1.7606399	-0.0227100	-0.1941516
PRD2a	-1.7335868	-0.0437561	-0.1582813
PC2b	-1.7585257	-0.0182187	-0.2062425
TS2b	-1.7645077	-0.0211557	-0.1980997
PRD2b	-1.7393415	-0.0399014	-0.1704491

Reference

(1) Schrock, R. R. *Chem. Rev.* **2002**, *102*, 145.

(2) (a) Fu, G. C.; Grubbs, R. H. *J. Am. Chem. Soc.* **1992**, *114*, 5426; (b) Fu, G. C.; Grubbs, R. H. *J. Am. Chem. Soc.* **1992**, *114*, 7324; (c) Fu, G. C.; Grubbs, R. H. *J. Am. Chem. Soc.* **1993**, *115*, 3800; (d) Fujimura, O.; Fu, G. C.; Grubbs, R. H. *J. Org. Chem.* **1994**, *59*, 4029; (e) Grubbs, R. H.; Miller, S. J.; Fu, G. C. *Acc. Chem. Res.* **1995**, *28*, 446 and references therein.

(3) Crowe, W. E.; Zhang, Z. J. *J. Am. Chem. Soc.* **1993**, *115*, 10998.

(4) (a) Schlund, R.; Schrock, R. R.; Crowe, W. E. *J. Am. Chem. Soc.* **1989**, *111*, 8004; (b) Schrock, R. R.; Murdzek, J. S; Bazan, G. C.; Robbins, J.; DiMare, M.; O'Regan, M. *J. Am. Chem. Soc.* **1992**, *112*, 3875.

(5) Schrock, R. R. *Acc. Chem. Res.* **1990**, *23*, 158.

(6) (a) Herndon, J. W. *Coord. Chem. Rev.* **1999**, *181*, 177; (b) Herndon, J. W. *Coord. Chem. Rev.* **2000**, *209*, 387; (c) Herndon, J. W. *Coord. Chem. Rev.* **2001**, *214*, 215 and references therein.

(7) Niu, X.; Gopal, L.; Masingale, M. P.; Braden, D. A.; Hudson, B. S.; Sponsler, M. B. *Organometallics* **2000**, *19*, 649.

(8) Conrad, J. C.; Amoroso, D.; Czechura, P.; Yap, G. P. A.; Fogg, D. E. *Organometallics* **2003**, *22*, 3634.

(9) Bolton, S. L.; Schuehler, D. E.; Niu, X.; Gopal, L.; Sponsler, M. B. *J. Organomet. Chem.* **2006**, *691*, 5298.

(10) Iyer, K.; Rainier, J. D. *J. Am. Chem. Soc.* **2007**, *129*, 12604.

(11) Nomura, K.; Onishi, Y.; Fujiki, M.; Yamada, J. *Organometallics* **2008**, *27*, 3818.

(12) Grisi, F.; Costabile, C.; Gallo, E.; Mariconda, A.; Tedesco, C.; Longo, P. *Organometallics* **2008**, *27*, 4649.

(13) (a) Walsh, P. J.; Baranger, A. M.; Bergman, R. G. *J. Am. Chem. Soc.* **1992**, *114*, 1708;

(b) Poise, J. L.; Anderson, R. A.; Bergman, R. G. *J. Am. Chem. Soc.* **1998**, *120*, 13405; (c) Anderson, L. L.; Schmidt, J. A. R.; Arnold, J.; Bergman, R. G. *Organometallics* **2006**, *25*, 3394.

(14) Vujkovic, N.; Ward, B. D.; Maisse-Francois, A.; Wadepohl, H.; Mountford, P.; Gade, L. H. *Organometallics* **2007**, *26*, 5522.

(15) Bennett, J. L.; Wolczanski, P. T. *J. Am. Chem. Soc.* **1997**, *119*, 10696.

(16) Eisenstein, O.; Hoffmann, R. *J. Am. Chem. Soc.* **1981**, *103*, 5582.

(17) (a) Rappé, A. K. ; Upton, T. H. *Organometallics* **1984**, *3*, 1440 ; (b) Upton, T. H.; Rappé, A. K. *J. Am. Chem. Soc.* **1985**, *107*, 1206.

(18) Cundari, T. R.; Gordon, M. S. *Organometallics* **1992**, *11*, 55.

(19) (a) Folga, E.; Ziegler, T. *Organometallics* **1993**, *12*, 325; (b) Woo, T. K.; Folga, E.; Ziegler, T. *Organometallics* **1993**, *12*, 1289; (c) Monteyne, K.; Ziegler, T. *Organometallics* **1998**, *17*, 5901.

(20) Cavallo, L. *J. Am. Chem. Soc.* **2002**, *124*, 8965.

(21) Bernardi, F.; Bottoni, A.; Miscione, G. P. *Organometallics* **2003**, *22*, 940.

(22) Suresh, C. H.; Koga, N. *Organometallics* **2004**, *23*, 76.

(23) Lippstreu, J. J.; Straub, B. F. *J. Am. Chem. Soc.* **2005**, *127*, 7444.

(24) Wu, Y.; Peng, Z. *J. Am. Chem. Soc.* **1997**, *119*, 8043.

(25) Straub, B. F.; Bergman, R. G. *Angew. Chem., Int. Ed* **2001**, *40*, 4632.

(26) Bailey, B. C.; Fan, H.; Huffman, J. C.; Baik, M.-H.; Mindiola, D. J. *J. Am. Chem. Soc.* **2006**, *128*, 6798.

(27) Becke, A. D. *Phys. Rev.* **1988**, *A38*, 3098.

(28) Becke, A. D. *J. Chem. Phys.* **1983**, *98*, 5648.

(29) Lee, C.; Yang, W.; Parr, R. G. *Phys. Rev.* **1988**, *B37*, 785.

(30) D. Andrae, U. Haeussermann, M. Dolg, H. Stoll, H. Preuss, *Theor. Chim. Acta.* **1990**, *77*, 123.

(31) (a) Hehre, W. J.; Ditchfield, R.; Pople, J. A. *J. Chem. Phys.* **1972**, *56*, 2257; (b) Hariharan, P. C.; Pople, J. A. Theor. Chim. Acta. 1973, 28, 213; (c) Hariharan, P. C.; Pople, J. A. *Mol. Phys.* **1974**, *27*, 209.

(32) Pou-Amérigo, R.; Merchán, M.; Widmark, P.-O.; Roos, B.O. *Theor. Chim. Acta.* **1995**, *92*, 149.

(33) (a) Dunning, T. H. Jr. J Chem Phys 1989, 90, 1007; (b) Woon, D. E.; Dunning, T. H. Jr. *J. Chem. Phys.* **1993**, *98*, 1358.

(34) Ochi, N.; Nakao, Y.; Sato, H.; Sakaki, S. *J. Am. Chem. Soc.* **2007**, *129*, 8615.

(35) Pople, J. A., et al. Gaussian 03, revision C.02; Gaussian, Inc.: Wallingford, CT, 2004.

(36) Schmidt, M. W.; Baldridge, K. K.; Boatz, J. A.; Elbert, S. T.; Gordon, M. S.; Jensen, J. H.; Koseki, S.; Matsunaga, N.; Nguyen, K. A.; Su, S.; Windus, T. L.; Dupuis, M.; Montgomery, J. A. *J. Comput. Chem.* **1993**, *14*, 1347.

(37) Nakano, H. J. Chem. Phys. 1993, 99, 7983; (b) Hirao, K. *Chem. Phys. Lett.* **1992**, *190*, 374.

(38) Reed, A. E.; Curtiss, L. A.; Weinhold, F. Chem. Rev. 1988, 88, 899.

(39) Flükiger, P.; Lüthi, H. P.; Portann, S.; Weber, J. MOLEKEL, v.4.3; Scientific Computing: Manno, Switzerland, 2002-2002. Portman, S.; Lüthi, H. P. CHIMIA **2000**, *54*, 766.

(40) (a) Kameno, Y.; Ikeda, A.; Nakao, Y.; Sato, H.; Sakaki, S. *J. Phys. Chem. A* **2005**, *109*, 8055; (b) Ikeda, A.; Nakao, Y.; Sato. H. *J. Phys. Chem. A* **2007**, *111*, 7124. (c) Ikeda, A.; Kameno, Y.; Nakao, Y.; Sato, H.; Sakaki, S. *J. Organomet. Chem.* **2007**, *692*, 299.

(41) Ohnishi, Y.-y.; Nakao, Y.; Sato, H.; Sakaki, S. *J. Phys. Chem. A* **2007**, *111*, 7915.

(42) Similar methods were reported in several literatures: (a) Kato, S.; Yamabe, S.; Fukui, K. *J. Chem. Phys.* **1974**, *60*, 572. (b) Dapprich, S.; Frenking, G. *J. Phys. Chem.* **1995**, *99*, 9352.

Chapter 4

New Palladium(II) Complex of P,S-Containing Hybrid Calixphyrin. Theoretical Study of Electronic Structure and Reactivity for Oxidative Addition

4.1. Introduction

Calixphyrin[1] is porphyrin analogue which contains several pyrroles bridged by sp^2- and sp^3-hybridized meso carbon atoms, as shown in Scheme 1A. This macrocyclic compound attracts considerable attention in porphyrin chemistry, host-guest chemistry, and coordination chemistry,[2-5] because its π-conjugation is partially interrupted by the sp^3-hybridized meso carbon, which leads to conformational flexibility of the macrocyclic frame.[6] Core-modified porphyrin is also promising, in which the nitrogen atoms of pyrrole moieties are substituted for heteroatoms such as phosphorus and sulfur atoms.[7] Considering these two promising porphyrin analogues, heteroatom-containing hybrid calixphyrins (see Scheme 1B) are expected to provide both unprecedented properties and conformational flexibility. However, reports of heteroatom-containing hybrid calixphyrins have been limited so far.[8] Also, the transition metal complex of heteroatom-containing hybrid calixphyrin and its reaction were not reported until the pioneering work reported recently by Matano et al.[9] They succeeded in the synthesis of a series of P,S-containing hybrid calixphyrins that contain phosphole, thiophene, and pyrrole rings bridged by sp^2- and sp^3-hybridized meso carbons, as shown in Scheme 1C. These P,S-containing hybrid calixphyrins are expected to play a role of ligand for transition metal element, because phosphorus-, sulfur-, and nitrogen-containing macrocyclic mixed-donor ligands provide characteristic chelating sites that are difficult to construct with their acyclic analogues.[10,11] Actually, they form palladium and rhodium complexes.[9b] Interestingly, the palladium complex of P,S-containing hybrid calixphyrin

Scheme 1[a]

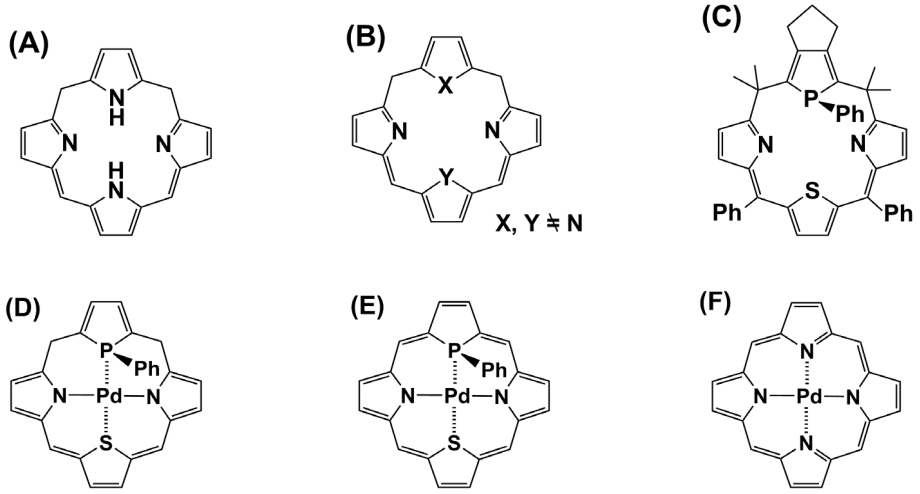

[a] These species mean (A) calixphyrin, (B) heteroatom-containing hybrid calixphyrin, (C) P,S-containing hybrid calixphyrin, (D) palladium model complex of P,S-containing hybrid calixphyrin **1**, (E) palladium complex of P,S-containing hybrid porphyrin **2**, and (F) palladium complex of conventional porphyrin **3**.

catalyzes the Heck reaction which is one of typical Pd-catalyzed reactions.[9a] Considering that even the palladium(0) species are not very reactive for oxidative addition,[12] the catalysis of this palladium complex for the Heck reaction is of considerable interest because the first step of this reaction is the oxidative addition. Several theoretical studies of core-modified porphyrins have been reported. Delaere and Nguyen investigated the groundstate electronic structure of unsubstituted monophospha- and diphosphaporphyrins with the DFT method and predicted the red-shifts of Q- and B-bands with the TD-DFT method.[13] Matano et al. investigated the aromaticity of core-modified porphyrins[14] and its transition metal complexes[15] with the DFT method. However, no theoretical study of heteroatom-containing hybrid calixphyrins and their transition metal complexes has been reported yet. In this theoretical study, we investigated the electronic structure of the palladium complex of a P,S-containing hybrid calixphyrin and the oxidative addition of phenyl bromide (PhBr) to its

Pd center. Our purposes here are to clarify the electronic structure of this palladium complex, to elucidate how and why this palladium complex is reactive for the oxidative addition of PhBr, and to show the difference in the reactivity for the oxidative addition among palladium complexes of P,S-containing hybrid calixphyrin (Scheme 1D), P,S-containing hybrid porphyrin (Scheme 1E), and conventional porphyrin (Scheme 1F). We emphasize that this is the first theoretical study of a transition metal complex of heteroatom-containing hybrid calixphyrin and its reaction.

4.2. Computational Details

The DFT method with the B3LYP functional[16] was used in this work, where two kinds of basis set system were used. In the smaller system (BS1) used for geometry optimization, core electrons of Pd (up to 3f) were replaced with effective core potentials (ECPs),[17] and its valence electrons were represented with (311111/22111/411) basis set.[17] For H, C, N, O, P, Cl, and S, 6-31G* basis sets were employed,[18] where an anion function was added to each N and Cl because these atoms are anionic in the palladium complex of P,S-containing hybrid calixphyrin. For Br, the 6-311+G* basis set was employed, because the basis set effect is somewhat large in Br.[20] We ascertained that the combination of BS1 and B3PW91 presents reliable results in geometry optimization; see Tables A1-A3 in Appendix.[21] In the better basis set system (BS2) used for evaluation of energy changes, two f polarization functions were added to Pd with the same ECPs as those of BS1.[17,22] For Br, the same basis set as that of BS1 was employed, and for H, C, N, O, P, Cl, and S, the 6-311G* basis sets[23] were employed, where an anion function was added to each N and Cl.[19,23] The DFT/BS2-calculated enthalpy changes are given in this work, where vibrational frequencies were evaluated with the DFT/BS1 method. In a model employed for calculation, four methyl groups on two sp^3-carbon atoms and two phenyl groups on two meso carbon atoms of P,S-containing hybrid calixphyrin (Scheme 1C) were replaced with six H atoms, and the

five-member ring fused with phosphole was replaced with two H atoms, because the P,S-containing hybrid calixphyrin is too large to optimize the transition state of reaction. The palladium complex of this model is named **1** hereafter; see Scheme 1D. Palladium complexes of the P,S-containing hybrid porphyrin and the conventional porphyrin are named **2** and **3**, respectively; see Schemes 1E and 1F. We selected **2** and **3** because they involve a P,S-containing well-conjugated macrocycle and a conventional porphyrin framework, respectively. The Gaussian 03 program package[24] was used for all calculations. Population analysis was carried out with the method of Weinhold et al.[25] Molecular orbitals were drawn with the MOLEKEL program package.[26]

4.3. Results and Discussion

4.3.1. Geometry and Electronic Structure of the Palladium Complex of P,S-Containing Hybrid Calixphyrin 1.

As shown in Scheme 2, there are two kinds of valence tautomer in the palladium complex of P,S-containing hybrid calixphyrin **1**: one is a Pd(II) form (Scheme 2A), in which the calixphyrin moiety possesses −2 charges and the Pd center takes +2 oxidation state in a formal sense, and the other is a Pd(0) form (Scheme 2B), in which the calixphyrin moiety is neutral and the Pd center takes zero oxidation state. We investigated the electronic structure and the Pd oxidation state of **1**. The optimized geometry of **1** agrees well with the experimental one reported by Matano et al.,[9a] as shown in Figure 1. Interestingly, the C^1-C^2 and C^3-C^4 distances are slightly longer than the C^2-C^3 distance in the pyrrole moiety, and the C^6-C^7 and C^8-C^9 distances are considerably longer than the C^7-C^8 distance in the thiophene moiety. Also, the C^4-C^5 distance is considerably longer than the C^5-C^6 distance. Optimized geometries of neutral P,S-containing hybrid calixphyrin **calix** and its dianion **calix**$^{2-}$ are also shown in Figure 1. Significantly large differences are observed in C^1-C^2, C^2-C^3, C^4-C^5, and C^5-C^6 bond distances between **calix** and **calix**$^{2-}$; for instance, the C^1-C^2

Scheme 2[a]

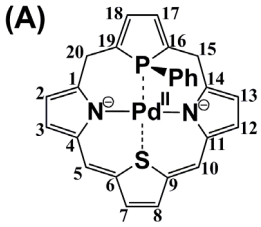

Pd(II) form

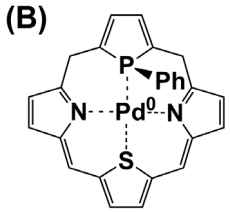

Pd(0) form

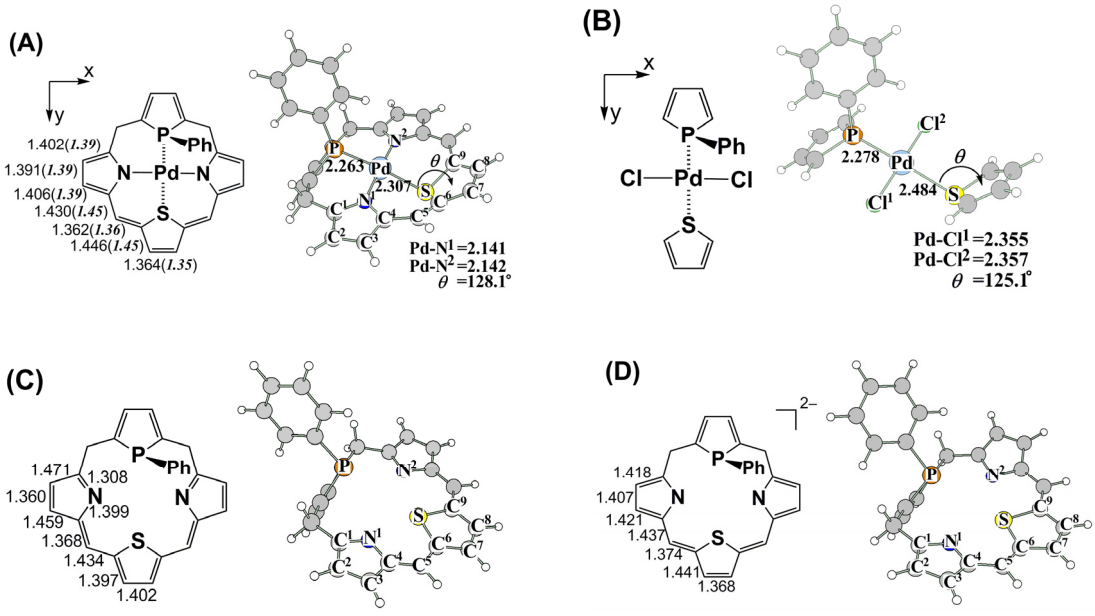

Figure 1. Optimized geometries of (A) palladium complex of P,S-containing hybrid calixphyrin **1**, (B) typical Pd(II) dichloro phosphole thiophene complex $\mathbf{1_M}$, (C) P,S-containing hybrid calixphyrin **calix**, and (D) its dianion $\mathbf{calix^{2-}}$. Bond lengths are in angstrom and angles are in degree. In parentheses are experimental values.[9c] The geometries of **1**, **calix**, and $\mathbf{calix^{2-}}$ are close to *Cs* symmetry.

distance is much longer in **calix** than in **calix**$^{2-}$, while the C^2-C^3 distance is much shorter in **calix** than in **calix**$^{2-}$. Also, the C^4-C^5 distance is much shorter than the C^5-C^6 distance in **calix** (Figure 1C) but much longer than the C^5-C^6 distance in **calix**$^{2-}$ (Figure 1D). It is noted that the geometry of the calixphyrin moiety in **1** is similar to that of **calix**$^{2-}$. These geometrical features of **1** suggest that the hybrid calixphyrin moiety possesses −2 charges and the Pd center takes +2 oxidation state in **1**; in other words, **1** takes the Pd(II) form. To inspect the oxidation state of the Pd center, we compared natural atomic orbital (NAO) occupancy of the Pd center between **1** and typical Pd(II) model complex, *trans*-$PdCl_2(C_4H_4S)(PPhC_4H_4)$ $\mathbf{1_M}$ (see Figure 1B), as shown in Table 1. The Pd oxidation state of $\mathbf{1_M}$ is +2 because of the presence of two Cl ligands. In $\mathbf{1_M}$, the NAO occupancy of d_{x2-y2} is 1.237 e and those of the other d_{xy}, d_{xz}, d_{yz} and d_{z2} are 1.973 e, 1.996 e, 1.968 and 1.957 e, respectively, which are close to 2.0 e. In **1**, the NAO occupancy of d_{x2-y2} is 1.233 e and those of the d_{xy}, d_{xz}, d_{yz}, and d_{z2} are 1.960 e, 1.976 e, 1.963 e, and 1.935 e, respectively. These d-orbital populations of **1** are similar to those of $\mathbf{1_M}$, suggesting that the Pd center takes +2 oxidation state in **1**. To investigate the electronic structure of **1** in more detail, molecular orbitals (MOs) of **1** are represented by linear combination of MOs of fragments, Pd, and **calix**, as follows:

$$\psi_i(\mathrm{AB}) = \sum_m C^A_{im}\varphi_m(\mathrm{A}) + \sum_n C^B_{in}\varphi_n(\mathrm{B}) \qquad (1)$$

$$\rho_m(\mathrm{A}) = \sum_i^{occ}\left[{C^A_{im}}^2 + \sum_n C^A_{im}C^B_{in}S_{mn} \right] \qquad (2)$$

where the ψ_i(AB) is the ith MO of AB system such as **1**, φ_m(A) is the mth MO of fragment A such as the Pd atom, and φ_n(B) is the nth MO of fragment B such as **calix**. C^A_{im} and C^B_{in} are expansion coefficients of the φ_m(A) and the φ_n(B), respectively. The Mulliken-type

Table 1. Natrual atomic orbital (NAO) occupancies of $\mathbf{1_M}$ and **1** evaluated with Weinhold's method.[26]

		NAO Occupancy		Mulliken population[b]
		$\mathbf{1_M}$	**1**	**1**
Pd	d_{xy}	1.973	1.960	1.934
	d_{xz}	1.996	1.976	1.926
	d_{yz}	1.968	1.963	1.949
	d_{z2}	1.957	1.935	1.915
	d_{x2-y2}	1.237	1.233	1.099
Calixphyrin	π* (LUMO)	–	–	1.464

[a] The DFT(B3LYP)/BS2 was employed. [b] Mulliken population was estimated by eq. 2 and 3.

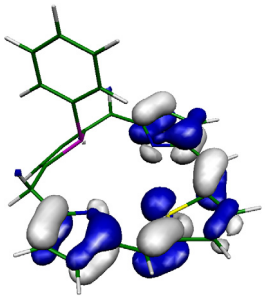

π* (LUMO)

Figure 2. The π* (LUMO) orbital of P,S-containing hybrid calixphyrin fragment of **1**. The surface value is 0.04.

population ρ_m(A) represents how much electron population the φ_m(A) possesses in the total system AB. This value is evaluated by eq 2, where the S_{mn} is the overlap integral between the φ_m(A) and the φ_n(B). As shown in Table 1, the Mulliken-type populations of the Pd d-orbital resemble well the NAO occupancies. It is noted that the Pd d_{x2-y2} orbital population is much smaller than the other d-orbitals such as $\mathbf{1_M}$, indicating that the Pd center takes +2 oxidation state (d^8 electron configuration) in a formal sense. Though the π*

(LUMO; see Figure 2) of neutral calixphyrin is unoccupied in free **calix**, its population is considerably large (1.464 e) in **1**, as shown in Table 1, indicating that the calixphyrin moiety in **1** takes a dianion form. However, the electron population of the LUMO is considerably smaller than the formal value of 2.0 for **calix**$^{2-}$. This is because its electron population decreases by the charge transfer from the LUMO to the Pd d^{x2-y2} orbital.[27] These results are consistent with the geometrical features discussed above. From all these results, it should be concluded that the calixphyrin moiety is dianion and the Pd center takes +2 oxidation state in **1**.

4.3.2. Geometry and Energy Changes in the Oxidative Addition of Phenyl Bromide (PhBr) to the Palladium Complex of P,S-Containing Hybrid Calixphyrin 1.

Although the oxidation state of Pd is +2 in **1**, the Heck reaction whose first step is the oxidative addition of PhBr to the Pd center is catalyzed by **1**.[9a] It is of considerable interest how and why the oxidative addition of PhBr to **1** occurs easily. There are several possible approaching courses of PhBr to the Pd center, as shown in Scheme 3. In one course, PhBr approaches the Pd center on the same side of the phenyl group of the calixphyrin moiety, which is called the "upward course". In the other course, PhBr approaches the Pd center on the opposite side of the phenyl group, which is called the "downward course". In the upward course, PhBr approaches the Pd center in two ways: in one way (up-I), Ph and Br approach the positions trans to the S and P atoms, respectively. In the other (up-II), they approach the positions trans to the P and S atoms, respectively. The two similar approaching ways in the downward course are named down-I and down-II. First, we will discuss the geometry changes in the up-I. PhBr approaches the Pd center of **1** to afford precursor complex **1PCa**, in which the Pd−Br distance is significantly long and the C−Br bond distance of PhBr is almost the same as that of free PhBr. These geometrical features indicate that the

Scheme 3

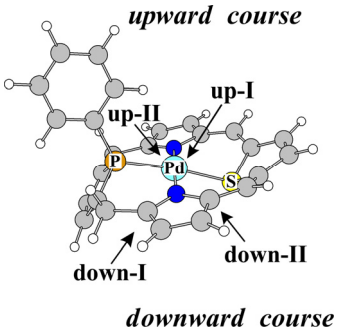

PhBr weakly interacts with the Pd center. Starting from **1PCa**, the PhBr further approaches the Pd center to afford intermediate **1INTa** through transition state **1TSa-I**, as shown in Figure 3A. Because the geometry of **1INTa** resembles well that of **1TSa-I**, **1TSa-I** is understood to be product-like, which is consistent with the fact that this process is considerably endothermic and the activation enthalpy is similar to the enthalpy change of reaction (see below). In **1TSa-I**, the Pd−Br distance decreases to 2.878 Å, which is much shorter than that of **1PCa**, and the Pd−N^1 distance moderately lengthens to 2.253 Å and the Pd−N^2 distance considerably lengthens to 2.970 Å. The distance (*h*) between the Pd center and the N^1−S−N^2 calixphyrin plane increases to 0.989 Å; in other words, the Pd center considerably moves upward above the N^1−S−N^2 plane. These geometrical features indicate that the interaction between the Pd center and the calixphyrin is becoming weak in **1TSa-I**. When going from **1PCa** to **1INTa**, the *h* distance considerably increases to 2.107 Å from −0.044 Å and the Pd−Br distance further shortens to 2.604 Å from 4.814 Å. The Pd−S, Pd−N^1, and Pd−N^2 distances considerably lengthen to 2.695 Å, 3.239 Å, and 3.244 Å from 2.308 Å, 2.141 Å, and 2.143 Å, respectively, while the Pd−P distance slightly shortens and the C−Br distance changes little in **1INTa**. These results indicate that pyrrole moieties do not coordinate to the Pd center and the hybrid calixphyrin plays a role of bidentate ligand in **1INTa**. Starting from **1INTa**, the C−Br σ-bond cleavage occurs through transition state

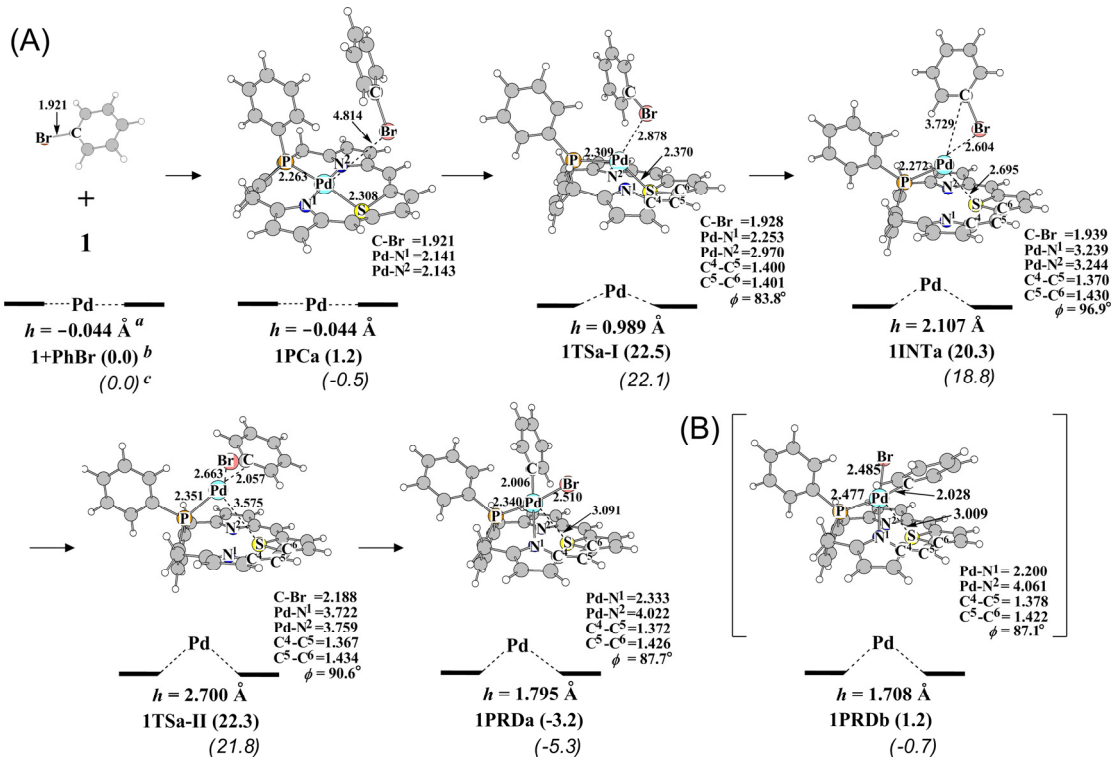

Figure 3. Geometry changes in the oxidative addition of PhBr to the palladium complex of P,S-containing hybrid calixphyrin **1** through the up-I reaction course. Bond lengths are in angstrom and bond angles are in degree. [a] In parentheses are the relative energies (kcal/mol unit) to **1** + PhBr, where the DFT(B3LYP)/BS2 method was employed. [b] The *h* indicates the distance between Pd center and N^1−S−N^2 plane.

1TSa-II to afford product **1PRDa**, as shown in Figure 3A. In **1TSa-II**, the C−Br distance of PhBr is elongated to 2.188 Å, which is moderately longer than that of **1INTa**. The Pd−C and Pd−Br distances decrease to 2.057 Å and 2.663 Å, respectively, which are considerably shorter than those of **1INTa** and similar to those of **1PRDa**. Also, the Pd−N^1, Pd−N^2, and Pd−S distances become considerably long but the Pd−P distance changes little. These geometrical features indicate that **1TSa-II** is understood to be a typical three-center transition state including a Pd monodentate phosphine ligand. In **1PRDa**, the Ph group and the Br atom take the positions trans to the N^1 atom and the phosphole moiety, respectively. The

Pd−N^1 distance becomes considerably short (2.333 Å), which is the usual Pd−N coordinate bond distance. Thus, **1PRDa** is understood to be a four-coordinate complex.[28] We will omit detailed discussion of the geometry changes in the up-II but mention several important differences in geometry changes; see Appendix Figure A1 for geometry changes in the up-II. In the product **1PRDb** of this course, Ph and Br exist at the positions trans to the phosphole and the pyrrole, respectively, as shown in Figure 3B. It is noted that the Pd−P bond distance is much longer in **1PRDb** than in **1PRDa** but the Pd−N^1 distance is much shorter in **1PRDb** than in **1PRDa**. These results indicate that the trans-influence effect of Ph is stronger than that of Br; note that the Ph group is at the position trans to the pyrrole in **1PRDa** but trans to the phosphole in **1PRDb**. Also, the Pd−Br distance is much longer in **1PRDa** than in **1PRDb**, indicating that the trans-influence effect of phosphole is stronger than that of pyrrole; note that the Br exists at the position trans to the phosphole in **1PRDa** but at the position trans to the pyrrole in **1PRDb**. Thus, **1PRDb** is less stable than **1PRDa**, as will be discussed below, because the Ph and the phosphole both possessing strong trans-influence effect exist at the positions trans to each other in **1PRDb** but at the positions cis to each other in **1PRDa**. The large difference is not, however, observed between **1TSa-II** and **1TSb-II**; see Figure 3 and Figure A1. This is because the Ph−Br bond cleavage has not been completed in **1TSa-II** and **1TSb-II**, and therefore the Ph moiety does not exhibit strong trans-influence effect yet. Also, **1TSa-I** is little different from **1TSb-I** in energy, because of the small trans-influence effect of PhBr; remember that the C−Br bond cleavage is not involved in **1TSa-I** and **1TSb-I**. In the downward courses, we skip detailed discussion except for the difference in geometry changes of the up-I and up-II, because the down-I and down-II are less favorable than the up-I and up-II, respectively. One of the important differences between the upward reaction courses and the downward ones is that the Pd center moves downward below the N^1−S−N^2 plane unlike in the up-I and up-II courses; see Appendix Figures A2 and A3 for the geometry changes. Except for this difference, the oxidative addition of PhBr occurs similarly to that of

the up-I and up-II courses. Activation enthalpy ($\Delta H^{o\ddagger}$) and enthalpy change of reaction (ΔH^{o}) were calculated as the enthalpy difference between **1TSn-I** (n = a, b, c, or d) and the sum of reactants and that between **1PRDn** and the sum of reactants, respectively, because **1TSn-I** is more unstable than **1TSn-II** and the **1PCn** is slightly less stable than the sum of reactants in enthalpy (see Figures 3, A1, A2, and A3). The negative ΔH^{o} value represents that the reaction is exothermic. The $\Delta H^{o\ddagger}$ value is moderate, 22.3 and 23.0 kcal/mol for the up-I and up-II, respectively, as shown in Table 2, though it is considerably large, 40.0 kcal/mol and 40.6 kcal/mol for the down-I and down-II, respectively. From these results, it should be concluded that the upward courses are much easier than the downward courses. The reason why the upward courses are easier than the downward ones is interpreted in terms of the position change of the Pd center; see Appendix pages 137-139. In summary, the oxidative addition of PhBr to **1** occurs through the up-I with moderate activation enthalpy. Although the activation enthalpy is little different between the up-I and up-II, the up-I is more favorable than the up-II from the thermodynamic viewpoint.

4.3.3. Changes in Electronic Structure Induced by the Oxidative Addition of PhBr to 1.

It is of considerable interest to clarify the electronic process of the oxidative addition of PhBr to **1**. First, we investigated the electron population changes in this reaction, as shown in Figure 4A. Several characteristic features are summarized, as follows: (1) The Pd d-orbital population slightly decreases when going from **1** to **1PCa** and then considerably increases when going to **1INTa** from **1PCa**. Going from **1INTa** to **1PRDa**, the d-orbital population considerably decreases, and finally it becomes almost the same as that of **1**. (2) The electron population of the calixphyrin slightly increases when going from **1** to **1PCa** but considerably decreases when going to **1PRDa** from **1PCa**. (3) Although the electron populations of Ph and Br little change upon going to **1INTa** from **1PCa**, their populations

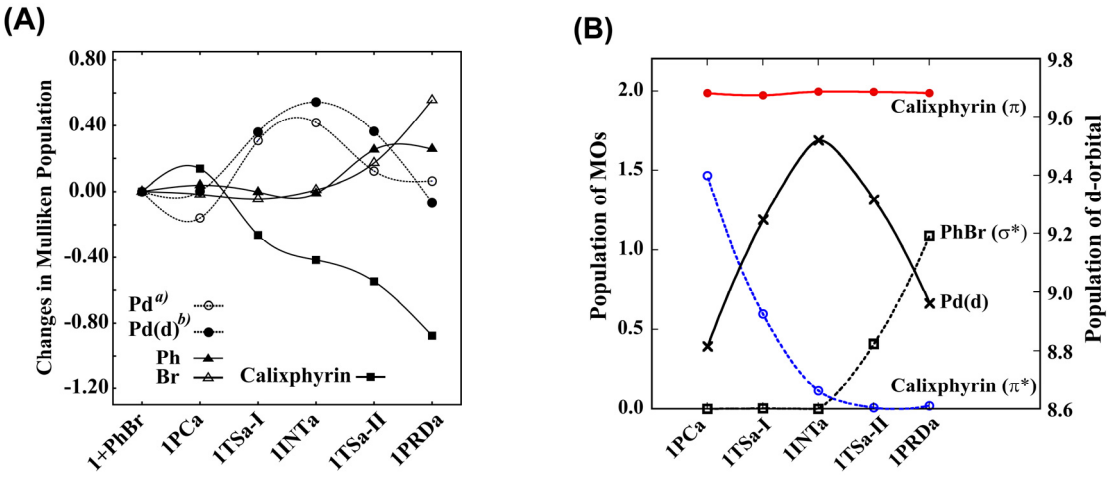

Figure 4. (A) Changes in Mullikene population and (B) population changes of MOs of fragments in the oxidative addition of PhBr to the palladium complex of P,S-containing hybrid calixphyrin **1**. The positive value represents the increase in electron population, and vice versa. The DFT(B3LYP)/BS2 method was employed. [a] Population of Pd atom. [b] Population of d-orbital of Pd atom.

Table 2. Activation barrier (E_a) and reaction energy (ΔE)[a] in the oxidative addition of phenyl bromide (PhBr) to the palladium complex of P,S-containing hybrid calixphyrin **1** through up-I, up-II, down-I, and down-II.

	up-I	up-II	down-I	down-I
E_a	22.6	23.1	40.3	41.0
ΔE	−5.3	−0.7	7.6	10.7

[a] kcal/mol unit. The DFT(B3LYP)/BS2 method was employed.

considerably increase when going from **1INTa** to **1PRDa**. These population changes suggest that the Pd d-orbital receives electron population from the calixphyrin moiety when going to **1INTa** from **1**, and then charge transfer occurs from the Pd d-orbital to the PhBr when going from **1INTa** to **1PRDa**. To present better understanding of population changes, we analyzed the molecular orbital ψ_i(ABC) of total system ABC with a linear combination of

molecular orbitals of fragments A, B, and C, as shown in eq 3, where ψ_i(ABC) represents the *i*th MO of the total system **1**··· PhBr, φ_m(A) is the *m*th MO of the Pd atom, φ_n(B) is the *n*th MO of PhBr, and φ_l(C) is the *l*th MO of the calixphyrin. Orbital populations, ρ_m(A), ρ_n(B), and ρ_l(C), are evaluated with eqs 4-6.

$$\psi_i(\mathrm{ABC}) = \sum_m C_{im}^A \varphi_m(\mathrm{A}) + \sum_n C_{in}^B \varphi_n(\mathrm{B}) + \sum_l C_{il}^C \varphi_l(\mathrm{C}) \tag{3}$$

$$\rho_m(\mathrm{A}) = \sum_i^{occ} \left[C_{im}^{A\,2} + \sum_n C_{im}^A C_{in}^B S_{mn}^{AB} + \sum_l C_{im}^A C_{il}^C S_{ml}^{AC} \right] \tag{4}$$

$$\rho_n(\mathrm{B}) = \sum_i^{occ} \left[\sum_m C_{im}^A C_{in}^B S_{mn}^{AB} + C_{in}^{B\,2} + \sum_l C_{in}^B C_{il}^C S_{nl}^{BC} \right] \tag{5}$$

$$\rho_l(\mathrm{C}) = \sum_i^{occ} \left[\sum_m C_{im}^A C_{il}^C S_{ml}^{AC} + \sum_n C_{in}^B C_{il}^C S_{nl}^{BC} + C_{il}^{C\,2} \right] \tag{6}$$

As shown in Figure 4B, the electron population of the π orbital of calixphyrin does not change at all in this reaction. On the other hand, the electron population of the π* orbital of the calixphyrin decreases to nearly zero when going to **1INTa** from **1PCa**, and simultaneously the Pd d-orbital population considerably increases. These results clearly indicate that the charge transfer considerably occurs from the π* orbital of the calixphyrin moiety to the Pd d-orbital when going to **1INTa** from **1PCa**. As a result, both the calixphyrin moiety and the Pd atom become nearly neutral in **1INTa**. Going to **1PRDa** from **1INTa**, the Pd d-orbital population considerably decreases but the electron population of the Ph-Br σ* orbital considerably increases, as shown in Figure 4B. In other words, the charge transfer occurs from the π* orbital of the calixphyrin to the Pd d-orbital to afford the Pd(0) form when going to **1INTa** from **1PCa**. Then, the charge transfer occurs from the Pd d-orbital to the σ* orbital of Ph-Br to induce the Ph-Br bond cleavage when going to **1PRDa** from **1INTa**. In **1PRDa**, the

oxidation state of Pd becomes +2 again. In summary, the oxidative addition to **1** occurs easily, because the Pd center changes to zero-oxidation state from +2 oxidation state when going to **1INTa** from **1** due to the charge transfer from the LUMO (π^*) orbital of the P,S-containing hybrid calixphyrin to the Pd d-orbital.

4.3.4. Oxidative Addition of PhBr to Palladium Complex of P,S-Containing Hybrid Porphyrin 2 and That of Conventional Porphyrin 3.

We investigated the oxidative additions of PhBr to the similar palladium(II) complex of P,S-containing hybrid porphyrin **2** and that of conventional porphyrin **3**, to make comparison of **1** with **2** and **3**; see Scheme 1E and 1F for **2** and **3**, respectively. In the oxidative addition to **2**, PhBr approaches the Pd center to form precursor complex **2PC**; see Figure A6 in Appendix. Then, the PhBr further approaches the Pd center through transition state **2TS-I** to form intermediate **2INT**. In **2TS-I**, the Pd center considerably moves upward. The activation enthalpy is 43.3 kcal/mol, indicating that the position change of Pd is very difficult. Then, the C−Br σ-bond cleavage occurs through **2TS-II** to afford product **2PRD**. The geometry of **2TS-II** is similar to that of **1TSa-I**. Because **2INT** is much more unstable than **2PC**, the total activation enthalpy to complete the reaction is the energy difference between **2TS-II** and the sum of reactants. This activation enthalpy is 49.1 kcal/mol and the enthalpy change of reaction is 18.1 kcal/mol, indicating that the oxidative addition to **2** is difficult. In the oxidative addition to **3**, intermediates such as **1INTa** are not formed; see Figure A7 for the geometry changes. In precursor complex **3PC**, PhBr is considerably distant from the Pd center. Starting from **3PC**, the C−Br σ-bond cleavage occurs through transition state **3TS** to yield product **3PRD**. In **3TS**, the C−Br distance (2.831 Å) of PhBr is considerably elongated, and the Pd−C and Pd−Br distances are similar to those of **3PRD**. These features indicate that **3TS** is product-like. Consistent with these geometrical features, the activation enthalpy (74.4 kcal/mol) and the enthalpy change of reaction (74.6 kcal/mol) are very large.

In **3PRD**, the porphyrin moiety is considerably distorted and the Pd center moderately moves upward. It is concluded that the oxidative addition of PhBr to **3** is very difficult, in contrast to **1**.

4.3.5. Reasons Why Palladium Complex of P,S-Containing Hybrid Calixphyrin Is Reactive for the Oxidative Addition, but Palladium Complexes of P,S-Containing Hybrid Porphyrin and Conventional Porphyrin Are Not.

In the oxidative addition to **2**, the π* orbital population of P,S-containing hybrid porphyrin considerably decreases and the Pd d-orbital population considerably increases when going to **2INT** from **2**, as shown in Figure 5A. Then, the σ* orbital population of PhBr considerably increases with concomitant decrease of the Pd d-orbital population when going to **2PRD** from **2INT**. These population changes are essentially the same as those of the oxidative addition to **1**, though the oxidative addition of PhBr to **2** is difficult unlike that to **1**. In the oxidative addition to **3**, electron populations of porphyrin π and π* orbitals are always about 2.0 e, as shown in Figure 5B, which indicates that charge transfer does not occur from the porphyrin moiety to the Pd center during the reaction. The Pd d-orbital population considerably decreases and the σ* orbital population of PhBr considerably increases when going to **3PRD** from **3PC**. These results indicate that the oxidation state of Pd changes from +2 to +4 in the reaction. It is worth investigating the reasons of the differences among **1**, **2**, and **3**. Although the π orbital energies are close to −5.5 eV in P,S-containing hybrid calixphyrin, P,S-containing hybrid porphyrin, and conventional porphyrin, the π* orbital energy is considerably different among them, as shown in Figure 6, where the π and π* orbital energies are calculated without the Pd atom. The π* orbital is doubly occupied in the Pd complexes **1**, **2**, and **3** and the conversion from the Pd(II) form to the Pd(0) form needs the charge-transfer from the doubly occupied π* orbitals to the Pd d orbital, as discussed above.

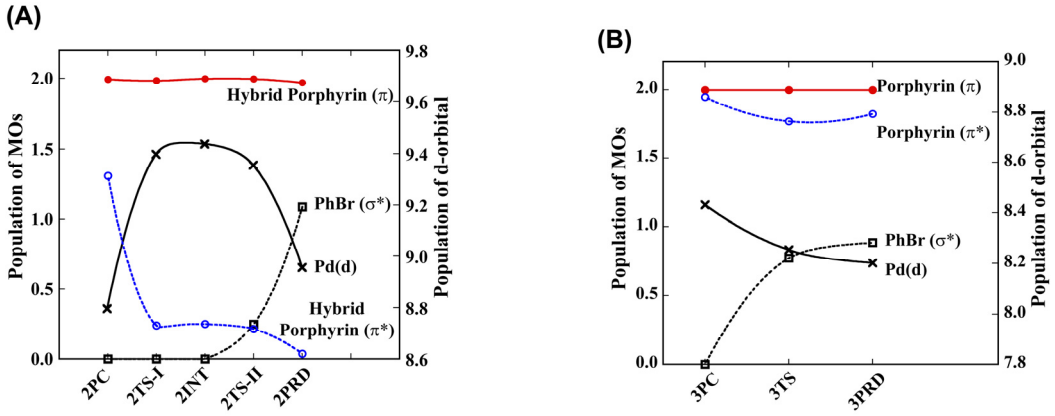

Figure 5. Population changes of important MOs of fragments in the oxidative addition of PhBr to (A) the palladium complexes of P,S-containing hybrid porphyrin **2** and (B) conventional porphyrin **3**. The DFT(B3LYP)/BS2 method was employed.

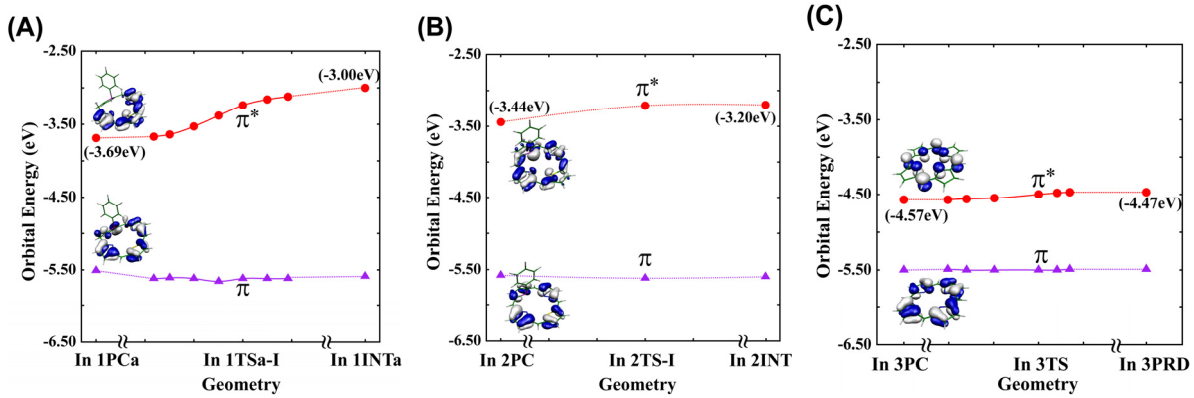

Figure 6. π and π* orbital energies of (A) P,S-containing hybrid calixphyrin moiety, (B) P,S-containing hybrid porphyrin moiety, and (C) conventional porphyrin moiety, where Pd atom is eliminated and the geometry is taken to be the same as the corresponding moiety of the palladium complex of P,S-containing hybrid calixphyrin **1**, the palladium complex of P,S-containing hybrid porphyrin **2**, and the conventional palladium porphyrin complex **3**. The DFT(B3LYP)/BS2 method was employed.

Because the π* orbital energy of conventional porphyrin is much lower than those of P,S-containing hybrid calixphyrin and P,S-containing hybrid porphyrin, the charge-transfer from the π* orbital to the Pd d-orbital occurs with much more difficulty in **3** than in **1** and **2**. Hence, the conversion of the Pd(II) form to the Pd(0) form is difficult in **3**. As a result, the Pd(II) center must change to Pd(IV) center in the oxidative addition to **3**, which is very difficult. It is noted that the π* orbital energy of P,S-containing hybrid porphyrin is similar to that of the hybrid calixphyrin in the geometry of **PC** but that of a conventional porphyrin is much more stable. These results suggest that the phosphole and thiophene moieties play an important role in raising the π* orbital energy. The π* orbital energy of hybrid calixphyrin considerably rises but that of hybrid porphyrin moderately rises when going from the geometry in **PC** to that in **INT**, though their π* orbital energies are similar to each other in their equilibrium structures. These results indicate that the charge transfer from the π* orbital of P,S-containing hybrid calixphyrin to the Pd d-orbirtal becomes easier than that from the P,S-containing hybrid porphyrin when going to **INT** from **PC**. This is because the π-conjugation of hybrid calixphyrin is interrupted by the presence of sp^3-carbon atoms. On the other hand, the π* orbital energy of hybrid porphyrin does not change easily, because the π-conjugation of hybrid porphyrin is strong due to the absence of the sp^3-carbon atom. From these results, it is concluded that the large reactivity of the palladium complex of P,S-containing hybrid calixphyrin **1** arises from the presence of the sp^3-carbon atom and phosphole and thiophene moieties.

4.3.6. Comparison of Reactivity among 1, Palladium(0) Bisphosphine Complex $Pd(PMe_3)_2$ 4, and Palladium(II) Dicholoro Bisphosphine Complex $PdCl_2(PMe_3)_2$ 5.

We make the comparison of **1** with palladium(0) bisphosphine complex $Pd(PMe_3)_2$ **4** in the oxidative addition of PhBr. The geometry and energy changes of the oxidative addition

to **4** are presented in Appendix Figure A9, because they were discussed previously.[29] The oxidative addition to **4** occurs with smaller activation enthalpy of 15.8 kcal/mol and larger enthalpy change of reaction (−18.0 kcal/mol) than those of the oxidative addition to **1**, indicating that **1** is less reactive for the oxidative addition than **4**. Also, we made the comparison of **1** with a typical palladium(II) complex, *trans*-$PdCl_2(PMe_3)_2$ **5**. The oxidative addition to **5** occurs with much larger activation enthalpy (51.2 kcal/mol) and much more positive enthalpy change of reaction (26.6 kcal/mol) than those of the oxidative addition to **1** (Appendix Figure A10). These results clearly indicate that **5** is much less reactive than **1**, similar to **2**, but more reactive than **3**; see above. It is likely that the larger reactivity of **5** than that of **3** arises from the more flexible geometry of **5** than that of **3**, indicating that the tight framework of the conventional porphyrin very much suppresses the oxidative addition. The activation enthalpy of the oxidative addition to **1** is only 2.0 kcal/mol relative to **1INTa**, which is similar to the activation enthalpy (0.5 kcal/mol) of the oxidative addition to a monodentate phosphine complex $Pd(PMe_3)$ **6**; see Figure A11. This means that the large activation enthalpy for **1** arises from the tautomerization from the Pd(II) form to the Pd(0) form, and the neutral form of the P,S-containing hybrid calixphyrin plays a role of ligand similar to monodentate phosphine.

4.4. Conclusions

There are two valence tautomers, Pd(II) form and Pd(0) form, in the palladium complex of P,S-containing hybrid calixphyrin **1**. The d-orbital populations indicate that **1** takes the Pd(II) form. Although the Pd(II) complex is unfavorable for the oxidative addition, the oxidative addition of PhBr to **1** occurs with moderate activation enthalpy, as follows: The valence tautomerization from the Pd(II) form to the Pd(0) form occurs concomitantly with the approach of PhBr to the Pd center and the position movement of the Pd center to afford intermediate **1INTa**. The activation enthalpy (20.3 kcal/mol) is moderate. Starting from

the Pd(0) form, the C−Br σ-bond activation of PhBr easily occurs with small activation enthalpy of 2.0 kcal/mol, relative to **1INTa**. Also, the oxidative addition to palladium complex of P,S-containing hybrid porphyrin **2** and that of conventional porphyrin **3** were investigated. The activation enthalpies are 49.1 and 74.4 kcal/mol in the reactions of **2** and **3**, respectively, which are much larger than that of **1**. In **1**, the tautomerization from the Pd(II) form to the Pd(0) form occurs with moderate activation enthalpy; see above. In other words, the oxidation state of Pd changes to zero from +2 prior to the oxidative addition. In **3**, the π* orbital population decreases little, indicating that the Pd oxidation state cannot change to zero. In **2**, the charge transfer occurs from the π* orbital to the Pd center by the tautomerization, while the activation enthalpy for this process is very large. These differences among **1**, **2**, and **3** are interpreted in terms of the π* orbital energy and its dependency on the geometry change. It should be concluded that the higher reactivity of **1** for the oxidative addition arises from the presence of phosphole and thiophene moieties and sp^3-carbon atoms in P,S-containing hybrid calixphyrin. Though **1** is more reactive than **2** and **3**, **1** is less reactive than palladium(0) bisphosphine complex $Pd(PMe_3)_2$ **4**. This is because the tautomerization from the Pd(II) form to the Pd(0) form needs large activation enthalpy.

Table A1. Optimized geometry of palladium complex of P,S-containing hybrid calixphyrin (the Pd(II) form) calculated with several basis sets

Basis set	**BS1**	**BS2**	**BS3**	**BS4**	Experiment[c]
Pd	ECP[a]+(311111/22111/411)	ECP[a]+(311111/22111/411)	ECP[a]+(311111/22111/411/11)	ECP[b]+(541/521/211)	
P, S	6-31G*	6-311G*	cc-pVTZ	6-31G*	
N	6-31+G*	6-311+G*	aug-cc-pVTZ	6-31+G*	
C	6-31G*	6-311G*	cc-pVTZ	6-31G*	
H	6-31G	6-311G	cc-pVTZ	6-31G	
Pd–P (Å)	2.257	2.260	2.258	2.264	2.2135(8)
Pd–N^1	2.130	2.133	2.135	2.139	2.079(2)
Pd–N^2	2.127	2.129	2.132	2.136	2.066(2)
Pd–S	2.312	2.316	2.317	2.321	2.2667(8)
P–Pd–N^1 (degree)	92.8	92.4	92.6	92.5	95.21(7)
P–Pd–N^2	88.6	88.9	88.6	88.8	85.75(7)
S–Pd–N^1	91.1	90.8	91.0	90.8	92.93(6)
S–Pd–N^2	87.4	87.9	87.7	87.8	85.77(7)

[a]Ref. 17. [b] Hay, P. J.; Wadt, W. R. *J. Chem. Phys.* **1985**, *82*, 299. [c] Matano, Y.; Miyajima, T.; Nakabuchi, T.; Imahori, H.; Ochi, N.; Sakaki, S. *J. Am. Chem. Soc.* **2006**, *128*, 11760.

Table A2. Optimized geometry of intermediate complex **1INTa** with several basis sets.

Basis set	**BS1**	**BS3**	**BS5**
Pd[a]	(311111/22111/411)	(311111/22111/411/11)	(311111/22111/411)
P, S	6-31G*	cc-pVTZ	6-31G*
C, O, H	6-31G*	cc-pVTZ	6-31G*
N	6-31+G*	aug-cc-pVTZ	6-31+G*
Br	6-311+G*	aug-cc-pVTZ	6-31+G*
Pd–Br (Å)	2.604	2.578	2.515
Pd–C	3.729	3.726	3.690
Pd–P	2.272	2.262	2.275
Pd–N[1]	3.239	3.230	3.247
Pd–S	2.695	2.722	2.739

[a] Ref. 17, 22.

Table A3. Optimized geometries of palladium complex of P,S-containing hybrid calixphyrin in the Pd(II) form and Pd(0) form calculated with several functionals

The Pd(II) form						**The Pd(0) form**			
	B3LYP	B3PW91	B3P86	BLYP	Experimental[a]		B3LYP	B3PW91	B3P86	BLYP
Pd–P (Å)	2.257	2.246	2.241	2.281	2.2135(8)	Pd–P (Å)	2.256	2.235	2.229	2.270
Pd–N^1	2.130	2.124	2.117	2.177	2.079(2)	Pd–S	2.489	2.427	2.412	2.481
Pd–N^2	2.127	2.124	2.117	2.176	2.066(2)	Pd–N^1	3.097	3.030	3.014	3.094
Pd–S	2.312	2.289	2.285	2.323	2.2667(8)	Pd–N^2	3.097	3.030	3.014	3.099
P–Pd–N^1 (degree)	92.8	91.5	91.5	91.4	95.21(7)	P–Pd–S (degree)	112.3	114.4	114.9	112.2
P–Pd–N^2	88.6	89.9	89.7	91.2	85.75(7)	N^1–Pd–N^2	104.7	107.3	107.7	105.7
S–Pd–N^1	91.1	89.9	90.1	88.6	92.93(6)					
S–Pd–N^2	87.4	88.6	88.5	88.3	85.77(7)					

[a] Matano, Y.; Miyajima, T.; Nakabuchi, T.; Imahori, H.; Ochi, N.; Sakaki, S. *J. Am. Chem. Soc.* **2006**, *128*, 11760.

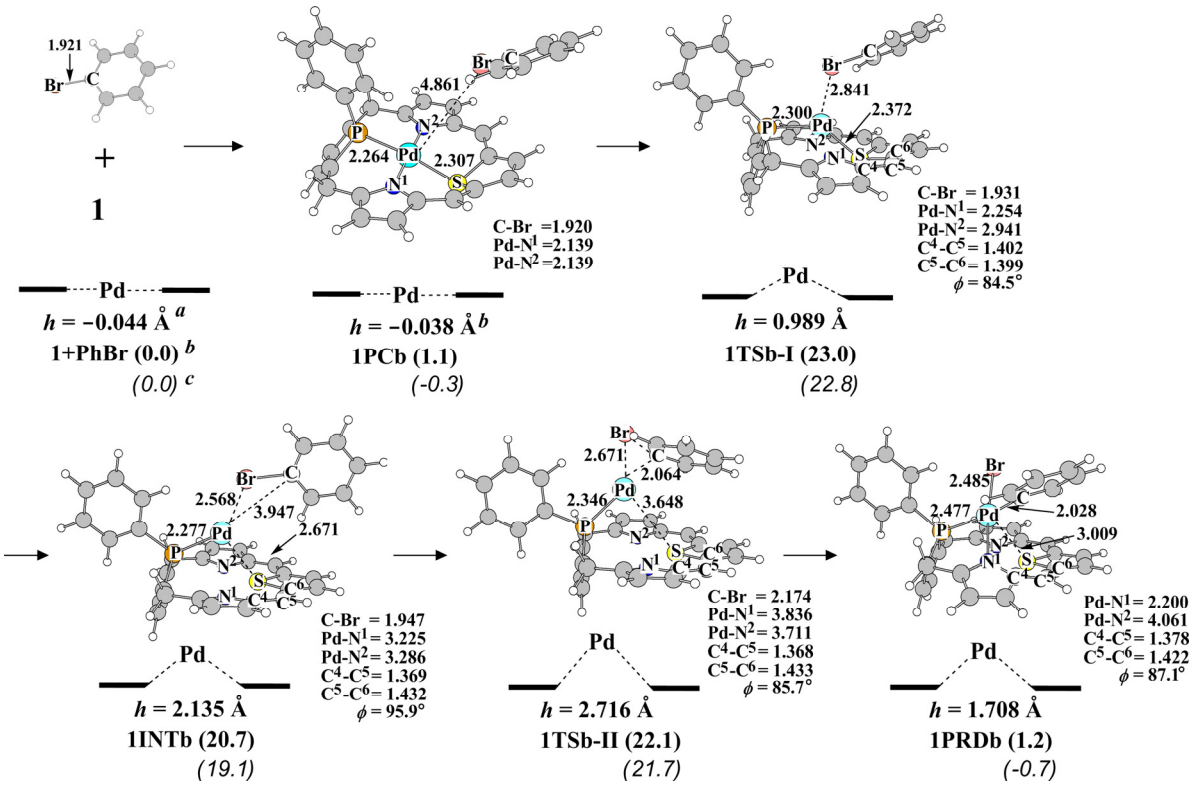

Figure A1. Geometry changes in the oxidative addition of PhBr to the palladium complex of P,S-containing hybrid calixphyrin **1** through up-II. Bond lengths are in angstrom and bond angles are in degree. [a] The *h* indicates the distance between Pd center and N^1−S−N^2 plane. [b] The relative enthalpies (kcal/mol unit) to **1** + PhBr, where the DFT(B3LYP)/BS2 method was employed. [c] The relative energies (kcal/mol unit) to **1** + PhBr, where the DFT(B3LYP)/BS2 method was employed.

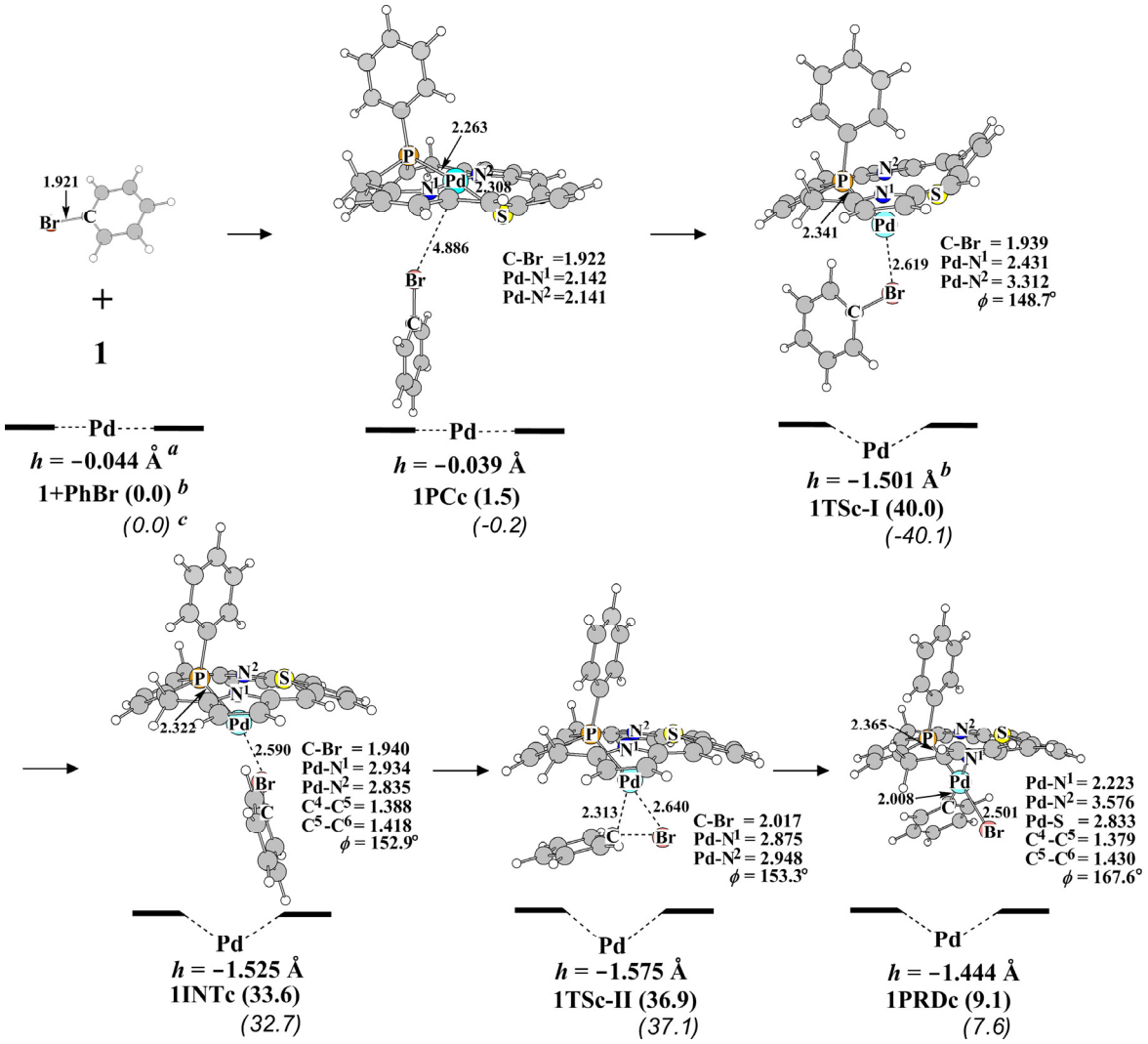

Figure A2. Geometry changes in the oxidative addition of PhBr to the palladium complex of P,S-containing hybrid calixphyrin **1** through the down-I reaction course. Bond lengths are in angstrom and bond angles are in degree. [a] The *h* indicates the distance between Pd center and N^1–S–N^2 plane. [b] The relative enthalpies (kcal/mol unit) to **1** + PhBr, where the DFT(B3LYP)/BS2 method was employed. [c] The relative energies (kcal/mol unit) to **1** + PhBr, where the DFT(B3LYP)/BS2 method was employed.

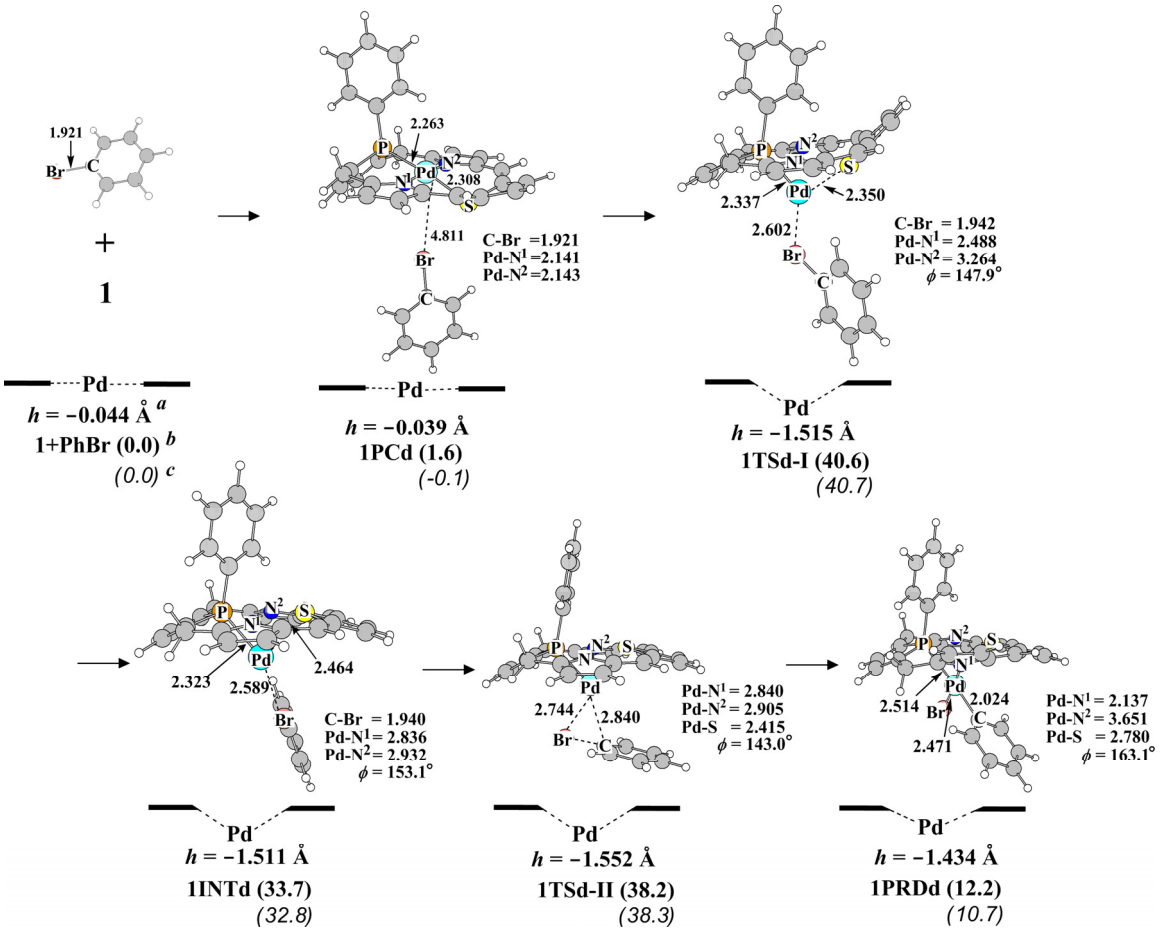

Figure A3. Geometry changes in the oxidative addition of PhBr to palladium complex of P,S-containing hybrid calixphyrin **1** through down-II reaction course. Bond lengths are in angstrom and bond angles are in degree. [a] The *h* indicates the distance between Pd center and N^1−S−N^2 plane. [b] The relative enthalpies (kcal/mol unit) to **1** + PhBr, where the DFT(B3LYP)/BS2 method was employed. [c] The relative energies (kcal/mol unit) to **1** + PhBr, where the DFT(B3LYP)/BS2 method was employed.

The reason why the upward courses are easier than the downward ones:

We wish to discuss the reason why the upward courses are more favorable than the downward courses. In **1TSn-I**, the position of Pd and the direction of phosphole are significantly different between the upward and downward courses. The dihedral angle ϕ between the phosphole moiety and the π-conjugated plane is 94.7 degrees in free P,S-containing hybrid calixphyrin. However, the ϕ of **1** is 111.1 degrees, indicating that the phosphole moiety is distorted in **1**. It becomes 83.8 and 84.5 degrees in **1TSa-I** and **1TSb-I**, respectively, which are close to that of free P,S-containing hybrid calixphyrin. But, it becomes 148.7 and 152.6 degrees in **1TSc-I** and **1TSd-I**, respectively, which are much larger than that of free P,S-containing hybrid calixphyrin. In other words, the geometry of the P,S-containing hybrid calixphyrin approaches that of the free calixphyrin in the upward course, whereas it is considerably distorted in the downward course. Because the interaction between Pd and PhBr is weak in all **1TSa-I** to **1TSd-I**, this interaction little contributes to the difference in E_a between the upward and downward courses. These results indicate that the direction change of the phosphole moiety is responsible for the E_a difference between the upward and downward courses. The potential energy curve was evaluated against the direction change of the phosphole moiety in Figure A4. Because the direction of the phosphole much more changes in **1TSc-I** and **1TSd-I** of the downward courses than in **1TSa-I** and **1TSb-I** of the upward course, the P,S-containing hybrid calixphyrin suffers from larger distortion energy in the downward courses than in the upward courses, as shown in Figure A4. As a result, the E_a value is much larger in the downward courses than in the upward courses. Thus, it should be concluded that the smaller distortion of the calixphyrin moiety in the upward courses is responsible to the smaller E_a value.

The next issue to be investigated is the reason why the dihedral angle ϕ decreases in the upward reaction course but increases in the downward reaction course. In the upward course, the Pd center moves upward above the calixphyrin plane to approach PhBr, which induces the

anti-clockwise geometry change of the phosphole moiety, as shown in Scheme A1A. As a result, the Pd center does not interact with the N and S atoms but only with the P atom in **1TSn'-I** (n' = a and b) and **1INTn'**. Because such Pd coordination is possible with the geometry of free calixphyrin, the geometry becomes similar to that of the free calixphyrin, as discussed above. In the downward courses, the Pd center moves downward below the calixphyrin plane, which induces the clockwise geometry change of the phosphole moiety, as shown in Scheme A1B. This geometry change increases the ϕ value and the geometry becomes much different from that of free calixphyrin; see above. This difference induces the large difference in the E_a between the upward and downward courses.

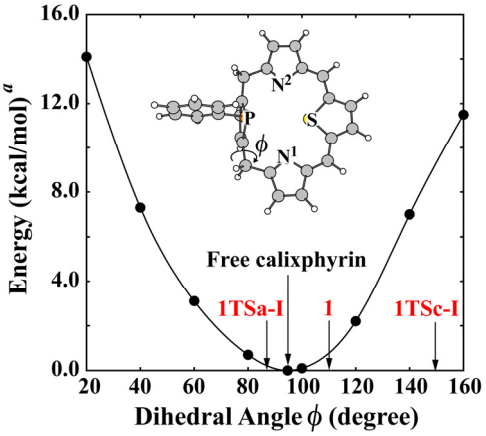

Figure A4. Potential energy surface against the dihedral angle ϕ between phosphole moiety and calixphyrin plane in P,S-containing hybrid calixphyrin **1**. [a] The DFT(B3LYP)/BS2 method was employed.

Scheme A1

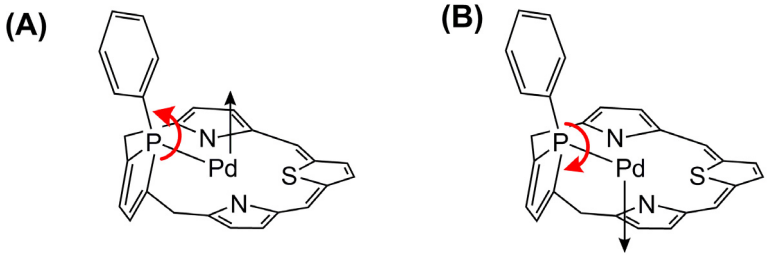

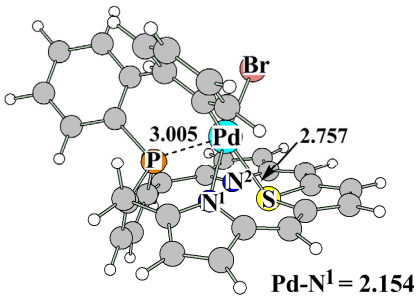

PRD$_S$ (10.8)[a]

Figure A5. Geometry of another possible product **1PRD$_S$**, in which the Pd coordinates to S and N^1. [a] In parenthesis is the relative value (kcal/mol unit) to **1PRDa**, where the DFT(B3LYP)/BS2 method was employed. Though this was expected to be one of possible products, this is much more unstable than **1PRDa** by 10.8 kcal/mol.

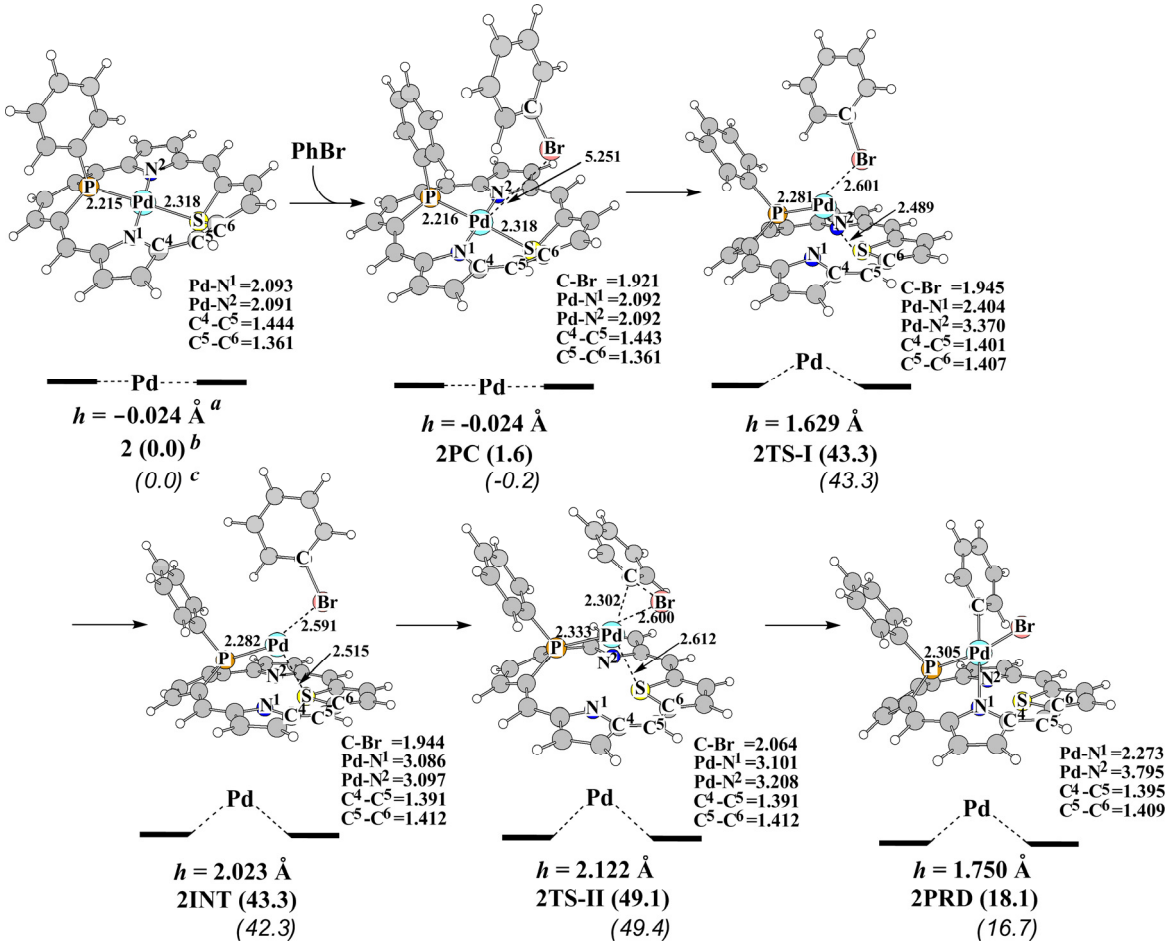

Figure A6. Geometry changes in the oxidative addition of PhBr to the palladium complex of P,S-containing hybrid porphyrin complex **2**. Bond lengths are in angstrom and bond angles are in degree. [a] The *h* indicates the distance between Pd center and N^1–S–N^2 plane. [b] The relative enthalpies (kcal/mol unit) to **2** + PhBr, where the DFT(B3LYP)/BS2 method was employed. [c] The relative energies (kcal/mol unit) to **2** + PhBr, where the DFT(B3LYP)/BS2 method was employed.

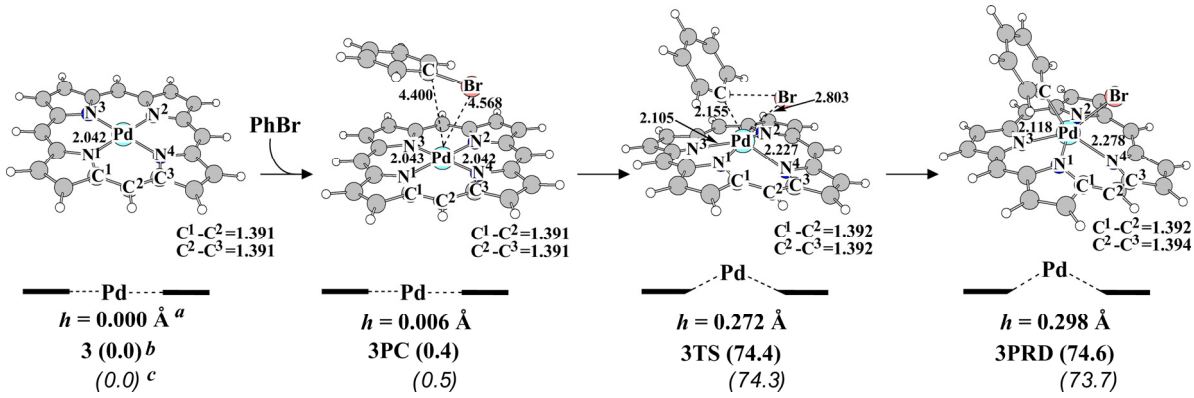

Figure A7. Geometry changes in the oxidative addition of PhBr to the palladium complex of conventional porphyrin **3**. Bond lengths are in angstrom and bond angles are in degree. [a] The *h* indicates the distance between Pd center and N^1–S–N^2 plane. [b] The relative enthalpies (kcal/mol unit) to **3** + PhBr, where the DFT(B3LYP)/BS2 method was employed. [c] The relative energies (kcal/mol unit) to **3** + PhBr, where the DFT(B3LYP)/BS2 method was employed.

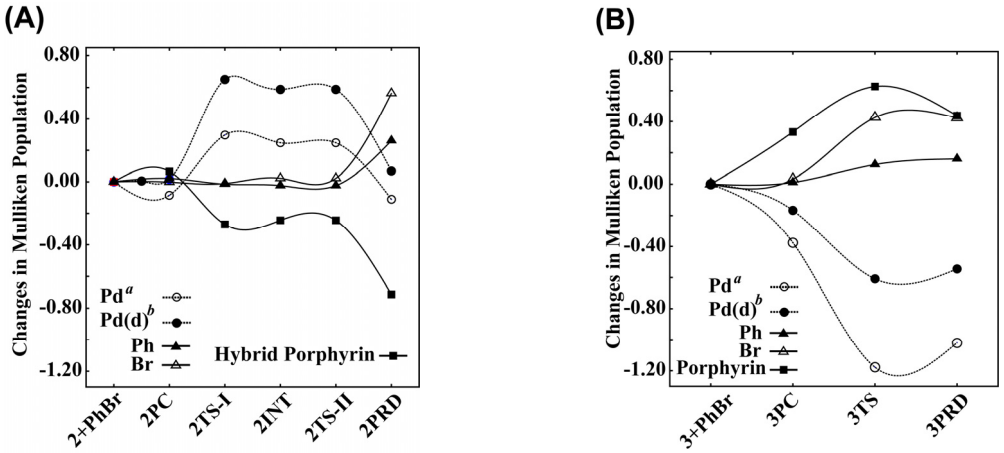

Figure A8. Mullikene population changes in the oxidative addition of PhBr to (A) the palladium complex of P,S-containing hybrid porphyrin **2** and (B) of conventional porphyrin complex **3**. The positive value represents the increase in electron population, and vice versa. The DFT(B3LYP)/BS2 method was employed. [a] Population of d-orbital of Pd atom.

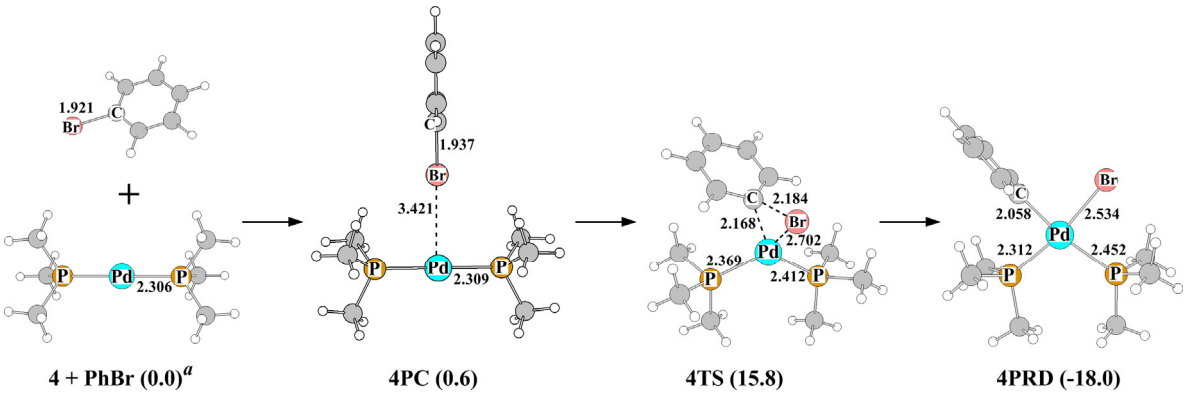

Figure A9. Geometry changes in the oxidative addition of PhBr to the typical palladium(0) complex $Pd(PMe_3)_2$ **4**. Bond lengths are in angstrom and bond angles are in degree. [a] In parenthesis is the relative value (kcal/mol unit) to **4** + PhBr, where the DFT(B3LYP)/BS2 method was employed.

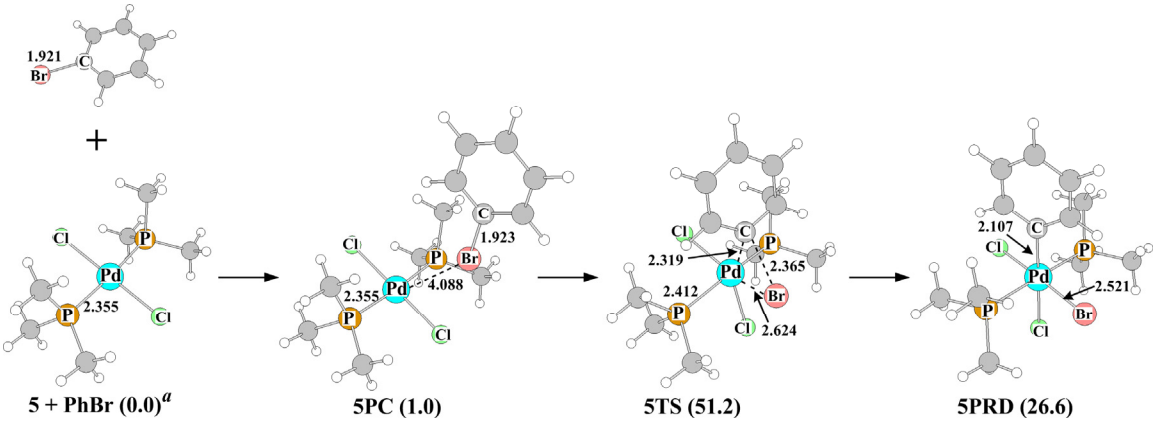

Figure A10. Geometry changes in the oxidative addition of PhBr to the typical palladium(II) complex Pd((PMe$_3$) **5**. Bond lengths are in angstrom and bond angles are in degree. [a] In parenthesis is the relative value (kcal/mol unit) to **5** + PhBr, where the DFT(B3LYP)/BS2 method was employed.

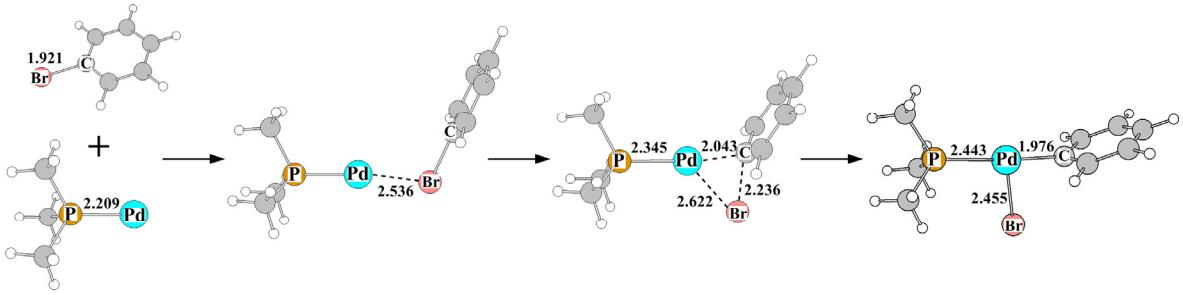

6 + PhBr (0.0) [a] **6PC (-10.6)** **6TS (-10.1)** **6PRD (-19.1)**

Figure A11. Geometry changes in the oxidative addition of PhBr to the monophosphine palladium complex Pd((PMe_3) **6**. Bond lengths are in angstrom and bond angles are in degree. [a] In parenthesis is the relative value (kcal/mol unit) to **6** + PhBr, where the DFT(B3LYP)/BS2 method was employed.

Reference

(1) The term *calixphyrin* was proposed by Sessler et. al to describe series of porphomethene, porphodimethene, porphotrimethene, and their analogues. Král, V.; Sessler, J. L.; Zimmerman, S. R.; Seidel, D.; Lynch, V.; Andrioletti, B. *Angew. Chem. Int. Ed.* **2000**, *39*, 1055.

(2) (a) Senge, M. O.; Kalisch, W. W.; Bischoff, I. *Chem. Eur. J.* **2000**, *6*, 2721. (b) Senge, M. O.; Runge, S.; Speck, M.; Ruhlandt-Senge, K. *Tetrahedron* **2000**, *56*, 8927. (c) Sessler, J. L.; Zimmerman, R. S.; Bucher, C.; Král, V.; Andrioletti, B. *Pure Appl. Chem.* **2001**, *73*, 1041. (d) Bischoff, I.; Feng, X.; Senge, M. O. *Tetrahedron*, **2001**, *57*, 5573. (e) Senge, M. O. *Acc. Chem. Res.* **2005**, *38*, 733.

(3) Bucher, C.; Zimmerman, R. S.; Lynch, V.; Král, V.; Sessler, J. L. *J. Am. Chem. Soc.* **2001**, *123*, 2099.

(4) (a) Benech, J.-M.; Bonomo, L.; Solari, E.; Scopelliti, R.; Floriani, C. *Angew. Chem., Int. Ed.* **1999**, *38*, 1957. (b) Bonomo, L.; Toranman, G.; Solari, E.; Scopelliti, R.; Floriani, C. *Organometallics* **1999**, *18*, 5198.

(5) (a) Krattinger, B.; Callot, H. J. *Tetrahedron Lett.* **1998**, *39*, 1165. (b) Harmjanz, M.; Gill, H. S.; Scott, M. J. *J. Org. Chem.* **2001**, *66*, 5374. (c) Bucher, C.; Devillers, C. H.; Moutet, J.-C.; Pécaut, J. ; Royal, G. ; Saint-Aman, E. ; Thomas, F. *Dalton Trans.* **2005**, 3620. (d) O'Brien, A. Y. ; McGann, J. P. ; Geier, G. R., III *J. Org. Chem.* **2007**, *72*, 4084.

(6) (a) Bucher, C.; Seidel, D.; Lynch, V.;Král, V.; Sessler, J. L. *Org. Lett.* **2000**, *2*, 3103. (b) Dolenský, B.; Kroulik, J.; Král, V.; Sessler, J. L.; Dvořáková, H.; Bouř, P.; Bernátková, M.; Bucher, C.; Lynch, V. *J. Am. Chem. Soc.* **2004**, *126*, 13714. (c) Bernátková, M.; Dvořáková, H.; Andrioletti, B.; Král, V.; Bouř, P. *J. Phys. Chem. A* **2005**, *109*, 5518.

(7) Review: (a) Chandrashekar, T. K.; Venkatraman, S. *Acc. Chem. Res.* **2003**, *36*, 676.

(b) Sessler, J. L.; Seidel, D. *Angew. Chem., Int. Ed.* **2003**, *42*, 5134. (c) Srinivasan, A.; Furuta, H. *Acc. Chem. Res.* **2005**, *38*, 10. (d) Chmielewski, P. J.; Latos-Grażyński, L. *Coord. Chem. Rev.* **2005**, *249*, 2510. (e) Gupta, I.; Ravikanth, M. *Coord. Chem. Rev.* **2006**, *250*, 468 and references therein.

(8) Recently, the synthese and structures of sulfur-containing phlorins were reported. Gupta, I.; Fröhlich, R.; Ravikanth, M. *Chem. Commun.* **2006**, 3726.

(9) (a) Matano, Y.; Miyajima, T.; Nakabuchi, T.; Imahori, H.; Ochi, N.; Sakaki, S. *J. Am. Chem. Soc.* **2006**, *128*, 11760. (b) Matano,Y.; Miyajima, T.; Ochi, N.; Nakabuchi, T.; Shiro, M.; Nakao, Y.; Imahori, H.; Sakaki, S. *J. Am. Chem. Soc.* **2008**, *130*, 990. (c) Matano,Y.; Miyajima, T.; Ochi, N.; Nakao, Y.; Sakaki, S.; Imahori, H. *J. Org. Chem.* **2008**, *73*, 5139.

(10) Recent Reviews: (a) Caminade, A.-M.; Majoral, J. P. *Chem. Rev.* **1994**, *94*, 1183. (b) Diloworth, J. R.; Wheatley, N. *Coord. Chem. Rev.* **2000**, *199*, 89, and references therein.

(11) (a) Fryzuk, M. D.; Kozak, C. M.; Bowdridge, M. R.; Jin, W.; Tung, D.; Patrick, B. O.; Retting, S. J. *Organometallics* **2001**, *20*, 3752. (b) Fryzuk, M. D.; Kozak, C. M.; Mehrkhodavandi, P.; Morello, L.; Patrick,, B. O.; Retting, S. J. *J. Am. Chem. Soc.* **2002**, *124*, 516. (c) Fryzuk, M. D.; Kozak, C. M.; Bowdridge, M. R.; Patrick, B. O.; Rettig, S. J. *J. Am. Chem. Soc.* **2002**, *124*, 8389. (d) Fryzuk, M. D.; Kozak, C. M.; Bowdridge, M. R.; Patrick, B. O. *Organometallics* **2002**, *21*, 5047.

(12) (a) Louie, J.; Hartwig, F. J. *Angew. Chem. Int. Ed. Engl.* **1996**, *35*, 2359. (b) Louie, J.; Paul, F.; Hartwig, F. J. *Organometallics* **1996**, *15*, 2794.

(13) Delaere, D.; Nguyen, M. T. *Chem. Phys. Lett.* **2003**, *376*, 329.

(14) Matano, Y.; Nakabuchi, T.; Miyajima, T.; Imahori, H.; Nakano, H. *Org. Lett.* **2006**, *25*, 5713.

(15) Matano,Y.; Nakabuchi, T.; Fujishige, S.; Nakao, Y.; Imahori, H. *J. Am. Chem. Soc.*

2008, *130*, 16446.

(16) (a) Becke, A. D. *J. Chem. Phys.* **1983**, *98*, 5648. (b) Becke, A. D. *Phys. Rev.* **1988**, *A38*, 3098. (c) Lee, C.; Yang, W.; Parr, R. G. *Phys. Rev.* **1988**, *B37*, 785.

(17) D. Andrae, U. Haeussermann, M. Dolg, H. Stoll, H. Preuss, *Theor. Chim. Acta* **1990**, *77*, 123.

(18) (a) Hehre, W. J.; Ditchfield, R.; Pople, J. A. *J. Chem. Phys.* **1972**, *56*, 2257. (b) Hariharan, P. C.; Pople, J. A. *Theor. Chim. Acta* **1973**, *28*, 213. (c) Hariharan, P. C.; Pople, J. A. *Mol. Phys.* **1974**, *27*, 209. (d) Francl, M. M.; Petro, W. J.; Hehre, W. J.; Binkley, J. S.; Gordon, M. S.; DeFrees, D. J.; Pople, J. A. *J. Chem. Phys.* **1982**, *77*, 3654.

(19) Clark, T.; Chandrasekhar, J.; Spitznagel, G. W.; Schleyer, P. V. R. *J. Comp. Chem.* **1983**, *4*, 294.

(20) Tuulmets, A.; Tammiku-Taul, J; Burk, P. *J. Mol. Struct.: THEOCHEM* **2004**, *674*, 233.

(21) (a) We carried out geometry optimization with B3PW91, B3P86, and BLYP functionals, because they were reported to be useful for geometry optimization of the second-row transition-metal complexes.[23b, c] (b) Waller, M. P.; Braun, H.; Hojdis, N.; Buhl, M. *J. Chem, Theory. Comput.* **2007**, *3*, 2234. (c) Schulz, N. E.; Zhao, Y.; Truhlar, D. G. *J. Phys. Chem. A*, **2005**, *109*, 4388.

(22) Martin, J. M. L.; Sundermann, A. *J. Chem. Phys.* **2001**, *114*, 3408.

(23) (a) Krishnan, R.; Binkley, J. S.; Seeger, R.; Pople, J. A. *J. Chem. Phys.* **1980**, *72*, 650. (b) McLean, A. D.; Chandler, G. S. *J. Chem. Phys.* **1980**, *72*, 5639. (c) Blaudeau, J.-P.; McGrath, M. P.; Curtiss, L. A.; Radom, L. *J. Chem. Phys.* **1997**, *107*, 5016. (d) Curtiss, L. A.; McGrath, M. P.; Blandeau, J-P.; Davis, N. E.; Binning, R. C.; Radom, Jr. L. *J. Chem. Phys.* **1995**, *103*, 6104.

(24) Pople, J. A., et al. Gaussina 03, revision C.02; Gaussian, Inc.: Wallingford, CT, 2004.

(25) Reed, A. E.; Curtiss, L. A.; Weinhold, F. *Chem. Rev.* **1988**, *88*, 899.

(26) Flükiger, P.; Lüthi, H. P.; Portann, S.; Weber, J. MOLEKEL, v.4.3; Scientific Computing: Manno, Switzerland, 2002-2002. Portman, S.; Lüthi, H. P. *CHIMIA* **2000**, *54*, 766.

(27) The charge transfer from **calix**$^{2-}$ to the Pd d_{x2-y2} orbital considerably increases the electron population of the Pd d_{x2-y2} orbital, as shown by the considerably large NAO occupancy of the d_{x2-y2} orbital.

(28) We examined another possible product in which Pd coordinates with the thiophene, and Ph and Br take the positions trans to S and N^1 atoms, respectively. However, this product is considerably less stable than **1PRDa** by 10.9 kcal/mol; see Figure A5 in Appendix.

(29) Fazaeli, R.; Ariafard, A.; Jamshidi, S.; Tabatabaie, E. S.; Pishro, K. A. *J. Organomet. Chem.* **2007**, *692*, 39.

Chapter 5

Interconversion between H_2 and H_2O by Hydroxo/Sulfido-Bridged Dinuclear Ruthenium-Germanium Complex. Theoretical Study

5.1. Introduction

Heterolytic activation of dihydrogen molecule (H_2) with transition metal complex is one of the most important subjects in biochemistry and organometallic chemistry,[1] because the heterolysis of H_2 is a key step of hydrogen metabolism in hydrogenase.[2] The hydrogenases are classified into three classes by considering what transition metal(s) is(are) involved in the active site; (1) hydrogenase containing iron-iron cluster, which is called [FeFe],[3,4] (2) hydrogenase containing nickel-iron cluster, which is called [NiFe],[5-7] and (3) hydrogenase containing only one iron center, which is called [Fe].[8-10] Among them, [NiFe]-hydrogenases are most widely investigated. To explore the catalysis of this hydrogenase, many experiments have been attempted to synthesize good model of [NiFe]-hydrogenase, so far. Actually, the activation of H_2 with such model of hydrogenase as Ir-Ir,[11,12] Rh-Rh,[13] Mo-Mo,[14] W-Ir,[15] and W-Ru[16] dinuclear complexes was reported. However, reports of interconversion of H_2 to protons and electrons have been limited.[17]

Recently, Matsumoto, Tatsumi, and their coworkers reported a hydroxo/sulfido-bridged Ru-Ge dinuclear complex $[Dmp(Dep)Ge(\mu\text{-}S)(\mu\text{-}OH)Ru(PPh_3)]^+(BAr^F{}_4)^-$ (Dmp = 2,6-dimesitylphenyl, Dep = 2,6-diethylphenyl, $Ar^F{}_4$ = 3,5-$(CF_3)_2C_6H_3$), as a functional hydrogenase model, as shown in Scheme 1.[18] This Ru-Ge dinuclear complex is considerably interesting, described below: (1) This Ru-Ge complex performs σ-bond activation of H_2 at room temperature to afford H_2O and $[Dmp(Dep)Ge(\mu\text{-}S)(\mu\text{-}H)Ru(PPh_3)]^+(BAr^F{}_4)^-$. (2) Addition of H_2O to the product induces reverse reaction to afford H_2 and the Ru-Ge complex,

Scheme 1

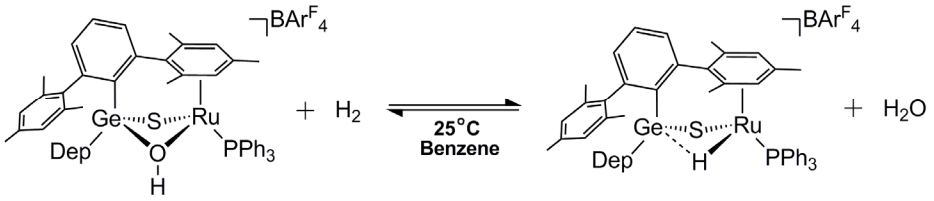

which indicates that the interconversion between H_2 and H_2O is catalyzed by this Ru-Ge complex. Although many H_2 σ-bond activations have been reported, this type of reversible reaction has been limited so far, to our knowledge. (3) This complex contains of sulfido bridged transition metal and non-transition metal elements. It is interesting to clarify whether the non-transition metal center plays important roles or not. (4) The product complex contains Ru-S-Ge-H four member-ring. Because the interaction between germanium and transition metal has not been reported except for a few pioneering works,[19] this four member-ring structure including Ru and Ge is interesting.

The H_2 activation with dinuclear complex has been theoretically investigated by several groups. Hoffmann and Trinquier investigated the four-center H_2 activation by $[Mn_2(CO)_6]$ with extended Hückel MO method and reported the transition state of H_2 activation.[20] Ienco and Mealli et al. investigated the activation of H_2 by sulfido-bridged rhodium dinuclear complex $[(PH_3)_3Rh(\mu\text{-}S)_2Rh(PH_3)_3]$ with the DFT method and reported that this dinuclear complex performs activation of H_2 with the Ru-(μ-S) moiety in heterolytic manner.[21] Nocera et al. investigated the reaction by di-iridium complex with the DFT method and disclosed the importance of cooperative roles of two Ir centers.[22]

In this theoretical work, we investigated the interconversion between H_2 and H_2O by the hydroxo/sulfido-bridged Ru-Ge dinuclear complex $[Dmp(Dep)Ge(\mu\text{-}S)(\mu\text{-}OH)Ru(PPh_3)]^+$

1. Our purposes here are to clarify the reaction course of this interconversion reaction and to understand what roles the germanium center plays in this reaction by comparing the reactivity of **1** with that of the Si analogue. Though the difference in reactivity between carbon and heavier 14 group elements was theoretically discussed,[23] the reactivity difference between them for the H-H σ-bond activation has not been reported yet. Also, we wish to present the theoretical understanding of bonding nature of $[Dmp(Dep)Ge(\mu\text{-}S)(\mu\text{-}H)Ru(PPh_3)]^+$ **PRD**, because this complex contains interesting four-member ring structure.

5.2. Computational Details

Geometries were optimized with ONIOM method, where the DFT method was used for the important moiety and the MM method with UFF force field was employed for whole system. In the important part, the Dmp, Dep, three phenyl groups of triphenyl phosphine, and three methyl groups of arene group coordinated with Ru center are replaced with H atoms. In DFT calculations, B3LYP functional was used for exchange-correlation term.[24-26] We named this computational procedure ONIOM(B3LYP:UFF) hereafter. We ascertained that each equilibrium geometry exhibited no imaginary frequency and each transition state exhibited one imaginary frequency. Two kinds of basis set systems were used. The smaller system (BS1) was used for geometry optimization. In this BS1, core electrons of Ru (up to 3f) were replaced with effective core potentials (ECPs),[27] and their valence electrons were represented with (311111/22111/411) basis set.[27] For H, C, O, P, and S, 6-31G* basis sets were employed.[28] The better basis set system (BS2) was used for evaluation of energy changes. In this BS2, (311111/22111/411/11) basis set[27, 30] was employed for Ru, where the same ECPs[27] as those of BS1 was employed for core electrons. For H, C, N, O, P, and S, the 6-311G* basis sets[31] were employed. In both of BS1 and BS2, a p-polarization function[29] was added for the H atoms of dihydrogen molecule, μ-OH, and H_2O. Zero-point energy was evaluated with the ONIOM(B3LYP/BS1:UFF) method under assumption of harmonic

oscillator.

The Gaussian 03 program package[32] was used for all calculations. Population analysis was carried out with the method of Weinhold et al.[33] Analysis of electron density distribution was performed using AIMPAC developed by Bader et al.[34] Molecular orbitals were drawn with the MOLEKEL program package.[35]

5.3. Results and Discussion

We investigated the interconversion reaction between H_2 and H_2O with **1**. As shown in Scheme 2, there are four courses for the approach of H_2 to the Ru center. After the dissociation of μ-OH group from the Ru center, H_2 coordinates with the Ru on either the μ-OH or the μ-S side of **1**. These courses are called paths 1O and 1S, respectively, hereafter. In these two paths, the arene group coordinates with the Ru center in η^6-manner. Also, there is a possibility that the η^6-arene changes into the η^4-arene form. In this case, H_2 coordinates with the Ru center in either μ-OH side or μ-S side of **1**, too. These are called paths 2O and 2S, respectively.

5.3.1. H_2 coordination reaction in paths 1O, 1S, 2O, and 2S

First, we investigate the geometry changes of the path 1O. Starting from **1**, the Ru-O distance becomes longer to afford intermediate complex **2** through transition state $\mathbf{TS_{1\text{-}2}}$, as shown in Figure 1. In $\mathbf{TS_{1\text{-}2}}$, the Ru-O distance considerably lengthens by 0.978 Å and the Ru-S distance moderately shortens by 0.120 Å. In **2**, the Ru-O distance (4.274 Å) is very long, indicating that the OH group does not coordinate with the Ru. It is noted that the Ru-S distance considerably shortens to 2.223 Å, which will be discussed bellow in more detail. In both **2** and $\mathbf{TS_{1\text{-}2}}$, the H_2 molecule is distant from the Ru center, indicating that **2** can not be considered to be H_2 σ-complex; Based on these features, **2** is understood to be an isomer of **1** in which the OH ligand interacts only with the Ge center. Starting from **2**, the H_2

Scheme 2[a]

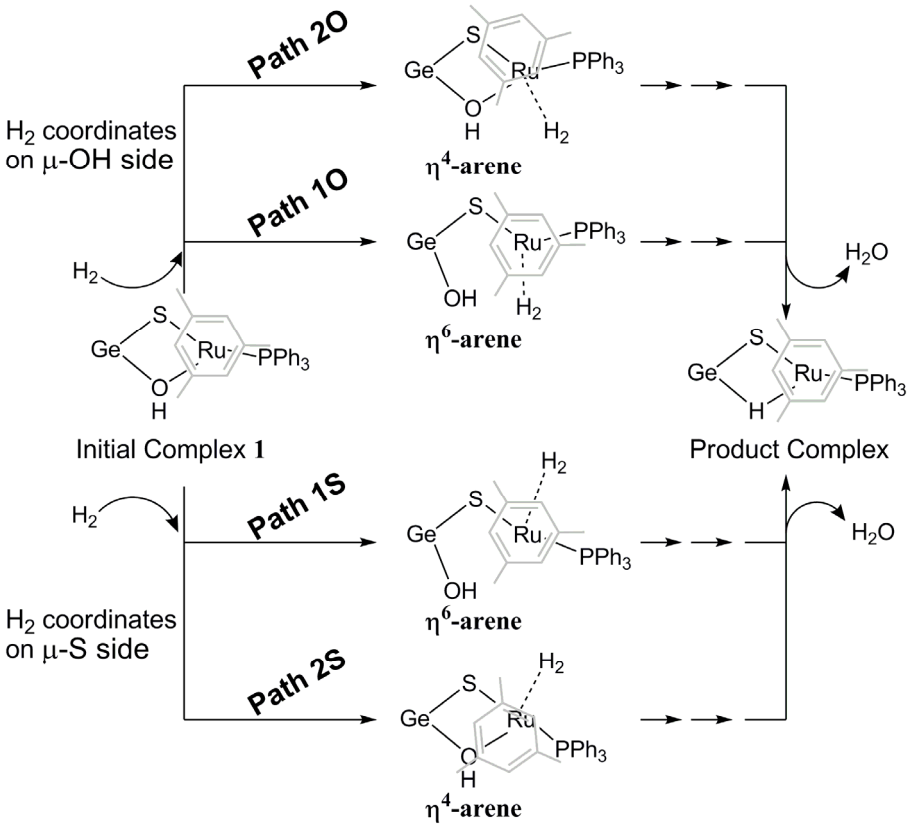

[a] Arene group drawn by gray indicates arene group coordinated to Ru center.

coordination with the Ru center occurs through transition state **TS$_{2\text{-}3}$** to afford H_2 σ-complex **3**. In **TS$_{2\text{-}3}$**, the Ru-H^{α} and Ru-H^{β} distances considerably shorten to about 2.5 Å and the H^{α}-H^{β} distance slightly lengthens to 0.752 Å, where H^{α} and H^{β} represent H atom approaching the Ru center and that approaching the OH group, respectively. In **3**, the H^{α}-H^{β} bond distance moderately lengthens to 0.892 Å and the Ru-S distance considerably lengthens to 2.425 Å again, which is close to that of **1**. Although we expected that H_2 coordination occurs concomitantly with the Ru-O bond lengthening, such transition state could not be found in our calculations.

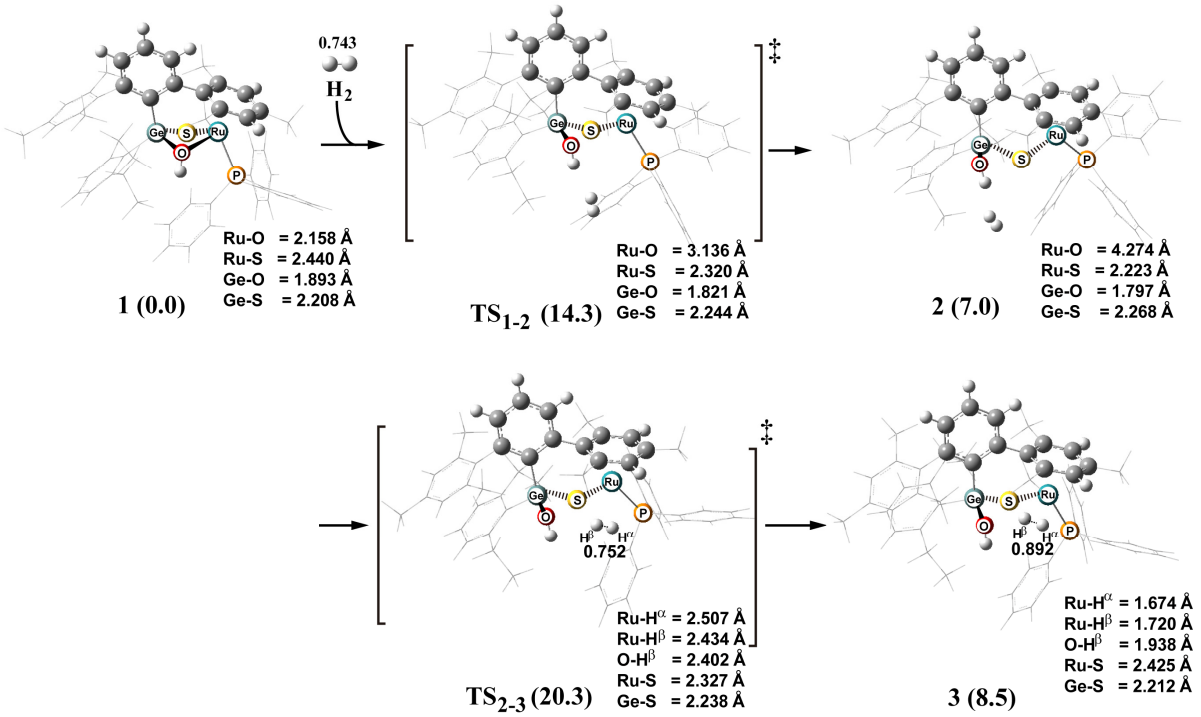

Figure 1. Geometry changes in H_2 coordination to $[Dmp(Dep)Ge(\mu\text{-}OH)(\mu\text{-}S)Ru(PPh_3)]^+$ **1** through path 1O. Bond lengths are in angstrom and angles are in degree. In parenthesis is the relative energy (kcal/mol unit) to **1** + H_2, where the ONIOM(B3LYP/BS2:UFF) method with solvation effect was employed. ‡ indicates the transition state.

We investigated another reaction course path 1S for the H_2 coordination in which H_2 approaches the Ru center in the μ-S side. Starting from **1**, the Ru-O distance considerably lengthens to 3.122 Å in $\mathbf{TS_{1\text{-}2S}}$ to afford intermediate $\mathbf{2_S}$, as shown in Figure 2, but the Ru-S distance little changes and the Ru-H_2 distance is very long. These results indicate that the Ru-O bond is completely broken but the H_2 does not coordinate with the Ru center like **2**. Thus, $\mathbf{2_S}$ is understood to be isomer of **1**, too. Then, the H_2 coordinates to the Ru center through $\mathbf{TS_{2S\text{-}3S}}$ to form the dihydrogen σ-complex $\mathbf{3_S}$. Though these geometry changes are similar to those of path 1O, we will present brief discussion here. The geometry of $\mathbf{TS_{1\text{-}2S}}$ is similar to that of $\mathbf{TS_{1\text{-}2}}$ except for the position of H_2; in the path 1S, the H_2 approaches the μ-S side but the μ-OH side in path 1O. The geometry of $\mathbf{2_S}$ is similar to that of **2**. This is

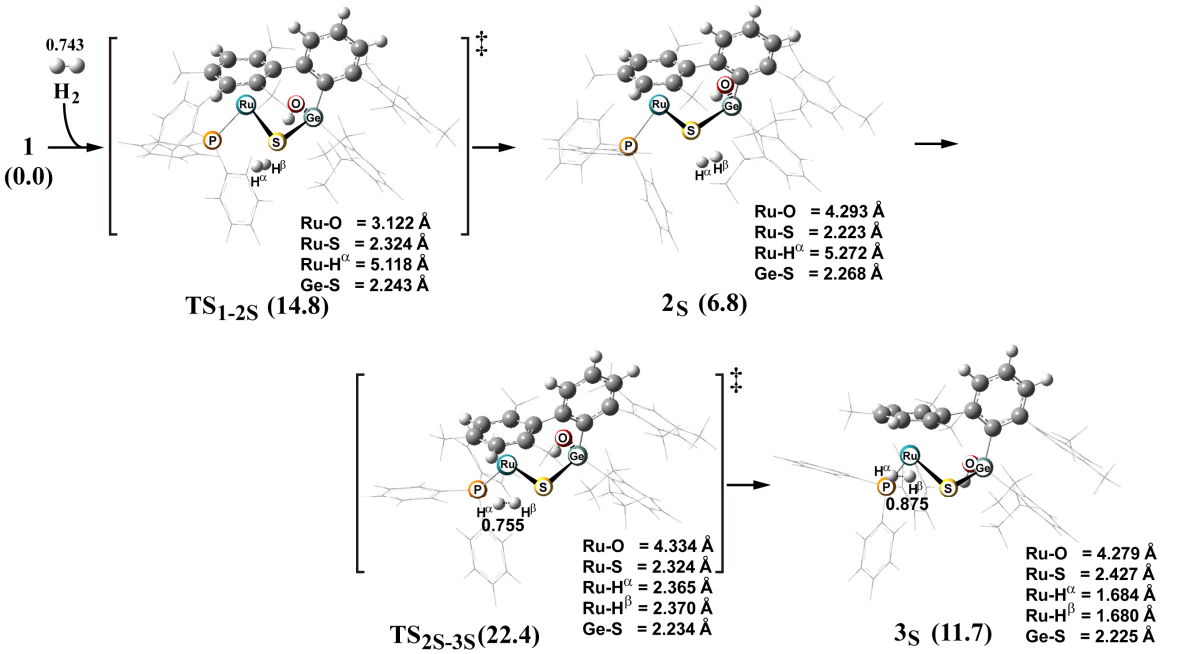

Figure 2. Geometry changes in H_2 coordination to $[Dmp(Dep)Ge(\mu\text{-}OH)(\mu\text{-}S)Ru(PPh_3)]^+$ **1** through path 1S. Bond lengths are in angstrom and angles are in degree. In parenthesis is the relative energy (kcal/mol unit) to **1** + H_2, where the ONIOM(B3LYP/BS2:UFF) method with solvation effect was employed. ‡ indicates the transition state.

because the interaction between H_2 and the Ru center is very weak. In $\mathbf{TS_{2S\text{-}3S}}$, the Ru-$H^{\alpha}$ and Ru-H^{β} distances shorten to 2.365 Å and 2.370 Å, respectively. In $\mathbf{3_S}$, the H^{α}-H^{β} distance lengthens to 0.875 Å, which is slightly longer than that of **3**.

We calculated energy changes by the H_2 coordination step in paths 1O and 1S with the ONIOM(B3LYP/BS2:UFF), where solvation effects of benzene in important part were evaluated with PCM method. As shown in Figure 3, $\mathbf{TS_{1\text{-}2}}$ and $\mathbf{TS_{2\text{-}3}}$ are more unstable than the sum of reactants, **1** + H_2, by 14.3 and 20.3 kcal/mol, respectively. These results indicate that the H_2 activation via $\mathbf{TS_{2\text{-}3}}$ occurs with more difficulty than the isomerization of the Ru-Ge complex via $\mathbf{TS_{1\text{-}2}}$. The intermediate **3** is 7.0 kcal/mol more unstable than the sum of reactants. In the path 1S, the activation barriers for $\mathbf{TS_{1\text{-}2S}}$ and $\mathbf{TS_{2S\text{-}3S}}$ are 14.8 and 22.4

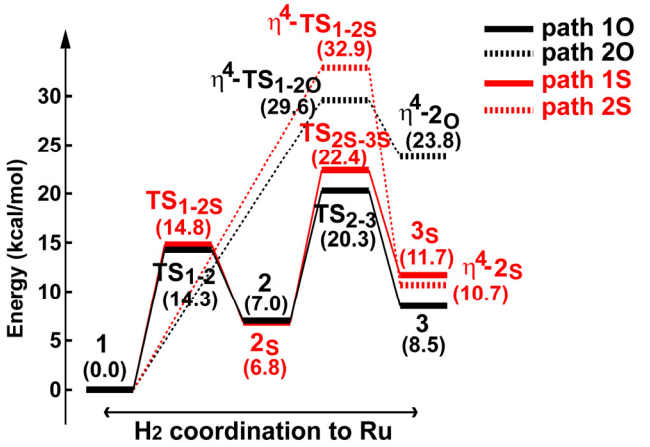

Figure 3. Energy changes in H_2 coordination to Ru center from μ-OH side through paths 1O, 1S, 2O, and 2S. Black solid and broken lines indicate energy changes in path 1O and 2O, respectively. Red solid and broken lines indicate energy changes in path 1S and 2S, respectively. These energies were corrected with zero-point energy.

kcal/mol, respectively, and the ΔE value for $\mathbf{3_S}$ is moderately larger than that for **3**, indicating that $\mathbf{3_S}$ exists in the solution to a lesser extent than **3**.

In the other reaction courses, paths 2O and 2S, the η^6-arene group changes to the η^4-arene form, as shown in Figure 4. When H_2 approaches **1** from the μ-OH side via path 2O, the H_2 coordination occurs through transition state $\mathbf{\eta^4\text{-}TS_{1\text{-}2O}}$ to afford intermediate $\mathbf{\eta^4\text{-}2_O}$. In $\mathbf{\eta^4\text{-}TS_{1\text{-}2O}}$, the Ru-$C^\alpha$ and Ru-C^β distances lengthen to 2.854 Å and 2.436 Å, respectively, while the Ru-C^α and Ru-C^β are 2.270 Å and 2.240 Å, respectively, in **1**. These geometry changes indicate that the η^6-arene is changing to the η^4-arene in $\mathbf{\eta^4\text{-}TS_{1\text{-}2O}}$. The Ru-$H^\alpha$ and Ru-H^β distances are 2.940 Å and 2.624 Å, respectively, and the H-H distance little changes from the equilibrium distance, indicating that the interaction between Ru and H_2 is still weak. In $\mathbf{\eta^4\text{-}2_O}$, the Ru-$H^\alpha$ and Ru-H^β distances shorten to 1.786 Å and 1.780 Å, respectively, indicating that the H_2 coordinates with the Ru center and $\mathbf{\eta^4\text{-}2_O}$ is understood to be a H_2

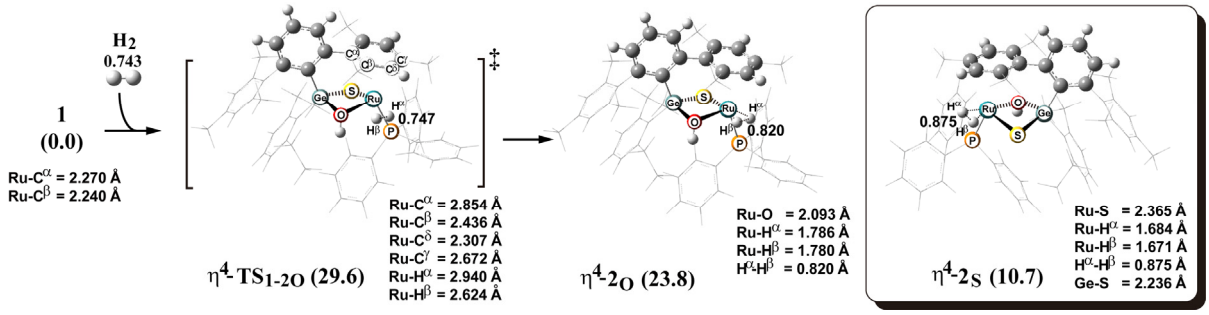

Figure 4. Geometry changes in H_2 coordination to μ-OH side of $[Dmp(Dep)Ge(\mu\text{-}OH)(\mu\text{-}S)Ru(PPh_3)]^+$ **1** through path 2O. Bond lengths are in angstrom and angles are in degree. In parenthesis is the relative energy (kcal/mol unit) to **1** + H_2, where the ONIOM(B3LYP/BS2:UFF) method with solvation effect was employed. η^4-**2S** surrounded by rectangle is intermediate complex where H_2 coordinates to Ru on μ-S side in path 2S. ‡ indicates the transition state.

σ-complex. These distances are longer than those in **3** and **3S**, suggesting that the interaction between the Ru and the H_2 is weaker in η^4-**2O** than in **3** and **3S**. Because the geometry changes in the path 2S are essentially the same as those in the path 2O, only H_2 σ-complex **η-2S** is shown in Figure 4; see Figure A1 for details. In η^4-**2S**, the Ru-H^α and Ru-H^β distances are 1.684 Å and 1.671 Å, respectively, which are shorter than those of η^4-**2O**.

The energy changes in the paths 2O and 2S are shown in Figure 3. In the path 2O, η^4-**TS1-2O** and η^4-**2O** are 29.6 kcal/mol and 23.8 kcal/mol above the sum of reactants **1** + H_2, respectively. In path 2S, η^4-**TS1-2S** and η^4-**2S** are 32.9 kcal/mol and 10.7 kcal/mol above the sum of reactants, respectively. Apparently the H_2 coordination easier occurs through paths 1O and 1S with smaller activation barrier of 20.3 - 22.4 kcal/mol than the paths 2O and 2S in which the activation barrier is 29.6 - 32.9 kcal/mol. Thus, we wish to skip discussion of the paths 2O and 2S.[36] We will discuss the H-H σ-bond activation starting from **3** and **3S**, below.

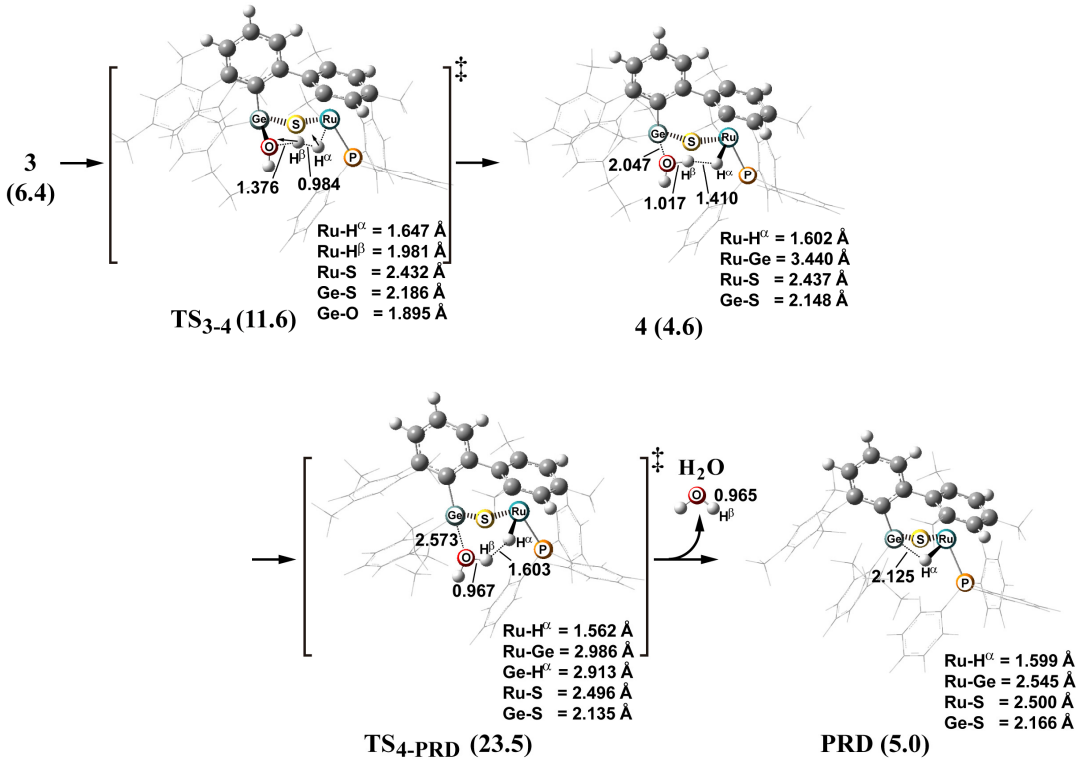

Figure 5. Geometry changes in H-H σ-bond activation and H_2O dissociation with [Dmp(Dep)Ge(μ-OH)(μ-S) Ru(PPh_3)]$^+$ **1** through path 1O. Bond lengths are in angstrom and angles are in degree. In parenthesis is the relative energy (kcal/mol unit) to **1** + H_2, where the ONIOM(B3LYP/BS2:UFF) method with solvation effect was employed. ‡ indicates the transition state.

5.3.2. H-H σ-bond activation and H_2O dissociation in paths 1O and 1S

Here, we wish to discuss H-H σ-bond activation and H_2O dissociation in the paths 1O and 1S. In the path 1O starting from **3**, the H-H σ-bond activation occurs through **TS$_{3\text{-}4}$** to afford intermediate **4**, as shown in Figure 5. In **TS$_{3\text{-}4}$**, the H^{α}-H^{β} distance considerably lengthens to 0.984 Å and the O-H^{β} distance shortens to 1.376 Å, indicating that the H^{β} is moving from the H^{α} toward the OH group in **TS$_{3\text{-}4}$**. This movement is also represented by the imaginary frequency: see **TS$_{3\text{-}4}$** in Figure 5 for the arrows which represent important movements of nuclei in the imaginary frequency. In **4**, the O-H^{β} distance considerably

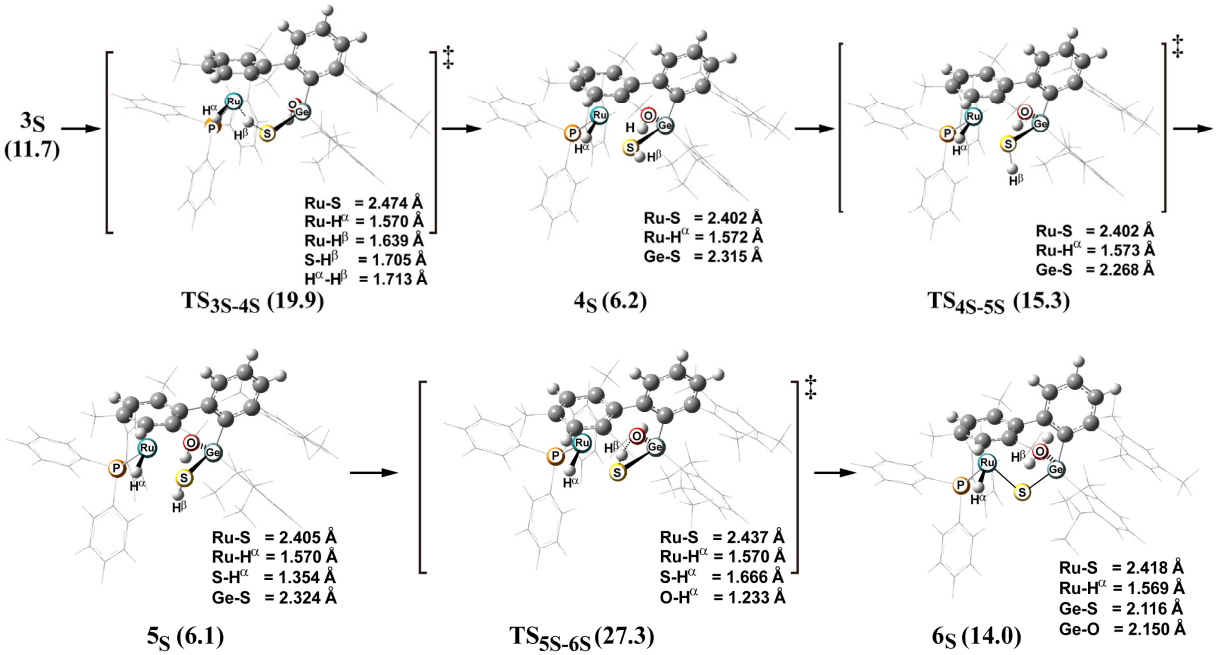

Figure 6. Geometry changes in H_2 coordination to Ru center of $[Dmp(Dep)Ge(\mu\text{-}OH)(\mu\text{-}S)Ru(PPh_3)]^+$ **1** from μ-S side through path 1S. Bond lengths are in angstrom and angles are in degree. In parenthesis is the relative energy (kcal/mol unit) to **1** + H_2, where the ONIOM(B3LYP/BS2:UFF) method with solvation effect was employed. ‡ indicates the transition state.

shortens to 1.017 Å which is almost the same as that of water and the Ge-O distance considerably lengthens to 2.047 Å. It is noted that the H^{α}-H^{β} distance (1.410 Å) is not very long even in **4**, suggesting that attractive interaction such as electrostatic interaction exists between them. This type of short H-H distance is often observed in the product of heterolytic H-H cleavage.[36] Then, the H_2O dissociates from the Ge center through $\mathbf{TS_{4\text{-}PRD}}$ to afford the final product **PRD** and H_2O. In $\mathbf{TS_{4\text{-}PRD}}$, the Ge-O and the H^{α}-H^{β} bond distances lengthen to 2.573 Å and 1.603 Å, respectively, which indicates that the H_2O is dissociating from the Ge. In **PRD**, the Ru-H^{α} bond distance (1.599 Å) is short, indicating that the Ru-H (hydride) bond is completely formed. It is noted here that the Ge-H^{α} distance

is 2.125 Å. The similar Ge-H^{α} distance is often observed in the germane σ-complex of transition metal complex.[37] This Ge-Ha distance will be discussed below in more detail.

In the path 1S, the H-H σ-bond is activated through transition state $\mathbf{TS_{3S\text{-}4S}}$ to afford intermediate $\mathbf{4_S}$. In $\mathbf{4_S}$, the H^{β} atom is bound with the μ-S, as shown in Figure 6. In $\mathbf{TS_{3S\text{-}4S}}$, the H^{α}-H^{β} distance considerably lengthens to 1.713 Å, indicating that the H-H σ-bond breaking occurs in this transition state. The Ru-H^{β} and S-H^{β} distances are 1.570 Å and 1.639 Å, respectively, indicating that the Ru-H (hydride) and S-H bond formations are almost completed. Although the H^{β} is bound with the μ-S in $\mathbf{4_S}$, the Ru-S distance becomes shorter when going from $\mathbf{TS_{3S\text{-}4S}}$ to $\mathbf{4_S}$, indicating that the SH group plays the role of bridging ligand between the Ru and Ge centers. Then, $\mathbf{4_S}$ isomerizes to $\mathbf{5_S}$ through transition state $\mathbf{TS_{4S\text{-}5S}}$, where the H^{β} is changing its position by the rotation of the SH group around the Ge-S bond. In the next step, the H^{β} migrates from the S atom to the OH group through transition state $\mathbf{TS_{5S\text{-}6S}}$, to afford $\mathbf{6_S}$. In $\mathbf{TS_{5S\text{-}6S}}$, the S-$H^{\beta}$ distance lengthens to 1.666 Å and the O-H^{β} distance shortens to 1.233 Å. In $\mathbf{6_S}$, the Ge-O distance (2.150 Å) is considerably long. $\mathbf{6_S}$ is more unstable than **4**, as will be discussed below. Thus, the isomerization of $\mathbf{6_S}$ to **4** must be examined. The H^{α} coordinates with the Ru at the position cis to H_2O in **4** but at the position trans to H_2O in $\mathbf{6_S}$. For this isomerization, PPh_3 needs to dissociate from the Ru center in $\mathbf{6_S}$ to afford $\mathbf{7_S}$, as shown in Figure 7; if the PPh_3 does not dissociate from the Ru, the H^{α} can not move to the position cis to H_2O. Starting form $\mathbf{7_S}$, the H^{α} migrates to the position cis to the H_2O through $\mathbf{TS_{7S\text{-}8S}}$ to afford $\mathbf{8_S}$. Finally, the PPh_3 coordinates with the Ru, again to afford **4**. After that, the H_2O dissociates from the Ge to afford **PRD** like in path 1O.

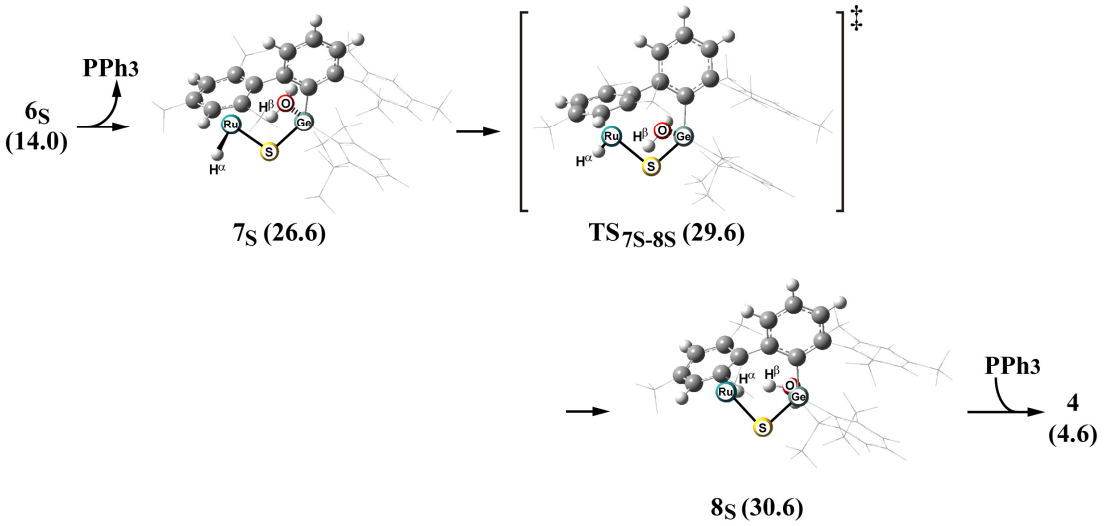

Figure 7. Geometry changes in H_2 coordination to Ru center of $[Dmp(Dep)Ge(\mu\text{-}OH)(\mu\text{-}S)Ru(PPh_3)]^+$ **1** from μ-S side through path 1S. Bond lengths are in angstrom and angles are in degree. In parenthesis is the relative energy (kcal/mol unit) to **1** + H_2, where the ONIOM(B3LYP/BS2:UFF) method with solvation effect was employed. ‡ indicates the transition state.

The energy changes are calculated with the ONIOM(B3LYP/BS2:UFF). In the path 1O, the H-H σ-bond activation occurs with small barrier of 11.6 kcal/mol, as shown in Figure 8. The final H_2O dissociation occurs with moderate activation barrier of 23.5 kcal/mol which is defined as the energy difference from the sum of reactants **1** + H_2. In the path 1S, the activation barrier is 27.3 kcal/mol for $\mathbf{TS_{5S\text{-}6S}}$, which is considerably larger than that of the most unstable transition state $\mathbf{TS_{4\text{-}PRD}}$ in the path 1O. Thus, it is clearly concluded that the path 1O is more favorable than the path 1S.[38] In the path 1O, the rate-determining step is the H_2O dissociation.

The reverse reaction of this conversion is experimentally observed by adding of excess H_2O. As shown in Figure 8, although **PRD** is moderately more unstable than **1** + H_2, the energy difference is small. Because the most unstable transition state is $\mathbf{TS_{4\text{-}PRD}}$, the rate-determining step is the H_2O coordination with the Ge through $\mathbf{TS_{4\text{-}PRD}}$ in the reverse

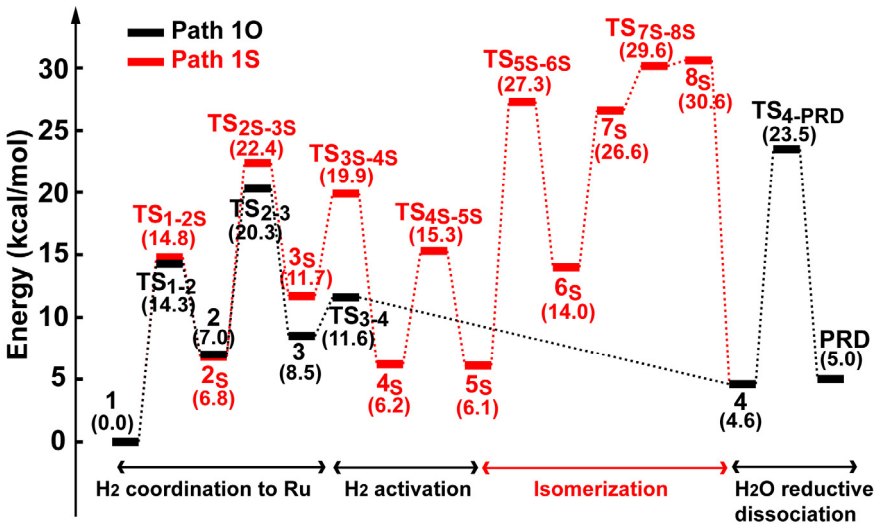

Figure 8. Energy changes in path 1O and 1S. Black and red lines indicate energy changes in path 1O and 1S, respectively. These energies were corrected with zero-point energy.

reaction. The activation barrier (E_a) of the reverse reaction is 18.5 kcal/mol. This E_a is moderately smaller than that of forward reaction. Because the difference between the E_a values of the forward and reverse reactions is very small, the present computational results clearly show that the interconversion between H_2 and H_2O is efficiently catalyzed by **1**.

5.3.3. Reliability of the ONIOM(B3LYP:UFF) Method

Another important issue to be examined here is to check if the MM method with UFF force field in the ONIOM calculation presents reliable result. We investigated the geometry changes in the path 1O with the real complex by DFT(B3LYP)/BS2//DFT(B3LYP)/BS1 method, because this path is considered to be the most favorable, as discussed above.

All of their geometries around the Ru and Ge moieties resemble well the ONIOM-optimized ones, as shown in Figure A3. Also, the DFT(B3LYP)/BS2//DFT(B3LYP)/BS1-calculated energy changes are very close to those of the ONIOM-computational results; see Figure A4. From these results, it is conclude that the

ONIOM(B3LYP/BS2:UFF) method presents reliable results.

5.3.4. Roles of the μ-OH and μ-S ligands in the conversion of H_2 to H_2O

The donating μ-OH group dissociates from the Ru center when going to **2** from **1**. It is noted that the H^{α} and H^{β} atomic populations of H_2 little change when going to $\mathbf{TS_{1\text{-}2}}$ from **1**, indicating that the H_2 coordination is not involved in this step. The Ru atomic population little changes when going to **2** from **1**, too, though the μ-OH group dissociates from the Ru center. On the other hand, the S atomic population somewhat decreases. These population changes indicate that the charge transfer from the S to the Ru becomes stronger in **2** than in **1**, to recover the decrease in the Ru atomic population by the OH group dissociation. This charge transfer leads to the shortening of the Ru-S distance in **2**; remember that the Ru-S distance is 2.441 Å in **1** and 2.221 Å in **2**. This shortening of the Ru-S bond contributes to the stabilization of **2**. Furthermore, the Ge-OH distance becomes shorter in **2** than in **1**, which also contributes to the stabilization of **2**. In other words, the isomerization of **1** to **2** easily occurs due to the strengthenings of the Ru-S and Ge-OH bonds. When going to **3** from **2**, the H_2 coordination with the Ru center occurs with moderate endothermicity (8.5 kcal/mol). In this step, the H^{α}-H^{β} electron population considerably decreases and the Ru atomic population considerably increases, indicating that the charge transfer from H_2 to the Ru center participates in the coordinate bond of H_2. Simultaneously, the Ru-S distance and the μ-S atomic population return to almost the same values as those of **1**. These results indicate that the μ-S group plays important roles to stabilize the coordinatively unsaturated species **2** and then recover the increase in the Ru atomic population by the H_2 coordination.

Interesting and important population changes are observed when going from **3** to **4**, as follows: The H^{α} atomic population moderately increases but the H^{β} atomic population considerably decreases when going to **4** from **3**, which indicate that this H-H σ-bond activation occurs in a heterolytic manner like hydrogenase.[2] Thus, **1** works well as

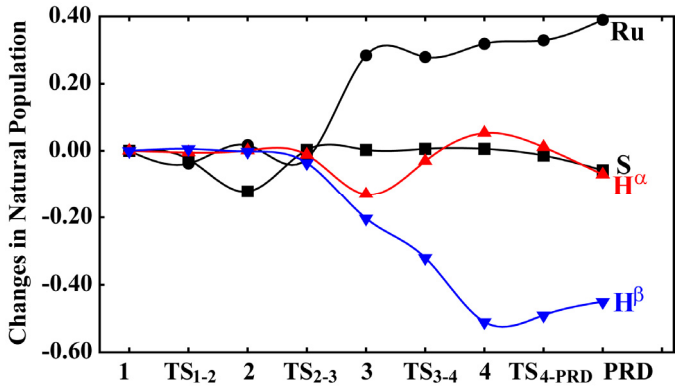

Figure 9. Electron population changes in the interconversion of H_2 to H_2O with ONIOM(B3LYP/BS2:UFF).

functional model of hydrogenase. Apparently, the OH group plays important roles in this heterolytic activation, as shown in **TS$_{3\text{-}4}$** of Figure 5. Interestingly, the Ru and Ge-OH moieties cooperatively participate in the H_2 activation, though they are separated from each other.

As shown in Figure 8, the rate-determining step is **TS$_{4\text{-}PRD}$**, in which the H_2O dissociates form the Ge center to afford free H_2O and **PRD**. In this step, the electron population of H_2O increases and the Ge atomic population further decreases because the CT from the H_2O to the Ge center becomes broken. Also, the H^{α} becomes almost neutral but the H^{β} becomes protonic. Because the H_2O dissociation from the Ge center is the rate-determining step, the Ge element plays important roles in this interconversion reaction. In a following section, we will discuss the role of germanium atom.

5.3.5. What roles does the germanium atom play in the interconversion reaction ?

To investigate the roles of the Ge atom, we investigated the reaction of H_2 with the Si analogue [Dmp(Dep)Si(μ-OH)(μ-S)Ru(PPh$_3$)]$^+$ **1$_{Si}$**, in which the Ge atom was replaced with the Si atom. The geometry changes are similar to those of the reaction by **1**, as shown in

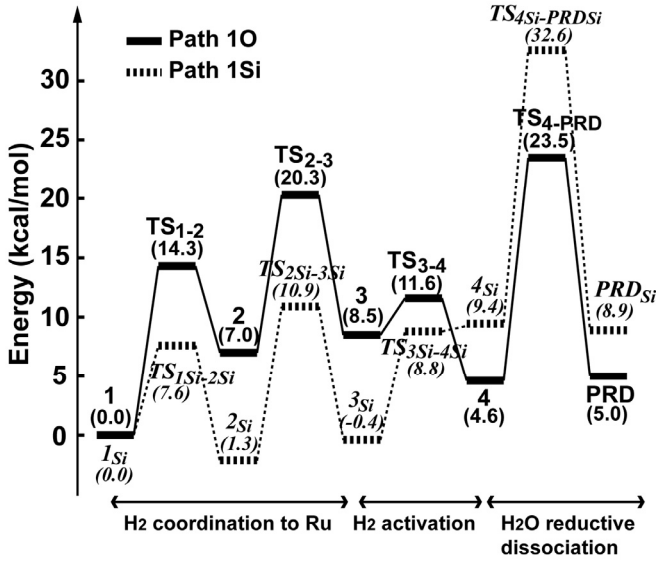

Figure 10. Energy changes in the interconversion of H and H_2O with $[Dmp(Dep)Ge(\mu\text{-}OH)(\mu\text{-}S)Ru(PPh_3)]^+$ **1** and $[Dmp(Dep)Si(\mu\text{-}OH)(\mu\text{-}S)Ru(PPh_3)]^+$ $\mathbf{1_{Si}}$. Solid and broken lines indicate energy changes of **1** and $\mathbf{1_{Si}}$, respectively.

Figure A5. As shown in Figure 10, the H_2 coordination occurs with activation barrier of 10.9 kcal/mol; see $\mathbf{TS_{2Si\text{-}3Si}}$ in Figure A5. The activation barrier of the H_2 σ-bond activation is close to that of the reaction by **1**. However, the H_2O dissociation requires much larger activation barrier of 32.6 kcal/mol than in the reaction by **1**; see $\mathbf{TS_{4Si\text{-}PRDSi}}$ in Figure A5. Because of this very large activation barrier, the Si analogue is not useful for this H-H σ-bond activation. To investigate this difference of activation barrier, we calculated the Si-OH_2 and Ge-OH_2 bond energies of model compounds $GePh_2(SH)(H_2O)^+$ $\mathbf{Ge_M}$ and $SiPh_2(SH)(H_2O)^+$ $\mathbf{Si_M}$, respectively. As shown in Figure 11, geometries of $\mathbf{Ge_M}$ and $\mathbf{Si_M}$ resemble those of Ge moiety in **4** and Si moiety in $\mathbf{4_{Si}}$. The sum of the C^1-Ge-C^2, C^1-Ge-S, and C^2-Ge-S angles in $\mathbf{Ge_M}$ is 353.5 degrees and that of the C^1-Si-C^2, C^1-Si-S, and C^2-Si-S angle of $\mathbf{Si_M}$ is 350.4 degrees. These large angles around Ge and Si centers indicate that the $GePh_2(SH)$ and $SiPh_2(SH)$ moieties are planer rather than tetrahedral, suggesting that the Ge and Si centers

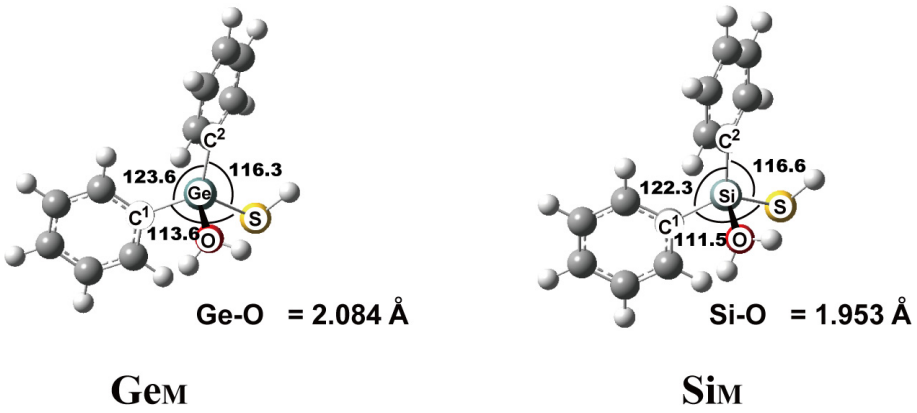

GeM **SiM**

Figure 11. Geometries of model complex $GePh_2(SH)(H_2O)$ $\mathbf{Ge_M}$ and $SiPh_2(SH)(H_2O)$ $\mathbf{Si_M}$.

are cation-like. As shown in Table 1, Si-OH_2 bond energy is much larger than the Ge-OH_2 bond energy. These results indicate that Ge-OH_2 dissociation occurs easier than the Si-OH_2 dissociation. The difference of bond energies can be interpreted in terms of orbital energy of unoccupied p orbital. As shown in Table 2, the unoccupied p orbital energy of $\mathbf{Ge_M}$ is higher than that of $\mathbf{Si_M}$, indicating that H_2O form strong CT with $[S_2Ph_2(SH)]^+$ than with the Ge analogue.

5.3.6. Bonding nature of $[Dmp(Dep)Ge(\mu\text{-}S)(\mu\text{-}H)Ru(PPh_3)]^+$ PRD and those of Si analogue complex $\mathbf{PRD_{Si}}$

We investigated that the bonding natures of **PRD** and $\mathbf{PRD_{Si}}$. The Ge-H^{α} distance (2.125 Å) of **PRD** is much longer than that of free GeH_4 (the optimized distance is 1.539 Å). But, the similar long Ge-H distance is observed in germane σ-complex, as mentioned above. The Ru-Ge distance (2.545 Å) of **PRD** and the Ru-Si distance (2.527 Å) of $\mathbf{PRD_{Si}}$ are somewhat longer than typical Ru-germyl and Ru-silyl bond distances, respectively. From these geometries, it is not clear whether or not Ru-Ge and Ru-Si bonds exist and whether or

Table 1. Bond energies of Si-OH_2 and Ge-OH_2 bond were calculated using DFT(B3LYP)/BS2 with PCM corrections.[a]

	Bond energy
Si-OH_2	39.6
Ge-OH_2	25.5

[a] In kcal/mol unit.

Table 2. Orbital energy (LUMO) of $\mathbf{Ge_M}$ and $\mathbf{Si_M}$ (in eV).

	DFT	HF
$\mathbf{Ge_M}$	-5.40	-2.12
$\mathbf{Si_M}$	-5.45	-2.21

not the Ge-H^{α} and Si-H^{α} bond exist. To shed light on the bonding nature, we investigated electron density distribution of **PRD** and $\mathbf{PRD_{Si}}$ with atoms in molecule (AIM) analysis. According to this AIM analysis, a molecular structure is defined as a network of atomic interaction lines linking nuclei. This network is called a molecular graph. As shown in Figure 12(A), three BCPs between Ru-Ge, Ru-S, and Ge-S were observed in the Ru-Ge-S plane. In Figure 12(B), two BCPs were observed in the Ru-Ge-H^{α}. These results indicate that the Ru is bonded with the Ge, the S, and the H^{α} bond and the Ge is bound with the S. However, it is noted that the BCP between Ge and H^{α} was not found, indicating that the Ge is not bound with the H^{α}. As shown in Figure 12(C), only two BCPs were observed in the Ru-Si-S plane, indicating the presence of the Ru-S and Si-S bonds and the absence of the Ru-Si bond. Also, two BCPs were found in the Si-Ru-H^{α} palne, as shown in Figure 12(D),

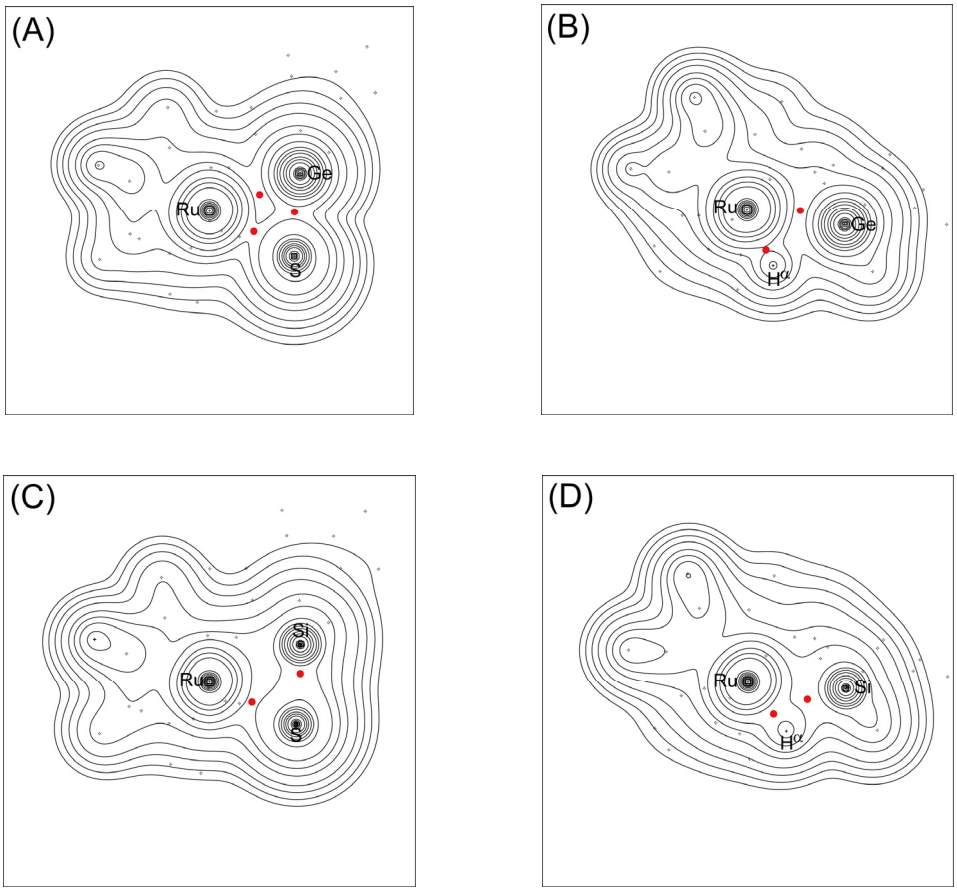

Figure 12. Electron density distribution of (A) Ru-Ge-S plane in **PRD**, (B) Ru-Ge-H^{α} plane in **PRD**, (C) Ru-Si-S plane of $\mathbf{PRD_{Si}}$, and (D) .Ru-Si-H^{α} plane of $\mathbf{PRD_{Si}}$. Red dots indicate the bond critical point.

indicating the presence of the Ru-H^{α} and Si-H^{α} bond. These results indicate that the Ge was not bound with the H^{α} and the Ru-Ge bond is formed in **PRD**, but that the Si-H^{α} bond was not cleaved and the Ru-Si was not formed in $\mathbf{PRD_{Si}}$. Similar results were reported by Kubas et al. These results arise from strength of Ru-Ge and Ge-H^{α}.

5.4. Conclusions

The interconversion between H_2 and H_2O by μ-hydroxo/sulfido dinuclear ruthenium-germanium complex $[Dmp(Dep)Ge(\mu\text{-}S)(\mu\text{-}OH)Ru(PPh_3)]^+$ **1** (Dmp = 2,6-dimesitylphenyl, Dep = 2,6-diethylphenyl) was investigated with ONIOM method. In the H_2 conversion to H_2O, the first step is H_2 coordination with Ru, in which the Ru-O distance considerably lengthens to afford the intermediate **2** containing the vacant coordination site with activation (E_a) 14.3 kcal/mol. Then the H_2 further approaches the vacant site through transition state $\mathbf{TS_{2\text{-}3}}$ with E_a of 20.3 kcal/mol to afford the H_2 σ-complex **3**. Starting from **3**, the H-H σ-bond activation by the Ru-OH moiety occurs with E_a 11.6 kcal/mol to form intermediate **4** in which hydride coordinates with the Ru and H_2O interacts with the Ge. Finally, the H_2O dissociates from the Ge with E_a of 23.5 kcal/mol to afford product complex $[Dmp(Dep)Ge(\mu\text{-}S)(\mu\text{-}H)Ru(PPh_3)]^+$ **PRD** and H_2O.

The analysis of electron redistribution of this reaction shows interesting features as follows: (1) The Ru atomic population little changes when going to **2** from **1**, too, though the donating μ-OH group dissociates from the Ru center. On the other hand, the S atomic population somewhat decreases. These population changes indicate that the charge transfer from the S to the Ru becomes stronger in **2** than in **1**, to recover the decrease in Ru atomic population by the μ-OH group dissociation. (2) The H^{α} atomic population moderately increases but the H^{β} atomic population considerably decreases when going to **4** from **3**, which indicate that this H-H σ-bond activation occurs in a heterolytic manner like hydrogenase.

In the Si analogue complex $[Dmp(Dep)Si(\mu\text{-}S)(\mu\text{-}OH)Ru(PPh_3)]^+$ $\mathbf{1_{Si}}$. The H-H σ-bond activation easily occurs with E_a of 10.9 kcal/mol, but dissociation of H_2O from Si needs considerably large E_a of 32.6 kcal/mol. This is understood in terms of E-O bond energy (E = Ge and Si), which are evaluated to be 25.5 and 39.6 kcal/mol, respectively.

5.5. Appendix

Table A1. Optimized geometries of [Dmp(Dep)Ge(μ-S)(μ-OH)Ru(PPh_3)]$^+$ **1** and this model complex with DFT(B3LYP) and ONIOM(B3LYP/BS1:UFF) methods. Bond lengths are in angstrom.

	Tiny	Small	Real	ONIOM	Expt.[a]
R^1	H	CH_3	Dmp[b]	Dmp[b]	Dmp[b]
R^2	H	CH_3	Dep[c]	Dep[c]	Dep[c]
R^3	H	CH_3	C_6H_5	C_6H_5	C_6H_5
R^4	H	H	CH_3	CH_3	CH_3
Ru-S	2.460	2.470	2.455	2.441	2.421
Ru-OH	2.178	2.187	2.151	2.156	2.137
Ge-S	2.213	2.209	2.219	2.224	2.189
Ge-OH	1.905	1.904	1.905	1.896	1.884

[a] Matsumoto, T.; Nakaya, Y.; Itakura, N.; Tatsumi, K. *J. Am. Chem. Soc.* **2008**, *130*, 2458. [b] Dmp = 2,6-dimesitylphenyl [c] Dep = 2,6-diethylphenyl

Scheme A1

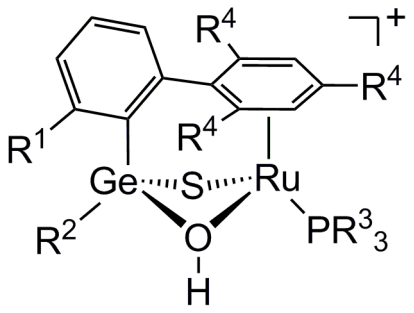

Table A2. Energy changes in H_2 coordination to Ru calculated with B3LYP/BS2 and ONIOM(B3LYP/BS2:UFF).

	2	**$TS_{2\text{-}3}$**	**3**
Tiny	1.1	8.8	2.5
Small	0.0	8.0	0.5
Real	6.1	17.3	6.5
ONIOM	3.1	17.4	6.4

[a] This is calculated with B3YLP/BS2 method. [b] This is calculated with ONIOM(B3YLP/BS2:UFF) method.

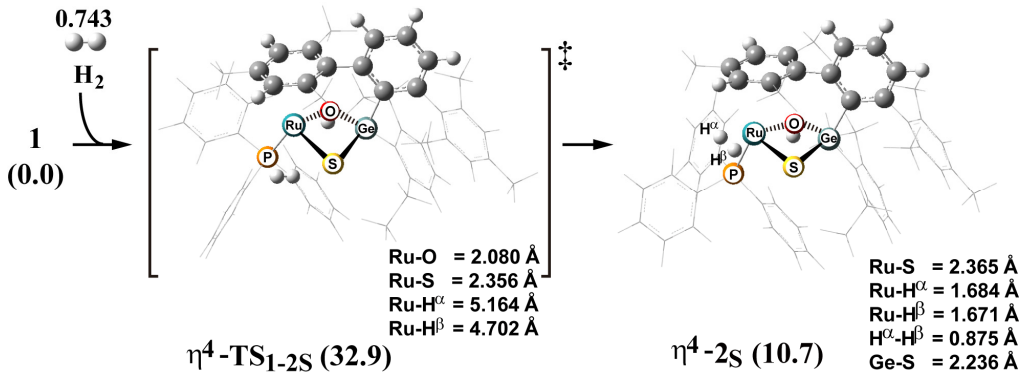

Figure A1. Geometry changes in H_2 coordination to μ-S side of $[Dmp(Dep)Ge(\mu\text{-}OH)(\mu\text{-}S)Ru(PPh_3)]^+$ **1** through path 2S. Bond lengths are in angstrom and angles are in degree. In parenthesis is the relative energy (kcal/mol unit) to **1** + H_2, where the ONIOM(B3LYP/BS2:UFF) method with solvation effect was employed. ‡ indicates the transition state.

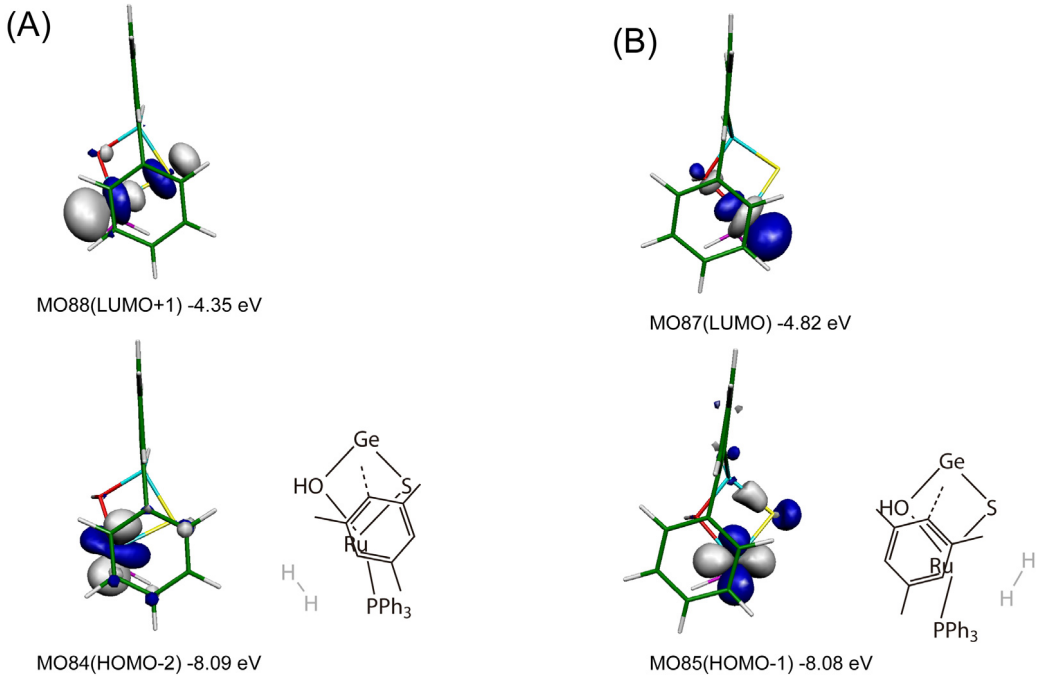

Figure A2. Important unoccupied orbitals and orbital energies of (A) η^4-arene RuGe dinuclear fragment in $\boldsymbol{\eta^4\text{-}2_O}$ and (B) in $\boldsymbol{\eta^4\text{-}2_S}$. These geometries of η^4-arene RuGe dinuclear fragments are fixed in $\boldsymbol{\eta^4\text{-}2_O}$ and $\boldsymbol{\eta^4\text{-}2_S}$, respectively.

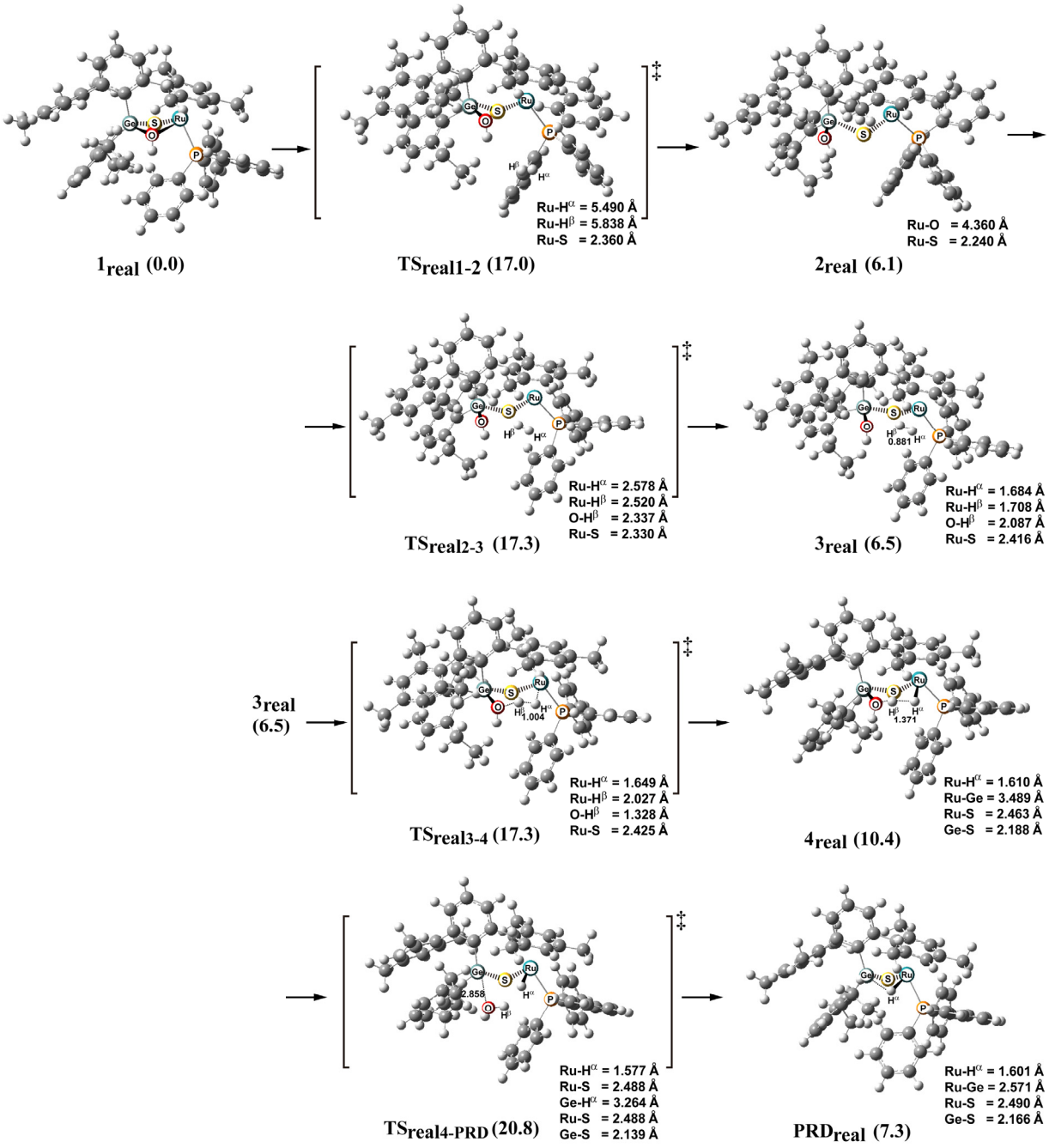

Figure A3. Geometry changes in interconversion with Real complex $[Dmp(Dep)Ge(\mu\text{-}OH)(\mu\text{-}S)Ru(PPh_3)]^+$ **1** with DFT(B3LYP)/BS1. In parenthesis is the relative energy (kcal/mol unit) to **1** + H_2, where the ONIOM(B3LYP/BS2:UFF) method with solvation effect was employed. ‡ indicates the transition state.

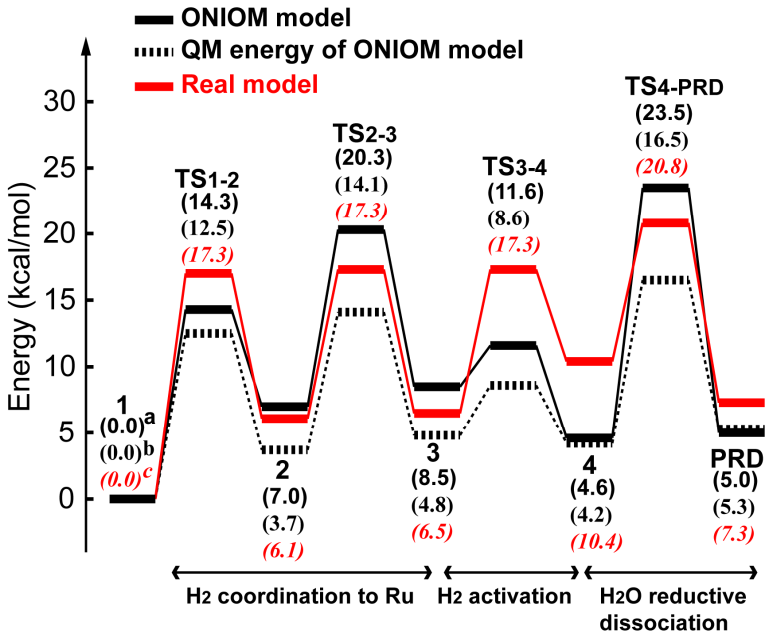

Figure A4. Energy changes in interconversion with ONIOM model **1**, QM moiety of **1**, and Real complex $[Dmp(Dep)Ge(\mu\text{-}OH)(\mu\text{-}S)Ru(PPh_3)]^+$ **1** with DFT(B3LYP)/BS2//DFT(B3LYP)/BS1. [a] The energy of ONIOM method. [b] The energy of QM region of ONIOM method. [c] The energy of real complex with DFT/BS1.

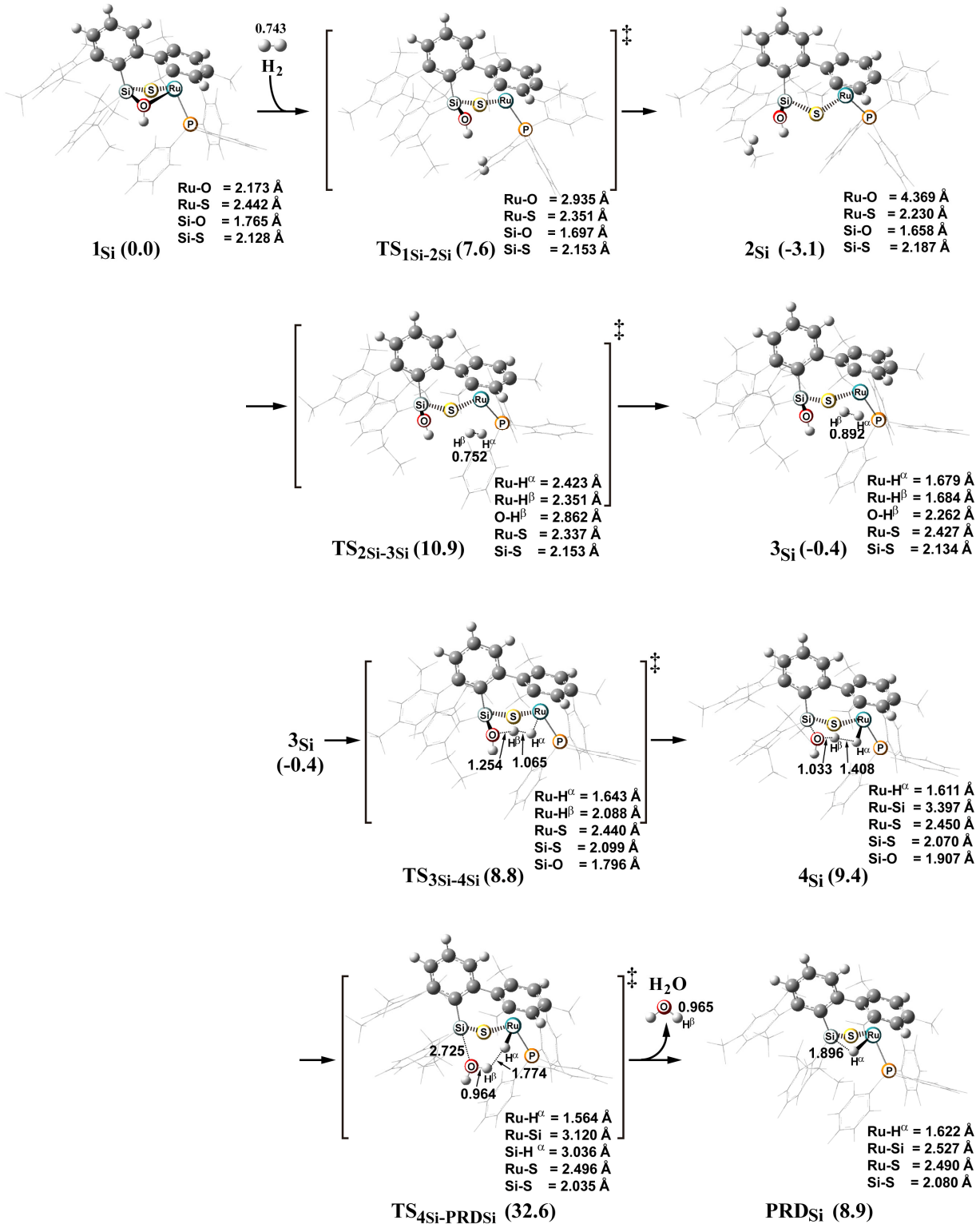

Figure A5. Geometry changes in interconversion with $[Dmp(Dep)Si(\mu\text{-}OH)(\mu\text{-}S)Ru(PPh_3)]^+$ **1**$_{Si}$ with ONIOM(B3LYP/BS1/UFF). In parenthesis is the relative energy (kcal/mol unit) to **1** + H_2, where the ONIOM(B3LYP/BS2:UFF) method with solvation effect was employed. ‡ indicates the transition state.

Reference

(1) (a) Kubas, G. J. *Comprehensive Organometallic Chemistry III* **2007**, *1*, 671. (b) Kubas, G. J. *Chem. Rev.* **2007**, *107*, 4152.

(2) Recent review; Lubitzs, W.; van Gastel, M.; Gärtner, W. In *Metal Ions in Life Science*; Sigel, A., Sigel, H., Sigel, R. K. O., Eds.; John Wiley & son, Ltd: New York, 2006; Vol. 2, pp 279-158. (b) Evans, D. J.; Pickett, C. J. *Chem. Soc. Rev*. **2003**, *32*, 268. (c) Vignais, P. M.; Billoud, B. *Chem. Rev.* **2007**, *107*, 4206. (d) Fontecilla-Camps, J. C.; Volbeda, A.; Cavazza, C.; Nicolet, Y. *Chem. Rev.* **2007**, *107*, 4273. (e) De Lacey, A. L.; Fernández, V.; Rousset, M.; Cammack, R. *Chem. Rev.* **2007**, *107*, 4304. (f) Lubitz, W.; Reijerse, E.; van Gastel, M. *Chem. Rev.* **2007**, *107*, 4331. (g) Siegbahn, P. E. M.; Tye, J. W.; Hall, M. B. *Chem. Rev.* **2007**, *107*, 4414.

(3) Nicolet, Y.; Lemon, B. J.; Fontecilla-Camps, J. C. ; Peters, J. W. *Trends Biochem. Sci.* **2000**, *25*, 138.

(4) Peters, J. W. *Curr. Opin. Struct. Biol.* **1999**, *9*, 670.

(5) Przbyla, A. E.; Robbins, J.; Menon, N.; Peck, H. D., Jr. *FEMS Microbiol. Rev.* **1992**, *8*, 109.

(6) Garcin, E.; Vernede, X; Hatchikian, E. C.; Volbeda, A.; Frey M.; Fibtecilla-Camps, J. C. *Structure* **1999**, *7*, 557.

(7) Teixeira, M.; Moura, I.; Xavier, A. V.;Huynh, B. H.; DerVartanian, D. V.; Peck, H. D., Jr.; LeGall, J.; Moura, J. J. G. *J. Bio;. Chem.* **1985**, *260*, 8942.

(8) Lyon, E. J.; Shima, S.; Boecher, R.; Thauer, R. K.; Grevels, F.-W.; Bill, E.; Roseboom, W.; Albracht, S. P. J. *J. Am. Chem. Soc.* **2004**, *126*, 14239.

(9) Shima, S.; Lyon, E. J.; Thauer, R. K.; Mienert, B.; Bill, E. *J. Am. Chem. Soc.* **2005**, *127*, 10430.

(10) Shima, S.; Pilak, O.; Vogt, S.; Schick, M.; Stagni, M. S.; Meyer-Klaucke, W.; Warjebtun, E.; Thauer, R. K.; Ermler, U. *Science* **2008**, *321*, 572.

(11) Linck, R. C.; Pafford, R. J.; Rauchfuss, T. B. *J. Am. Chem. Soc.* **2001**, *123*, 8856.

(12) Gray, T. G.; Veige, A. S.; Nocera, D. G. *J. Am. Chem. Soc.* **2004**, *126*, 9760.

(13) Bianchini, C.; Mealli, C.; Meli, A.; Sabat, M. *Inorg. Chem.* **1986**, *25*, 4617.

(14) (a) DuBois, M. R.; VanDerveer, M. C.; DuBois, D. L.; Haltiwanger, R. C.; Miller, W. K. *J. Am. Chem. Soc.* **1980**, *102*, 7456. (b) DuBois, M. R. *Chem. Rev.* **1989**, *89*, 1. (c) Laurie, J. C. V.; Duncan, L.; Haltiwanger, R. C.; Weberg, R. T.; DuBois, M. R. *J. Am. Chem. Soc.* **1986**, *108*, 6234.

(15) Kato, H.; Seino, H.; Mizobe, Y.; Hidai, M. *J. Chem. Soc., Dalton Trans.* **2002**, 1494.

(16) Ohki, Y.; Matsuura, N.; Marumoto, T.; Kawaguchi, H.; Tatsumi, K. *J. Am. Chem. Soc.* **2003**, *125*, 7978.

(17) (a) Ogo, S.; Kabe, R.; Uehara, K.; Kure, B.; Nishimura, T.; Menon, S. C.; Harada. R.; Fukuzumi, S.; Higuchi, Y.; Ohhara, T.; Tamada, T.; Kuroki, R. *Science* **2007**, *316*, 585. (b) Matsumoto, T.; Kure, B.; Ogo, S. *Chem. Lett.* **2008**, *37*, 970. (c) Wilson, A. D.; Shoemaker, R. K.; Miedaner, A.; Muckerman, J. T.; Dubois, D. L.; Dubois, R. M. *Proc. Natl. Acad. Sci. U.S.A.* **2007**, *104*, 6951.

(18) Matsumoto, T.; Nakaya, Y.; Itakura, N.; Tatsumi, K. *J. Am. Chem. Soc.* **2008**, *130*, 2458.

(19) Vincent, J. L; Luo, S.; Scott, B. L.; Butcher, R.; Unkefer, C. J.; Burns, C. J.; Kubas, G. J.; Lledos, A.; Maseras, F.; Tomas, J. *Organometallics* **2003**, *22*, 5307.

(20) Trinquier, G.; Hoffmann, R. *Organometallics* **1984**, *3*, 370.

(21) Ienco, A.; Calhorda, M. J.; Reinhold, J.; Reineri, F.; Bianchini, C.; Peruzzini, M.; Vizza, F.; Mealli, C *J. Am. Chem. Soc.* **2001**, *126*, 11954.

(22) Gray, T. G.; Veige, A. S.; Nocera, D. G. *J. Am. Chem. Soc.* **2004**, *126*, 9760.

(23) Suzuki, H.; Tokitoh, N.; Okazaki, R.; Nagase, S.; Goto, M. *J. Am. Chem. Soc.* **1998**, *120*. 11096.

(24) Becke, A. D. *Phys. Rev.* **1988**, *A38*, 3098.

(25) Becke, A. D. *J. Chem. Phys.* **1983**, *98*, 5648.

(26) Lee, C.; Yang, W.; Parr, R. G. *Phys. Rev.* **1988**, *B37*, 785.

(27) D. Andrae, U. Haeussermann, M. Dolg, H. Stoll, H. Preuss, *Theor. Chim. Acta* **1990**, *77*, 123.

(28) (a) Hehre, W. J.; Ditchfield, R.; Pople, J. A. *J. Chem. Phys.* **1972**, *56*, 2257. (b) Hariharan, P. C.; Pople, J. A. *Theor. Chim. Acta* **1973**, *28*, 213. (c) Hariharan, P. C.; Pople, J. A. *Mol. Phys.* **1974**, *27*, 209. (d) Francl, M. M.; Petro, W. J.; Hehre, W. J.; Binkley, J. S.; Gordon, M. S.; DeFrees, D. J.; Pople, J. A. *J. Chem. Phys.* **1982**, *77*, 3654.

(29) Clark, T.; Chandrasekhar, J.; Spitznagel, G. W.; Schleyer, P. V. R. *J. Comp. Chem.* **1983**, *4*, 294.

(30) Martin, J. M. L.; Sundermann, A. *J. Chem. Phys.* **2001**, *114*, 3408.

(31) (a) Krishnan, R.; Binkley, J. S.; Seeger, R.; Pople, J. A. *J. Chem. Phys.* **1980**, *72*, 650. (b) McLean, A. D.; Chandler, G. S. *J. Chem. Phys.* **1980**, *72*, 5639. (c) Blaudeau, J.-P.; McGrath, M. P.; Curtiss, L. A.; Radom, L. *J. Chem. Phys.* **1997**, *107*, 5016. (d) Curtiss, L. A.; McGrath, M. P.; Blandeau, J-P.; Davis, N. E.; Binning, R. C.; Radom, Jr. L. *J. Chem. Phys.* **1995**, *103*, 6104.

(32) Pople, J. A., et al. Gaussina 03, revision C.02; Gaussian, Inc.: Wallingford, CT, 2004.

(33) Reed, A. E.; Curtiss, L. A.; Weinhold, F. *Chem. Rev.* **1988**, *88*, 899.

(34) Bader, R. F. W. *Atoms in molecules. A quantum theory*; Oxford: 1990.

(35) Flükiger, P.; Lüthi, H. P.; Portann, S.; Weber, J. MOLEKEL, v.4.3; Scientific Computing: Manno, Switzerland, 2002-2002. Portman, S.; Lüthi, H. P. *CHIMIA* **2000**, *54*, 766.

(36) Experimental studies in (a) Peris, E.; Lee, J. C.; Rambo, J. R.; Eisenstein, O.; Crabtree, R. H. *J. Am. Chem. Soc.* **1995**, *117*, 3485. (b) Wessel, J.; Lee, J. C.; Peris, E.; Yap, G. P. A.; Fortin, J. B.; Ricci, J. S.; Sini, G.; Albinati, A.; Koetzle, T. F.; Eisenstein, O.;

Rheingold, A. L.; Crabtree, R. H. *Angew. Chem. Int. Ed. Engl.* **1995**, *34*, 2507.; Theoretical studies in (c) Liu, Q.; Hoffmann, R. *J. Am. Chem. Soc.* **1995**, *117*, 10108. (d) Orlova, G.; Scheiner, S. *J. Phys. Chem. A* **1998**, *102*, 260.

(37) Cygan, Z. T.; Kampf, J. W.; Holl, M. M. B. *Inorg. Chem.* **2003**, *42*, 7219.

(38) As shown in supporting information (Figure A2), important orbitals of RuGe dinuclear fragment is unoccupied and occupied d-orbitals because stability of H_2 coordination arises from donation and back-donation. Although the orbital energies of occupied d-orbital are close each other, orbital energies of unoccupied d-orbital are different. In $\mathbf{2_{S\eta4}}$, the orbital energy of LUMO is -4.82 eV. In $\mathbf{2_{O\eta4}}$, that of LUMO+1 is -4.35 eV. These results indicate that back-donation in $\mathbf{2_{S\eta4}}$ occurs more than that in $\mathbf{2_{O\eta4}}$.

(39) Though the activation barrier (29.6 kcal/mol) for $\mathbf{TS_{7S\text{-}8S}}$ relative to **1** + H_2 is much larger than that of $\mathbf{TS_{4\text{-}PRD}}$ in the path 1O, this value decreases by entropy effect.

General Conclusion

In this thesis, I mainly investigated the σ-bond activation with transition metal complex by electronic structure theory. These studies provide us with well understanding of σ-bond activation, which is difficult to obtain from the experimental study. Such understanding is indispensable for rational design of catalysts and improving performance of catalysts. The important conclusions presented in this thesis are summarized, as follows:

In chapter 1, the C-H σ-bond activation of methane and the N-H σ-bond activation of ammonia by $(Me_3SiO)_2Ti(=NSiMe_3)$ **1** were theoretically investigated with DFT, MP2 to MP4(SDQ), and CCSD(T) methods. The C-H σ-bond activation of methane takes place with activation barrier (E_a) of 14.6 (21.5) kcal/mol and reaction energy (ΔE) of -22.7 (-16.5) kcal/mol to afford $(Me_3SiO)_2Ti(Me)\{NH(SiMe_3)\}$, where DFT- and MP4(SDQ)-calculated values are given without and in parentheses, respectively, hereafter. The electron population of the CH_3 group increases but the H atomic population decreases upon going to the transition state from the precursor complex, which indicates that the C-H σ-bond activation occurs in heterolytic manner unlike the oxidative addition. The Ti atomic population considerably increases upon going to the transition state from the precursor complex, which indicates that the charge-transfer (CT) occurs from methane to Ti. These population changes are induced by the orbital interactions among the d_π-p_π bonding orbital of the $Ti=NSiMe_3$ moiety, the Ti d_{z2} orbital and the C-H σ-bonding and σ*-anti-bonding orbitals of methane. The reverse regioselective C-H σ-bond activation which leads to formation of $(Me_3SiO)_2Ti(H)\{NMe(SiMe_3)\}$ occurs with larger E_a value and smaller exothermicity. The reasons are discussed in terms of Ti-H, Ti-CH_3, Ti-NH_3, N-H, and N-CH_3 bond energies and orbital interactions in the transition state. The N-H σ-bond activation of ammonia occurs in

a heterolytic manner with larger E_a value of 19.0 (27.9) kcal/mol and considerably larger exothermicity of -45.0 (-39.4) kcal/mol than those of the C-H σ-bond activation. The N-H σ-bond activation of ammonia by Ti-alkylidyne complex, [(PNP)Ti(≡CSiMe$_3$)] **3** (PNP = N-[2-(PH$_2$)$_2$-phenyl]$_2^-$]) was also investigated. This reaction occurs with smaller E_a value of 7.5 (15.3) kcal/mol and larger exothermicity of -60.2 (-56.1) kcal/mol. These results lead us to prediction that the N-H σ-bond activation of ammonia can be achieved by these complexes.

In chapter 2, the O-H σ-bond activation of methanol, the Si-H σ-bond activation of silane, and the Si-C σ-bond activation of methylsilane by titanium(IV)-imido complex (Me$_3$SiO)$_2$Ti(NSiMe$_3$) were theoretically investigated with DFT and MP2 to MP4(SDQ) methods. The O-H σ-bond activation of methanol occurs with small activation barrier (E_a) of 7.1 (14.6) kcal/mol and large exothermicity (E_{exo}) of 65.8 (61.4) kcal/mol to afford (Me$_3$SiO)$_2$Ti(OCH$_3$)[NH(SiMe$_3$)], indicating that the O-H σ-bond activation occurs easier than the C-H σ-bond activation (E_a = 14.6 (21.5) kcal/mol and E_{exo} = 22.7 (16.5) kcal/mol), where DFT- and MP4(SDQ)-calculated values are presented without and in parenthesis hereafter. Though the OCH$_3$ group becomes anionic and the H atom becomes proton-like in this activation reaction, population changes moderately occur compared to those of the C-H σ-bond activation. This is because the H-OCH$_3$ bond is already polarized in methanol. In the Si-H σ-bond activation, two reaction courses were investigated; in one course, the product is (Me$_3$SiO)$_2$Ti(SiH$_3$)[NH(SiMe$_3$)] in which the H atom and the SiH$_3$ group are bound with the N atom and the Ti center, respectively, while in the other course the product is (Me$_3$SiO)$_2$Ti(H)[N(SiH$_3$)(SiMe$_3$)] in which the H atom and the SiH$_3$ group are bound with the Ti center and the imido N atom, respectively. Though the former reaction occurs with small E_a value and large exothermicity, the latter reaction occurs easier with further smaller E_a value of 2.6 (4.3) kcal/mol and larger E_{exo} value of 32.5 (34.1) kcal/mol than the former reaction. This is because the Ti-H bond energy is much larger than the Ti-SiH$_3$ one. The Si-C σ-bond activation occurs with moderate activation barrier of 19.1 (18.6) kcal/mol and considerably

large exothermicity of 33.9 (37.7) kcal/mol. Based on these results, I wish to propose theoretical prediction that the titanium(IV)-imido complex is useful for O-H, Si-H, and Si-C σ-bond activation reactions.

In chapter 3, the {2 + 2} cycloaddition of alkynes across the titanium-imido bond of $[(H_3SiO)_2Ti(=NSiH_3)]$ **1** was theoretically investigated with DFT and CCSD(T) method. Though this cycloaddition is symmetry forbidden in a formal sense by the Woodward-Hoffmann rule, the {2 + 2} cycloaddition of 2-butyne (MeC≡CMe) easily occurs with moderate activation barrier (7.6 kcal/mol) and considerably large exothermicity (41.0 kcal/mol), where the CCSD(T)-calculated values are presented hereafter. This result is interpreted in terms of the highly polarized Ti=N bond; Because the d_π-p_π bonding orbital largely consists of the p_π orbital of N and moderately of the d_π orbital of Ti, the π* orbital of 2-butyne overlaps with the d_π-p_π bonding orbital so as to form C-N bonding interaction, into which the π orbital of 2-butyne mixes in an anti-bonding way with the p_π orbital of N. As a result, the C-C bond of 2-butyne is polarized and the symmetry forbidden character becomes weak, which leads to the small activation barrier. The {2 + 2} cycloaddition of 1-methoxy-1-propyne ($MeC^\alpha{\equiv}C^\beta OMe$) occurs with smaller activation barrier (3.2 kcal/mol) than that of 2-butyne, when the C^α and C^β approach the Ti and N, respectively. The higher reactivity of this alkyne is interpreted in terms of the polarized C≡C bond of 1-methoxy-1-propyne. From these results, it is expected that the regioselective {2 + 2} cycloaddition can be performed by introducing the π-electron donating group on the C atom of alkyne and in the major product the N and Ti are bound with the C atom bearing the π-electron donating group and the other C atom, respectively.

In chapter 4, the palladium complex of P,S-containing hybrid calixphyrin **1** was investigated with the DFT method. There are two kinds of valence tautomer in **1**: one is a Pd(II) form in which the calixphyrin moiety possesses -2 charges and the Pd center takes +2 oxidation state, and the other is a Pd(0) form in which the calixphyrin is neutral and the Pd

center takes zero oxidation state. Complex **1** takes the Pd(II) form in the ground state. Though the Pd center takes +2 oxidation state, DFT computations clearly show that the oxidative addition of phenyl bromide (PhBr) to **1** occurs with moderate activation enthalpy, as experimentally proposed. The first step of the oxidative addition is the coordination of PhBr with the Pd center to form intermediate **1INTa**, in which the Pd center and the calixphyrin moiety are neutral; in other words, the valence tautomerization from the Pd(II) form to the Pd(0) form occurs in the palladium calixphyrin moiety. The activation enthalpy is 22.5 kcal/mol, and the enthalpy change of reaction is 20.3 kcal/mol. The next step is the C-Br σ-bond cleavage of PhBr, which occurs with activation enthalpy of 2.0 kcal/mol relative to **1INTa**. On the other hand, the oxidative additions of PhBr to palladium complex of P,S-containing hybrid porphyrin **2** and that of conventional porphyrin **3** need much larger activation enthalpies of 49.1 and 74.4 kcal/mol, respectively. The differences in the reactivity among **1**, **2**, and **3** were theoretically investigated; in **1**, the valence tautomerization occurs with moderate activation enthalpy to afford the Pd(0) form which is reactive for the oxidative addition. In **2**, the tautomerization from the Pd(II) form to the Pd(0) form needs very large activation enthalpy (43.3 kcal/mol). In **3**, such valence tautomerization does not occur at all, indicating that the Pd(II) must change to the Pd(IV) in the oxidative addition of PhBr to **3**, which is a very difficult process. These differences are interpreted in terms of the π* orbital energies of P,S-containing hybrid calixphyrin, hybrid porphyrin, and conventional porphyrin and the flexibility of their frameworks.

In chapter 5, the interconversion between H_2 and H_2O by hydroxo/sulfido-bridged dinuclear ruthenium-germanium complex $[Dmp(Dep)Ge(\mu\text{-}S)(\mu\text{-}OH)Ru(PPh_3)]^+$ **1** (Dmp = 2,6-dimesitylphenyl, Dep = 2,6-diethylphenyl) is theoretically investigated with ONIOM method. In the conversion of H_2 to H_2O, the first step is the isomerization of **1**, in which the Ru-O bond is broken with activation (E_a) of 14.3 kcal/mol to afford the intermediate **2** containing the vacant coordination site. Then, the H_2 further approaches the vacant site

through transition state **$TS_{2\text{-}3}$** with E_a of 20.3 kcal/mol to afford the H_2 σ-complex **3**. Starting from **3**, the H-H σ-bond activation by the Ru and the Ge-OH moieties occurs with E_a of 11.6 kcal/mol to form intermediate **4** in which hydride coordinates with the Ru and H_2O interacts with the Ge. Finally, the H_2O dissociates from the Ge with E_a of 23.5 kcal/mol to afford products, $[Dmp(Dep)Ge(\mu\text{-}S)(\mu\text{-}H)Ru(PPh_3)]^+$ **PRD** and H_2O. The E_a of reverse reaction is moderately smaller than that of the forward reaction, indicating that **1** catalyzes well the interconversion between H_2 and H_2O. This result indicates that this reaction can reversibly occur. The population changes clearly indicate the H-H σ-bond activation occurs in heterolytic manner, similar to the σ-bond activation by hydrogenase. Interestingly, this heterolytic σ-bond activation is performed by separated two reaction centers, the Ru and Ge-OH moieties. In the Si analogue complex $[Dmp(Dep)Si(\mu\text{-}S)(\mu\text{-}OH)Ru(PPh_3)]^+$ **1_{Si}**, the H-H σ-bond activation easily occurs with smaller E_a of 10.9 kcal/mol, but the dissociation of H_2O from the Si needs considerably large E_a of 32.6 kcal/mol. This is understood in terms of the strong Si-OH_2 bond; the Ge-OH_2 and Si-OH_2 bonds are evaluated to be 25.5 and 39.6 kcal/mol, respectively.

As described above, new and valuable understanding of σ-bond activation reaction by transition metal complexes is presented in this thesis. For instance, the σ-bond activation by titanium-imido complex occurs in heterolytic manner. Based on the careful studies, important orbital interaction in heterolytic σ-bond activation is clearly disclosed here. Also, the C-Br σ-bond activation by palladium complex of P,S-containing hybrid calixphyrin was discussed and the importance of flexible behavior of P,S-containing hybrid calixphyrin in the reaction was shown as important process. I believe that these computational results are useful for finding a new catalyst and presenting well understanding of σ-bond activation reaction.

List of Publications

Publications included in this thesis

Chapter 1

"Theoretical Study of C-H and N-H σ-Bond Activation Reactions by Titanium(IV)-Imido Complex. Good Understanding Based on Orbital Interaction and Theoretical Proposal for N-H σ-Bond Activation of Ammonia"

Noriaki Ochi, Yoshihide Nakao, Hirofumi Sato, Shigeyoshi Sakaki

J. Am. Chem. Soc., **2007**, *129*, 8615-8624.

Chapter 2

"Theoretical Prediction of O-H, Si-H, and Si-C σ-Bond Activation Reactions by Titanium(IV)-Imido Complex"

Noriaki Ochi, Yoshihide Nakao, Hirofumi Sato, and Shigeyoshi Sakaki

Can. J. Chem., **2009**, *87*, 1415-1424.

Chapter 3

"{2 + 2} Cycloaddition of Alkyne with Titanium-Imido Complex. Theoretical Study of the Determining Factors of Reactivity and Regioselectivity"

Noriaki Ochi, Yoshihide Nakao, Hirofumi Sato, and Shigeyoshi Sakaki

J. Phys. Chem. A, in press.

Chapter 4

"New Palladium(II) Complex of P,S-Containing Hybrid Calixphyrin. Theoretical Study of Electronic Structure and Reactivity for Oxidative Addition"

Noriaki Ochi, Yoshihide Nakao, Hirofumi Sato, Yoshihiro Matano, Hiroshi Imahori, and Shigeyoshi Sakaki

J. Am. Chem. Soc., **2009**, *131*, 10955-10963.

Chapter 5

"Interconversion between H_2 and H_2O by Hydroxo/Sulfido-Bridged Dinuclear Ruthenium-Germanium Complex. Theoretical Study"

Noriaki Ochi, Tsuyoshi Matsumoto, Takeya Dei, Yoshihide Nakao, Hirofumi Sato, Kazuyuki Tatsumi, and Shigeyoshi Sakaki

To be submitted.

Other publications

1. "Oxidation Reaction by Xanthine Oxidase. Theoretical Study of Reaction Mechanism"
   Tatsuo Amano, Noriaki Ochi, Hirofumi Sato, Shigeyoshi Sakaki
   J. Am. Chem. Soc., **2007**, *129*, 8131-8138.

2. "Heterolytic σ-Bond Activation by Transition Metal Complexes"
   Shigeyoshi Sakaki, Noriaki Ochi, Yu-ya Ohnishi
   Computational Modeling for Homogeneous and Enzymatic Catalysis. A Knowledge-Base for Designing Efficient Catalysis. Morokuma, K. and Musaev, D. G. (Eds.); Wiley: Weinheim, 2008.